SYMPOSIUM ON SURFACE SCIENCE 2012

St. Christoph am Arlberg, Austria
March 11 - 17, 2012

CONTRIBUTIONS

EDITORS
Friedrich Aumayr, Ulrike Diebold, Christoph Lemell, and Peter Varga
TU Wien

A PASSION FOR PERFECTION

PFEIFFER VACUUM

PFEIFFER VACUUM

adixen
by PFEIFFER VACUUM

Perfect Vacuum Solutions!

Two strong brands combined for your success

- Best-in-class products
- Leading vacuum technology know-how
- Worldwide sales and service support

Are you looking for a perfect vacuum solution? Please contact us:

Pfeiffer Vacuum Austria GmbH
T +43 1 8941704 · F +43 1 8941707
office@pfeiffer-vacuum.at

www.pfeiffer-vacuum.com

NUR BIS 27. 4. 2012:
KLIMAKREDIT MIT BIS ZU EUR 600,– UMWELTBONUS.

Sie malen sich Ihr Traumhaus aus.

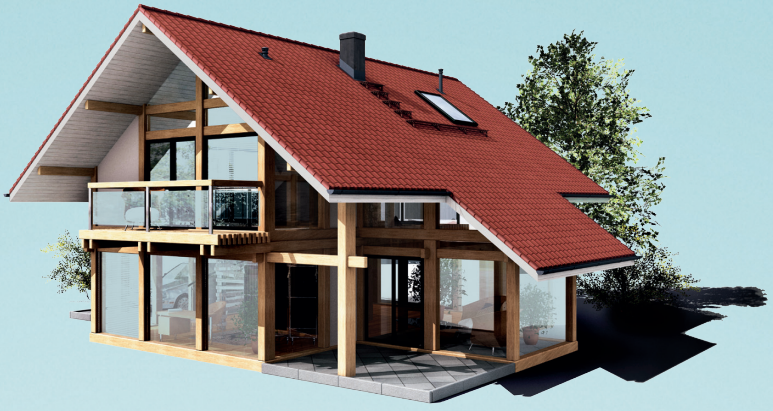

Wir helfen Ihnen bei der Verwirklichung.

Es gibt nichts Schöneres, als Träume, die Wirklichkeit werden. Egal ob Hausbau, Wohnungskauf, Umbau oder Sanierung – die Bank Austria bietet individuelle WohnFinanzierungen um Ihren Wohntraum maßgeschneidert und unkompliziert zu erfüllen.
finanzierungen.bankaustria.at

Das Leben ist voller Höhen und Tiefen. Wir sind für Sie da.

Willkommen bei der
Bank Austria
Member of UniCredit

SYMPOSIUM ON SURFACE SCIENCE 2012

St. Christoph am Arlberg, Austria
March 11 - 17, 2012

CONTRIBUTIONS

EDITORS
Friedrich Aumayr, Ulrike Diebold, Christoph Lemell, and Peter Varga
TU Wien

This symposium is organized by

Friedrich Aumayr, Ulrike Diebold and Peter Varga
Institute of Applied Physics (IAP)
Vienna University of Technology (TU Wien)
Wiedner Hauptstr. 8-10/E134
1040 Vienna, Austria

Medieninhaber: F. Aumayr, U. Diebold und P. Varga, Institut für Angewandte Physik, Technische Universität Wien, Adresse: Wiedner Hauptstr. 8-10/E134, A-1040 Wien
Druck: R. & W. Smutny OEG, A-1110 Wien

PREFACE

We welcome all participants and accompanying persons to the 25th Symposium on Surface Science (3S). The 3S was founded as a winter school by members of the Institute of Applied Physics of the Vienna University of Technology (TU Wien) in 1983. The conference seeks to promote the growth of scientific knowledge and its effective exchange among scientists in surface physics and chemistry and in related areas, including applied topics. Its format is similar to that of Gordon Conferences, with ample time for discussions and joint outdoor activities. The number of participants has been kept below 100 in order to guarantee active communication between all attendees.

Initially the 3S was held exclusively in Austria and took place every other year. It became an annual event in 1990, when the site started to alternate between locations in France and Austria. In 1998 the 3S evolved into a truly global conference with venues in the US, Canada, Bulgaria, Japan, Switzerland, Spain, and France, always returning to Austria in alternate years. This year we are happy to again host the 3S in Austria; for the 6th time in the Arlberg area.

We hope that all participants will experience a lively and successful meeting while enjoying the surroundings in this beautiful mountain region.

Fritz Aumayr Ulrike Diebold Peter Varga

Dates and locations of 3S conferences:

1983	(31.01.-04.02.)	Obertraun	A	2001	(07.01.-13.01.)	Furano	J
1985	(27.01.-02.02.)	Obertraun	A	2002	(03.03.-09.03.)	St.Christoph/Arlberg	A
1988	(22.05.-28.05.)	Kaprun	A	2003	(30.03.-05.04.)	La Plagne	F
1990	(11.03.-17.03.)	La Plagne	F	2004	(29.02.-06.03.)	St.Christoph/Arlberg	A
1991	(10.02.-16.02.)	Obertraun	A	2005	(13.03.-19.03.)	Les Arcs 1800	F
1992	(15.03.-21.03.)	La Plagne	F	2006	(05.03.-11.03.)	St. Christoph/Arlberg	A
1993	(09.05.-15.05.)	Kaprun	A	2007	(11.03.-17.03.)	Les Arcs 2000	F
1994	(06.03.-12.03.)	Les Arcs	F	2008	(02.03.-08.03.)	St. Christoph/Arlberg	A
1995	(23.04.-29.04.)	Kaprun	A	2009	(08.03.-14.03.)	St. Moritz	CH
1997	(26.01.-31.01.)	Aussois	F	2010	(07.03.-13.03.)	St. Christoph/Arlberg	A
1998	(29.03.-04.04.)	Park City	US	2011	(06.03.-12.03.)	Baqueira Beret/Lleida	ES
1999	(21.02.-27.02)	Pamporova	BUL	2012	(11.03.-17.03.)	St. Christoph/Arlberg	A
2000	(15.02.-18.02.)	Kananaskis	CAN				

SYMPOSIUM ON SURFACE SCIENCE 2012

St. Christoph am Arlberg, Austria
March 11-17

Time Schedule

Sunday, 11 March 2012

16:00 – 18:30	**Registration**
20:00 – 20:20	**Opening**
	Chair: P. Varga
20:25 – 20:45	**M. Scheffler** *Role of van der Waals Interactions in Adsorption of Organic Molecules at Inorganic Surfaces*
20:45 – 21:05	**C. Wöll** *Liquid-phase epitaxy of functional metal-organic frameworks on modified Au substrates*
21:05 – 21:25	**C. Draxl** *Manipulating the Dirac cone: Molecules on graphene studied from first-principles*

Monday, 12 March 2012

Chair: P. M. Echenique

08:00 – 08:20 **F. J. Giessibl**
The Phantom Force

08:20 – 08:40 **A. Gölzhäuser**
The Helium Ion Microscope: A New Instrument for Surface Studies

Chair: D. Sanchez-Portal

16:30 – 16:50 **H. Brune**
Magnetism of Co on graphene/Pt(111)

16:50 – 17:10 **M. Weinelt**
Femtomagnetism in Gadolinium and Terbium studied by X-ray Spectroscopy

17:10 – 17:30 **W. Eberhardt**
Magnetism in small mass selected Clusters

17:30 – 17:50 **L. Johansson**
Structure, morphology and magnetic properties of ultrathin Mn germanide films on Ge(111)

17:50 – 18:10 **U. Starke**
Ambipolar doping and formation of p-n junctions in quasifree epitaxial graphene on SiC(0001) controlled by Ge intercalation

18:10 – 18:30 **J. Knudsen**
Stability of graphene and graphene supported clusters in a gas atmosphere

Chair: M. Altman

19:30 – 19:50 **K. Reuter**
Beat the heat: Watching phonons cool down during O_2 dissociation on Pd(100)

19:50 – 20:10 **A. Hellman**
A detailed investigation of the active phase of palladium during methane oxidation

20:10 – 20:30 **A. Borg**
Oxidation and reduction of single crystal Pd-based alloy surfaces – the case of $Pd_{75}Ag_{25}(100)$

20:30 – 20:50 **M. A. Schneider**
Adsorption of small and large molecules on thin cobalt oxide films

Tuesday, 13 March 2012

Chair: U. Heinzmann

08:00 – 08:20 **T. Greber**
The four hills of Graphene on Ru(0001) 25 on 23

08:20 – 08:40 **F. Mittendorfer**
Graphene on Ni(111): Strong Interaction and Weak Adsorption

Chair: E. Taglauer

16:30 – 16:50 **H. Dil**
Self-protecting spin-polarized surface states in ternary topological insulators

16:50 – 17:10 **T. Okuda**
Development of high-resolution spin and angle-resolved photoelectron spectrometer and its applications

17:10 – 17:30 **H. Ibach**
Electron energy loss spectroscopy: a new spectrometer, high resolution spectra of surface spin waves, and a new mode of lens operation

17:30 – 17:50 **Ch. Linsmeier**
Chemically resolved depth profiles from synchrotron XPS of oxygen ion-driven reactions with Be_2W

17:50 – 18:10 **W. Steurer**
Surface processes under strong homogeneous external DC fields

18:10 – 18:30 **A. Klimov**
Surface scattering of electrons in thin PbSnTe:In films with space-charge-induced limitation of electric current

Chair: P. Muller

19:30 – 19:50 **G. Renaud**
Substrate-enhanced supercooling in AuSi droplets

19:50 – 20:10 **F. Leroy**
Si nanoparticles motion onto SiO_2 driven by chemical reaction: a real time study

20:10 – 20:30 **J. E. Ortega**
Tuning the superlattice bands of the Ag/Cu(111) triangular dislocation network

20:30 – 20:50 **E. V. Chulkov**
On the origin of 2DEG states at the surface of layered topological insulators

Wednesday, 14 March 2012

Chair: H. Kisch

08:00 – 08:20 **E. Lundgren**
Pd and PdAg aerosol nanoparticles for catalysis

08:20 – 08:40 **A. Stierle**
Atomic structure of graphene supported metal nanoparticles

Chair: L. Hammer

16:30 – 16:50 **T. U. Kampen**
From basic research in UHV to applied research under ambient conditions: Recent developments in Surface Science Equipment

16:50 – 17:10 **M. Maier**
A new type of detector for dynamic XPS measurements

Chair: G. Rupprechter

17:10 – 18:30 **Poster Introduction**

M. S. Altman
Step Permeability on the Pt(111) Surface

J. Baran
A first-principles determination of the thickness of the protective oxide layer of aluminum

P. Bauer
Electronic excitations of slow ions in a free electron gas metal: evidence for charge exchange effects

U. Bovensiepen
Electron dynamics in Pb/Si(111) investigated with time-resolved photoelectron spectroscopy

M. Buchholz
UHV-IR-spectroscopy on metal oxide surfaces

V. Chis
Phonon dispersion curves of Bi_2Se_3 ultra-thin quintuple layers

K. Dobes
Sputtering of tungsten and a-C:H surfaces by nitrogen ions – investigation of transient and molecular effects

M. H. Farstad
Oxidation of the PdCu(100) surface

R. Fasel
Graphene Nanoribbon Heterojunctions

T. Frederiksen
H-atom relay reactions in real space

L. Hammer
Tuning the growth orientation of oxide films via the interface chemistry

U. Heinzmann
Time-resolved femtosecond Se 3d core level photoemission spectroscopy at the Mott insulator $TiSe_2$

R. Kalousek
Theoretical Description of Material Transport During Germanium Nanowire Growth

H. Kisch
Carbon and Nitrogen/Carbon Modified Titania for Visible Light Photocatalysis

S. Yu. Krylov
Hidden problem of atomic scale friction: Critical damping

T. Ladnorg
Site-selective epitaxial growth of substrate supported metal-organic framework by using AFM nanografting

C. Lemell
Phase diagram for nanostructuring CaF_2 surfaces by slow highly charged ions

N. Müller
Spin-resolved photoemission spectroscopy of $[Mn^{III}{}_6Cr^{III}]^{3+}$ single-molecule magnets (SMM) deposited on surfaces and of Mn compounds as reference substances, cross comparison with XMCD

P. Müller
Nature of the peak-to-peak spacing oscillations measured by RHEED during epitaxial growth

S. Müller
Hybrid materials design with DFT: Silane coupling agent on TiO_2 rutile surfaces

Z. Novotny
Surface Terminations of $Fe_3O_4(001)$

G. Rupprechter
The true explanation is typically rather simple

D. Sánchez-Portal
Electronic and Magnetic Properties of Partially Sulphur-Terminated Graphene Nanoribbons on Au(111)

W.-D. Schneider
Dynamical Coulomb blockade observed in nano-sized electrical contacts

V. M. Silkin
Low-energy collective electronic excitations in thin metallic films

Y. Suchorski
CO oxidation on individual grains of polycrystalline Pd: Laterally-resolved reaction kinetics by PEEM

F. C. Tabak
MEMS devices as fast STM scanners: options and difficulties, an overview

E. Taglauer
Information depth of low-energy ion scattering in the reionization regime

H. Takei
Cap-shaped noble metal particles adsorbed on a solid support as a platform for surface-enhanced colorimetric, fluorescence, and Raman spectroscopies

A. S. Terekhov
The relative influence of work function and stoichiometry of GaAs(001) surface on Cs -promoted oxygen adsorption

I. Thomé
Formation and spectroscopic analysis of conditioning films on self-assembled monolayers

19:30 – 21:30 **Postersession**

Thursday, 15 March 2012

Chair: U. Bovensiepen

08:00 – 08:20 **J. V. Barth**
Porphyrin nanochemistry – a 2D perspective

08:20 – 08:40 **M. Buck**
Pore Modified Supramolecular Networks as Templates

Chair: W.-D. Schneider

16:30 – 16:50 **L. Grill**
Hierarchical covalent molecular linking by sequential activation

16:50 – 17:10 **H. Marbach**
Direct observation of molecular switching at and close to room temperature by STM

17:10 – 17:30 **B. Hendriksen**
SPM study of inorganic molecular electronics

17:30 – 17:50 **M. Messing**
Protein interactions with the surface of gold nanoparticles: possible means of determining particle toxicity

17:50 – 18:10 **A. Winkler**
Nucleation and growth of rod-like organic molecules on inert substrates: 6P on mica

18:10 – 18:30 **G. Pirug**
Line-on-line growth mode of HCOOH on Au (111): Energetic balance between intermolecular and adsorbate-substrate interaction

Chair: P. Bauer

19:30 – 19:50 **A. Arnau**
Evidence of a strong hybridization between surface states and 1-D quasimolecular states of a Cu-O chain in the reconstructed O(2x1)/Cu(110) surface

19:50 – 20:10 **A. Garcia-Lekue**
Theoretical investigation of intermolecular hydrogen-bond mediated core level shifts

20:10 – 20:30 **P. Cabrera-Sanfelix**
One Dimensional Structures at Low Water Coverage on Cu(110)

20:30 – 20:50 **F. P. Netzer**
The self-assembly of $(WO_3)_3$ clusters on Cu(110) surfaces

Friday, 16 March 2012

Chair: F. Aumayr

08:00 – 08:20 **K. Morgenstern**
Field states and their lifetime on nano

08:20 – 08:40 **F. Esch**
Dynamics of truly monodisperse clusters under the STM

Chair: U. Diebold

16:30 – 16:50 **J. Gustafson**
CO oxidation over Pt group metals studied by in situ high pressure XPS

16:50 – 17:10 **J. Libuda**
Liquid Organic Hydrogen Carriers: Surface Science and Model Catalytic Studies

17:10 – 17:30 **V. Navarro**
Fischer-Tropsch synthesis followed at high pressures with STM and SXRD

17:30 – 17:50 **S. Blomberg**
Laser Induced Fluorescence applied to catalysis

17:50 – 18:10 **D. Menzel**
Photochemistry on nanoparticles. An overview of a typical system

Chair: R. Fasel

18:30 – 18:50 **T. Koshikawa**
Development of novel high brightness and high spin-polarized SPLEEM and application to spintronics

18:50 – 19:10 **Y. Suchorski**
Kinetic transitions and light-off in catalytic CO oxidation on Pt: from mesoscopic to nanoscale

19:10 – 19:35 **Giant Slalom Race Award Ceremony**

20:00 – **Conference Dinner**

VG SCIENTA

a gammadata company

Content

CONTRIBUTIONS

Sunday

Role of van der Waals Interactions in Adsorption of Organic Molecules at Inorganic Surfaces

Matthias Scheffler

Fritz-Haber-Institut der Max-Planck-Gesellschaft, Faradayweg 4-6, 14195 Berlin, Germany

Dispersive or van der Waals (vdW) interactions are crucial for the formation, stability, and function of many molecules and materials. They typically dominate in regions where the overlap of electron densities is small, i.e., at medium to long interatomic distances. Interestingly, the commonly applied implementations of density-function theory (e.g. LDA, GGAs, hybrids) are completely lacking the vdW tail. And also at short interatomic distances these approaches do not provide the correct physical/chemical description in systems were nonlocal correlation (vdW being the long-range limit) is playing a noticeable role.

In this talk I will review recent advances in electronic-structure theory, in particularly I will highlight the exceptionally accurate and truly parameter-free "*exact exchange (EX) plus random phase approximation to correlation (cRPA)*" approach and recent corrections to cRPA.[1]

Furthermore, I will discuss approximations that are computationally more efficient, as, for example the linkage of the Tkatchenko-Scheffler [2] and Landau-Zaremba-Kohn methods [3]. This provides an accurate description of vdW interactions between adsorbates and metal surfaces at the cost of a DFT-PBE calculation.

As particular applications I will discuss PTCDA [4], Xe, and benzene @ metals [3], F4TCNQ @ ZnO [5], and benzene @ Si (100) [6].

[1] J. Paier,1 X. Ren, P. Rinke, G. E. Scuseria, A. Grüneis, G. Kresse, and M. Scheffler, *Assessment of correlation energies based on the random-phase approximation*, submitted to New J. Phys.

[2] A. Tkatchenko and M. Scheffler, *Accurate molecular van der Waals interactions from ground-state electron density and free-atom reference data*. Phys. Rev. Lett. **102**, 073005 (2009).

[3] V.G. Ruiz, W. Liu, E. Zojer, M. Scheffler, and A. Tkatchenko, *Density-functional theory with screened van der Waals interactions for the modeling of hybrid inorganic/organic systems*, submitted for publication.

[4] A. Tkatchenko, L. Romaner, O.T. Hofmann, E. Zojer, C. Ambrosch-Draxl, and M. Scheffler, *Van der Waals interactions between organic adsorbates and at organic/inorganic interfaces*. MRS Bulletin **35**, 435-442 (2010).

[5] R. Schlesinger1, Y. Xu, S. Winkler, J. Frisch, J. Niederhausen, A. Vollmer, P. Rinke, M. Scheffler, and N. Koch, *Controlling the work function of ZnO over wide ranges with a strong molecular acceptor,* in preparation.

[6] H.-J. Kim, A. Tkatchenko, J.-H. Cho, and M. Scheffler, *Benzene adsorbed on Si(001): The role of electron correlation and finite temperature*. Phys. Rev. B (RC), in print (2012).

Liquid-phase epitaxy of functional metal-organic frameworks on modified Au-substrates

Christof Wöll
Institute of Functional Interfaces (IFG)
Karlsruhe Institute of Technology (KIT)
76021 Karlsruhe, FRG

Supramolecular chemistry holds unique prospects for the fabrication of novel functional materials. In 2D, the assembly of organic molecules (ligands) via hydrogen bonds or ionic interactions into porous meshes supported on flat metal substrates has been significantly advanced in recent years.[1]
Here we extend the fabrication of surface-anchored networks beyond the formation of planar, 2D adlayers by growing highly-ordered, 3D porous metal-organic frameworks (MOFs) on organic surfaces exposed by different types of self-assembled thiolate-based monolayers (SAMs). We will demonstrate the principle of liquid phase epitaxy [2] for the case of $[Cu_3(BTC)_2(H_2O)_n]$ (HKUST-1) deposited on COOH- and OH-terminated SAMs using Cu(II) acetate as the metal precursor and BTC (benztricarboxylic acid) as the organic ligand. SPR (surface plasmon resonance) spectroscopy and a quartz crystal microbalance (QCM) are used to monitor the growth (and the subsequent loading of the porous adlayers) in-situ [3]. XRD data reveal the formation of oriented, highly ordered crystalline MOF thin-films with a structure identical to that observed in the bulk. The orientation is, interestingly, found to depend on the particular type of SAM used.
The availability of porous frameworks rigidly anchored to solid surfaces opens the prospect of adding additional functionality to these ultrathin surface coatings by placing nanoobjects inside the pores within the MOFs, e.g. metal clusters or dye molecules [5], or by achieving chiral recognition via enantiopure ligands used to build the MOFs [6].

[1] J.V. Barth, *Ann Rev. Phys. Chem.* ***58***, 375 (2007)
[2] O. Shekhah et al., *J.Am.Chem.Soc.* **129**, 15118 (2007)
[3] O. Shekhah et al., Angew. Chem. Int. Ed., **48**, 5038 (2009)
[4] O. Shekhah, J. Liu, R.A. Fischer, Ch. Wöll, Chem. Soc. Rev., **40**, 1081 (2011)
[5] H.K. Arlsan, O. Shekhah, D.C.F. Wieland, M. Paulus, C. Sternemann, M. A. Schroer, S. Tiemeyer, M. Tolan, R.A. Fischer, Ch. Wöll, J. Am. Soc., **133**, 8158 (2011)
[6] B. Liu, O. Shekhah, H. K. Arslan, J. Liu, Ch. Wöll, R. A Fischer, Angew. Chemie, in print (2012)

Manipulating the Dirac cone: Molecules on graphene studied from first-principles

Peiman Amiri[1], Peter Puschnig[1], and Claudia Draxl[1,2]

[1]*Chair of Atomistic Modelling and Design of Materials, Montanuniversität Leoben, Franz-Josef-Straße 18, A-8700 Leoben, Austria*
corresponding author: C. Draxl, e-mail: claudia.draxl@physik.hu-berlin.de

[2]*Institut für Physik, Humboldt-Universität zu Berlin, Newtonstraße 15, D-12489 Berlin, Germany*

The double Dirac cone, i.e., allowing for a massless charge transport, has made graphene one of the most studied materials during the last years. In order to exploit graphene for logic device applications, much effort is put nowadays into opening the gap between these two cones. Here, we show that this is possible through the adsorption of organic molecules or polymers. With the example of the poly-para-phenylene (PPP) we demonstrate that the polymer significantly affects the band structure of graphene.

When investigating the absorption of PPP on graphene by density-functional theory (DFT), we find that the system is van-der Waals bound, where the electron density shows only weak surface dipoles with zero total charge transfer from the polymer to the surface and vice versa. Hence we can expect that the polymer and graphene bands in the combined system should hardly be altered compared to the electronic structures of its components. In fact, when performing DFT calculations for the interface, the HOMO-LUMO gap of PPP remains unchanged upon adsorption onto graphene. However, DFT misses the image-charge effect which can change the band gap of semiconductors in the vicinity of a polarizable surface. It has been shown by Neaton and coworkers [1] that the band gap of benzene is strongly diminished when the molecule is absorbed on a graphite surface, and this many-body effect can be captured by the so-called *GW* approach. Indeed, when applying this method to PPP@graphene, we observe a significant reduction of the PPP band gap, which amounts to 1.1 eV at an adsoption distance of 3.25Å.

What has not been observed so far, is the fact that the polymer, in turn, can renormalize the electronic structure of graphene. We show that, upon adsorption of PPP, a gap of about 0.4 eV is opened at the Dirac point due to the presence of the polymer which breaks the symmetry and affects folded-back Dirac-cones unequally due to the polymer's anisotropic polarizability. Thus, our calculations suggest that tailored manipulation of the Dirac cone is possible by choosing molecules or polymers with specific dielectric properties.

[1] J. B. Neaton, M. S. Hybertsen, and S. G. Louie, Phys. Rev. Lett. 97, 216405(2006).

Monday

The Phantom Force

A. J. Weymouth, T. Wutscher, J. Welker, T. Hofmann, F. J. Giessibl

Institute of Experimental and Applied Physics, University of Regensburg, D-93053 Regensburg, Germany, franz.giessibl@ur.de

Scanning tunneling microscopy (STM) allows to image surfaces at a relatively large tip-sample distance. The tunneling current increases by approximately a factor of ten when decreasing the tip-sample distance by 100 pm. Because tunneling currents can typically be measured with a good signal-to-noise ratio (SNR) within at least a range of five decades (e.g. 1 pA to 100 nA), atomic resolution can be obtained within a distance interval of 0.5 nm.

In atomic force microscopy (AFM), the distance interval where atomic resolution can be achieved is typically much smaller, because obtaining a good SNR is usually more difficult in AFM than in STM. Small tip-sample distances, where forces are large, are typically required to observe a force image with a good SNR.

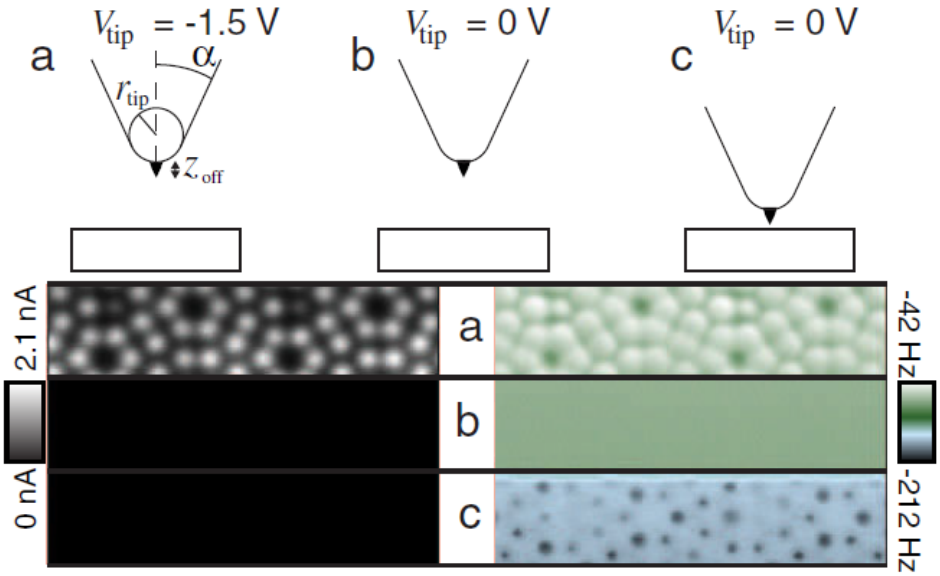

Recently, we found in combined STM and AFM experiments [1] that apparently, high contrast in the frequency shift can be obtained at large distances, where the chemical bonding forces are thought to have a negligible magnitude, as well. The image above shows constant height data of tunneling current (left column) and frequency shift (proportional to the average force gradient between tip and sample, right column). Part a) shows data recorded at a relatively large distance with a minimal tunneling impedance of 1.5V/2.1 nA = 5/7 GΩ. The right section of a) shows a pronounced frequency shift signal that is more positive at the adatom sites, pointing to an apparent repulsive interaction. When reducing the bias voltage to zero in part b), the atomic contrast is of course lost in the tunneling current, but also in the frequency shift, suggesting that this apparently repulsive force is caused by the presence of a

tunneling current. In part c), the tip sample distance is reduced by 340 pm and the chemical bonding forces between tip and sample cause the expected negative (i.e. attractive) contrast in the frequency shift. Chemical bonding forces at the distance range of parts a) and b) are known to be much smaller than the large effect apparent in a), and inspired by Webster's definition of "something apparently sensed but having no physical reality" as "phantom" [2], we called this force the phantom force.

We identified the origin of this phantom force as an electrostatic effect induced by the tunneling current. The tunneling current induces a local shift in the electrostatic potential as indicated by the blue area in the sample in the figure below. This reduction in the local tip-sample potential mimicks a local repulsive force. The voltage drop is proportional to the tunneling current and the resistance of the sample. Adding a resistor in the current path from the sample to the tunneling current amplifier decreases the current contrast, but increases the phantom force, as can be seen in the figure to the left.

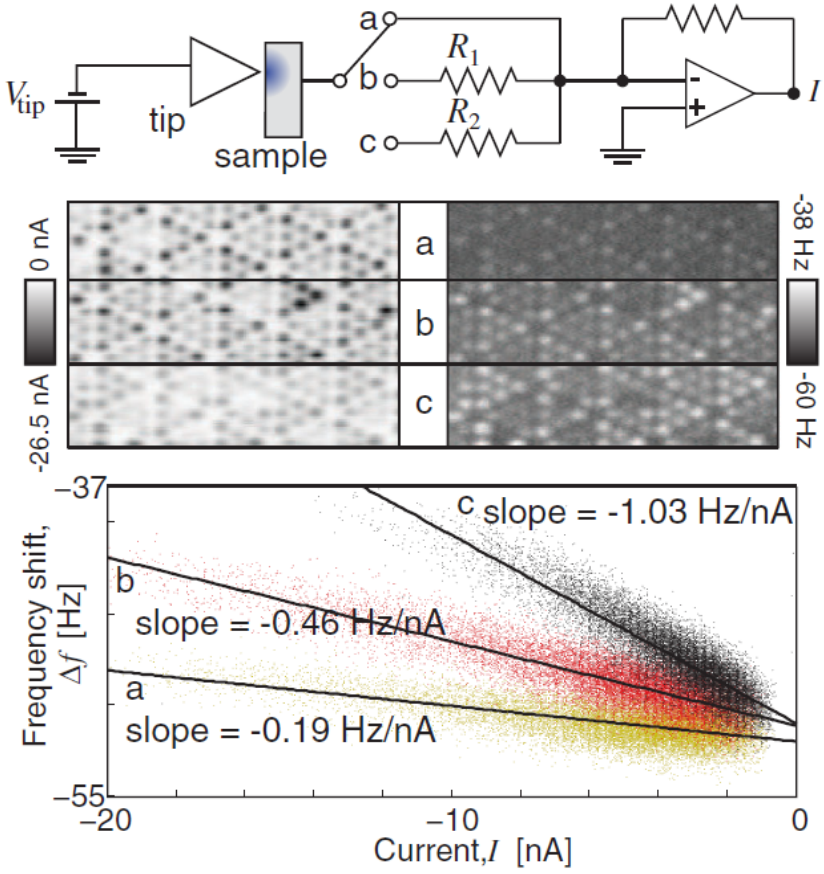

It is important to note that the phantom force is always present when a tunneling current can flow, no matter if that force is measured. Also, the phantom force exists even when the tunneling current is not measured. The phantom force is expected to influence Kelvin Probe measurements. Whenever conductive AFM tips are used and a nonzero bias voltage between tip and sample is applied, the phantom force will influence the force measurements. The magnitude of the phantom force depends on the resistivity of the sample – a high specific resistance (e.g. for semiconductors and adsorbed molecules) will cause a strong phantom force and for samples with a high conductivity such as metals, the phantom force is negligible.

[1] A.J. Weymouth, T. Wutscher, J. Welker, T. Hofmann, F.J. Giessibl, *Phys. Rev. Lett.* **106**, 226801 (2011).
[2] http://www.websters-online-dictionary.org/definitions/phantom

The Helium Ion Microscope: A New Instrument for Surface Studies

André Beyer, Henning Vieker, Xianghui Zhang, Andreas Winter, Nils Eike Weber, Nils Mellech, Andrey Turchanin, Armin Gölzhäuser

Department of Physics, University of Bielefeld, Germany

A Helium Ion Microscope (HIM) operates with a highly focussed He^+ ion beam that is scanned over a sample surface. The impact of the helium ions generates secondary particles, such as secondary electrons (SE) or Rutherford backscattered ions (RBI) that are ejected from the surface. By utilizing electron and ion detectors, the spatial variations of the SE and RBI intensities are recorded. Like in a scanning electron microscope (SEM), highly magnified pictures of the sample are produced by the conversion of these secondary particle intensities into greyscale images [1].

The helium ion source is realized by a field ion microscope with an atomically sharp metal tip that is terminated by a trimer of atoms [2]. Due to the short de Broglie wavelength of the helium ions and the atomic source size, the He^+ beam is highly focused and the HIM is capable to resolve image features with sizes below ~0.3 nm, i. e. ~10x smaller than an SEM. Due to the complex interactions of helium ions with matter, HIM images (SE as well as RBI) also show more pronounced chemical contrasts than SEM images. Hence, HIM images combine high spatial resolution and materials contrast. We report on a HIM study of different nanomaterials focusing on Self-Assembled Monolayers (SAMs), 1 nm thick carbon nanomembranes (CNMs), and gold nanowires [3]. We also demonstrate the capability of the HIM for nanolithography of organic surfaces.

[1] L. Scipioni, L. A. Stern, J. Notte, S. Sijbrandij, B. Griffin: Helium Ion Microscope *Advanced Materials & Processes 16*6, 27 (2008).

[2] R. Hill, J. Notte, B. Ward: The ALIS He ion source and its application to high resolution microscopy, *Physics Procedia 1*, 135 (2008).

[3] K. Gries, H. Vieker, A. Gölzhäuser, S. Agarwal, A. Greiner: Preparation of continuous Gold Nanowires via Electrospinning of high concentration aqueous Dispersions of Gold Nanoparticles, *Small, in press* (2012).

Correspondence: ag@uni-bielefeld.de

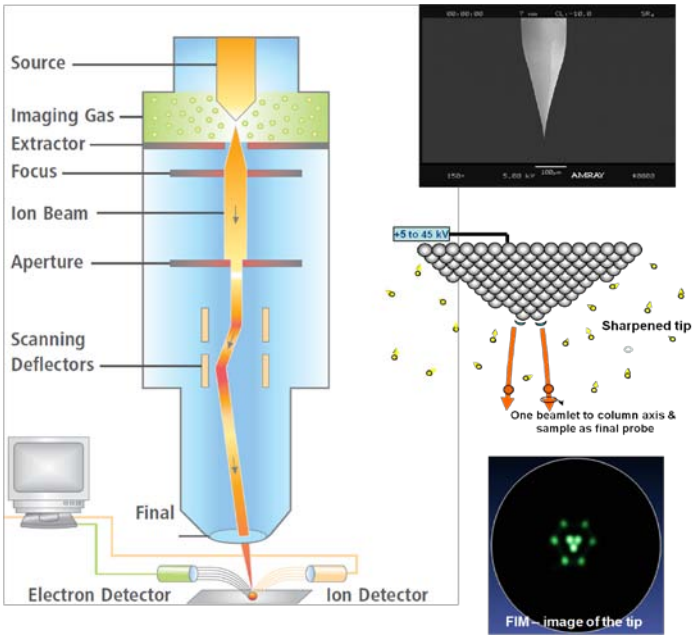

Fig. 1: Schematic of a Helium Ion Microscope (HIM): A He^+ gas ion source, realized by a metal tip sharpened in a field ion microscope (FIM) to form an atomic trimer at the tip apex

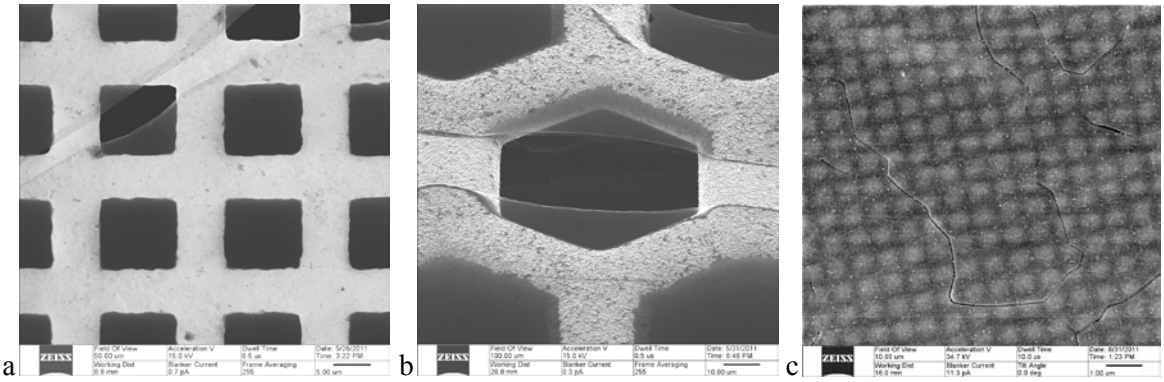

Fig 2: HIM micrographs of 1 nm thick carbon nanomembranes free-standing onto different Cu grids with openings of (a) 10 µm and (b) 40 µm. (c) HIM micrograph of a patterned SAM on a gold surface.

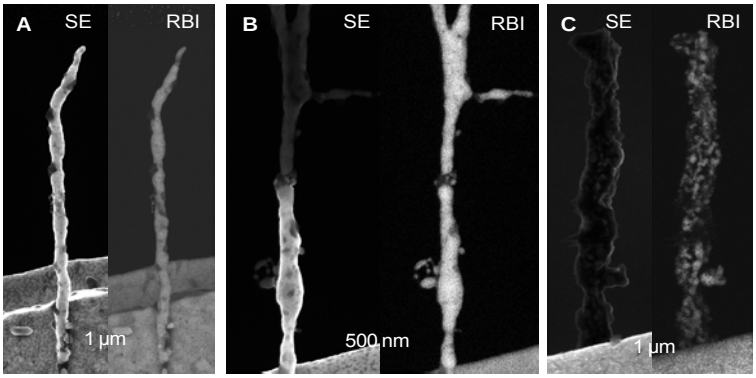

Fig 3: A-C: HIM images of Au nanowires in SE and RBI contrast. SE and RBI images show the same samples. The wire in B contains a slice of carbon (arrow) leading to charging of its upper part. Charging is only visible in the SE, but not in RBI image.

Magnetism of Co on graphene/Pt(111)

Q. Dubout, F. Donati, and H. Brune

Institute of Condensed Matter Physics (ICMP), Station 3, Ecole Polytechnique Fédérale de Lausanne (EPFL), CH-1015 Lausanne, Switzerland
(Corresponding author: H. Brune, e-mail: harald.brune@epfl.ch)

We present low-temperature STM results on the magnetic properties of single Co atoms adsorbed on graphene on Pt(111). The choice of Pt(111) as substrate is motivated by the fact that graphene is particularly weakly bound on this surface compared with other close-packed metal surfaces [1]. Therefore we expect results that are close to Co on free-standing graphene.

The state-of-the-art for Co on graphene is as follows. Co atoms on graphene/SiO_2 grown on Si wafers (crystallographic orientation not specified) showed inelastic STS conductance steps at ±5 meV that were attributed to vibrational excitations [2]. DFT calculations predict for Co on free-standing graphene that the adsorption site on-top of the C_6 ring is by 0.53 eV more stable than the site on-top a C atom [3]. Finally, a giant magnetic anisotropy has been predicted for a Co dimer adsorbed on a C_6 ring [4]; a result that might well be relevant also for Co/graphene.

We have grown graphene on Pt(111) in the ($\sqrt{67}$ x $\sqrt{67}$) moiré structure [5] by ethylene CVD at 1230 K followed by a flash to 1400 K. The expose was adjusted such as to leave clean Pt(111) parts. The Co atoms dosed at 19 K are immobile on the clean Pt parts leading to 99.5 % single atoms and only to 0.5 % dimers at the employed coverages. Therefore the Co coverage can precisely be calibrated by simply counting the density of protrusions in the STM images. Comparing this density with the one on g enables to determine the mean feature size on graphene, which evaluates to single Co adatoms. Co/Pt is further used as spectroscopy reference characterizing the LDOS of the tip and finally we use it as reference in order to detect a possible H contamination that shows up by high intensity inelastic STS conductance steps known from our previous study.

We find four adsorption states, labeled A, B, C, and D. They are clearly distinguished by their apparent height and spectroscopic features. Transformation between the first 3 states can be achieved with tunnel voltage pulses of 150 mV, the last state is obtained for pulses of 250 mV and more, and this transformation is irreversible. Upon H-exposure type A is most abundant and type D entirely disappears. From this, and from comparison with the Co atoms on clean Pt, we conclude that A–C are H-contaminated, and D clean Co.

Spectra recorded at 0.5 K over the clean Co atom reveal a single pair of inelastic conductance steps, which splits into two at finite out-of-plane magnetic fields. Figure 1 shows the raw data as dots together with numerically smoothed data as full curves and their numerical derivative, from which the peak energies marked by arrows, can best be retrieved. Our results yield with the effective spin Hamiltonian [5] an effective spin of $S = 1$, and anisotropy parameter of $D =$

(1.7 ± 0.2) meV, and a Landé factor of $g = 2.19 \pm 0.13$. The magnetic ground state is $m_z = 0$ and the excited states are $m_z = \pm 1$, as represented in Fig. 1c. A finite field lifts the degeneracy of the excited states leading to two conductance steps.

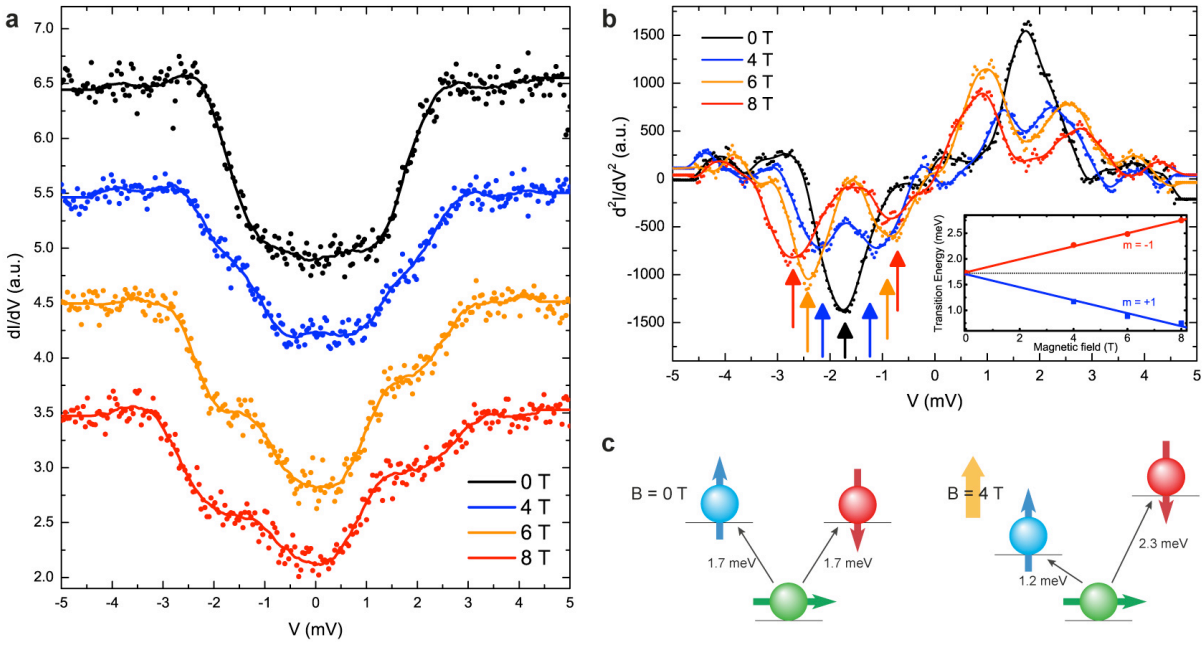

Fig. 1. (a) and (b) show low-T STS of type A versus out-of-plane magnetic field. Spectra obtained on three different adatoms have been averaged. As above, dots are raw data and full lines smoothened data (tip stabilization at -20 mV, 100 pA, 0.45 K, 611 Hz, modulation amplitude $\Delta V = 200\ \mu V$ peak-to-peak, acquisition time 200 s). The arrows show the inelastic peaks splitting with B. The inset shows the position of each inelastic peak obtained from Lorentzian fits as function of B.

We note that *ab-initio* calculations obtain $S = 1/2$ for Co in its most stable adsorption site on free-standing graphene [3]. This corresponds to a Co3*d*9 and therefore Co^{2-} configuration. Charge transfer from graphene to Pt(111) has been reported [5]; this could lead to Co3*d*8 for Co/graphene/Pt which would explain the observed spin.

Support by the Swiss National Science Foundation is gratefully acknowledged.

[1] J. Wintterlin and M. L. Bocquet, Surf. Sci. **603**, 1841 (2009).

[2] V. W. Brar, R. Decker, H. M. Solowan, Y. Wang, L. Maserati, K. T. Chan, H. Lee, Ç. O. Girit, A. Zettl, S. G. Louie, M. L. Cohen and M. F. Crommie, Nat. Phys. **7**, 43 (2011).

[3] T. O. Wehling, A. V. Balatsky, M. I. Katsnelson, A. I. Lichtenstein and A. Rosch, Phys. Rev. B **81**, 115427 (2010).

[4] R. J. Xiao, D. Fritsch, M. D. Kuz'min, K. Koepernik, M. Richter, K. Vietze and G. Seifert, Phys. Rev. B **82**, 205125 (2010).

[5] M. Gao, Y. Pan, L. Huang, H. Hu, L. Z. Zhang, H. M. Guo, S. X. Du and H. J. Gao, Appl. Phys. Lett. **98**, 033101 (2011).

[6] C. F. Hirjibehedin, C. Y. Lin, A. F. Otte, M. Ternes, C. P. Lutz, B. A. Jones and A. J. Heinrich, Science **317**, 1199 (2007).

Femtomagnetism in Gadolinium and Terbium studied by X-ray Spectroscopy

Martin Weinelt
Freie Universität Berlin, Fachbereich Physik, Arnimallee 14, 14195 Berlin, Germany

In current technical implementations changes in the magnetization of ferromagnetic materials are induced thermally, by magnetic fields, or by combining both stimuli. While this conventional switching happens on nanosecond timescales, various magneto-optical experiments demonstrate that the spin system of ferromagnets exhibits a reduced magnetization in less than 1 ps after laser excitation [1]. Unifying concepts have been put forward, but the associated microscopic processes are still notional [2]. On ultrashort timescales the electronic, spin, and lattice subsystems are not in equilibrium. Hot electrons equilibrate with the lattice through electron-phonon scattering in 1-2 ps as described by the two-temperature model [3]. Concerning the spin subsystem the situation is less clear. Direct interaction between electrons and spins, as well as demagnetization upon phonon-mediated spin-flip-scattering of excited carriers have been proposed [2]. The latter mechanism is usually favored, since angular momentum conservation requires that a loss of magnetization is compensated, *e.g.*, via spin-orbit coupling.

Here we address the optical demagnetization of Gadolinium and Terbium, studying their electronic structure by VUV and X-ray spectroscopies. The lanthanides are local ferromagnets with distinct magnetic properties as a function of $4f$ occupation. While the spin quantum number decreases as the $4f$ shell is more than half-filled (Gd $S = 7/2$, Tb $S = 6/2$), the orbital quantum number increases (Gd $L = 0$, Tb $L = 3$). The large localized magnetic moment of the $4f$ shell polarizes the spins of the itinerant $(5d6s)^3$ valence electrons, which in turn align the moments of adjacent atoms in an indirect exchange interaction. Gd and Tb films were optically demagnetized by IR laser pulses with a wavelength of 800 nm, fluences of $1 - 4$ mJ/cm^2, and pulse durations of ≤ 300 fs.

In a first experiment we combined IR pump - synchrotron probe experiments at the MBI-BESSY II beamline of the Helmholtz-Zentrum-Berlin [4]. We studied the magnetic linear dichroism of the Gd $4f^{\uparrow}$ core-level photoemission line as a measure of the film magnetization [5]. Core-level spectra of epitaxial Gd(0001) films on W(110) were recorded at a photon energy of 60 eV for opposite in-plane magnetization directions. Under IR excitation conditions where the lattice temperature reaches the Curie temperature, the magnetization of the Gd film is lowered but remains finite at about 80% of the equilibrium value, *i.e.*, significantly smaller than expected from thermal modeling. Only after 80 ps the recovery of the magnetization follows the cooling of the laser spot and can be well described by the lattice temperature. This deviation of the data from the thermal estimate suggests that equilibrium between the Gd spin-system and lattice is not established before 80 ps have elapsed. In Gd the $4f$ spin-lattice relaxation thus takes much longer than the electron-lattice equilibration [6].

To investigate the subpicosecond timescale of $4f$ demagnetization we used time-resolved X-ray magnetic circular dichroism (XMCD) [7]. Optical pump - X-ray probe experiments were performed at the femtosecond slicing facility of BESSY II [8]. Here we recorded the X-ray transmission of poly-crystalline Gd and Tb films grown in between yttrium buffer layers on a free-standing Al substrate. The X-ray photon energy was tuned to resonantly excite the $3d_{5/2}$ core-level electrons to the unoccupied $4f^{\downarrow}$ states of Gd and Tb. These experiments confirm the slow quasi-equilibrium demagnetization of Gd and establish a timescale of 40 ps for the indirect spin-orbit coupling ($L = 0$). For Tb we identify in contrast a faster time constant of 8 ps suggesting a strong direct spin-lattice coupling ($L = 3$). Moreover, we disentangle for both lanthanides the ultrafast subpicosecond demagnetization process, which is only active while hot electrons are present. It must involve a photo-induced enhancement of the spin-lattice coupling leading to an increase in the momentum transfer rates from magnetization to lattice.

To resolve further details of this ultrafast process we have built a high-order harmonics VUV source and beamline. To create harmonics, 40 fs pulses from a Ti:Sapphire laser amplifier running at 10 kHz repetition rate are focused into an argon-filled gas cell. The VUV photon energy ($h\nu$ = 35 eV) and energy resolution (150 meV) are selected using a toroidal grating monochromator. Since photoelectron spectroscopy probes the magnetic properties on the electrons coherence length of a few lattice constants, it provides a direct microscopic view of magnetic correlations. Therefore we obtain a picture of magnetism complimentary to the dichroism experiments described above. After excitation by an IR pulse, we follow the response of the exchange-split Gd and Tb valence bands. As a signature of ultrafast demagnetization, we see a rapid reduction of the exchange-splitting in the valence band of both metals, with the time constant comparable to the XMCD experiment. This proves that upon laser excitation the magnetic moment is indeed reduced and the sample does not only break into domains. Moreover, we observe significant differences between the responses of the minority and majority bands for Gd in the first picosecond. This ultrafast response is in contrast to quasi-equilibrium thermal demagnetization, and reveals a spin dependence to the exchange coupling between the valence and $4f$ states responsible for magnetic ordering. The ultrafast response of the $4f$ system observed in XMCD is attributed to the direct coupling among the spins of the $5d6s$ valence and $4f$ core electrons. It reflects only the average response of the system. Laser excitation drives the system even out of magnetic equilibrium on the picosecond timescale. We furthermore corroborate that due to its large spin-lattice coupling, the response of Tb to laser excitation is much stronger. On a microscopic level the coupling of $4f$ spins and hot lattice establishes in Tb a quasi-equilibrium of electron, lattice, and spin subsystems on the time scale of electron cooling.

Acknowledgement

It is a pleasure to thank all the coworkers who contributed to this work. Dichroism in $4f$ photoemission was studied in collaboration with the group of U. Bovensiepen [5]. This work was carried on with the XMCD measurements, which were accomplished together with the femtoslicing research team of BESSY II [7]. The high-order harmonics beamline was established at the Max Born Institute (MBI) by R. Carley, C. Döbrich, B. Frietsch, C. Gahl, and M. Teichmann in collaboration with O. Scharzkopf and P. Wernet from the Helmholtz-Zentrum-Berlin. The MBI group performed the HHG experiments.

References

[1] E. Beaurepaire, J.-C. Merle, A. Daunois, and J.-Y. Bigot, Phys. Rev. Lett. **76**, 4250 (1996); J. Hohlfeld, E. Matthias, R. Knorren, and K. H. Bennemann, Phys. Rev. Lett. **78**, 4861 (1997); L. Guidoni, E. Beaurepaire, and J.-Y. Bigot, Phys. Rev. Lett. **89**, 017401 (2002); B. Koopmans, M. van Kampen, and W. J. M. Jonge, J. Phys.: Condens. Matter **15**, S723 (2003); C. D. Stanciu *et al.*, Phys. Rev. Lett. **99**, 047601 (2007); I. Radu, *et al.*, Nature **472**, 205 (2011).

[2] B. Koopmans, J. J. M. Ruigrok, F. D. Longa, and W. J. M. de Jonge, Phys. Rev. Lett. **95**, 267207 (2005); M. Cinchetti, *et al.*, Phys. Rev. Lett. **97**, 177201 (2006); B. Koopmans *et al.*, Nature Materials **9**, 259 (2010); M. Battiato, K. Carva, and P. M. Oppeneer, Phys. Rev. Lett. **105**, 027203 (2010).

[3] S. I. Anisimov, B. L. Kapeliovich, and T. L. Perel'man, Sov. Phys. JETP **39**, 375 (1974); U. Bovensiepen, J. Phys.: Cond. Matter **19**, 083201 (2007).

[4] T. Gießel, D. Bröcker, P. Schmidt, and W. Widdra, Rev. Sci. Instrum. **74**, 4620 (2003).

[5] A. Melnikov, H. Prima-Garcia, M. Lisowski, T. Gießel, R. Weber, R. Schmidt, C. Gahl, U. Bovensiepen, and M. Weinelt, Phys. Rev. Lett. **100**, 107202 (2008).

[6] A. Vaterlaus, T. Beutler, and F. Meier, Phys. Rev. Lett. **67**, 3314 (1991); W. Hübner and K. H. Bennemann, Phys. Rev. B **53**, 3422 (1996).

[7] M. Wietstruk, A. Melnikov, C. Stamm, T. Kachel, N. Pontius, M. Sultan, C. Gahl, M. Weinelt, H. A. Dürr, and U. Bovensiepen, Phys. Rev. Lett. **106**, 127401 (2011).

[8] C. Stamm *et al.*, Nature Materials **6**, 740 (2007).

Magnetism in small mass selected Clusters

S. Peredkov[1], M. Neeb[2], J. Meyer[3], M. Tombers[3], H. Kampschulte[3], G. Niedner-Schatteburg[3], and W. Eberhardt[1]

[1]*Technische Universität Berlin, Institut für Optik und Atomare Physik, Str. d. 17 Juni 135, 10623 Berlin, Germany*
[2]*Helmholtz-Zentrum Berlin für Materialien und Energie, BESSY II, Albert-Einstein-Str. 15, 12489 Berlin, Germany*
[3]*Fachbereich Chemie und Forschungszentrum OPTIMAS, TU Kaiserslautern, 67663 Kaiserslautern, Germany*

Most atoms are magnetic, since according to Hundt's rule the highets spin configuration corresponds to the lowest energy state. As solids, on the other hand, only a few transition metals and rare earths exhibit stable magnetic phases. Electron delocalization is largely responsible for quenching the orbital moment and even if there is a net spin configuration at individual atoms, with the absence of orbital magnetisation these spin moments are not aligned. Thus macroscopically magnetic order is not observed. An intriguing question remains how this development from the atom to the solid manifiests itself for small clusters containing only a few atoms. Clusters are ideal test objects, since the exact size, i.e. the number of atoms, can be readily determined by mass spectroscopy. Atomic magnetic moments larger than in the solid state should be expected, however the question is open whether these are aligned within the particle. If thermal fluctuations are too strong, alignment still may be introduced by an external magnetic field. This has also important technological implications, since small metallic particles are the basis of magnetic recording materials. With ever increasing storage densities, these particles become smaller and smaller and there is a question about the fundamental limits of this technology.

Total magnetic moments of mass selected clusters have been determined earlier by observing the deflection in a Stern Gerlach experiment [1-3]. This however does not allow to deduce the orbital and spin moments. Magnetic circular dichroism, at the L-edge of transition metals is a very well established probe which has been extensively used in the determination of the spin and orbital element specific moments in materials. We have applied this spectroscopic technique to determine the individual spin- and orbital moments of mass selected Co clusters stored in a magnetic trap installed at the BESSY-II storage ring in Berlin. The temperature of the clusters could be adjusted by collisional cooling in He buffer gas at a specified temperature. The experiment setup has been described in more detail in [4].

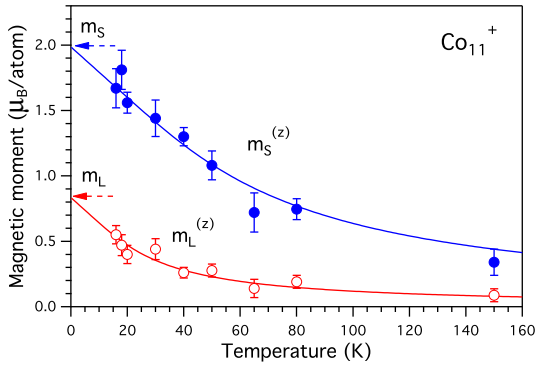

Fig. 1 displays the orbital and spin moment of an intermediate size cluster, Co_{11}^+, as a function of temperature. The values were obtained from the XMCD signal using the well established sum rules [5]. Since the particles are rotating freely in space, in this analysis it is assumed that the T_z term averages out to a value close to 0. The solid lines are the result of a Langevin fit using

Fig. 1 Orbital and spin moments of Co_{11}^+ as a function of temperature

the 7T magnetic field and the temperature as parameters. The zero temperature extrapolated values for m_S and m_L are larger than in the solid phase, whereby the orbital moment m_L (m_{Lsolid} = 0.15μ_B) is enhanced much more than the spin moment m_S (m_{Ssolid} = 1.65 μ_B). Moreover upon closer inspection of the Langevin fits it becomes obvious, that the two components exhibit a different temparature behavior. This indicates that the spin orbit coupling is at least partially lifted by the 7T field of the ion trap and both moments are fluctuating independent of each other. Such a behavior was postulated by M. Knickelbein earlier [6].

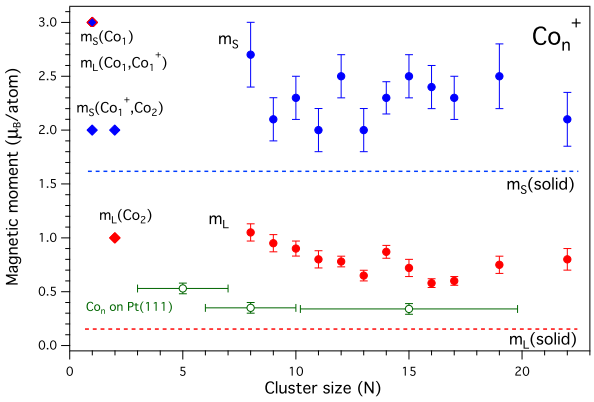

Fig. 2 Spin and orbital moments of small clusters

The spin and orbital moments of all clusters measured here are shown in Fig. 2. The spin moment exhibits an even–odd oscillation up to cluster sizes less than 13 atoms. For the positively charged clusters it can be expected that the even numbered clusters, which have an odd number of s-electrons exhibit a larger spin total moment. A similar even-odd oscillation was also observed in earlier photoemission spectra of Ni clusters [7]. For larger clusters the geometry causes stronger modifications of the electronic structure, such that a simple electron counting scheme, which is at the heart of such even-odd oscillations, is not applicable anymore.

The absolute values of the moments reported here are substantially larger than the values given in earlier publications [1-3] We attribute this to the more extensive analysis including temperature variation and especially the capability to separate the spin and orbital moments by the XMCD technique. A slight trend of a reduction with size towards the bulk values might be noted for the orbital moments, but in general in this size range the magnetism of the particles is determined individually for each cluster by its geometry and electronic properties.

This work was supported by the DFG through a large equipment grant. A more extended version, including a detailed discussion of the data analysis has been published recently[8].

[1] M. L. Billas, A. Chatelain, and W. A. de Heer, Science **265**, 1682 (1994)
[2] S. E. Apsel, J. W. Emmert, J. Deng, and L. A. Bloomfield, Phys. Rev. Lett. **76**, 1441 (1996).
[3] M. B. Knickelbein, J. Chem. Phys **125**, 044308 (2006).
[4] S. Peredkov, A. Savci, S. Peters, M. Neeb, W. Eberhardt, H. Kampschulte, J. Meyer, M. Tombers, B. Hofferberth, F. Menges, and G. Niedner-Schatteburg, J. Electron Spectrosc. and Relat. Phenom. **184**, 113 (2011)
[5] C.T. Chen, Y. Idzerda, H.J. Lin, N.V. Smith, G. Meigs, E. Chaban, E. Ho, G. Pellegrin, F. Sette, Phys. Rev. Lett. **75**, 152 (1995)
[6] M. B. Knickelbein, J. Chem. Phys **121**, 5281 (2004)
[7] G. Ganteför, W. Eberhardt, Phys. Rev. Lett **76**, 4975 (1996)
[8] S. Peredkov, M. Neeb, J. Meyer, M. Tombers, H. Kampschulte, G. Niedner-Schatteburg, W. Eberhardt, Phys. Rev. Lett **107**, 233401(2011)

Structure, morphology and magnetic properties of ultrathin Mn germanide films on Ge(111)

J. Hirvonen Grytzelius, H. M. Zhang, and L. S. O. Johansson

Department of Physics, Karlstad University, SE-65188, Karlstad, Sweden
(corresponding author: L. Johansson, e-mail: lars.johansson@kau.se)

The interest in transition metal layers on semiconductors has increased over the last years. One reason is the possibility to combine semiconducting and magnetic properties. Introducing the spin degree of freedom to the standard charge based electronics would lead to great improvements in e.g. data storage and memory handling [1]. To achieve this, it is of great interest to understand the fundamental properties of those materials that are candidates for this new technology.

We have recently investigated the surface electronic of Mn_5Ge_3 on Ge(111) by angle resolved photoemission, and scanning tunnelling microscopy and spectroscopy (STM/STS) [2]. In the present work, we continue our studies of thin manganese germanide films grown on Ge(111) by investigating morphology, structure and magnetic properties. The Mn germanide films were formed by solid phase epitaxy, and were investigated by low energy electron diffraction (LEED), high-resolution photoelectron core-level spectroscopy (CLS), X-ray magnetic circular dichroism (XMCD) and STM. The CLS and XMCD studies were performed at MAX-lab, Lund, Sweden. The manganese depositions were done with various substrate coverages from 3 to 32 monolayers (ML). After each deposition the samples were annealed at 260° C and 330° C for 20 min. The core-level spectra and STM images were recorded from the above surfaces. XMCD measurements were done with Mn coverages of 8, 16 and 32 ML .

Ge 3*d* spectra were recorded with various photon energies and different emission angles, in order to vary the surface sensitivity. The Ge 3*d* spectra could be decomposed into several components, identified as originating from the Ge bulk and from the Mn germanide. The germanide surfaces displayed a simple $\sqrt{3}\times\sqrt{3}$ LEED pattern or triple split $\sqrt{3}\times\sqrt{3}$ LEED spots depending on the annealing temperatures. As shown in Ref. 3, the $\sqrt{3}\times\sqrt{3}$ LEED pattern formed after annealing of as-deposited Mn films above 300° C is associated with the formation of the ordered Mn_5Ge_3 phase. The STM images recorded from the Mn germanide surfaces mostly show a honeycomb pattern but a hexagonal pattern was also observed. These patterns are explained as arising from Mn atoms in the top layer, and Mn and Ge atoms in the sublayer arranged in triangular structures, respectively. An XMCD signal was measured already at coverage of 8 ML. An example of the XMCD data at a coverage of 16 ML is given below in Fig. 1. Based on these results, the atomic and electronic structure, and magnetic properties of ultrathin manganese germanide films will be discussed.

This work was supported by the Swedish Research Council.

[1] S. A. Wolf, D. D. Awschalom, R. A Buhrman, J. M. Daughton, S. von Molnar, M. L. Roukes, A. Y. Chtchelkanova and D. M. Treger, Science **294**, 1488 (2001).

[2] J. Hirvonen Grytzelius, H. M. Zhang, and L. S. O. Johansson, Phys. Rev. B **84**, 195306 (2011).

[3] C. Zeng *et al.*, Appl. Phys. Lett. **83**, 24 (2003); C. Zeng *et al.*, Phys. Rev. B **70**, 205340 (2004).

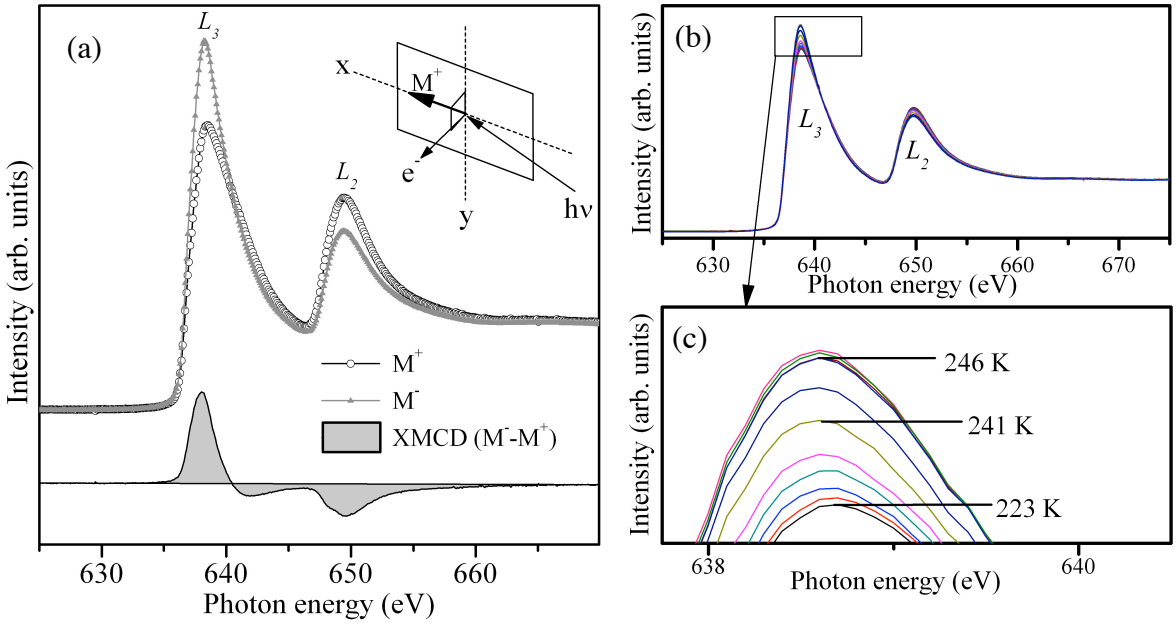

Figure 1. (a) XMCD spectrum measured at the L_2 and L_3 absorption edges of the MnGe(111) film at 100 K. (b) XAS spectra recorded at different sample temperature. (c) Close up image of the L_3 absorption edge.

The in-plane XMCD spectra were obtained by recording two XAS (x-ray absorption spectroscopy) spectra at liquid nitrogen temperature, with opposite surface magnetization. Before recording each spectrum, the sample was magnetized with a magnetic field pulse of 250 Gauss in the horizontal plane along the positive and negative x-directions, respectively (M^+ and M^-, see inset in fig. 1(a)). The L-edge XAS spectrum was measuring with 70% circularly polarized light at an incidence angle of 75° in the positive x-direction. The intensity of the XMCD signal of the L_2 and L_3 absorption edges is shown as the difference between the XAS spectra recorded with opposite magnetization (M^+ and M^-), as seen in figure 1(a). The Curie temperatur (T_C) was found by following the L_3 absorption edge in the M^+ XAS spectra during sample warm up, figure 1(b) and 1(c). T_C was estimated to 246 K which is 50 K lower than that found in thicker Mn germanide films.

Ambipolar doping and formation of p-n junctions in quasi-free epitaxial graphene on SiC(0001) controlled by Ge intercalation

U. Starke, K.V. Emtsev, A.A. Zakharov[1], C. Coletti[*], and S. Forti

Max-Planck-Institut für Festkörperforschung, Heisenbergstr. 1, D-70569 Stuttgart, Germany (corresponding author: U. Starke, u.starke@fkf.mpg.de)

[1]MAX-lab, Lund University, Lund, S-22100, Sweden

[*]present address: Center for Nanotechnology Innovation @NEST, Istituto Italiano di Tecnologia, Piazza San Silvestro 12, 56127 Pisa, Italy

Large scale epitaxial graphene (EG) grown on SiC single crystal wafers promises to be a suitable candidate for carbon based electronics [1]. However, the electronic and structural properties of EG are influenced by the SiC substrate. Notably, they can be manipulated on an atomic scale, e.g. by hydrogen to passivate interface states [2]. Here, we use Ge intercalation to modify the carrier concentration in epitaxial graphene on a lateral scale down to 100 nm [3]. The electronic structure is analyzed using angle-resolved photoemission spectroscopy (ARPES). The spatial formation of graphene layers and areas of different doping was studied *in situ* by low energy electron microscopy (LEEM) and photoelectron microscopy (PEEM).

The $(6\sqrt{3}\times6\sqrt{3})R30°$-reconstructed first carbon layer on SiC(0001) has graphene-like topology and bond lengths, however, with strong covalent bonds to the SiC substrate [4] and thus exhibits no π-bands, cf. Fig. 1(a). It can be turned into quasi-free standing monolayer graphene by intercalating an atomically thin germanium film. The interface bonds are broken upon in-diffusion of Ge atoms so that the C-layer is structurally decoupled from the SiC surface. This leads to a complete recovery of the electronic structure of graphene, as shown in Fig. 1(b). Depending on the annealing temperature moderate *p*- or *n*-doping can be achieved, as shown in Fig. 1(b and d) by the shift of the Dirac point with respect to the Fermi energy. Interestingly, an intermediate stage shown in Fig 1(c) is characterized by the coexistence of both doping regions, i.e., at this stage the surface splits into lateral graphene *p*-*n* junctions.

In Fig. 2(a) we show the LEEM micrograph of the initial quasi-free standing graphene layer (*p*-phase, see Fig. 1(b)) obtained after intercalation of germanium. The graphene layer is quite homogeneous and covers the entire surface. Graphene domains are determined by the size of the SiC substrate terraces, that is, of the order of 3-5 μm in width. Initial and later stages of the *n*-doped graphene phase formation are presented in Fig. 2(b) and in Fig. 3, respectively. The corresponding PEEM image in Fig. 3(b) reveals a significant contrast in intensity of the Ge 3d core level signal for the two graphene phases. Contrast in PEEM is determined by the concentration of Ge atoms located beneath the epitaxial graphene layer and coincides with the contrast obtained in LEEM. Apparently, the *n*-phase is induced upon a partial desorption of germanium from under the surface, i.e. partial de-intercalation. Surprisingly, the process is not initiated at the step edges but rather on the terraces (see Fig. 2(b)). This leads to the formation

of *n*-doped induced graphene islands with the size as small as 100 nm embedded into the *p*-doped graphene sheet. With further annealing the islands grow in size and coalesce forming extended *n*-doped graphene areas.

Acknowledgements: C.C. acknowledges the Alexander von Humboldt Foundation for financial support. This research was partially funded by the European Community's Seventh Framework Programme (FP7/2007-2013) under grant agreement no. 226716. We are indebted to the staff at MAX-Lab (Lund, Sweden) and SLS (Villigen, Switzerland) for their advice and support.

[1] K.V. Emtsev, A. Bostwick, K. Horn, et al. Nature Materials **8**, 203-207 (2009).

[2] C. Riedl, C. Coletti, T. Iwasaki, et al. Phys. Rev. Lett. **103**, 246804 (2009).

[3] K.V. Emtsev, A.A. Zakharov, C. Coletti, S. Forti, and U. Starke, Phys. Rev. B **84**, 125423 (2011),

[4] K.V. Emtsev, F. Speck, Th. Seyller, L. Ley, and J.D. Riley, Phys. Rev. B **77**, 155303 (2008).

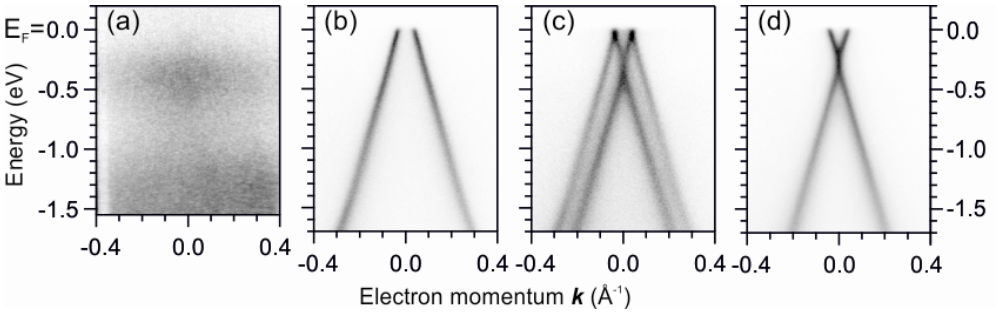

Fig. 1. Photoemission valence band maps (energy *vs* electron momentum) in the vicinity of the K-point (***k***=0) of the graphene Brillouin zone taken from: (a) the (6√3×6√3)R30° surface and after deposition of 5 ML of Ge followed by vacuum annealing at (b) T=720°C, (c) 820°C, and (d) 920°C. The photon energy was 90 eV.

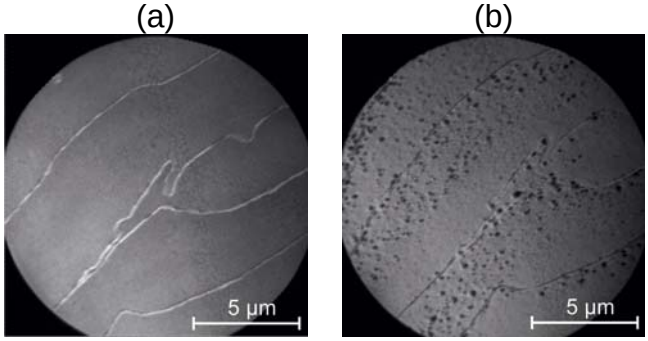

Fig. 2. LEEM micrographs of the quasi-free standing graphene layer obtained by intercalation of Ge atoms at the interface with SiC(0001) surface: (a) homogeneous p-doped graphene phase, and (b) initial stage of the graphene p-n junction formation. Dark inclusions in (b) correspond to the n-doped graphene islands embedded into the p-doped graphene.

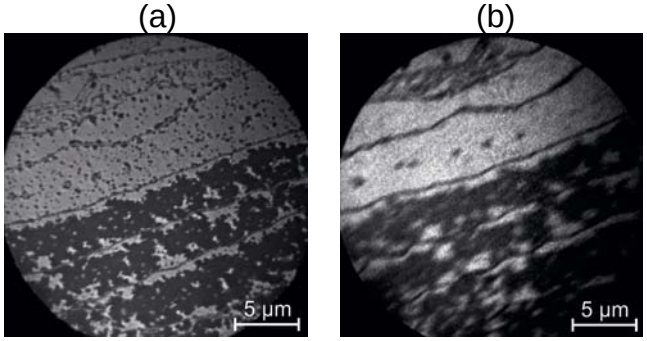

Fig. 3. (a) - LEEM micrograph and (b) - PEEM Ge3d intensity map of the graphene *p-n* coexistence stage (see also Fig. 1(c)). Bright (*dark*) regions in (a) correspond to p-doped (*n-doped*) quasi-free standing graphene regions.

Stability of graphene and graphene supported clusters in a gas atmosphere

J. Knudsen[1], E. Grånäs[1], T. Gerber[2], P. J. Feibelman[3], U. Schröder[2], M. A. Arman[1], P. Stratmann[2], K. Schulte[4], T. Michely[2], and J. N. Andersen[1, 4]

Division of Synchrotron Radiation Research, Lund University, Box 118, SE-221 00, Sweden (corresponding author: J. Knudsen, e-mail: jan.knudsen@sljus.lu.se)

[1] *Division of Synchrotron Radiation Research, Lund University, Box 118, SE-221 00, Sweden*

[2] II. Physikalisches Institut, Universität zu Köln, 50937 Köln, Germany

[3] *Sandia National Laboratories, Albuquerque, New Mexico 87185-1415, USA*

[4] *MAX IV Laboratory, Lund University, Box 118, 22 100 Lund, Sweden*

Graphene is an attractive support material for catalytic model systems since it is chemically inert at room temperature and has a high thermal stability in ultra-high vacuum (UHV). Furthermore, arrays of nanoparticles with an extremely narrow size distribution can be grown on graphene [1,2]. Such uniform nanoparticles are excellent model systems for systematic studies of gas adsorption and reactivity on nanoparticles. As real reactivity measurements require both elevated temperatures and gas exposure it is essential to test the stability of both the clusters and graphene at these conditions.

In this contribution we will discuss the stability of small Pt-clusters supported by graphene/Ir(111) in O_2 and CO. Further, we will discuss the stability of graphene without particles in the same gases in the entire pressure interval from $1 \cdot 10^{-9}$ mbar to ~1 mbar.

As a starting point we considered how Pt-clusters binds to graphene grown on Ir(111). For pristine graphene without particles we find a linear correlation between C-atom height and the C 1s binding energy in a graphene adlayer on Ir(111). Upon Pt-cluster adsorption the graphene film is pinned to the Ir(111) surface, as the C-atoms below the clusters rehybridize from the sp^2 bonding characteristic of graphene to diamondlike sp^3. The sp^3 hybridized carbon atoms then bind with their fourth bond normal to the average carbon plane alternately to substrate Ir atoms directly below or metal atoms directly above. Due to the pinning and an increased height modulation a broad C 1s shoulder develops at the high binding energy side. Comparing our measured high resolution X-ray photoemission spectra with density functional theory we show that this shoulder should be assigned to C atoms both under and in the vicinity of the Pt-clusters [3].

Room temperature CO or O_2 adsorption leads to a reduced Pt-induced C 1s shoulder and we interpret this as a weakened bonding of the Pt-clusters. Further, support for this interpretation comes from STM movies that show cluster diffusion and coalescence upon CO exposure for small clusters with an average size below 10 atoms. To prevent cluster coalescence in the early stages of cluster growth and to obtain the most regular Pt-cluster superlattices the CO/O_2 partial pressure during Pt deposition should be minimal. Otherwise adsorbed CO/O causes unpinning and subsequent coalescence of small intermediate clusters already during growth.

Following our discussion of Pt-clusters on graphene we continue with considering the stability of graphene itself in O_2 and CO. In contrast to atomic oxygen that forms oxygen species on top of graphene [4, 5] we find that exposure to molecular oxygen exclusively leads to intercalated oxygen species formed below the film. Upon oxygen saturation we unambiguously assign the intercalated oxygen phase to a p(2×1)-O structure similar to the one observed clean Ir(111). Further, we reveal that holes in the graphene film are essential for oxygen intercalation and facilitate complete intercalation already at 400 K. The oxygen intercalation is reflected as a C 1s CLS of -0.5 eV and we explain this by the decoupling of the graphene layer from the surface. Using STM, we observe that Pt-particles grow very different on the O-intercalated phase as compared to pristine graphene. This observation is consistent a mechanism, where sp^2 to sp^3 re-hybridization is responsible for the binding of the Pt-clusters, since the re-hybridization is impossible on the O-intercalated and decoupled graphene.

Finally, we consider the stability of graphene in CO. Using a combination of high pressure XPS taken in-situ and STM images of pre-exposed samples we reveal that CO intercalation is possible already at room temperature, but only if pressures close to 1 mbar are used.

Altogether, our studies show that Ir(111) supported graphene and particles supported by graphene are dynamic systems, that quickly responds to gas dosing. For Pt-particles supported by graphene we show that CO and O_2 exposure often result in cluster diffusion and coalescence. Even clean graphene films without particles are unstable in CO and O_2, since both molecules can intercalate the film. For oxygen we find that small holes in the film and temperatures above ~350 K are essential for intercalation. CO intercalation is observed already at room temperature but only at pressures close to 1 mbar.

[1] A.T. N'Diaye et al., Phys. Rev. Lett. 97, 215501 (2006)
[2] A.T. N'Diaye et al., New J. Phys. 11, 103045 (2009)
[3] J. Knudsen et al., Phys. Rev. B. Accepted
[4] N. A. Vinogradov et al., J. Phys. Chem. C, 115, 9568 (2011)
[5] R. Larciprete et al., JACS, 133, 17315 (2011)

Beat the heat: Watching phonons cool down during O_2 dissociation on Pd(100)

Jörg Meyer and Karsten Reuter

Lehrstuhl für Theoretische Chemie, Technische Universität München,
Lichtenbergstr. 4, D-85747 Garching, Germany
(corresponding author: K. Reuter, e-mail: karsten.reuter@ch.tum.de)

Energy conversion at interfaces is at the center of the rapidly growing field of basic energy science. This concerns not only desired conversions, such as from solar to chemical energy, but also unavoidable by-products, such as the dissipation of chemical energy into heat. An atomistic understanding of the elementary processes involved is in all cases only just emerging but is likely to question established views and macro-scale concepts. With respect to the dissipation of heat freed during exothermic surface chemical reactions, the prevailing view is that of a rapid equilibration, with the local heat bath provided by the solid surface. The view is nurtured by the rare event dynamics resulting from the typically sizably activated nature of surface chemical processes: while the actual elementary processes take place on a picosecond time scale, times between such rare events are orders of magnitude longer. The understanding is then that in these long inter-process time spans, any released chemical energy is rapidly distributed over a sufficiently large number of surface phononic degrees of freedom to warrant a description in terms of a mere heat bath with defined local temperature. At the atomic scale, this equilibration with the surface heat bath leads to an efficient loss of memory of the adsorbates about their history on the solid surface between subsequent rare events. This motivates the description in terms of a Markovian state dynamics that is, e.g., underlying all present-day microkinetic formulations in heterogeneous catalysis [1-3]. In turn, the freed reaction energy only enters the determination of the local heat bath temperature, commonly achieved through a continuum heat-balancing equation [4-5].

Aiming to scrutinize this view through first-principles multiscale modeling we develop a novel QM/Me approach that extends the power of embedding techniques to metallic systems. A huge atomistically described bath can thus be included in *ab initio* molecular dynamics (AIMD) simulations of chemical reactions at model catalyst surfaces. This allows to quantitatively account for the heat dissipation into the phononic system without being riddled by spurious phonon reflections as in conventional supercell AIMD simulations, while simultaneously maintaining the correct description of the metallic band structure of the extended surface. We apply our scheme to the O_2 dissociation at Pd(100) as a representative showcase system, where around 2.6 eV (!) are released during the exothermic surface reaction. With the competing dissipation channel in form of electron-hole pair excitations only taking up a negligible share of this energy [6], we quantify the dissipation into the

phononic system through a projection scheme that allows to explicitly follow the excitation of individual modes during the adsorption dynamics.

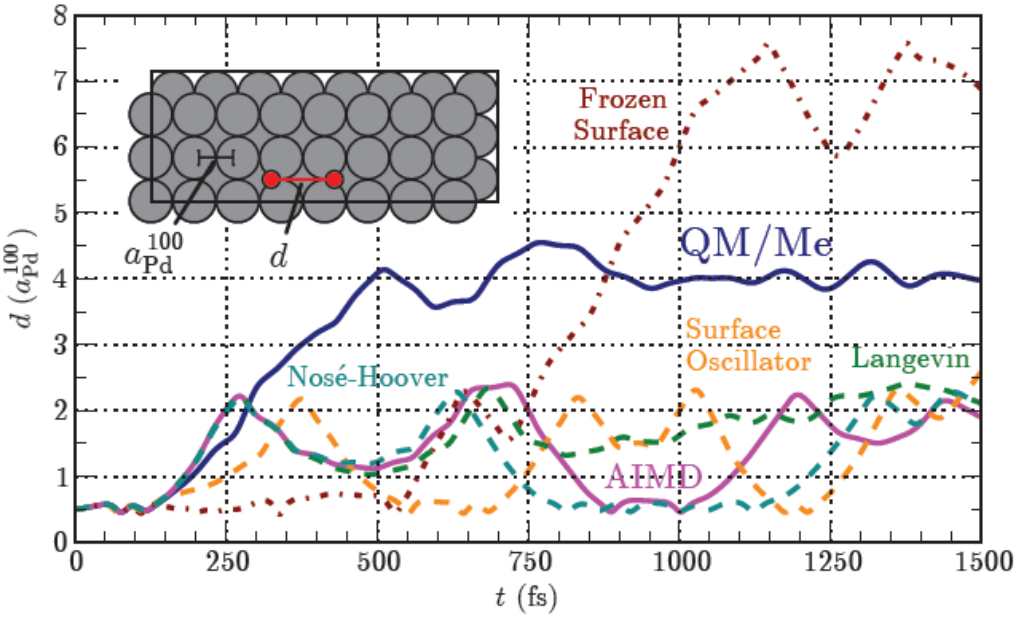

Fig. 1: Time evolution of the separation distance of the oxygen atoms on the Pd(100) surface after O_2 dissociation as resulting from prevalent energy sink models and QM/Me.

For the first time we can thus unravel the detailed role of e.g. surface phonons in the dissociation process or check on the validity of commonly employed approximations like the harmonic solid underlying state-of-the-art generalized Langevin equation treatments. Not surprisingly, the new first-principles perspective questions some established views, with the obtained hot adatom motion, cf. Fig. 1, prominently challenging prevalent Markov-based microkinetic formulations.

[1] J. Dumesic, D. Rudd and L. Aparicio, *The Microkinetics of Heterogeneous Catalysis*, Washington D.C., American Chemical Society (1993)

[2] I. Chorkendorff and H. Niemantsverdriet, *Concepts of Modern Catalysis and Kinetics*, Weinheim, Wiley (2003)

[3] K. Reuter, First-Principles Kinetic Monte Carlo Simulations for Heterogeneous Catalysis: Concepts, Status and Frontiers, in *Modeling Heterogeneous Catalytic Reactions: From the Molecular Process to the Technical System*, Ed. O. Deutschmann, Weinheim, Wiley (2011)

[4] O. Deutschmann, Computational Fluid Dynamics Simulations of Catalytic Reactors, in Handbook of Heterogeneous Catalysis, Ed. G. Ertl, H. Knözinger, F. Schüth, J. Weinkamp, 2nd edn, Weinheim, Wiley (2008)

[5] S. Matera and K. Reuter, Catal. Lett. 133, 156 (2009); Phys. Rev. B 82, 085446 (2010)

[6] J. Meyer and K. Reuter, New. J. Phys. 13, 085010 (2011)

A detailed investigation of the active phase of palladium during methane oxidation

A. Hellman[1], A. Resta[2], N. M. Martin[3], J. Gustafson[3],
A. Trinchero[1], P. –A. Carlsson[1], O. Balmes[2], R. Felici[2], R. van Rijn[2,4],
J. W. M. Frenken[4], J. N. Andersen[3], E. Lundgren[3], and H. Grönbeck[1]

[1] *Department of Applied Physics and Competence Centre for Catalysis, Chalmers University of Technology, SE- 41296, Göteborg, Sweden*
(corresponding author: A. Hellman, e-mail: ahell@chalmers.se)

[2] *ESRF, 6 rue Jules Horowitz – 38000 Grenoble, France*

[3] *Division of Synchrotron Radiation Research, Lund University, Box 118, SE-22100, Lund, Sweden*

[4] *Kamerlingh Onnes Laboratory, Leiden University, P.O. Box 9504, 2300 RA Leiden, The Netherlands*

Determining the active phase of a heterogeneous catalyst during operating conditions is a well-recognized challenge. This, in particular, applies for structurally ill-defined catalysts that are realized as metal particles dispersed on a porous oxide. One example is the active phase of palladium during complete methane (CH_4) oxidation to water and carbon dioxide. This important reaction has recently regained interest because of the usage of bio- and natural gas as fuels in automotive applications. Methane is the main component in such fuels and there is currently a pressing need for catalysts with enhanced low temperature activity. The high activity measured for catalysts based on supported palladium has previously been attributed to different Pd/PdOx phases [1], such as, reduced (metallic) palladium, metal supported surface oxides and bulk metal oxide.

Here, the active phase of Pd during methane oxidation is investigated by density functional theory calculations in combination with *in situ* surface x-ray diffraction measurements. Low activation energies for methane dissociation are calculated for either under-coordinated Pd sites in PdO or metallic surfaces. The results are in full agreement with the experiments.

Density functional theory calculations [2,3,4] are performed to investigate relevant reaction barriers and stability of intermediates for a large set of palladium and palladium oxide surfaces. In addition, a first-principles based micro-kinetic model is constructed to calculate turnover frequencies for methane oxidation and coverages of surface species. The methodology enables comparisons between calculations and measurements both for methane conversion into CO_2 and H_2O and the state of the surface as measured by *in situ* surface x-ray diffraction.

The rate determining step (RDS) in CH_4 oxidation is generally assumed to be the removal of the first H atom, whereupon adsorbed CH_3 and H are formed. The present work support this view, and the dissociate adsorption of methane can be used as a measure of the catalytic activity. The present results show that a low barrier for methane dissociation is obtained either on under-coordinated Pd-sites in PdO or on metallic Pd. The atomistic rational behind the high activity of metallic sites is their ability to polarize methane during the dissociation. On the other hand, the high activity of the PdO(101) surface is an intrinsic balance between the electronic structure and the geometrical structure of the under-coordinated Pd site. The difference is analyzed and found to be an interesting consequence of the detailed electronic structure.

The experiments consider Pd(100) for which an oxide film is formed during oxidizing conditions. A high CH_4 conversion is observed in the presence of a thick epitaxial [PdO(101)] film supported on the metal surface or when the temperature is high enough to decompose the oxide.

To conclude, the active site for methane dissociation of Pd has been determined by density functional theory calculations in combination with *in situ* surface x-ray diffraction. The results may be used for design of catalysts with enhanced low temperature activity.

This work is supported by the Swedish Foundation for Strategic Research and the Swedish Research Council. Computational resources were provided by SNIC.

[1] Burch R., Loader P.K., and Urbano F.J., Catalysis Today 27 (1996) 243.

[2] Mortensen J.J., Hansen L.B., and K.W. Jacobsen K.W., Phys. Rev. B 71 (2005) 035109.

[3] Blöchl P., Phys. Rev. B, 50 (1994) 17953.

[4] Perdew, J.P., Burke K., Ernzerhof M., Phys. Rev. Lett. 77 (1996) 3865.

Oxidation and reduction of single crystal Pd-based alloy surfaces – the case of $Pd_{75}Ag_{25}(100)$

V. Fernandes[1], L. E. Walle[1], S. Blomberg[2], M. H. Farstad[1], H. Grönbeck[3], J. Gustafson[2], J.N. Andersen[2], E. Lundgren[2] and A. Borg[1]

[1] *Dept. of Physics, Norwegian University of Science and Technology, 7491 Trondheim, Norway (corresponding author: A. Borg, e-mail: anne.borg@ntnu.no)*

[2] *Div. of Synchrotron Radiation Research, Institute of Physics, Lund University, Sweden*

[3] *Competence Centre for Catalysis and Dept. of Applied Physics, Chalmers University of Technology, Gothenburg, Sweden*

Palladium exhibits high selectivity and permeability for hydrogen and is thus a suited material for hydrogen separation membranes. Furthermore Pd is a versatile catalyst among others for hydrogenation and dehydrogenation reactions. Upon exposure to hydrogen pure palladium is susceptible to embrittlement due to the formation of hydride phases and poisoning [1-3]. To overcome such limitations alloys are commonly applied. Alloying with 23wt% silver has shown to improve permeability and durability of Pd-based membranes while maintaining high selectivity [4,5]. Recent studies indicate that surface oxides formed on Pd and PdAg alloys may improve the catalytic activity and the membrane resistance to poisons [6]. The underlying mechanism for this behaviour is still poorly understood.

In the present work, we have investigated oxidation and reduction of the $Pd_{75}Ag_{25}(100)$ surface as model system for PdAg membrane surfaces. The observed behaviour is compared to that of Pd(100). We have applied high-resolution photoemission spectroscopy measurements performed at beam line I311 of the MAX-lab synchrotron facility in Lund, Sweden, in combination with density function theory (DFT) calculations. The $Pd_{75}Ag_{25}(100)$ alloy surface is found to be silver terminated after the cleaning procedure consisting of Ar ion sputtering followed by annealing to about 900K, in agreement with observations by Wouda et al. [7]. Unlike Pd(100), which has a surface core level shift to lower binding energies compared to the Pd 3d bulk contribution, clean $Pd_{75}Ag_{25}(100)$ displays a contribution to higher binding energy. The DFT results reveal that this shift originates from Pd atoms in the surface region embedded in the silver rich surface.

Before onset of bulk oxide formation a $(\sqrt{5}\times\sqrt{5})R27°$ surface oxide is formed on Pd(100) [8,9]. By low energy electron diffraction (LEED) experiments we observe a similar, but less pronounced, oxide structure on $Pd_{75}Ag_{25}(100)$. The LEED images for the $(\sqrt{5}\times\sqrt{5})R27°$ structure on Pd(100) and $Pd_{75}Ag_{25}(100)$ surfaces are shown in Fig. 1 along with the corresponding Pd $3d_{5/2}$ core level spectra. These photoemission results show significant similarities supporting that a Pd-oxide is also formed on the alloy surface. Observed differences in the spectra can be understood from an Ag interface layer being formed between the surface oxide and the bulk alloy.

The reduction behaviour of the $(\sqrt{5}\times\sqrt{5})R27°$ surface oxides due to CO and H_2 exposure was monitored *in situ* by photoemission spectroscopy, illustrated in Fig. 2 for the case of CO

exposure at $5x10^{-8}$mbar and temperature 120°C. The reduction rates were found to be significantly slower in the case of $Pd_{75}Ag_{25}(100)$ compared to Pd(100). The origin of this behaviour will be discussed.

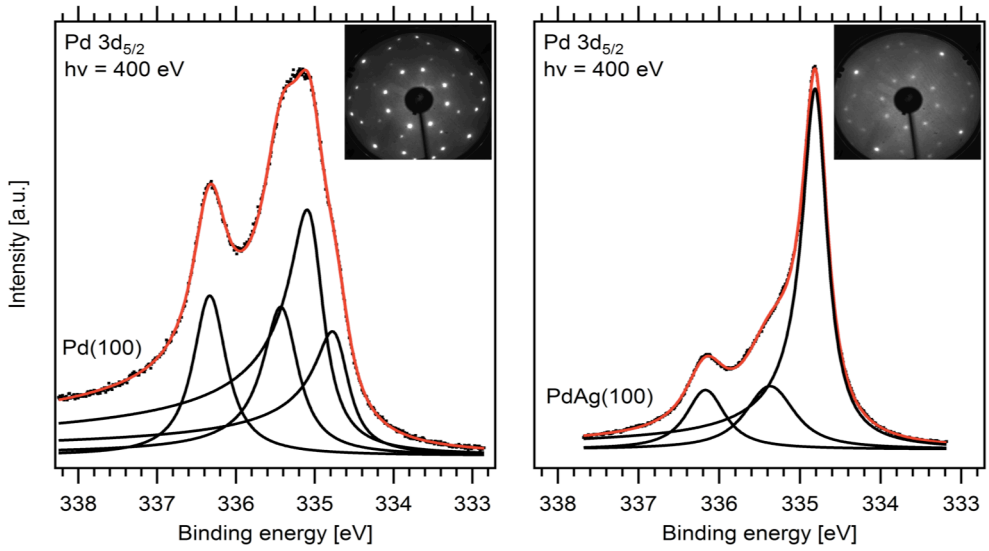

Figure 1. *Pd $3d_{5/2}$ core level spectra of the (√5×√5)R27° surface oxides on Pd(100) (left) and $Pd_{75}Ag_{25}(100)$ (right). The corresponding LEED patterns are shown in the insets.*

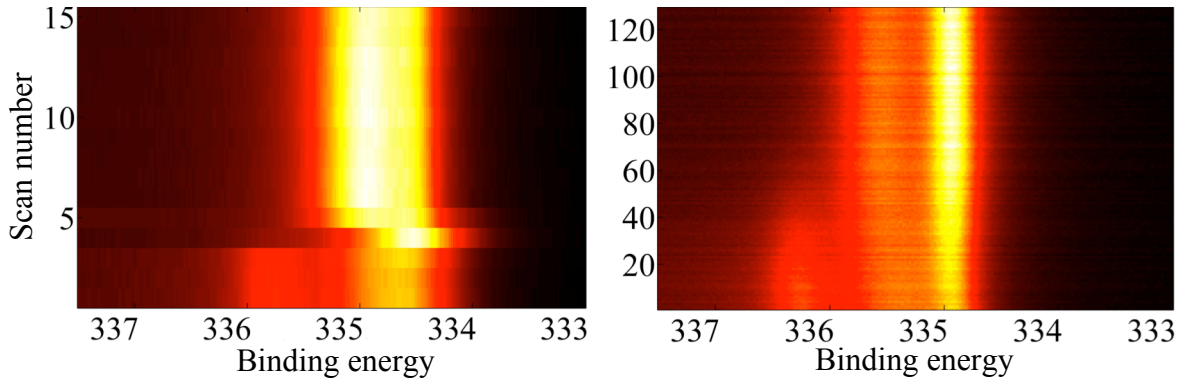

Figure 2. *In situ recording of CO induced reduction of the (√5×√5)R27° surface oxides on Pd(100) (left) and $Pd_{75}Ag_{25}(100)$ (right) at temperature 120°C and CO pressure $5x10^{-8}$mbar.*

References

[1] R. Hughes, Membr. Tech. **131**, 9 (2001).
[2] G. J. Grashoff et al., Plat. Met. Rev. **27**, 157 (1983).
[3] A. K. M. Kibria Fazle et al., Int. J. Hydrogen Energy **23**, 891 (1998).
[4] J. Rogal et al., Phys. Rev. Lett. **98**, 046101 (2007).
[5] S. Uemiya et al., J. Membr. Sci. **56**, 315 (1991).
[6] A. L. Mejdell et al., J. Membr. Sci. **350**, 371 (2010).
[7] P. T. Wouda et al. Surf. Sci. **417**, 292 (1998).
[8] M. Todorova et al., Surf. Sci. **541**, 101 (2003).
[9] P. Kostelnik et. al, Surf Sci. **601**, 1574 (2007).

Adsorption of small and large molecules on thin cobalt oxide films

M.A. Schneider, T. Schmitt, M. Reuschl, C. Tröppner, L. Hammer

Lehrstuhl für Festkörperphysik, Universität Erlangen-Nürnberg, D-91058 Erlangen, Germany
(corresponding author: M.A. Schneider, e-mail: alexander.schneider@physik.uni-erlangen.de)

Apart from its structural richness [1-4] cobalt oxide thin films offer two interesting aspects for basic research and applications. First, cobalt oxide is known to promote CO oxidation at low-temperatures [5] and also other oxidation reactions are catalytically enhanced. The proper reaction mechanisms are unknown from a microscopic point of view. Here, the structurally well characterized cobalt oxide films on Ir(100) may serve as a model catalyst surface that can be accessed by surface-science methods. Secondly, the interaction of larger (organic) molecules on oxide surfaces is an important topic relevant for organic electronics, solar energy conversion, sensors, catalysis, etc.. Here, thin cobalt oxide films are an interesting playground where the mechanisms of molecular self-assembly and functionalization can be tested on a technologically relevant oxide surface. In this talk we will present first experiments showing the adsorption properties of metalophthalocyanines and CO on thin CoO films by low-temperature STM.

Fe-Pc deposited at room temperature by thermal evaporation on a 1 bilayer (1BL) CoO(111)-c(10x2) on Ir(100) shows that the majority of molecules is adsorbed in a standing configuration. The adsorption as a flat lying molecule is rare and observed only at specific sites presumably allowing for an optimal interaction between the metal ion and the oxide surface. This interaction appears less site specific on a 2BL CoO film where standing molecules have not been observed.

On the other hand, CO is readily oxidised at an ultra-thin cobalt oxide film (CoO-(3x3) on Ir(100)) leaving defects that can be healed by dosing oxygen. Atomic scale images of adsorbed CO reveal that the structure offers various adsorption sites compatible with the molecules bridging oxygen sites. However, a repulsive interaction prevents the unit cell from being occupied by molecules fully. This results in the formation of molecular stripes on the surface.

[1] M. Gubo, C. Ebensperger, W. Meyer, L. Hammer, and K. Heinz, Phys. Rev. B 83, 075435 (2011)
[2] C. Ebensperger, M. Gubo., W. Meyer, L. Hammer, K. Heinz, Phys. Rev. B 81, 235405 (2010)
[3] K. Biedermann, M. Gubo, L. Hammer, K. Heinz, J. Phys. Condens. Matt. 21, 185003 (2009)
[4] L. Gragnaniello, et al., Surface Science 604, 2002 (2010)
[5] X.Xie, Y. Li, Z.-Q. Liu, M. Haruta, S. Shen, Nature 458, 746 (2009)

Tuesday

The four hills of Graphene on Ru(0001) 25 on 23

Marcella Iannuzzi,[1] Haifeng Ma,[2] Irakli Kalichava,[3] Steven Leake,[3] Haitao Zhou,[4] Geng Li,[4] Yi Zhang,[4] Oliver Bunk,[3] Hongjun Gao,[4] Jürg Hutter,[1] Phil Willmott,[3] and Thomas Greber[2]

[1] *Physikalisch Chemisches Institut der Universität Zürich, Switzerland*
[2] *Physik-Institut der Universität Zürich, Switzerland*
[3] *Swiss Light Source, Paul Scherrer Institut, Villigen, Switzerland*
[4] *Institute of Physics, Chinese Academy of Sciences, Beijing, 100190, China*

(corresponding author: T. Greber, e-mail: greber@physik.uzh.ch)

A single layer of sp^2 hybridized carbon on ruthenium (g/Ru) forms a 23x23 superstructure. The unit cell corresponds to a coincidence lattice of 25x25 graphene units (1250 atoms) on top of 23x23 ruthenium unit cells with *four* hill-like protrusions (see Figure 1) [1]. These hills impose *lateral* electric fields, which depend on the height of the hills or corrugation [2]. The corrugation is also important for the understanding of proposed quantum dot arrays [3].

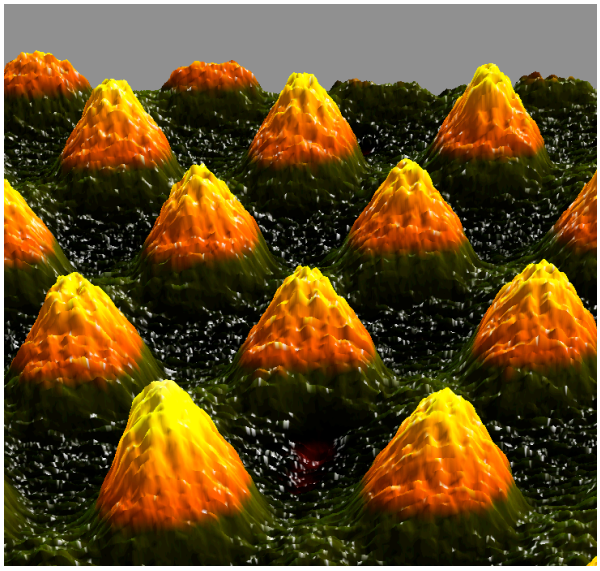

*Fig. 1: Three-dimensional representation of a tunneling microscopy image of the g/Ru superstructure with atomic resolution. The corrugation, i.e. physical height of the "hills" with a distance of about 3 nm is of crucial importance for the understanding of this structure and its functionality (Data HG. Zhang, cover JPCM **22** No 30 (2010)).*

A large density functional theory (DFT) calculation on the 25 on 23 unit cell shows 4 hills with very similar heights i.e. a corrugation of 120 pm, which is in line with a recent result on a single hill calculation in a 11x11 super cell, i.e. a 12 on 11 coincidence lattice [4].

However, and this is the main message of this talk, the four hills have not the same registry of their peak positions with respect to the carbon atoms. The theoretical prediction is one hill with a tetrahedral (Y) peak consisting in 4 carbon atoms, and three omega (Ω) peaks, with a carbon six-ring on the crest.

Comparison with atomically resolved large scale scanning tunneling microscopy (STM) images, shows that the four different hills can be observed with STM.

The surface x-ray diffraction (SXRD) data of Ref.1 and the structural model obtained without help of DFT [5] are revisited. The present DFT model leads a better R-factor without

adjustment of any parameter and a lower graphene straining (Keating) energy than the model with chiral hills [5].

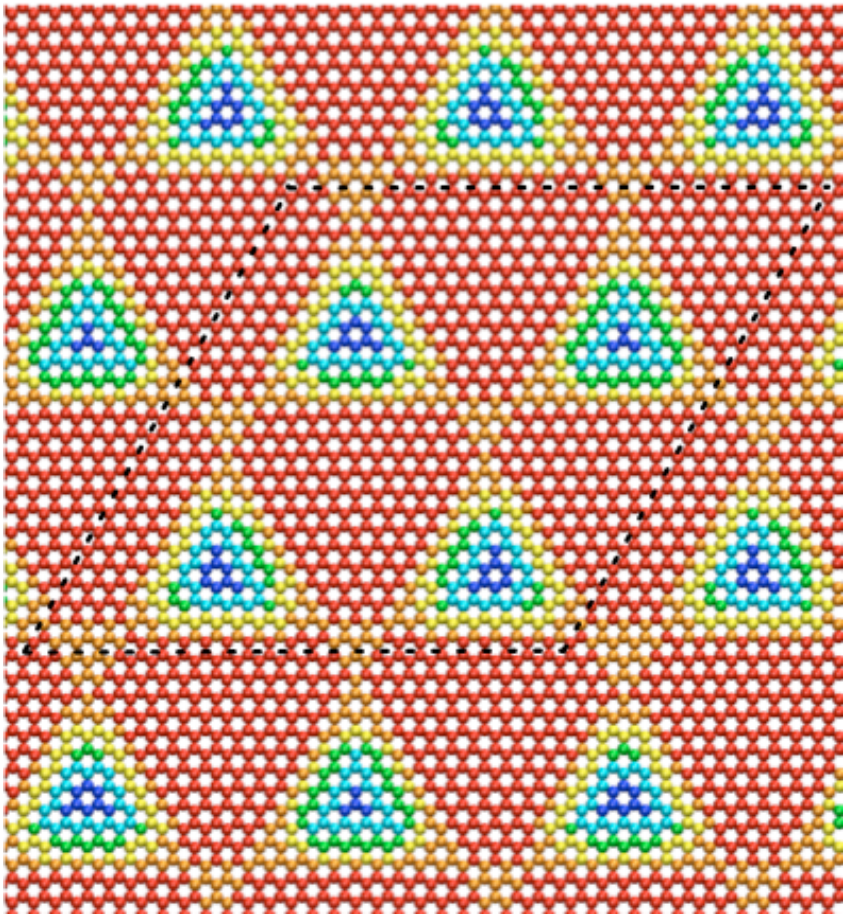

Fig.2: Theoretical result of the arrangement of the 25x25 carbon atoms in the 25 on 23 g/Ru(0001) structure. The color indicates the height of the C atoms over the Ru substrate and ranges from 325 pm (blue) to 209 pm (red). Note the two different types of hills: 1 Y-type hill with one carbon atom on the peak and 3 W types with 6 carbon atoms on the crest of the peak.

In conclusion we present a structural model for the 23 on 25 structure of graphene on ruthenium. Two different types of hills with similar height, though different terminations are predicted by DFT and confirmed with STM and SXRD. We expect this finding to further extend the opportunities for self-assembling of atoms and molecules, since the different terminations will have distinct reactivities.

[1] Martoccia et al. Phys. Rev. Lett., 101 (2008) 126102.
[2] Brugger, et al., Phys. Rev. B, 79 (2009) 045407.
[3] Zhang et al., J. Phys.: Condens. Matter, 22 (2010) 302001.
[4] Stradi et al., Phys. Rev. Lett., 106 (2011) 186102.
[5] Martoccia et al. New J. of Physics, 12 (2010) 04302.

Graphene on Ni(111): Strong Interaction and Weak Adsorption

F. Mittendorfer

Institut für Angewandte Physik und Center for Computational Materials Science,
Technische Universität Wien, A-1040 Wien, Austria
(corresponding author: F. Mittendorfer,
e-mail: Florian.Mittendorfer@tuwien.ac.at)

The discovery of the exceptional electronic properties of graphene, such as the linear band dispersion in the vicinity of the Dirac point or the ambipolar field effect, has led to a wide range of proposed applications for graphene-based electronics. For example, the interface between graphene and a ferromagnetic metal, such as Ni, is of special interest, as it might open the path for the design of spin-filtering devices needed for spintronics.

Nevertheless, the precise nature of the interaction of graphene and a metallic surface is not well understood. In addition, the need for both an accurate description of the van der Waals (vdW) interactions and the metallic substrate make the theoretical treatment of the system demanding. While density functional theory (DFT) based methods usually offer reliable structural models and energetics, and allow to treat systems containing several hundreds of atoms, the accuracy of commonly used semi-local functionals for adsorption studies is severely limited: Depending on the functional, they either yield too high surface energies or too low adsorption energies, but fail to predict both quantities correctly. In addition, non-local (van der Waals) contributions are completely neglected. In a recent publication [1], we could demonstrate that the evaluation of the correlation energy in a many-electron approach based on the adiabatic-connection fluctuation-dissipation theorem (ACFDT) in the random phase approximation (RPA) leads to a significant improvement.

In this presentation, I will discuss our recent results [2] for the adsorption of graphene on Ni(111) on the basis of RPA calculations. Although we find a significant hybridization between the graphene π orbitals and Ni d z^2 states at an optimized binding distance of 2.17 Å, the adsorption energy is still in the range of a typical physisorption (67 meV per carbon). An analysis of the contributions to the binding energy allows to identify the origin of seeming

contradiction of a strong interaction (hybridization), but only a low adsorption energy: An important contribution to the binding energy is related to a decrease in the exchange energy resulting from a localization of the electrons due to the broken symmetry in the graphene layer.

The energetics can be well reproduced using the computationally significantly cheaper van der Waals density functional theory (vdW-DF) with an appropriately chosen exchange-correlation functional.

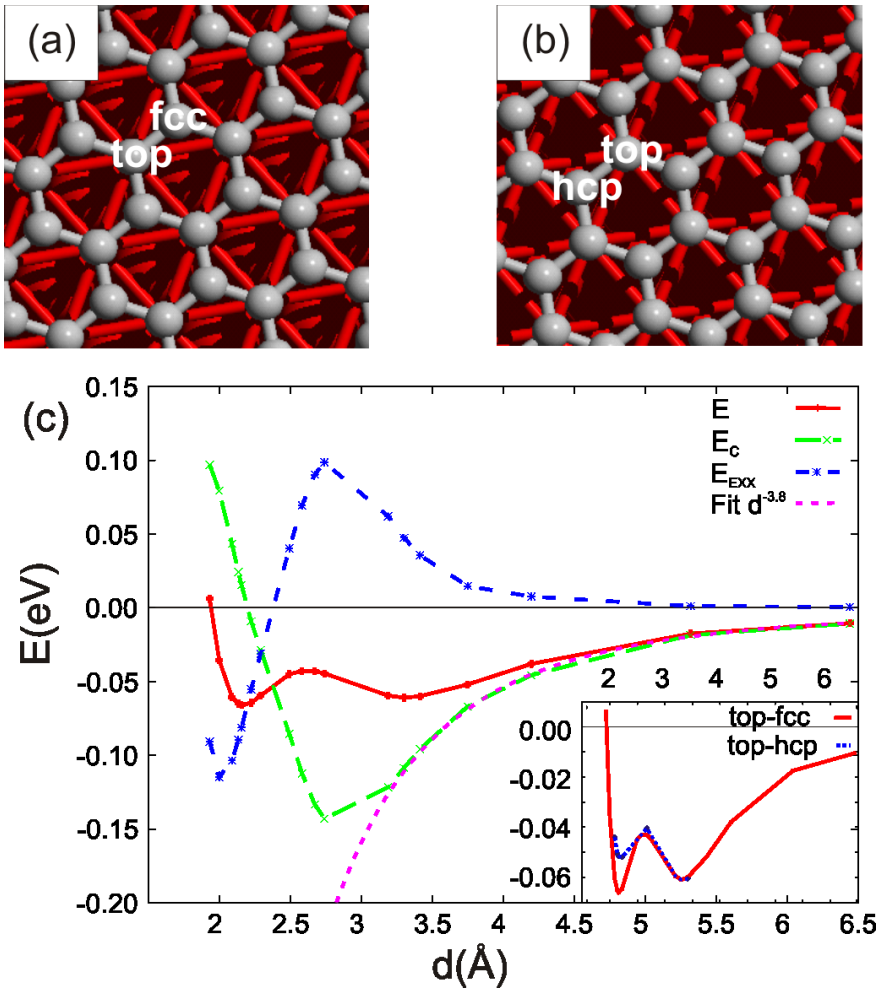

Fig.1: Adsorption of graphenen on Ni(111) a) and b) Structural models, c) contributions to the adsorption energy as a function of the distance to the surface.

Support by the European Science Foundation (ESF) under the EUROCORES project EUROGRAPHENE /SpinGraph and the Fonds zur Förderung der Wissenschaftlichen Forschung (projects I422-N16 and ViCom) is gratefully acknowledged.

[1] L. Schimka, J. Harl, A. Stroppa, et al., Nature Materials 9, 741 (2010).

[2] F. Mittendorfer, A. Garhofer, et al., Phys. Rev. B 84, 201401 (R) (2011)

Self-protecting spin-polarized surface states in ternary topological insulators.

Hugo Dil[1,2], Gabriel Landolt[1,2], Bartosz Slomski[1,2] Sergey Eremeev[3,4], Andreas Eich[5], Alexander Khajetoorians[5], Jens Wiebe[5], Evgueni Chulkov[4,6] and Jürg Osterwalder[1]

[1]Physik-Institut, Universität Zürich, 8057 Zürich, Switzerland
(corresponding author: Hugo Dil, jan-hugo.dil@psi.ch)
[2]Swiss Light Source, Paul Scherrer Institute, 5232 Villigen, Switzerland
[3]Tomsk State University, 634050, Tomsk, Russia
[4]Donostia International Physics Center (DIPC), Paseo de Manuel Lardizabal, 4, 20018 San Sebastián/Donostia, Basque Country, Spain
[5]Institute of Applied Physics, University of Hamburg, Jungiusstrasse 11, Hamburg, Germany
[6]The Basque Country University, 20080, San Sebastian, Spain

In a simple picture topological insulators can be viewed as bulk band insulators with metallic surface states. The unique properties of this novel class of materials arises from the fact that the spin-orbit interaction causes an odd number of parity inversions of the bulk bands around the Fermi level. Combined with spin-orbit interaction this parity inversion induces an odd number of spin-polarized Fermi level crossings of the surface states [1]. Together with time reversal symmetry, the odd number of crossings guarantees the metallic nature of the surface.

Whereas initial three dimensional topological insulators were based on binary systems [2,3], ternary systems give more parameters to induces changes in the band structure and spin properties. Here we will present scanning tunneling microscopy (STM) and spin- and angle-resolved photoemission spectroscopy (SARPES) [4] results on the ternary three dimensional topological insulators $PbBi_4Te_7$ and $TlBiSe_2$. Combined with spin-resolved DFT calculations the important difference between topological states and trivial surface states with respect to their self-protection will be explored.

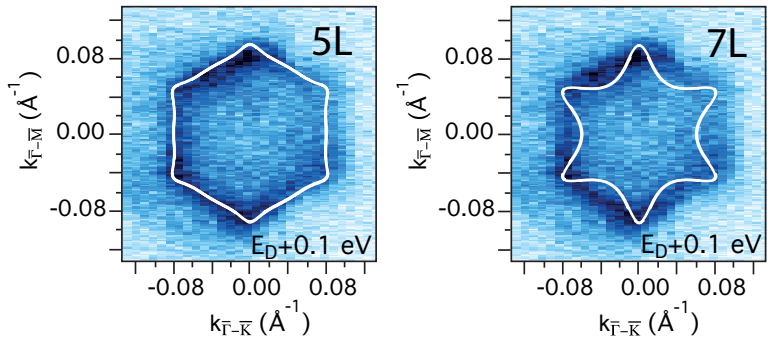

Figure 1: Constant energy surface measured with ARPES 100meV above the Dirac point for $PbBi_4Te_7$. The white solid lines indicate the expected constant energy contours from DFT for the respective surface terminations indicated in the plot.

Because $PbBi_4Te_7$ has a layered structure consisting of alternating 5 atomic layer (5L) and 7 atomic layer (7L) blocks the crystal has two possible surface terminations upon cleaving, either 5L or 7L is the topmost block. DFT predicts two rather different surface state band structures for the two terminations, but as depicted in Figure 1 we observe only the 5L termination. On the other hand STM results show that both terminations are present. Here it will be shown how this apparent paradox can be resolved and gives information about the self-protecting nature of the topological state. Furthermore, it will be shown that the hexagonal warping of the states induces an out-of-plane spin component with three-fold symmetry.

In $TlBiSe_2$ the number of possible surface terminations is even higher because there is no clear van der Waals gap where the crystal would preferentially cleave. All possible surface terminations are expected to yield trivial surface states besides the topological states [5]. However, no trivial surface states have been observed in ARPES or SARPES experiments up to date [6]. Here again a combination of SARPES, STM and DFT can resolve this apparent paradox. Our interpretation also provide strong indications on why in recent ARPES experiments the topological state in Bi_2Se_3 seemed to disappear after very mild Ne^+ sputtering [7].

[1] M.Z Hasan and C.L. Kane, Rev. Mod. Phys. **82**, 3045–3067, (2010).

[2] D. Hsieh et al. Science **323**, 919 (2009).

[3] D. Hsieh et al. Nature **460**, 1101 (2009).

[4] J. H. Dil, J. Phys.: Condens. Matter **21**, 403001 (2009).

[5] S.V. Eremeev et al. Phys. Rev. B **83**, 205129 (2011).

[6] Kuroda et al. Phys. Rev. Lett. **105**, 146801 (2010); Sato et al. Phys. Rev. Lett. **105**, 136802 (2010); Xu et al. Science **332**, 560 (2011).

[7] R.C. Hatch et al. Phys. Rev. B **83**, 241303(R) (2011)

Development of high-resolution spin- and angle-resolved photoelectron spectrometer and its applications

T. Okuda, Y. Takeichi[1], K. Miyamoto, H. Miyahara[2], K. Kuroda[2], A. Kimura[2], H. Namatame, M. Taniguchi, and A. Kakizaki[1]

Hiroshima Synchrotron Radiation Center (HSRC), Hiroshima University, Higashi-Hiroshima 739-0046, Japan
(corresponding author: T. Okuda, e-mail: okudat@hiroshima-u.ac.jp)

[1]*Synchrotron Radiation Laboratory, Institute for Solid State Physics, The University of Tokyo, Kashiwa 277-8581, Japan*

[2] *Graduate School of Science, Hiroshima University, Higashi-Hiroshima 739-8526, Japan*

Spin- and angle-resolved photoelectron spectroscopy (SARPES) which can directly observe the spin-resolved band dispersions, is one of the most suitable and powerful experimental techniques for the investigation of spin-related materials. As the discovery of the high-*Tc* superconductors promoted the development of high-resolution angular resolved photoelectron spectroscopy (ARPES), recent discovery of peculiar spin texture of surface states by the spin-orbit interaction, such as surface Rashba spin splitting state or helical spin state of topological insulators stimulates to develop high-performance SARPES machines. However, the low efficiency of the spin polarimeters that utilized the spin-orbit interaction of the electrons such as Mott detector, spin LEED detector and so on has hampered to realize the high-resolution SARPES experiment.

Here we report our newly developed highly efficient spin- and angle-resolved photoelectron spectrometers at the ISSP beamline in Photon Factory (KEK)[1] and at beamline BL-9B of Hiroshima Synchrotron Radiation Center (HSRC)[2], which realize the high-resolution SARPES measurements. By utilizing high-efficient spin detector based on very low energy electron diffraction (VLEED)[3] by ferromagnetic target (Fe(001)p1x1-O) as the spin detector and combining it with high-resolution hemispherical analyzers (PHOIBOS 150 at PF, SCIENTA R4000 at HSRC), high-efficient and high-resolution SARPES experiment has been realized[1,2]. Especially, the machine at HSRC which is named ESPRESSO (Efficient SPin REsolved SpectroScOpy) was designed to improve the performance of the first prototype machine at ISSP and resolution of 7.5 meV in energy and ±0.18◦ in angle has been achieved with spin resolution[2]. With ESPRESSO one can observe both in-plane and out-of-plane spin components by the aid of a 90 degree electron deflector. In addition, the integrated two dimensional electron detector for usual spin-integrated ARPES measurement can realize quick and precise observation of the electronic band structure and Fermi surfaces of the samples in advance. Therefore, one can find the specific electronic structure in *k*-space, which

is interested in to observe the spin structure and measure the spin structure with high-resolution efficiently.

As examples to demonstrate the high performance of the machines we present the observation of the spin-textures of Au induced one-dimensional surface state on vicinal Si(111) surface which has peculiar doubly splitting band structure with very steep dispersion[4]. The high-resolution SARPES observation reveals that origin of the splitting band is Rashba effect caused by the spin-orbit interaction of Au[5]. Interestingly, the state has considerable out-of-plane spin component which deviates from the tangential spin structure of normal Rashba spin-splitting state. The unexpected large out-of-plane spin component is due to the highly anisotropic wave function of the gold which is confirmed by first principle calculation[5].

As the second example, we present the investigation of the precise spin structure of Bi(111) film which has been reported that the spin structure shows significant out-of-plane spin component and oscillation of in-plane spin polarization[6]. Our precise observation affirms the quite high out-of-plane spin polarization which is reflecting the three-fold symmetry of the Bi(111) crystal and well reproduced by the analysis based on the $k \cdot p$ theory like an warping effect of the Fermi surface of Dirac cone in 3D topological insulators[7]. However, the oscillation of the in-plane tangential spin component has not been observed and the spin-polarization difference among different k-points probably can be explained by photoemission final state effect[8].

TO acknowledges Dr. T. Kinoshita, and Dr. F. U. Hillebrecht for their helps and advices for the development of the new spin detector. TO also thanks to Prof. T. Oguchi, Dr. T. Shishidou and Prof. Matsuda for the fruitful discussion. This work was partly supported by KAKENHI (19340078, 23244066, 23244066), Grant-in-Aid for Scientific Research (B, A, and B) of Japan Society for the Promotion of Science. Some of the experiments were performed under the PF proposal No. 2008G561 and HSRC proposal No. 11-C-1.

[1] T. Okuda, Y. Takeichi, Y. Maeda, A. Harasawa, I. Matsuda, T. Kinoshita, and A. Kakizaki, Rev. Sci. Instrum. **79**, 123117 (2008).

[2] T. Okuda, K. Myamoto, H. Miyahara, K. Kuroda, A. Kimura, H. Namatame, and M. Taniguchi, Rev. Sci. Instrum. **82**, 103302 (2011).

[3] D. Tillmann, R. Thiel, and E. Kisker, Z. Phys. B **77**, 1 (1989).

[4] J. N. Crain, J. L. McChesney, F. Zheng, M. C. Gallagher, P. C. Snijders, M. Bissen, C. Gundelach, S. C. Erwin, and F. J. Himpsel, Phys. Rev. B **69**, 125401 (2004), and references therein.

[5] T. Okuda, K. Miyamoto, Y. Takeichi, H. Miyahara, M. Ogawa, A. Harasawa, A. Kimura, I. Matsuda, A. Kakizaki, T. Shishidou, and T. Oguchi, Phys. Rev. B **82**, 161410 (R) (2010).

[6] A. Takayama, T. Sato, S.Souma and T. Takahashi, Phys. Rev. Lett. **106**, 166401 (2011).

[7] L. Fu, Phys. Rev. Lett. **103**, 266801 (2009).

[8] H. Miyahara *et al.* unpublished.

Electron energy loss spectroscopy: a new spectrometer, high resolution spectra of surface spin waves, and a new mode of lens operation.

J. Rajeswari[1,3], H. Ibach[2,3], and C. M. Schneider[1,3]

(*corresponding author:H. Ibach, e-mail: h.ibach@fz-juelich.de*)

Peter Grünberg Institut [1](PGI-6), [2](PGI-3), Forschungszentrum Jülich, 52425 Jülich, Germany

[3]Jülich Aachen Research Alliance - (JARA), Germany

Surface spin waves and other electronic energy losses have a small cross section for inelastic interaction with low energy electrons, much smaller than phonons. On the other hand, there is less demand on high energy resolution. Conventional spectrometers for electron energy loss spectroscopy (EELS) designed for studies of surface vibrations do not meet the requirements for studies of surface spin waves in the high momentum regime. A first break through in the struggle for intensity was achieved in 2003 with the development of a special spectrometer featuring a combination of 90°/180° monochromators and a spin-polarizing cathode [1]. In the meantime a considerable number of studies on surface spin waves have been performed using this spectrometer (see e.g. [2-4]). A theoretical study of the electron optics including the electron deflection by its own space charge showed however that the 90°/180° monochromator is not ideal. Up to seven times higher monochromatic currents are obtained using the classical combination of two 143° deflectors as monochromator [5]. Based on those ideas but also on extensive further electron optical calculations with newly developed codes that include the diffuse scattering at a surface we have now realized a new spectrometer. While it looks rather conventional at first sight the spectrometer differs in some important details from previous designs [6]. These details include the addition of a second monochromator with low angle aberrations and the addition of an angle aperture in the plane perpendicular and parallel to the scattering plane, respectively. Using this spectrometer we have been able to resolve the surface spin waves on fcc cobalt films with 7meV FWHM energy resolution (Fig. 1).

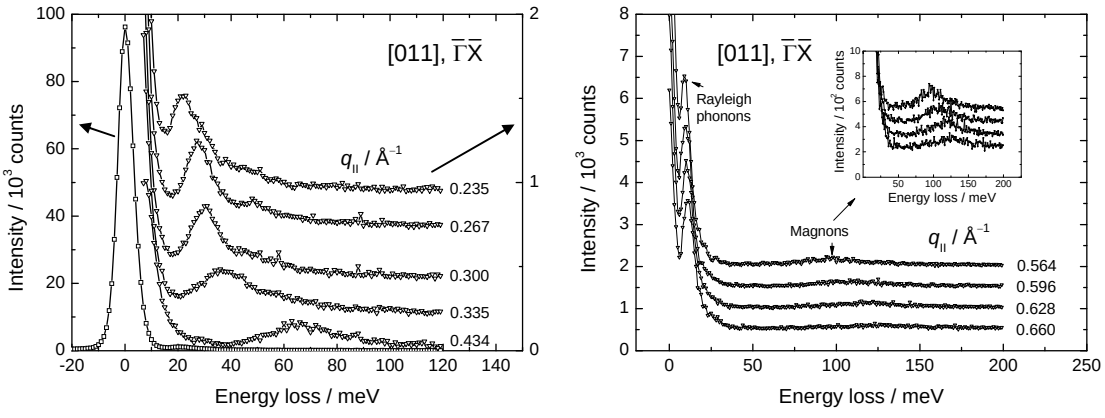

Fig. 1: High resolution spectra of surface spin waves along [011] showing also the Rayleigh phonon.

The spectra in the right panel additionally display energy losses due to Rayleigh waves with their much higher intensity, demonstrating nicely the need for a higher sensitivity in studies of spin wave energy losses.

The high energy resolution in combination with a controlled momentum resolution allows the determination of the spin wave dispersion down to low wave vectors and a reliable determination of the energy width of the spin wave losses. We have furthermore extended the study to the [001] ($\overline{\Gamma}\overline{\mathrm{M}}$) direction and to cobalt surfaces covered with thin layers of nickel and copper. Details will be reported on the meeting.

In the course of our electron optical calculation we discovered a new mode of operation of the lens system which uses higher voltages. It brings the cardinal plane closer to the sample and thereby increases the solid angle that is probed by the spectrometer. The mode is easily adapted to conventional EELS spectrometers. For lower impact energies the required voltages are within the range of the standard commercial control units. Fig. 2 shows an example of the gain of intensity.

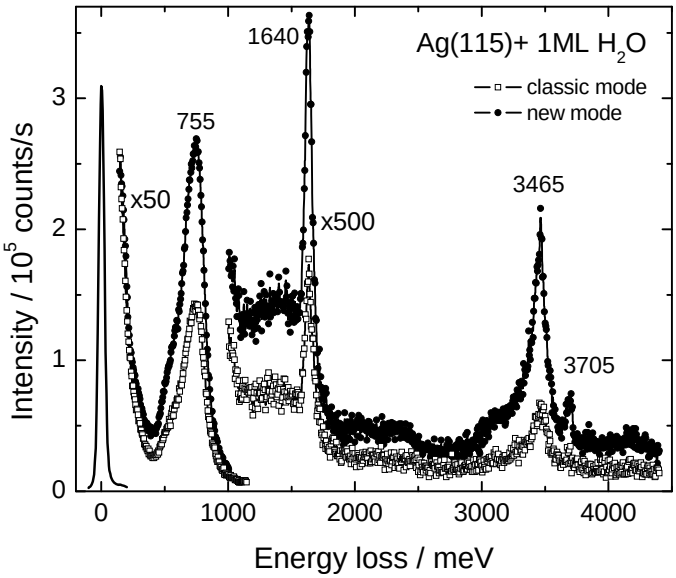

Fig. 2: Spectrum of adsorbed water on an Ag(115) surface taken in the conventional and the new mode of operation.

One of us (J. R.) expresses her sincere gratefulness to the NRW Research School "Forschung mit Synchrotronstrahlung in den Nano- und Biowissenschaften" for financial support..

[1] H. Ibach, D. Bruchmann, R. Vollmer, M. Etzkorn, P. S. A. Kumar, J. Kirschner, Rev. Sci. Instrum. 74 (2003) 4089.
[2] R. Vollmer, M. Etzkorn, P. S. A. Kumar, H. Ibach, J. Kirschner, Phys. Rev. Lett. 91 (2003) 147201.
[3] W. X. Tang, Y. Zhang, I. Tudosa, J. Prokop, M. Etzkorn, J. Kirschner, Phys. Rev. Lett. 99 (2007) 087202.
[4] Y. Zhang, P. A. Ignatiev, J. Prokop, I. Tudosa, T. R. F. Peixoto, W. X. Tang, K. Zakeri, V. S. Stepanyuk, J. Kirschner, Phys. Rev. Lett. 106 (2011) 127201.
[5] H. Ibach, M. Etzkorn, J. Kirschner, Surface and Interface Analysis 38 (2006) 1615.
[6] H. Ibach, J. Rajeswari, C. M. Schneider, Rev. Sci. Instrum., in press.

Chemically resolved depth profiles from synchrotron XPS of oxygen ion-driven reactions with Be_2W

M. Köppen, K. Schmid, H. Löchel[1], T.-V. Phan, J. Riesch, A. Vollmer[1] and Ch. Linsmeier

Max-Planck-Institut für Plasmaphysik, EURATOM Association,
Boltzmannstr. 2, 85748 Garching b. München, Germany
(corresponding author: Ch. Linsmeier, e-mail: linsmeier@ipp.mpg.de)

[1] *Helmholtz Zentrum Berlin für Materialien und Energie GmbH, Wilhelm-Conrad-Röntgen Campus BESSY II, Albert-Einstein-Str. 15, 12489 Berlin, Germany*

In this study we present a newly developed model to derive quantitative depth profiles from energy-resolved synchrotron XPS spectra. The model is applied to oxygen ion induced reactions with the alloy Be_2W, motivated by the materials selected for the first wall of the fusion device ITER: beryllium and tungsten.

XPS experiments performed at a synchrotron allow to change the excitation energy of the X-ray photons. Thus, the kinetic energy of the emerging photoelectron can be chosen for a given core level. Since the inelastic mean free path (IMFP) of electrons in a solid depends on their kinetic energy the information depth can be adjusted. By recording spectra with different excitation energies (leading to identical photoelectron kinetic energies) it is possible to access chemical information of selected core level binding energies from the same depths of the sample. Unfortunately this information is always depth-integrated. Thus, direct access to chemical information in a specific depth interval is not available. As a second challenge the signal contribution to the XPS intensity decays exponentially with increasing depth. Therefore, a direct quantitative comparison of spectra recorded at different photon energies is not possible.

In order to gain access to quantitative depth profiles, the recorded high-resolution spectra are normalised by element and experiment specific parameters, like e.g. excitation cross section, angular dependence, analyzer transmission, and photon flux. The areal density for an element in a specific chemical state is determined and is used as input for modelling the depth distributions.

The modelling approach is based on forward calculations of XPS spectra for a given elemental depth distribution. The calculated spectra are fitted to the experimental data by the application of numerical methods. Thus, the elemental depth distributions are improved in an iterative procedure.

In this presentation we show the results of this new evaluation method for a typical surface chemistry problem at the first wall of ITER: the implantation of energetic oxygen ions as a

reactive plasma impurity into the beryllium-tungsten alloy Be_2W, formed at the first wall due to plasma-wall interaction processes. In this experiment, carried out in a d edicated preparation chamber directly attached to the SurICat end station at BESSY II, oxygen is implanted in several steps with acceleration voltages of 1000 and two times 500 V at fluences of 5 x 10 ^{14} cm^{-2}. Between the single implantation steps the sample is heated for 30 min at 600 K in order to investigate both ion-induced and thermally driven reactions. Photoelectron spectra with six different photon energies per core level are recorded after each preparation step. The results of this evaluation are depth profiles on the nanometer scale of the chemical compounds.

The figure shows a depth profile which is the result of the quantitative analysis after the first implantation step of oxygen with 1 kV. The depth resolution (layer thickness) applied here is 1.4 nm, based on the IMFP calculations after Gries [1]. The dominating species in the first and third layer is BeO. The beryllium oxide in the first layer originates mainly from the surface oxidation of Be with residual gas. The beryllium oxide in the third layer (2.8 – 4.2 nm) is formed due to the implanted oxygen. In the layer in between, only species containing tungsten can be found.

The results of the chemically resolved depth profiles determined by t his approach are compared to implantation depth profiles simulated with the kinematic code SDTrim.SP.

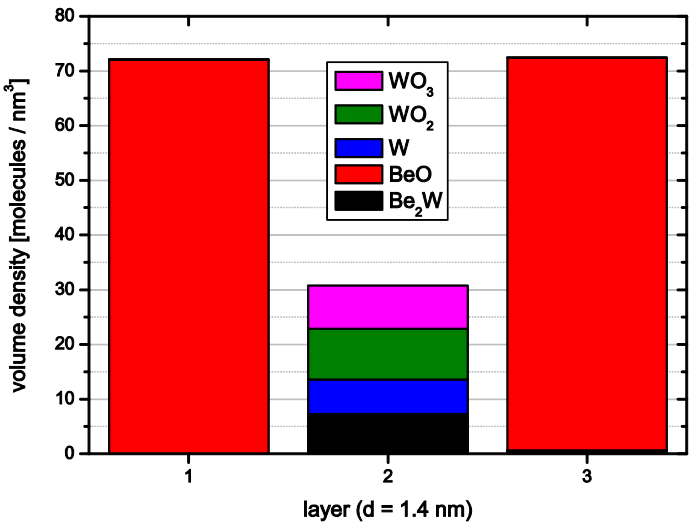

Chemically resolved depth profile of after oxygen ion implanted into the beryllium-tungsten alloy Be_2W at 1 kV. For better clarity, species with less than five molecules per nm^3 are omitted.

[1] W. Gries, Surf. Interface Anal. 24 (1996) 38

Surface processes under strong homogeneous external DC fields

W. Steurer, T. Obermüller, S. Surnev, F. P. Netzer

Institute of Physics, University of Graz, Universitätsplatz 5, Graz, A-8010, Austria

Dynamic processes such as growth, melting and crystallization, or chemical reactions are ubiquitous in many areas of surface science. The influence of external parameters beyond the usual temperature and pressure are, however, rarely considered. Yet, a substantial influence is expected when dynamic phenomena occur in the presence of external fields. Here we report on experiments where Ag(100) surfaces (bare or covered with NiO or MnO nanolayers) are exposed to spatially-extended homogeneous external electric fields up to 2 V/nm. Such high fields are obtained in a setup resembling a plate capacitor, in which the Ag(100) substrate acts as the cathode with a counter electrode placed 800nm apart. Several new surface phenomena are discussed in this talk:

1. E-field induced smoothing of Ag(100) in the presence of oxygen

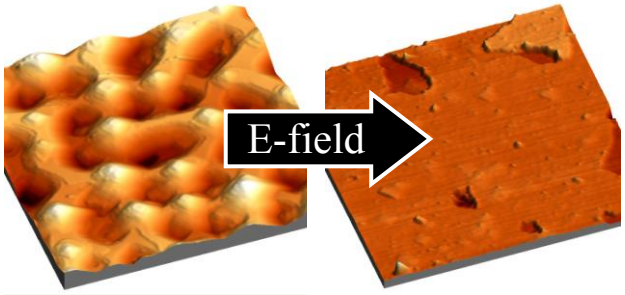

While, in general, strong electric fields ($E > 10^9$ Vm^{-1}) give rise to a coarsening of metal surfaces [1], we find a significant flattening of the Ag surface if an oxygen partial pressure ($p = 5x10^{-6}$ to $1x10^{-7}$ mbar) is present in the gap between the silver surface and the anode. The field emission current, which is very sensitive to the surface roughness, decreases exponentially upon leaking oxygen into the UHV chamber; the exponential decay constant depends strongly on the oxygen partial pressure. Subsequently performed LEED and AES measurements do not show any signs of an oxidized silver surface. STM images recorded on sputtered Ag(100) surfaces after electric-field exposure in the presence of oxygen show large, step-free terraces demonstrating the smoothing effect. In contrast, and in agreement with Ref. [1], we observe a coarsening of the silver surface if strong electric fields are applied under UHV conditions ($p_{O2} < 1x10^{-9}$ mbar).

2. Reduction of Ni-oxide nanostructures for E-fields > 0.9 V/nm

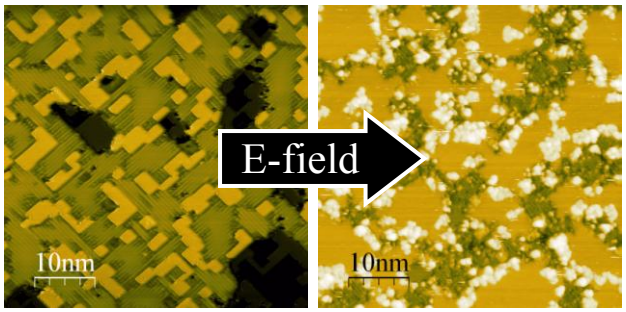

Ultrathin Ni-oxide nanostructures immersed into an Ag(100) substrate have been grown by reactive evaporation [2] and have subsequently been exposed to electric fields in the range of 0.5-1.6 V/nm. For fields exceeding the threshold of 0.9 V/nm, oxygen atoms are removed from the surface, thus, efficiently reducing the initially highly-ordered Ni-oxide film. The remaining Ni atoms on the surface are highly mobile and cluster together. No oxide reduction is observed if the field polarity is inverted.

3. E-field induced transition of (2x1) MnO/Ag(100)

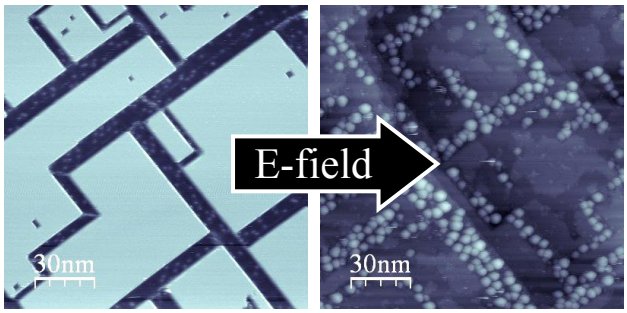

Well-ordered Mn-oxide films on Ag(100) have been grown by evaporation of 0.4-2 ML Mn at room temperature and post-oxidation at 800K. If exposed to strong electric fields, the planar (2x1) phase converts into uniformly sized clusters (mean diameter: 6 nm), which do not exist in the absence of the electric field. The clusters are only weakly bound to the Ag(100) substrate and aggregate into bigger clusters under the influence of the inhomogeneous electric-field of an STM tip.

This work is supported by the ERC Advanced Grant “SEPON”.

[1] V. Gill, PR Guduru, and BW Sheldon, “Electric field induced surface diffusion and micro/nano-scale island growth”, *International Journal of Solids and Structures*, 45(3-4), 943–958 (2008)

[2] W. Steurer, F. Allegretti, S. Surnev, G. Barcaro, L. Sementa, F. Negreiros, A. Fortunelli, and F. P. Netzer, “Metamorphosis of ultrathin Ni oxide nanostructures on Ag(100)”, *Physical Review B 84,* 115446 (2011)

Surface scattering of electrons in thin PbSnTe:In films with space-charge-induced limitation of electric current

A. Klimov, V. Shumsky and V. Epov

Rzhanov Institute of Semiconductor Physics, SB RAS, 6300090 Novosibirsk, Russia
(corresponding author: A. Klimov, e-mail: klimov@thermo.isp.nsc.ru)

Solid solution $Pb_{1-x}Sn_xTe$ is a narrow-gap semiconductor whose band-gap energy at T=4.2 K decreases approximately from E_g=0.2 eV at x=0 down to zero at x≈0.35. Doping of PbSnTe with indium to 1-3 at.% results in that in a narrow interval of compositions, x≈0.24-0.28, the Fermi level in PbSnTe:In takes up position deep in the forbidden band. In such a material, the resistivity at helium temperatures may reach a value in excess of 10^{10}-10^{12} Ohm·cm, quite comparable with the resistivity of ordinary insulators. However, unlike in insulators, the mobility of free charge carriers in PbSnTe:In remains high, reaching at T=4.2 K a value over 10^5 $cm^2 \cdot V^{-1} \cdot s^{-1}$. In addition, the regime with space-charge-induced limitation of electric current in PbSnTe:In films can easily be attained due to the low height of the potential barriers at injecting contacts since the band-gap width in PbSnTe:In is comparatively small (E_g≈0.06 eV in the material examined in the present study) while the static dielectric permittivity at T=4.2 K is high, ε ≥ 2000-3000. That is why space-charge-limited injection currents typical of insulators can easily be measured in PbSnTe:In using samples with contacts spaced apart by a distance of several ten micrometers or even millimeters.

In the present study, we examined 1-μm thick $Pb_{0.74}Sn_{0.26}Te$:In films grown by molecular-beam epitaxy on BaF_2 substrates. On the surface of the films, two aluminum electrodes were formed, separated from each other with 30-μm inter-electrode spacing. The length of the gap between the electrodes was 0.2 cm. The current-voltage characteristics of non-illuminated structures measured in the dark at T=4.2 K were indicative of the electric regime with space-charge-induced limitation of the injection current [1, 2].

The magnitude of the electric current I through the films was examined as a function of magnetic field intensity for various orientations of the magnetic field B with respect to the electric-field direction and the normal to the substrate. The experimental procedure was similar to that described in [3]. Figure 1 shows how the relative change in the current I, $I_B/I_{B=0}$, for two values of I at B=0 depends on the angle between the direction of the magnetic (B=4 T) and electric fields on «rotation» of the field B in the plane of the substrate. Engaging attention here is a distinct asymmetry of the observed minima of $I_B/I_{B=0}$ for I=1 and 10 μA, and also the angular shift of the minima away from the angles α=90° and α=180° under conditions with B⊥E. A giant (over three orders of magnitude) asymmetric variation of the electric-current value in a magnetic field in samples with space-charge-induced limitation of

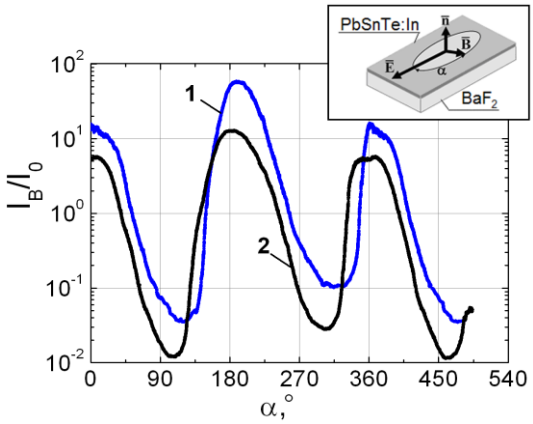

Fig. 1. Relative change of the current I during rotation of the magnetic field B in the plane of the substrate. 1 – I=1 μA, 2 – I=10 μA. B=4T.

electric current was previously observed in [3]. Qualitatively, this effect was explained assuming anisotropy of dielectric permittivity in PbSnTe:In at T=4.2 K.

Figure 2 shows data obtained during «rotation» of the field B in the plane normal to the electric-field direction. It is seen from the figure that the shape of the local maxima observed at α=90° (at this orientation of B, electrons are deflected in the field B towards the interface with the substrate) differs substantially from the shape of the local maxima at α=270° (in the latter case, electrons are deflected towards the free surface). The half-width of the maxima at α=90° is approximately one order of magnitude smaller than the half-width of the maxima at α=270°, and at I=1 μA the maxima observed at α=270° exhibit a «thin structure». Both effects can be a consequence of different mechanisms governing the scattering of electrons by imperfections at the free surface of the film and at the film-substrate interface and/or be a result of different densities of electron traps in the near-surface/interface regions of the films.

The obtained data can be considered the first observational evidence of the influence the electron scattering by film surfaces has on the transport phenomena in PbSnTe:In. We would like to emphasize here that the effect of surfaces on the transport properties of PbSnTe:In thin-film samples can hardly be examined by other experimental techniques, including capacitive or field methods, because of the high (over 1000-2000) magnitude of ε in PbSnTe:In and the Fermi level pinning phenomenon in this material, including the Fermi level pinning at the surface of the samples.

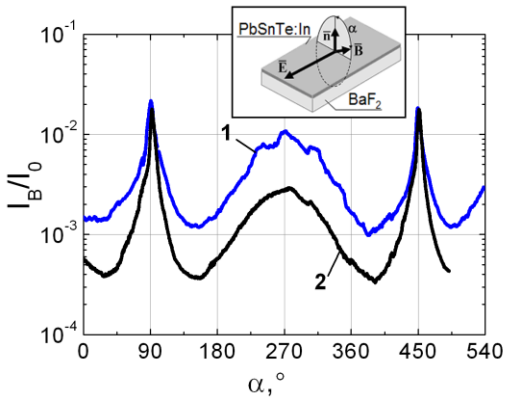

Fig. 2. Relative change of the current I during rotation of B in the plane normal to the electric field. 1 – I=1 μA, 2 – I=10 μA.

Finally, we discuss the effect of surface morphology on the observed effect and, also, the possibility of application of the experimental procedure used in the present study for revealing similar effects in other materials.

This work was supported by the Russian Foundation for Basic Research (Grant No. 11-02-12141-ofi-m-2011), by the Presidium of the Russian Academy of Sciences (Programs Nos. 1.13.17 and 4.5.14), and by the Government of the Russian Federation (Contract No. 14.740.11.0058).

[1] M.A. Lampert and P. Mark, *Current Injection in Solids,* N.Y.-London, Academic Press (1970)

[2] A.N. Akimov, V.G. Erkov, A.E. Klimov, E.L. Molodtsova, S.P. Suprun, and V.N. Shumsky, Semiconductors 39, 563 (2005)

[3] A.E. Klimov, V.N. Sherstyakova and V.N. Shumsky, Ferroelectrics 378, 101 (2009)

Substrate-enhanced supercooling in AuSi droplets

T. U. Schülli[1], R. Daudin, G. Renaud and A. Pasturel[3]

CEA, Institut Nanosciences et Cryogénie, SP2M, 17 rue des martyrs, 38054 Grenoble, France (corresponding author: G. Renaud, e-mail: gilles.renaud@cea.fr)

[1] ESRF, BP-220, F-38043 Grenoble, France

[2]SIMAP INPG, BP 75, 38402 Saint Martin d'Hères Cedex. France, Austria

Supercooling in metals i.e. the preservation of a disordered, fluid phase in a metastable state well below the melting point has led to speculations that local atomic structure configurations of dense, symmetric, but non-periodic packing act as the main barrier for crystal nucleation. For liquids in contact with solids, crystalline surfaces induce layering of the adjacent atoms in the liquid and may prevent or lower supercooling. This seed effect is supposed to depend on the local lateral order adopted in the last atomic layers of the liquid in contact with the crystal. Although it has been suggested that there might be a direct coupling between surface induced lateral order and supercooling, no experimental observation of such lateral ordering at interfaces is available [1]. We present evidence for surface and interface induced supercooling of nanometric gold-silicon (AuSi) eutectic droplets laying on a silicon substrate, which stay liquid far below the bulk eutectic solidification temperature (T_E=360ºC) . *In situ* x-ray scattering measurements show that the silicon surface orientation and structure strongly influences the degree of supercooling, its maximum being observed on a gold-induced Si(111)-(6×6) surface reconstruction presenting gold atoms in pentagonal arrangement onto which solidification is observed at 230 ºC. *Ab initio* molecular dynamics simulations confirm the possibility of supercooling in a confined $Au_{81}Si_{19}$ alloy, revealing in addition a large proportion of local icosahedral order with a five-fold local ordering similar to that of the reconstructed surface. This reveals that pentagonal atomic arrangements of Au atoms at this interface favour a lateral-ordering stabilization process of the liquid phase [2]. This interface-enhanced stabilization of the liquid state proves the importance of solid–liquid interaction on the structure of the adjacent liquid layers as well as for the stability of liquids under confined conditions. Such processes are important for present and future technologies since fluidity and crystallization play a key role in soldering and casting as well as for processing and controlling chemical reactions for microfluidic devices and for the catalytic properties of such eutectic alloys for the vapor-liquid-solid growth of semiconductor nanowires.

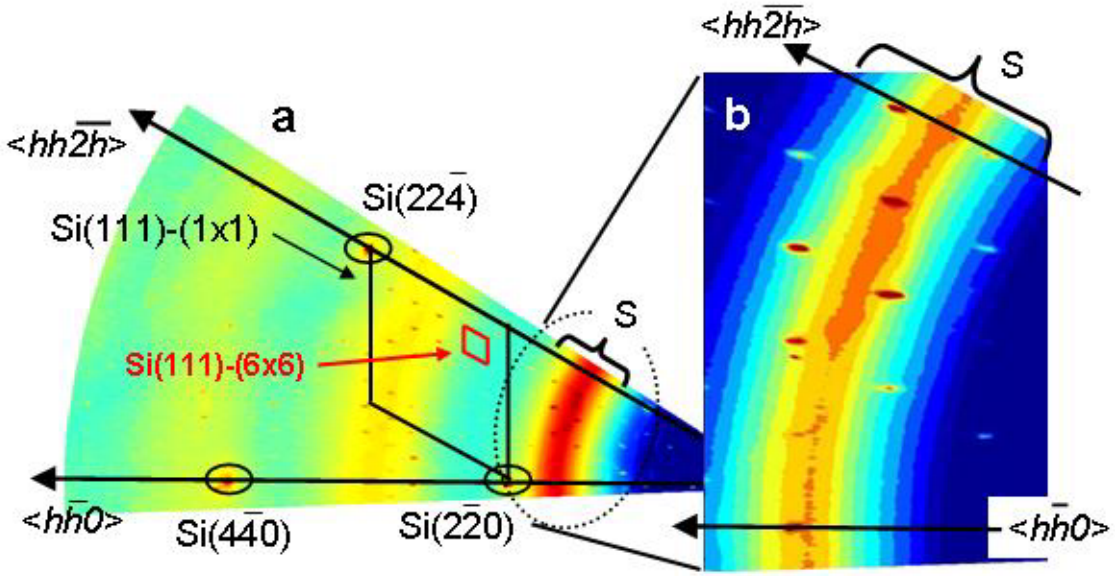

Figure 1: (a): Reciprocal space map of the liquid in its supercooled state on a (6×6) reconstructed Si(111) surface (b):First order maximum of the liquid structure factor in the vicinity of strong (6×6) reconstruction peaks.

[1] A. Greer, Nat. Mater. **5**, 13-14(2006).

[2] T. U. Schülli, R. Daudin, G. Renaud, et al. Nature **464**, 1174 (2010) and A. Lindsay Greer, Nature **464**, 1137 (2010).

Si nanoparticles motion onto SiO_2 driven by chemical reaction: a real time study

F. Leroy, F. Cheynis, Y. Saito, E. Bussmann, T. Passanante, P. Müller

CINaM-CNRS, UPR 3118,Campus de Luminy Case 913, 13288 Marseille cedex 9, France
(corresponding author: F. Leroy, e-mail:leroy@cinam.univ-mrs.fr)

In the literature, recent examples of spontaneous motion of droplets have been provided, especially for liquid droplets on solid surfaces [1-6]. In particular it has been shown that a chemical reaction between a nanoparticle and its underlying substrate can modify locally the interface free energy. The induced asymmetry of the solid/liquid contact can generate a self-propulsion [2]. From a fundamental respect, the motion of a reactive triple-line and its interaction with a time-evolving substrate surface is of high interest.

Here we report on the motion of solid state 3D Si nanoparticles onto SiO_2 substrate. The Si nanoparticles are obtained by dewetting of a thin Si film (20nm thick) onto an amorphous SiO_2 layer [7,8] when annealed at high temperature (T> 750°C). Increasing the temperature in the range 950-1100°C we have measured *in situ* and in real time, by Low Energy Electron Microscopy (LEEM), the motion of Si nanoparticles. This process is concomitant with the chemical reaction $Si_{(3D)} + SiO_{2(substrate)} \rightarrow 2\ SiO_{(g)}$ resulting in a progressive shrinking of the nanoparticles [9] and consumption of the SiO_2 substrate. Following the centre of mass of each nanoparticle we put in evidence that the motion in the small timescale limit is random whereas at late time nanoparticles get trapped inside the hole formed in the SiO_2 substrate induced the chemical reaction. At the very end the Si nanoparticles have completely disappeared giving rise to a conic hole into the SiO_2 layer [9].

From the kinetics of the Si nanoparticles motion an effective diffusion coefficient D_{eff} could be extracted as function of temperature and nanoparticle size. The first stage of Brownian motion is thermally activated with an activation energy E_a=4.1 eV. A clear size-dependent behaviour is also put in evidence $D_{eff} \sim R^{-1/2}$. The shrinking of the nanoparticules is analysed assuming a chemical reaction rate occurring at the interface with gas expelled at the triple line. These experimental results are highlighted by Monte Carlo simulations based on a solid on solid model including surface diffusion processes and chemical reaction kinetics.

Support by ANR PNANO (ANR 08-Nano-036) is gratefully acknowledged.

[1] J. Tersoff, et al. Science 324, 236 (2009).
[2] A. K. Schmid, N. C. Bartelt, R. Q. Hwang, Science 290, 1561 (2000).
[3] C. D. Bain, G. D. Burnett-Hall, R. R. Montgomerie, Nature 372, 414 (1994).
[4] F. D. Dos Santos, T. Ondarçuhu, Phys. Rev. Lett. 75, 2972 (1995).
[5] Y. Sumino, N. Magome, T. Hamada, K. Yoshikawa, Phys. Rev. Lett. 94, 068301 (2005).
[6] K. Ichimura, S.-K. Oh, M. Nakagawa, Science 288, 1624 (2000).
[7] E. Bussmann, et al., New Journal of Physics 13, 043017 (2011).
[8] F. Cheynis et al., Phys. Rev. B in press (2011).
[9] K. Sudoh et al. J. Appl. Phys. 108, 083520 (2010).

Tuning the superlattice bands of the Ag/Cu(111) triangular dislocation network

Zakaria Abd-el-Fattah[1,2], Frederik Schiller[2], F. Javier García de Abajo[3], Manfred Matena[4], and J.Enrique Ortega[1,2,4]

[1] *Departamento de Física Aplicada I, Universidad del País Vasco UPV/EHU, Paseo Manuel Lardizábal 5, E-20018 San Sebastian, Spain*
[2] *Centro de Física de Materiales, Centro Mixto CSIC-UPV/EHU, San Sebastian, Spain*
[3] *Instituto de Optica CSIC, Serrano 121, 28006 Madrid, Spain,*
[4] *Donostia International Physics Center DIPC, San Sebastian, Spain*

Free-electron-like Shockley states of noble metal surfaces are known to scatter strongly at surface defects, such as steps and dislocations. Both types of defects may cristallyze, respectively, in vicinal surfaces, which self-arrange forming one-dimensional (1D) monatomic step lattices, and strained noble metal overlayers, which frequently exhibit two-dimensional (2D) strain-relief patterns. At the 2-4 nm scale such 1D and 2D networks match the Shockley state Fermi wavelength $\lambda_F/2$, leading to Fermi energy gapping, and generally, to strong Fermi surface modulation [1-4].

The Ag/Cu(111) system is a model 2D noble metal dislocation network that exhibits a strongly modulated band structure [1]. Triangular dislocation loops at the Cu substrate form spontaneously by mild annealing, as a way of relaxing on-top positions in the hexagonal Ag/Cu moiré pattern. As a result, the free-electron-like parabola of the strained Ag/Cu moiré transforms into a strongly featured band structure in the strain-free array of triangles, at energies around E_F. Moreover, the threefold symmetry of the array lifts completely the degeneracy at the *K* symmetry point, giving rise to a 25 meV band gap that extends over the entire Brillouin zone [2]. The phenomenon is analogous to that studied in graphene, although in the present case the sixfold symmetry is reduced to threefold by relieving strain, in contrast to the enhanced strain needed to break the sixfold symmetry in graphene.

In the past few years, we have searched the possibility of tuning the Ag/Cu(111) superlattice band gap around the Fermi energy [2-4]. Using potassium as adsorbate one can rigidly shift the surface band, and hence sweep the gap across E_F, but at the cost of increasing inelastic lifetime broadening of surface states [3]. Tuning the temperature also gives us a small tuning range, enough to shift E_F from 30 meV below the gap at 300 K, up to midgap position at 4 K [2]. The most successful method is substrate alloying [4]. Diluting Au in the Cu matrix lowers the surface potential without affecting the scattering properties of the Shockley state in the Ag overlayer. The Figure summarizes the main observations. The band structure shifts down rigidly as a function of the Au concentration, such that the band gap moves entirely across the Fermi energy. A complete Lifshitz transition is thus observed, in which the hole-pocket-like Fermi

surface of the bare Ag/Cu(111) interface turns electron-pocket-like in the Au-alloyed Cu substrate.

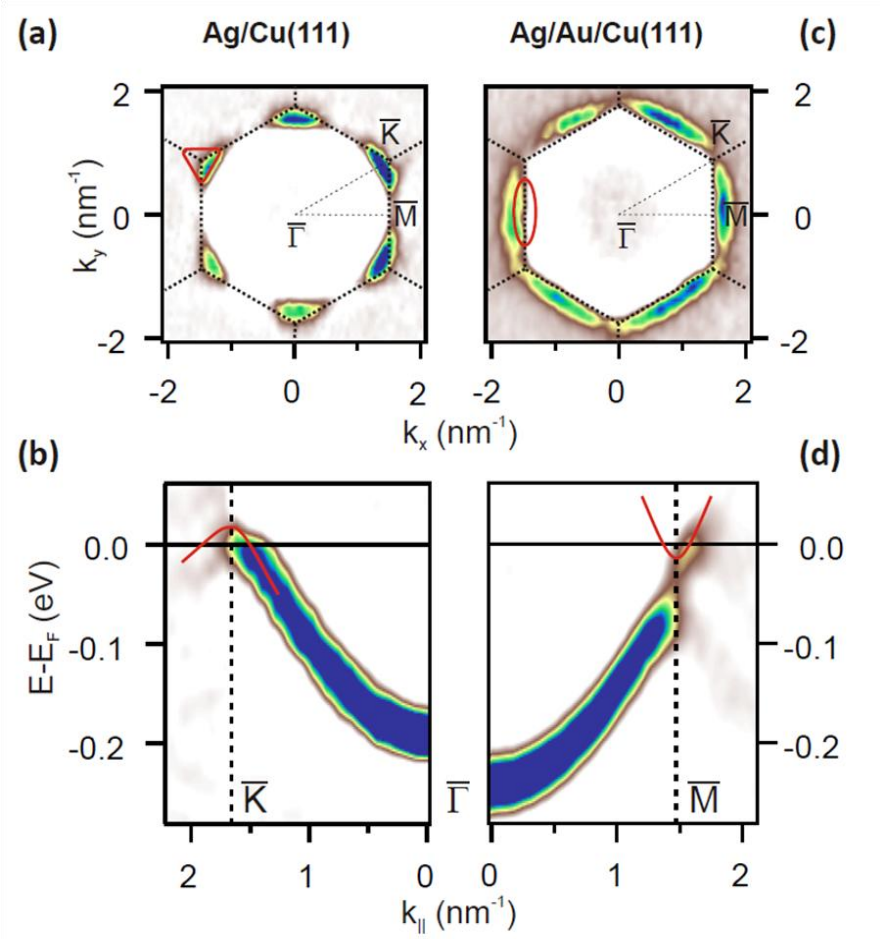

Lifschitz transition in the Ag/Cu(111) dislocation network triggered by adding small amounts of Au to the Cu substrate. *(a) Fermi surface and (b) band dispersion along ΓK for the bare Ag/Cu(111), showing hole pockets at the K point. (c) Fermi surface and (d) band dispersion along ΓX for the alloyed substrate. The intensity moves to the X point where elongated electron pockets arise.*

Support by the Spanish Ministry of Economy (MAT2010-21156-C03-01 and -C03-03) and the Basque Government (IT-257-07) is gratefully acknowledged.

[1] F. Schiller, J. Cordón, D. Vyalikh, A. Rubio, and J. E. Ortega, Phys. Rev. Lett. **94**, 016103 (2005); *ibid* Phys. Rev. Lett. **96**, 029702 (2006).

[2] D. Malterre, B. Kierren, Y. Fagot-Revurat, C. Didiot, F. J. García de Abajo, F. Schiller, J. Cordón and J. E. Ortega, New J. of Phys. **13**, 013026 (2011).

[3] F. J. García de Abajo, J. Cordón, M. Corso, F. Schiller, and J. E. Ortega, Nanoscale **2**, 717-721 (2010).

[4] Z. M. Abd-el-Fattah, M. Matena, M. Corso, F. J. García de Abajo, F. Schiller, and J. E. Ortega, Phys. Rev. Lett. **107**, 066803 (2011).

On the origin of 2DEG states at the surface of layered topological insulators

E.V. Chulkov[1,2], S.V. Eremeev[3,4], M.G. Vergniory[1], T.V. Menshchikova[3],

[1] *Donostia International Physics Center (DIPC), 20018 San Sebastian/Donostia, Basque Country, Spain*
(corresponding author: E.V. Chulkov, e-mail: waptctce@ehu.es)

[2] *Departamento de Fisica de Materiales UPV/EHU, Centro de Fisica de Materiales CFM - MPC and Centro Mixto CSIC-UPV/EHU, 20080 San Sebastian/Donostia, Basque Country, Spain*

[3] *Tomsk State University, 634050, Tomsk, Russia*

[4] *Institute of Strength Physics and Materials Science, 634021, Tomsk, Russia*

The recently discovered three-dimensional topological insulators belong to a class of insulators in which the bulk gap is inverted due to the strong spin-orbit interaction [1]. A direct consequence of such bulk band structure arises at the surface: the spin-polarized topologically protected massless metallic states, forming a Dirac cone. These surface states (SS) exhibit many interesting properties resulting from the fact that the spin of electron is locked perpendicular to its momentum, thus forming a SS spin structure that protects electrons from backscattering. This makes topological insulators potentially promising materials for creation of new quantum devices.

Recently it has been demonstrated by using angle-resolved photoemission spectroscopy (ARPES) that beside the Dirac cone the 2DEG states arise at the surface of Bi2Se3 after a few hours of exposition in vacuum [2], upon deposition of various magnetic [3,4] and non-magnetic atoms [4,5] and molecules as well [6]. These states form a parabolic band(PB) in the energy gap just below the conduction band and M-shaped band in the local gap of bulk-projected valence band. The former bands show an appreciable Rashba spin- splitting Moreover, for several adsorbates [2-6] at the saturation deposition time a second and even third pair of spin-split parabolic states emerges below the conduction band minimum. In the most of these papers the emergence of PB states was ascribed to a confinement of the conduction band states in a quantum well formed by band bending potential produced by adsorption of metallic atoms or residual gases, although in Ref. [6] it was pointed out that the potential gradient from band bending cannot alone be responsible for their Rashba-splitting. Indeed, a model calculation exploiting band bending approach based on the coupled solution of the Poisson and Schrödinger equations yielded the Rashba spin-orbit coupling parameter α_R which is significantly smaller than that extracted from the ARPES data [6]. Moreover, this

approach doesn't reproduce the M-shaped band [2]. The most surprising experimental finding is the absence of interband scattering of the Dirac state electrons in the presence of the PB spin-split states after the deposition of any kind of metal atoms [4]. A study of a naturally aged surface of Bi2Se3 also reveals that scattering rate in the topologically protected state is unaffected by the potential createdby adsorbed atoms or molecules [7].

Here we show on the basis of ab-initio calculations using the VASP code that the driving mechanism of the simultaneous emergence of the parabolic and M-shaped bands in layered TIs Bi2Se3, Bi2Te3, and Sb2Te3, is a widening of the outermost vdW spacing. This scenario also explains the Rashba-type splitting for the PB. We find that besides the emergence of PB states, which are localized in the detached QL the expansion of the vdW spacing results in a relocation of the Dirac state to the lower QL that makes topological and PB states separated in space. This fact explains the observable absence of interband scattering [4,7]. We also show that the expansion of various vdW gaps produces multiple 2DEG states.

[1] M. Z. Hasan and C. L. Kane, Rev. Mod. Phys. 82, 3045 (2010)
[2] M. Bianchi, et al., Nature Comm. 1:128 DOI:10.138/ncomms1131 (2010)
[3] L.A. Wray, et al., Nature Phys. 7, 32 (2011)
[4] Z.-H. Pan, et al., arXiv:1104.0966v1
[5] Z.-H. Zhu, et al., Phys. Rev. Lett. 107, 186405 (2011).
[6] H.M. Benia, et al., Phys. Rev. Lett. 107, 177602 (2011).
[7] S.R. Park, et al., Phys. Rev. B 81, 041405(R) (2010)

Wednesday

Pd and PdAg aerosol nanoparticles for catalysis

S. Blomberg[(1)], N. M. Martin[(1)], J. Gustafson[(1)], J. N. Andersen, E. Lundgren[(1)], L. E. Walle[(2)], A. Borg[(2)], M. E. Messing[(3)], K. Deppert[(3)] and H. Grönbeck[(4)]

(corresponding author: E. Lundgren, e-mail: edvin.lundgren@sljus.lu.se)

[(1)] Div. of Synchrotron Radiation Research, Institute of Physics, Lund University, Sweden

[(2)] Dept. of Physics, Norwegian University of Science and Technology (NTNU), Norway

[(3)] Div. of Solid State Physics, Lund University, Lund, Sweden

[(4)] Competence center for catalysis, Chalmers University, Göteborg, Sweden

Due to the potential economic and environmental rewards, one major goal in catalysis related research is to create cheaper catalysts. As catalysis happens on the surface of the catalyst, one possible way to realize this would be to dilute the more expensive active material with a less costly one, providing that the active material stays at the surface. This could be achieved by using a material which is less prone to interact with the reactant gases, such as a noble metal. In most catalysts, the active material is dispersed in a high area complex oxide support as nanoparticles. In order to maintain a high activity, it would be necessary to ensure that the active material is at the surface of the nanoparticle.

We have initiated a project to investigate whether this approach towards cheaper catalysts is viable. In the present contribution we report on our findings from attempts to produce Pd [1] and PdAg alloy particles using an aerosol deposition technique [2, 3]. Starting with the Pd nano particles, we will in detail describe their production, cleaning, oxidation and reduction. We will also report on their catalytic behavior in the catalytic oxidation of CO and CH_4.

In the second part we will present our results from PdAg nanoparticles. The use of PdAg is motivated by the observation that Pd segregates to the surface in the presence of a reactive gas while Ag segregates in UHV [4] and that Ag is less expensive than Pd.

In Fig, 1(a) we show a Scanning Electron Microscope (SEM) image from aerosol produced PdAg particles with a diameter of 10 nm deposited on a SiO_x substrate. To produce the PdAg particles, one Pd rod and one Ag rod was used as electrodes for the discharge sublimation of both materials with the aim to produce fully alloyed nanoparticles. It can be seen from the SEM image that the particles have a narrow size distribution; however no information on the composition can be obtained. In Fig. 1(b) we show a Transmission Electron Microscope (TEM) image from a PdAg particle with a diameter of 15 nm. X-ray Energy Dispersive Spectoscopy (XEDS) analysis indicates that approximately 65-75% of each particle consists of Pd. Unfortunately, the XEDS does not reveal whether the particle is an alloy or a mixed metal particle with separate Pd and Ag phases.

High Resolution Core Level Spectroscopy performed at I311 at Maxlab and the HPXPS beamline 9.3.2 at ALS, Berkeley provides additional information. In Fig. 1(c) we show the Ag $3d_{5/2}$ spectra from a clean Ag(110) single crystal surface (bottom), the clean $Pd_{75}Ag_{25}(100)$ surface (middle) and from the aerosol PdAg nanoparticles (top) after oxidation using 1 mbar of O_2 and reduction by CO following the cleaning procedure in Ref. [1]. The Ag $3d_{5/2}$ bulk binding energy displays a shift of 0.5 eV between the pure metal and the $Pd_{75}Ag_{25}$ alloy [5]. Previous measurements [6, 7] and our Density Functional Theory (DFT) calculations [5] confirm the large alloy induced Ag $3d_{5/2}$ shift. Comparing the Ag $3d_{5/2}$ bulk binding energy in $Pd_{75}Ag_{25}(100)$ with the bulk Ag $3d_{5/2}$ binding energy from the PdAg particles, it is immediately clear that they are almost identical. We therefore conclude that the aerosol PdAg alloy particles consist of an alloy and not Ag and Pd in

separate phases. Turning to Fig. 1(d) we show the Pd $3d_{5/2}$ core level from the Pd(100) (bottom), the $Pd_{75}Ag_{25}$(100) (middle) and from the PdAg nanoparticles (top). The surface core level shift of the alloy is opposite to that of the pure metal, an observation confirmed by theory [4]. Again, the bulk binding energy of the Pd $3d_{5/2}$ from the PdAg particles coincides with that from the $Pd_{75}Ag_{25}$(100) and deviates from the pure Pd metal. Further, most of the intensity from the spectra originates from a CO induced shifted Pd component indicating Pd at the surface of the nanoparticles after reduction.

Armed with the above described characterization of the PdAg particles, we have studied the oxidation and CO reduction of these particles using HPXPS. These studies will be compared to the results from the Pd nanoparticles.

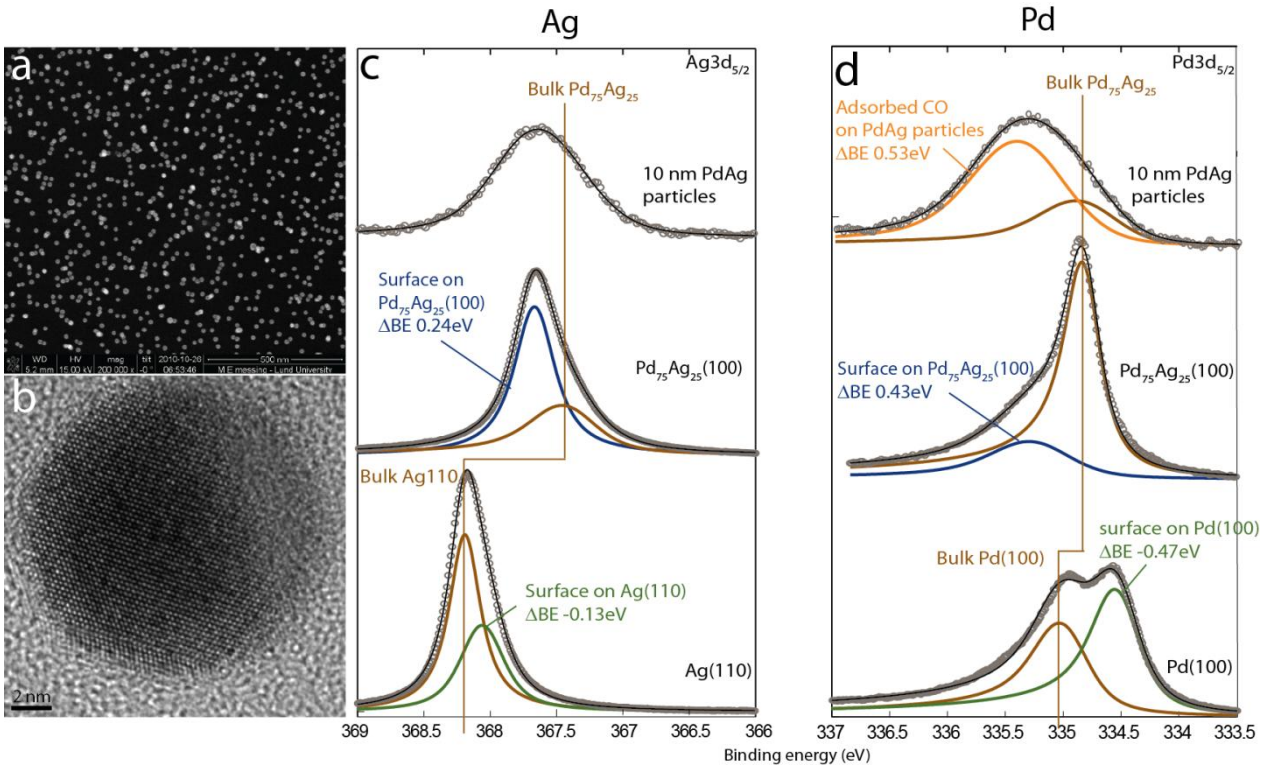

Figure 1 (a) SEM image from 10 nm large aerosol deposited PdAg particles on SiOx. **(b)** TEM image of a 15 nm large PdAg particle on a TEM grid. **(c)** Ag $3d_{5/2}$ core level spectra from Ag(110), $Pd_{75}Ag_{25}$(100) and the aerosol PdAg particles. Note the shift between the bulk binding energy of the pure metal and the alloy. **(d)** Pd $3d_{5/2}$ core level spectra from Pd(100), $Pd_{75}Ag_{25}$(100) and the aerosol PdAg particles after oxidation and CO reduction.

References

[1] R. Westerström *et al*, Phys. Rev. B. **83** (2011) 115440.
[2] M. E. Messing, K. A. Dick, L. R. Wallenberg, K. Deppert, Gold Bull. **42** (2009) 20.
[3] M. E. Messing *et al* J. Phys. Chem. C. **114** (2010) 9257.
[4] L. E. Walle *et al*, in preparation.
[5] P.T. Wouda, M. Schmid, B.E. Nieuwenhuys, P. Varga, Surf. Sci. **417** (1998) 292.
[6] W. Olovsson, L. Bech, T. H. Andersen, Z. Li, S. V. Hoffmann, B. Johansson, I. A. Abrikosov, J. Onsgaard, Phys. Rev. B **72** (2005) 075444.
[7] N.A. Khan , A. Uhl, S. Shaikhutdinov, H.-J. Freund Surf. Sci. **600** (2006) 1849.

Atomic structure of graphene supported metal nanoparticles

A. Stierle, D. Franz, V. Kilic, U. Hejral, T. Gerber[1], T. Michely[1]

AG Festkörperphysik / Grenzflächen, Universität Siegen, D-57072 Siegen, Germany
(corresponding author: A. Stierle, e-mail: andreas.stierle@uni-siegen.de)

[1] *II. Physikalisches Institut, Universität zu Köln, D-50937 Köln, Germany*

Supported metal nanoparticles play an important role as heterogeneous catalysts for a huge variety of chemical reactions, which makes a fundamental, atomic scale understanding of their working principles desirable. In many cases nanoparticles with a diameter < 10 nm are employed to enhance the active surface area and to benefit from effects such as higher reactivity from undercoordinated atoms at corners, edges and in the vicinity to the support or size dependent electronic effects. A pronounced size dependence of the catalytic activity for CO oxidation was e.g. reported for Au at a particle size of 3 nm [1]. To be able to implement structure – activity relationships an atomic scale characterization of the nanoparticles is needed preferably under in-situ reaction conditions, which is a highly demanding task for a real catalyst material because of its complexity. To overcome this difficulty, we have recently developed synchrotron radiation based x-ray diffraction schemes [2,3], which allow an atomic scale characterization of model catalysts composed of epitaxial metal nanoparticles on oxide single crystal supports.

In my presentation I will demonstrate how this approach can be extended to the characterization of nanoparticles / clusters with a diameter smaller than 1-2 nm, which may exhibit not only enhanced catalytic activity but also interesting magnetic and electronic properties. By the use of graphene on an Ir(111) as a template, extremely well ordered high density arrays of nearly identical nanoparticles can be prepared [4,5], giving rise to superlattice diffraction peaks, which disclose atomic scale structural information on the clusters and their interface to the graphene / Ir(111) substrate.

Support by the German Federal Ministry of Research and Education (BMBF) within the project “NanoXcat” is gratefully acknowledged.

[1]: M. Valden, X. Lai, D. W. Goodman, Science 281, 1647 (1998)

[2]: P. Nolte, A. Stierle, N. Y. Jin-Phillipp, N. Kasper, T. U. Schulli, H. Dosch, Science 321, 1654 (2008)

[3]: P. Nolte, A. Stierle, N. Kasper, N. Y. Jin-Phillipp, H. Reichert, A. Rühm, J. Okasinski, H. Dosch, S. Schöder, Phys. Rev. B 77, 115444 (2008)

[4]: A. T. N’Diaye, S. Bleikamp, P. J. Feibelman und T. Michely, Phys. Rev. Lett. 97, 215501 (2006)

[5]: A. T. N’Diaye, T. Gerber, C. Busse, J. Myslivecek, J. Coraux, T. Michely, New J. Phys. 11, 103045 (2009)

From basic research in UHV to applied research under ambient conditions: Recent developments in Surface Science Equipment

T. U. Kampen, S. Mähl, and S. Schmitt

SPECS Surface Nano Analysis GmbH, Voltastr. 5, 13355 Berlin, Germany
(corresponding author: T. U. Kampen, e-mail:Thorsten.Kampen@specs.com)

Two of the most important tasks for research and development are: miniaturization for sophisticated applications down to the nanoscale, and designing low cost large scale devices. In both fields the device performance is strongly determined by materials quality, composition, combination and last but not least by processes at materials surfaces and interfaces.

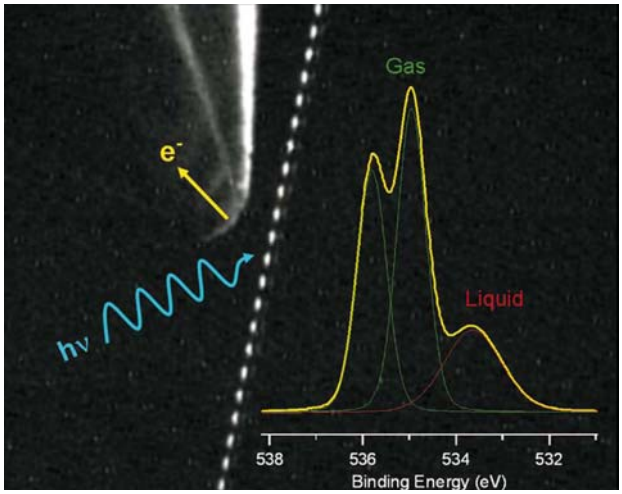

Figure 1:
Stroboscopic photograph of a droplet jet prepared from a 40% ethanol solution in front of the entrance aperture (diameter 0.3 mm) of the differentially PHOIBOS analyzer. The O1s spectrum of the methanol solution droplets is recorded with an incident photon energy of 938 eV. Both gas phase and liquid phase photoemission peaks are visible in the spectrum [1].

Two of the most established techniques for surface and interface analysis are photoelectron spectroscopy (PES) and scanning probe microscopy (SPM). Both techniques already reveal important insights in classical well defined model experiments under ultra-high vacuum conditions. But analysis of materials and devices in near ambient conditions and even in-situ during operation is a mandatory prerequisite for the development and quality management of functional thin films and devices. In this respect the application of techniques like Near Ambient Pressure XPS, XPS from liquids and solid liquid interfaces, hard x-ray PES (HAXPS), as well as Near Ambient Pressure SPM for microscopy studies on the dynamics of

surface reactions is the challenging task for manufacturing companies of surface analytical equipment.

Nowadays, electron spectrometers can be operated in a kinetic energy range from nearly zero electron volt up to 15 keV and more, with acceptance angles of 60° and an angular resolution of well below 0.1°. For data acquisition under such conditions detectors have been improved in sensitivity, lateral and time resolution. Nowadays spectroscopic features with a count rate of 5 counts/second or less can be detected. In addition, these spectrometers can now be operated at pressures up to 25 mbar due to an intelligent design of differentially pumped electron optics. As an example Figure 1 shows a photograph taken during an experiment, where a droplet jet of an ethanol solution is investigated by photoemission spectroscopy.

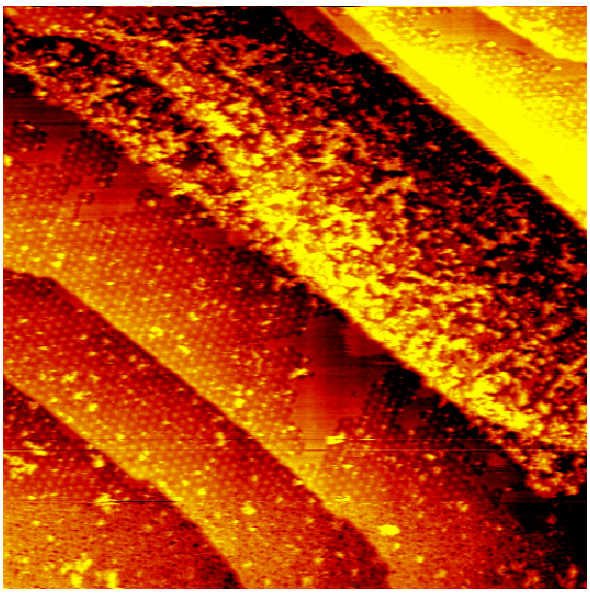

Figure 2:
Graphene and O(2x2) on Ru(0001). STM image has been taken at 11mbar and 510K sample temperature.

One key design parameter for both, Near Ambient Pressure XPS and Near Ambient Pressure SPM, is to reduce the gas load on the analysis system to a minimum. This is achieved by minimizing the volume in which the reactions and the in-situ analysis takes place. As a result experimental conditions are highly reproducible, minimum amounts of reactants are used, and times for sample transfer are reduced. The data shown in Figure 2 has been taken in a Near Ambient Pressure SPM, where the reaction cell consists of just the STM head and the sample stage. The image was taken under a pressure of 11 mbar and a sample temperature of 510 K.

[1] D. E. Starr, E. K. Wong, D. R. Worsnop, K. R. Wilson and H. Bluhm, Phys. Chem. Chem. Phys. 10, 3093 (2008)

A new type of detector for dynamic XPS measurements

P. Baumann, B.Krömker, G. Prümper, K.Winkler, M.Maier, A. Feltz

Omicron NanoTechnology GmbH, D-65599 Taunusstein, Germany
(corresponding author: M. Maier, e-mail: m.maier@omicron.de)

Real time observation of fast processes occurring in a time window of a few milliseconds to a few minutes have always been difficult to observe by x-ray excited photoemission (XPS) studies under laboratory conditions. However, the demand to understand the chemistry of surface processes e.g. during heating processes, electro migration and diffusion is of high relevance in various research fields.

In this contribution, we will report on first results of a new multi-anode detector concept with 128 individual anodes, preamplifiers and counters. It has the capability to allow of quantitative XPS studies on fast time scales with good signal to noise ratio excited with a monochromated Al Kα laboratory source. The detector can be operated in snapshot XPS mode. This mode allows recording an energy window in the spectrum versus time with high repetition-rates and good energy resolution, e.g. a 15 eV detectable energy window with an approximate energy resolution of 0.5 eV.

As an early application we report on results of removing an in-situ grown SiO_2 layer on a Si substrate. The measurement was made during a sample temperature ramp from 600 to 900° Celsius within a time frame of one hour. The target of the experiment was to analyze the time window in which the oxide was removed.

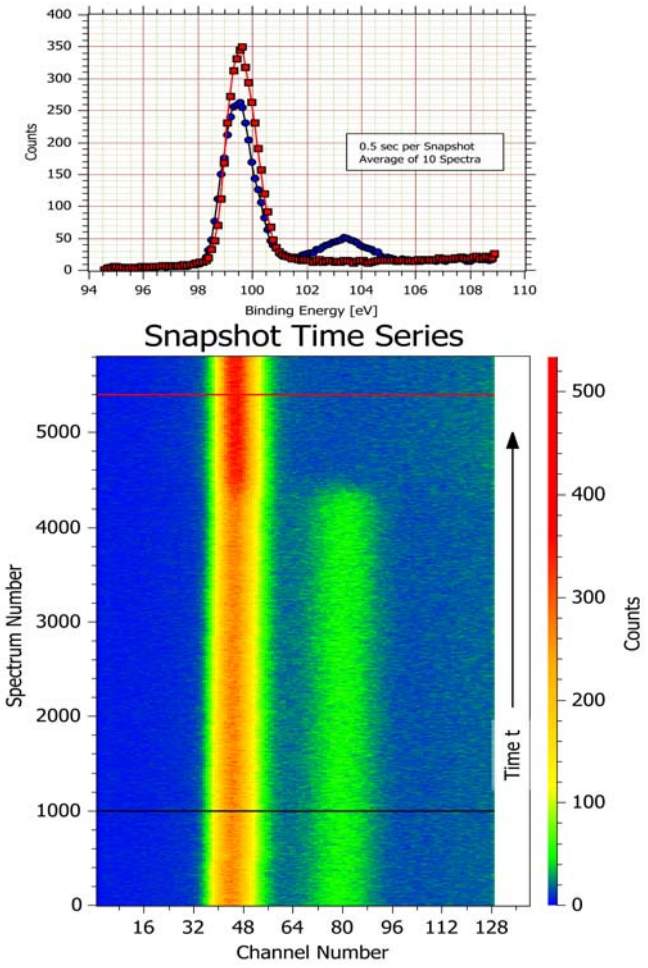

Fig. 1: Bottom: XPS snapshot series of about 6000 spectra recorded with a 128 channel detector on the Si 2p peak with a time span of one hour. Sample: SiO_2/Si. Top: Spectra before (black) and after (red) the removal of the oxide. The two lines indicate the position of the spectra in time.

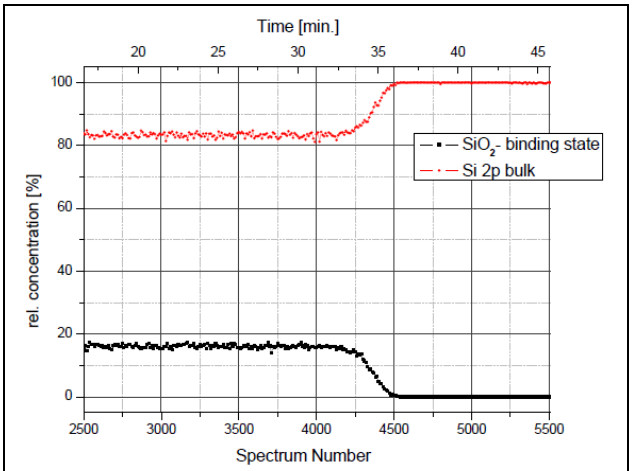

Fig. 2: Relative concentration of the SiO_2-binding state and Si 2p bulk component vs. time.

Snapshot spectra have been recorded with an acquisition time of 0.5 seconds per spectrum to follow the evolution of the subcomponents $Si4^+$ to Si^0 during the heating process of the Silicon, see Fig.1. The snapshot series with >5000 spectra shows the evolution of the peak versus time. The complete removal of the oxide occurred at a very small temperature window around 850°C. A closer look into the data revealed that the removal of the oxide from the silicon took place in about 2.5 minutes. Within this transition time 300 spectra have been recorded.

Postersession

Step Permeability on the Pt(111) Surface

K.L. Man and M.S. Altman

Department of Physics, Hong Kong University of Science and Technology,
Clear Water Bay, Kowloon, Hong Kong
(corresponding author: M.S. Altman, e-mail: phaltman@ust.hk)

Atomic steps are common defects at surfaces that may influence surface properties and can play an important role in many physical and chemical phenomena. The key role that steps play, for example, as sites for incorporation or removal of atoms is particularly evident in the changes in step morphology that occur when steps move during crystal growth, sublimation and coarsening. The resulting step morphology will be affected, or can even be dictated, by the nature of the kinetic processes that mediate step motion. Step motion kinetics are collectively defined in terms of surface diffusion, step attachment/detachment and step permeability. Step permeability, in particular, refers to the diffusive motion of an atom between adjacent terraces without attachment at the intervening step. Asymmetry of step attachment with respect to the direction an atom approaches a step is recognized to be an important and possibly common cause of step morphological instabilities during step flow growth [1,2]. However, manifestation of this effect depends upon the relative rates of surface diffusion and step attachment, i.e., the rate-limiting step or kinetic regime, as well as upon the status of step permeability [3]. Although surface diffusion and the origins of step attachment asymmetry have been studied extensively, experimental investigations of step permeability are extremely rare, and nothing is known about permeability on metal surfaces. Part of the problem is that reliable methods for evaluating permeability are lacking. The scarcity of experimental results pertaining to step permeability undoubtedly contributes to the fact that its physical origins at the atomistic level are still not well understood. Furthermore, without reliable experimental information on this overlooked phenomenon, it cannot be treated appropriately in theoretical modeling of epitaxial growth, particularly in step morphological evolution.

In the present work, we have investigated step permeability on the Pt(111) surface using a new experimental approach. Information about permeability is obtained from measurements of step velocity during step flow growth that were made using low energy electron microscopy (Fig. 1). In accordance with basic expectations, step velocity is found to increase with decreasing step density. The dependence of step velocity upon adjacent terrace width also provides qualitative evidence of asymmetric step attachment and step permeability. In particular, for fixed sum of the leading and trailing terrace width, steps bounded by larger leading terrace move faster than those bounded by larger trailing terrace. This is consistent with the known presence of an Ehrlich-Schwoebel barrier on this surface [4]. Permeability is evident in the fact that step velocity extrapolated to zero terrace width is non-zero.

Step velocity is modeled by solving the diffusion equation simultaneously on several adjacent terraces subject to boundary conditions at intervening steps that include asymmetric step attachment and step permeability. This analysis allows a quantitative evaluation of step permeability and the kinetic length, which characterizes the rate-limiting step continuously between the diffusion and attachment/detachment limited regimes. This work provides information that is greatly needed to set physical bounds on the parameters that are used in theoretical treatments of growth. The observation that steps are permeable even on a simple metal surface should also stimulate more experimental measurements and theoretical treatments of this effect.

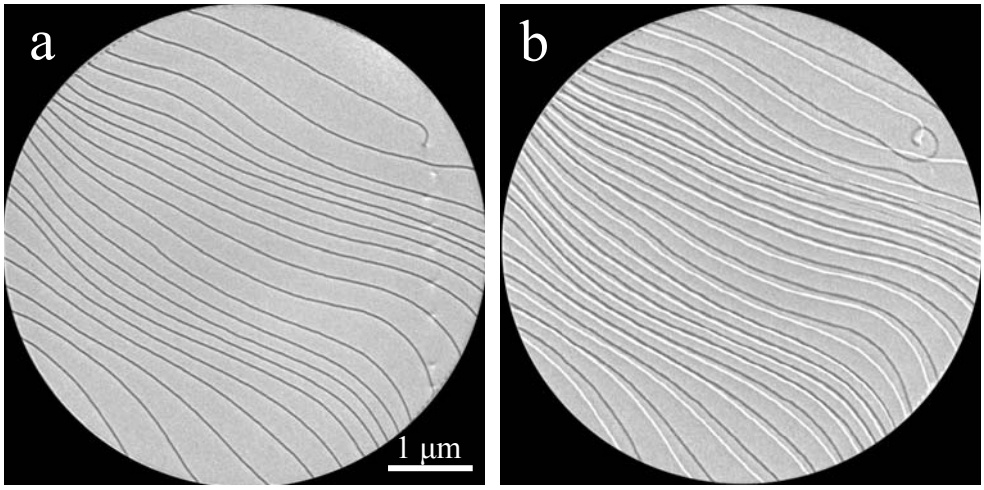

Fig. 1: LEEM images reveal atomic step motion during step flow growth on the Pt(111) surface at 800K. The dark lines indicate step positions (a) initially before growth and (b) after deposition of 0.8 ML. The initial step positions are also indicated by white lines in (b). Steps move from the upper right to the lower left except for the spiral growth around the screw dislocation in the upper right.

This work was supported by the Hong Kong Research Grants Council under Grant No. HKUST600108.

References

[1] R.L. Schwoebel and E.J. Shipsey, J. Appl. Phys. **37**, 3682 (1966).

[2] G.S. Bales and A. Zangwill, Phys. Rev. B **41**, 5500 (1990).

[3] W.F. Chung and M.S. Altman, Phys. Rev. B **66**, 075338 (2002).

[4] K. Kyuno and G. Ehrlich, Phys. Rev. Lett. **81**, 5592 (1998).

A First-Principles Determination of the Thickness of the Protective Oxide Layer of Aluminum.

Jakub D. Baran, Henrik Grönbeck and Anders Hellman

Competence Centre for Catalysis and Department of Applied Physics
Chalmers University of Technology, SE-412 96, Göteborg, Sweden
jakub.baran@chalmers.se

Aluminum is readily oxidized when exposed to an oxidizing environment. However, bulk oxidation is prevented by the formation of a thin nanometer sized protective metal-oxide layer. The kinetics of the growth of thin oxide film is generally described by the Cabrera-Mott (CM) model [1]. In this model, negatively charged oxygen atoms are formed on the surface by electron tunneling through the film from the metal and the created electric field drives ionic transport and further oxidation. Although conceptually very powerful, the CM model lacks the support from first-principles calculations. Recently, however, a novel bond mechanism for molecular adsorbates on metal supported ultrathin oxide films has been suggested [2-4]. The bond mechanism is long ranged and provides an interpretation of the CM model in terms of the electronic structure of the oxide/metal system.

Here we present first-principles calculations of O_2 adsorption on Al_2O_3 supported on Al(111) that can explain the thickness of the protective oxide layer.

[1] N. Cabrera, N. F. Mott, Rept. Progr. Phys. 12 (1948-49) 163.
[2] G. Pacchioni, L. Giordano, M. Baistrocchi, Phys. Rev. Lett. 94 (2005) 226104.
[3] H. Grönbeck, J. Phys. Chem. B, 100 (2006) 11977.
[4] A. Hellman, H. Grönbeck, Phys. Rev. Lett. 100 (2008) 116801.

Electronic excitations of slow ions in a free electron gas metal: evidence for charge exchange effects

D. Primetzhofer, S. Rund, D. Roth, D. Goebl, and P. Bauer

Institut für Experimentalphysik, Johannes-Kepler Universität Linz, A-4040 Linz, Austria

The interaction of ions with an electron gas is considered to be a robust and reliable concept. Many years ago it was successfully applied to model electronic stopping of light ions in metals [1 - 5]. As a striking result, theory predicted that in an electron gas of sufficiently low density (like in Mg or in alkali metals), He ions lose less energy due to electron-hole pair excitation than H ions, when they are sufficiently slow ($v << v_0 = c/137$) [4]. This prediction, however, has not been confirmed up to now, although many attempts were made [6 - 9].

Here, we present a study of electronic energy loss of light ions transmitted through nm-films of Al at very low ion velocities [10]. For hydrogen, the electronic stopping power S is found to be perfectly proportional to velocity, as expected for a free electron gas. For He, S shows a transition between two distinct regimes, in both of which S is velocity proportional – however with remarkably different slopes. This finding can be explained as a consequence of charge exchange in close encounters between He and Al atoms, which represents an additional energy loss channel, independent of electron-hole pair excitation in a binary collision. Since these processes exhibit a strong distance dependence, a pronounced coupling between elastic collisions and inelastic energy loss results.

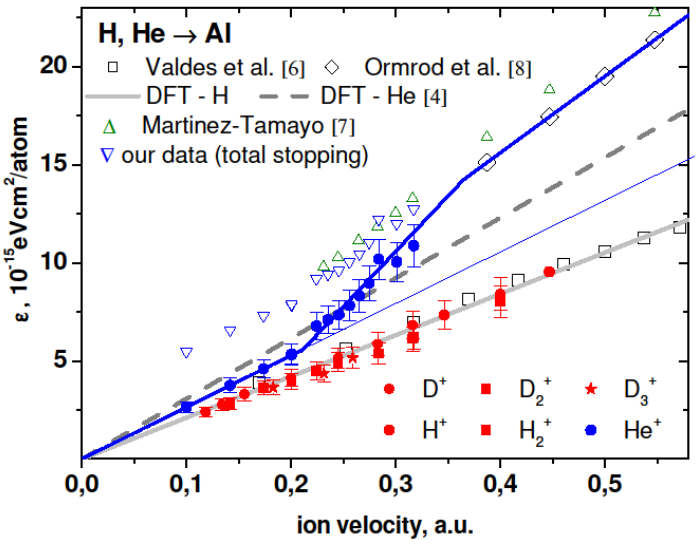

Fig.1 Electronic stopping power S of H,D, and He ions in Al as a function of velocity. Also shown are data from [6 - 8]. Predictions from DFT for slow H and He in a FEG are shown as full and dashed grey line respectively [4].

These findings are not a peculiarity of the He-Al system, but of general relevance: on the one hand, it explains why slow He ions exhibit stronger electronic interactions in FEG metals than predicted by theory [9]. On the other hand, the effectiveness of electronic energy loss of He ions in large band gap insulators like SiO_2 can be understood [11].

Consequently, the validity of theory is confirmed for H ions up to velocities $v/v_0 \approx 1$. In contrast, for He ions it is restricted to sufficiently low velocities, where projectiles, which experienced charge exchange in a close collision, do not contribute to the experimental signal. For He and Al, this corresponds to $v/v_0 < 0.2$. For higher He velocities, a realistic description of the energy loss has to include a distance dependent contribution to the energy loss due to electronic excitations in charge changing collisions is important. Also a dependence of effective electronic energy loss on the experimental geometry has to be anticipated in this regime. For a more detailed understanding, a thorough theoretical analysis of the underlying processes is requested, and further experiments on appropriate systems will be elucidative.

Support by the Fonds zur Förderung der Wissenschaftlichen Forschung (projects P19595 and P20831) is gratefully acknowledged. The authors express their gratitude to P. Zeppenfeld and A. W. Hassel for interesting discussions.

[1] E. Fermi and E. Teller, Phys. Rev. 72 (1947) 399.
[2] J. Lindhard, Mat. Fys. Medd. Dan. Vid. Selsk. 28 (1954) 57.
[3] R.H. Ritchie, Phys. Rev. 114 (1959) 644.
[4] P.M. Echenique, R.M. Nieminen, and R.H. Ritchie, Solid State Commun. 37 (1981) 779.
[5] A. Mann and W. Brandt, Phys. Rev. B24 (1981) 4999.
[6] J.E. Valdes, G. Martinez Tamayo, G.H. Lantschner, J.C. Eckardt, N.R. Arista, Nucl. Instrum. Meth. 73 (1993) 313.
[7] G. Martinez Tamayo, J.C. Eckardt, G.H. Lantschner, and N. R. Arista , Phys. Rev. A54 (1996) 3131.
[8] J.H. Ormrod, J.R.Mac Donald, and H.E. Duckworth, Can. J. Phys. 43, (1965) 275
[9] M. Bergsmann, P. Hörlsberger, F. Kastner, and P. Bauer, Phys. Rev. B58 (1998) 5139.
[10] D. Primetzhofer, S. Rund, D. Roth, D. Goebl, and P. Bauer, Phys. Rev. Lett. 107 (2011) 163201.
[11] S. N. Markin, D. Primetzhofer, and P. Bauer, Phys. Rev. Lett. 103 (2009) 113201.

Electron dynamics in Pb/Si(111) investigated with time-resolved photoelectron spectroscopy

L. Rettig[1,2], P. S. Kirchmann[3], X. Zubizarreta[4,5], V. M. Silkin[4,5], E. V. Chulkov[4,5], M. Sandhofer[1], P. Zhou[1], M. Ligges[1], U. Bovensiepen[1]

[1] *Fakultät für Physik und Zentrum für Nanointegration (CeNIDE), Universität Duisburg-Essen, 47048 Duisburg, Germany*

(corresponding author: U. Bovensiepen, e-mail: uwe.bovensiepen@uni-due.de)

[2] *Fachbereich Physik, Freie Universität Berlin, Arnimallee 14, 14195 Berlin, Germany*

[3] *Physikalische Chemie, Fritz-Haber-Institut der MPG, Faradayweg 4-6, 14195 Berlin, Germany*

[4] *Donostia International Physics Center (DIPC), Paseo de Manuel Lardizabal, 4, 20018 San Sebastian/Donostia, Basque Country, Spain*

[5] *Departamento de Física de Materiales, Facultad de Ciencias Químicas, UPV/EHU, 20080 San Sebastian, Basque Country, Spain*

Relaxation of optically excited, hot electrons proceeds in metals on ultrafast timescales typically within femtoseconds. The microscopic processes responsible for this relaxation comprise electron-electron, electron-phonon, and electron-impurity scattering. A detailed analysis of these processes was performed at surfaces and interfaces using conventional and femtosecond time-resolved photoelectron spectroscopy, which facilitated a separation of the individual scattering contributions [1]. A first step towards an analysis on a similar microscopic level of electronic relaxation in bulk metals could be made by such studies for epitaxial metallic films. Here results of time-resolved two-photon photoemission, time-resolved linear photoemission, and a line width analysis of data from laser photoemission as a function of temperature will be presented for epitaxial Pb films on Si(111).

Pb is adsorbed at 100 K on the Si(111)-$\sqrt{3}\times\sqrt{3}$-R30°-Pb reconstruction that serves as a wetting layer for the epitaxial film growth. In order to analyze films at thicknesses of integer number of monolayers (ML) films are grown in a wedge shape by moving the substrate with respect to a fixed shutter edge. As a result of the reflection of the electron wave functions in the energy interval of the Si band gap electron quantum well states (QWS) are formed in the Pb film. Occupied and unoccupied states are analyzed as a function of film thickness by combining linear (1PPE) and two-photon photoemission (2PPE), respectively. The well known [2,3] intensity contrast with a close to two ML periodicity for odd and even number of ML is reproduced in 1PPE and extended to the unoccupied energy range by 2PPE. Time-resolved measurements establish a similarly strong contrast in the electronic lifetimes for odd and even number of ML, which is explained by the respective difference in binding energy with respect to the Fermi level E_F. We find a remarkable quantitative agreement with a

parameter-free description of the hot electron lifetimes following the Fermi-Liquid theory for the QWS within the Si band gap, which represents relaxation through e-e scattering. For QWS resonant with the Si conduction band lifetimes are overestimated by the Fermi-liquid description, which we explain by electron transfer contributions to the substrate in the measured relaxation rates [4]. A time-resolved analysis of the occupied QWS unveils a photoinduced increase in binding energy up to 60 meV within 100 fs, i.e. at time delays where the excess energy resides in the electronic system. An analysis of the binding energy change as a function of film thickness leads us to the conclusion that this effect originates from an ultrafast modification of the Fermi level pinning which is determined by the photoinduced charge transfer across the Pb/Si interface [5].

In addition, we have analyzed the e-ph contribution to the scattering rates by a temperature-dependent analysis of the photoemission line width of occupied QWS for 40 K < T < 170 K. An earlier study suggested that the e-e and e-ph contribution are comparable for states in the vicinity of the Si band gap [6]. In our recent study we find an e-ph coupling constant λ=0.8 (2) which is clearly smaller than earlier theoretical results [6]. Note that temperatures up to 170 K anneal the Pb films which we can identify from an anomalous temperature dependent line width above 120 K and a line width reduction measured at 40 K from 110 meV before to 90 meV after thermal cycling. These results establish the Pb/Si(111) system as very promising for future angle-dependent 2PPE studies with the goal to analyze defect mediated scattering directly in the time domain.

Support from the Deutsche Forschungsgemeinschaft through Sfb 616 and BO 1823/2 and from Ministerio de Ciencia y Tecnologia (grant FIS2007-66711-C02-01) is gratefully acknowledged.

[1] U. Bovensiepen, H. Petek, M. Wolf, (eds.), *Dynamics at solid state surfaces and interfaces,* Vol. 1, Wiley-VCH, Weinheim, 2010.

[2] M. H. Upton, C. M. Wei, M. Y. Chou, T. Miller, T.-C. Chiang, Phys. Rev. Lett. **93**, 026802 (2004).

[3] J. H. Dil, J. W. Kim, T. Kampen, K. Horn, A. R. H. F. Ettema, Phys. Rev. B **73**, 161308 (2006).

[4] P. S. Kirchmann, L. Rettig, X. Zubizarreta, V. M. Silkin, E. V. Chulkov, U. Bovensiepen, Nature Physics **6**, 782 (2010).

[5] L. Rettig, P. S. Kirchmann, U. Bovensiepen, submitted.

[6] I.-P. Hong, C. Brun, F. Patthey, I. Y. Sklyadneva, X. Zubizarreta, R. Heid, V. M. Silkin, P. M. Echenique, K. P. Bohnen, E. V. Chulkov, W.-D. Schneider, Phys. Rev. B **80** (R), 81409 (2009).

UHV-IR-spectroscopy on metal oxide surfaces

Maria Buchholz[1], Mingchun Xu[1], Yuemin Wang[2], Alexei Nefedov[1], Christof Wöll[1]

Institute of Functional Interfaces, Karlsruhe Institute of Technology,
76344 Eggenstein-Leopoldshafen, Germany
(corresponding author: M. Buchholz, e-mail: maria.buchholz@kit.edu)

[1] *Chair of Industrial Chemistry, Ruhr University Bochum, 44801 Bochum, Germany*

The role of metal oxides is central in many technological areas such as gas sensing, catalysis and thin film growth. In particular, zinc and titanium oxides are very important for photocatalysis and photooxidation[1]. Moreover, in the Graetzel-cell, organic molecules bound to TiO_2 substrates via carboxylate bonds effectively convert photons into electric energy. Owing to the fact that many Dye Sensitized Solar Cells (DSSCs) consist of dyes grafted to the oxide support via carboxylate groups, determination and control of the adsorption of carboxylic acids on oxide substrates is fundamental for understanding the energy transfer from the molecule to the substrate.

In last decades numerous IR investigations of metal oxide powders, including the different modifications of TiO_2, have been reported, however an unambiguous assignment of the features in the complex IR spectra recorded for molecules bound to the oxide powders is quite complicate. Otherwise, it could be possible on the basis of data recorded for well-defined reference systems, e.g. surfaces of single crystals, but, unfortunately, studies on oxide single crystals are extremely scarce due to the fact that the sensitivity of reflection IR-spectroscopy for molecular adsorbates is two orders of magnitude lower for oxides than for metal single crystals. Only recently it became possible to overcome these technical problems by employing a novel, advanced spectrometer.[2]

Here, we demonstrate the performance of this highly sensitive IRRAS-setup by presenting high-quality IR-spectra obtained for different molecules, namely small acids and alcohols. For the present experiments, monolayers of terephthalic acid (TPA) and benzoic acid (BA), as well as methanol and ethanol were deposited under UHV conditions on a rutile $TiO_2(110)$ surface at room temperature. Subsequently the sample was transferred in the main chamber for a characterization in a highly sensitive UHV IRRAS system. The deposition and measurement of the alcohols on the surface were done directly in the analysis chamber. While for BA the expected bidentate carboxylate bonding is observed, for TPA molecule the presence of two carboxylic acid groups leads to interesting complications. The IR-spectra allow, in particular, to answer on the question which could not be answered by the results from x-ray absorption spectroscopy and the scanning probe techniques[3], whether the carboxylic acid group is still protonated for the TPA species on the surface. Since we can detect the carbonyl stretching vibration and the carboxylic acid stretching vibration we conclude that the TPA molecules adsorb on the $TiO_2(110)$ surface in the protonated state.

M. Buchholz gratefully acknowledges the financial support from the Helmholtz Research School "Energy-Related Catalysis".

[1] M. C. Xu, Y. K. Gao, E. M. Moreno, M. Kunst, M. Muhler, Y. M. Wang, H. Idriss, C. Wöll, *Phys. Rev. Lett.* **2011**, *106*, 138302.
[2] Y. Wang, A. Glenz, M. Muhler, C. Wöll, *Rev. Sci. Instrum.* **2009**, *80*, 113108-113106.
[3] P. Rahe, M. Nimmrich, A. Nefedov, M. Naboka, C. Wöll, A. Kühnle, *Journal of Physical Chemistry C* **2009**, *113*, 17471-17478.

Phonon dispersion curves of Bi_2Se_3 ultra-thin quintuple layers

Vasse Chis[1] and Eugen V. Chulkov[1,2]

[1] *Donostia International Physics Center - DIPC,*

Paseo Manuel de Lardizabal 4, 20018 Donostia-San Sebastian, Spain,

vasse.chis@yahoo.com

[2] *CFM, Centro Mixto CSIC-UPV/EHU,*

Departamento de Fisica de Materiales, UPV/EHU,

Apdo. 1072, 20080 San Sebastian, Spain

Density functional perturbation theory is applied to calculate the dynamical properties of ultra-thin quintuple layers (QL) of Bi_2Se_3. Bi_2Se_3 is considered as a layered material where the building blocks consist of alternating bismuth and selenium layers in the form of QL's. The work is partially motivated by the lack of theoretical predictions of the dynamical properties of the class of materials from *first-principles* calculations[1].

Previous experimental[2–4] studies of semi-infinite crystal surface and down to ultra-thin QL of Bi_2Se_3 were carried out by means of Raman spectroscopy which gives access to Raman active zone center phonon modes in the vicinity of a surface. A more recent study employing Helium Atom Scattering (HAS) reveal several modes dispersing along the surface Brillouin zone symmetry directions with surface character. A surprising reported result from the HAS experiments[5] is the occurrence of a Kohn-anomaly at long wave lengths for a surface/resonance phonon mode. Although the experiments were carried out for a semi-infinite Bi_2Se_3 crystal surface, we are able to address and characterize several features that appears within the experimental results. HAS is a very surface sensitive spectroscopy tool where the helium atoms are scattered by the phonon induced modulation of the charge density at distances of 2-4 Ångström away from the surface. Within the energy resolution of the experiments we find that most of the reported modes, either they are pure surface modes or surface resonance modes, have their largest vibrational amplitude within the second atomic layer of the QL's. The modes with predominantly selenium character have much higher energy than modes with bismuth character due to the

large bismuth selenium weight ratio of about 2.5. A different consequence of the large weight ratio is that now the Rayleigh mode is located within the second layer and with only a small signature in the first layer. For normal non-layered materials the Rayleigh mode has its highest amplitude within the first atomic layer with the displacement field rapidly decaying into the bulk layers.

[1] W. Cheng *et. al.*, Phys. Rev. B **83**, 094301 (2011)

[2] W. Dang *et. al.*, Nano Lett. **10**, 2870-2876 (2010)

[3] S. Y. F. Zhao *et. al.*, Appl. Phys. Lett. **98**, 141911 (2011)

[4] J. Zhang *et. al.*, Nano Lett. **11**, 2407-2414 (2011)

[5] X. Zhu *et. al.*, Phys. Rev. Lett. **107**, 186102 (2011)

Sputtering of tungsten and a-C:H surfaces by nitrogen ions – investigation of transient and molecular effects

K. Dobes, P. Naderer and F. Aumayr

Institute of Applied Physics, TU Wien, Association EURATOM-ÖAW, Austria, EU
(Corresponding author: K. Dobes, e-mail: dobes@iap.tuwien.ac.at)

In present fusion experiments plasma-facing components are made of tungsten and/or carbon because of the advantageous thermal properties of these materials. In order to radiatively cool the plasma edge and thereby reduce the power load on highly exposed plasma-facing components, nitrogen seeding is presently used in fusion devices like ASDEX Upgrade. Hence the interaction of low energy (eV – keV) nitrogen ions with both, carbon and tungsten surfaces, is of considerable interest.

Using a highly sensitive quartz crystal microbalance (QCM) technique developed at TU Wien, we investigated total sputtering yields under bombardment of nitrogen ions, of tungsten surfaces as well as amorphous hydrogenated carbon (a-C:H) thin films, which are representative for co-deposited, hydrogen isotope containing carbon layers in fusion devices. The target material of interest was deposited onto one of the gold electrodes of a stress compensated (SC) cut quartz crystal. The quartz was then transferred to an ion beam facility at the TU Vienna. Nitrogen ions were extracted from an ECR ion source and selected according to their m/q ratio in a sector field. The change of the resonance frequency of the quartz under ion irradiation is a direct measure of the total mass change of the surface film. In this way, total sputtering yields can be determined in situ and in real time. In addition, transient effects such as the formation of a modified surface layer upon ion impact can be studied.

When bombarding a freshly deposited 370 nm thick a-C:H film (with a hydrogen content of 50 %) with nitrogen ions, we observe a sputtering yield, which decreases exponentially with fluence until a steady state value is reached after a typical fluence of some 10^{15} N_2^+ ions per cm^2 (see figure 1, red dots). The fact that reaching this steady state roughly corresponds to the removal of a surface layer of a thickness similar to the ion penetration depth suggests a correlation of this transient phase to the formation of a hydrogen depleted, nitrogen containing modified surface layer. In steady state this top layer is dynamically reformed and its underlying bulk becomes thinner.

Following a model of Hopf *et al*. [1] a set of rate equations is used to describe this transient behavior. In the proposed model, beside physical sputtering, also chemical sputtering and depletion of hydrogen as well as the implantation and chemical sputtering by nitrogen projectiles is taken into account. Within the framework of our model, both the transient as

well as the steady state sputtering yield can be reproduced quite well (see figure 1, red solid line) [2].

Furthermore sputtering yields of a polycrystalline, 500 nm thick tungsten surface during bombardment with atomic N^+ and molecular N_2^+ ions were determined (see figure 2). The obtained results compare well with existing experimental data. At ion energies below 1 keV, a distinct molecular effect was found, i.e. the sputtering yield per nitrogen atom for N_2^+ molecular ions is up to 25 % higher than that of a single N^+ ion with the same impact velocity. In the investigated energy regime a N_2^+ ion can thus not be considered as two independent nitrogen atoms impinging on the surface. This molecular effect can be explained with an energy transfer model assuming an effective mass for the molecular projectile, which depends

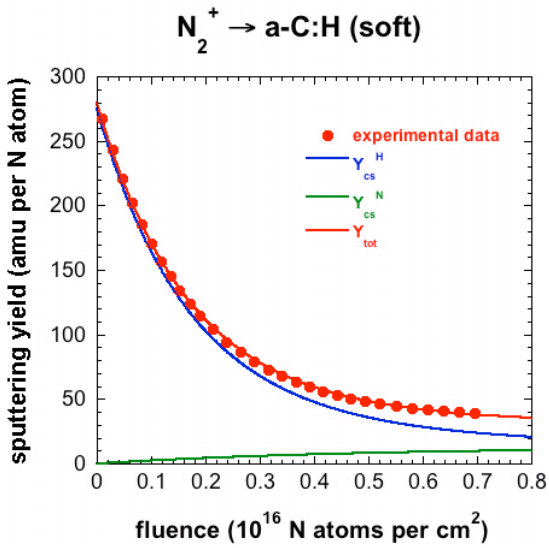

Figure 1: Comparison of the modeled total sputtering yield of soft a-C:H (red solid line) with results obtained from the experiment (red circles). The underlying modeled evolution of the chemical sputtering yield of hydrogen (blue solid line) as well of the chemical sputtering of nitrogen (green solid line) is also shown.

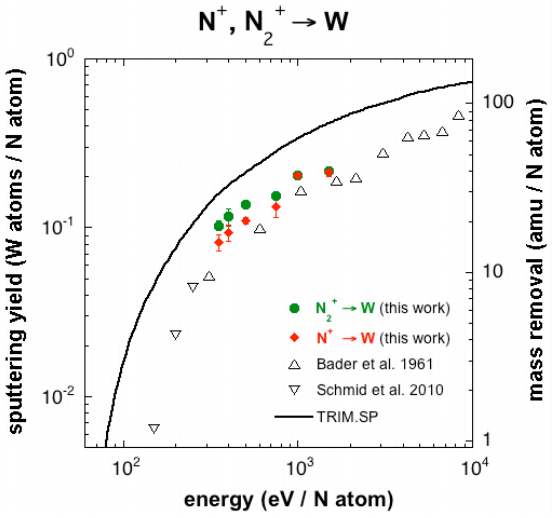

Figure 2: Sputtering yield per nitrogen atom of polycrystalline tungsten bombarded by molecular N_2^+ ions (full circles) and by atomic N^+ ions (full diamonds) vs. projectile energy per nitrogen atom. Previously published data are included for comparison: (△) [4], (▽) [5]. The continuous line represents a fit to TRIM.SP [6].

on the time scales of the molecular vibration as compared to the collision interaction [3].

[1] C. Hopf, A. von Keudell and W. Jacob, J. Appl. Phys. **94**, 2373 (2003)

[2] K. Dobes, P. Naderer, N. Lachaud, C. Eisenmenger-Sittner and F. Aumayr, Phys. Scr. **T145**, 014017 (2011)

[3] K. Dobes, P. Naderer, C. Hopf, T. Schwarz-Selinger and F. Aumayr, NIMB in print

[4] M. Bader, F. C. Witteborn and T. W. Snouse, NASA Technical Report NASA-TR-R-105 (1961)

[5] K. Schmid, A. Manhard, C. Linsmeier, A. Wiltner, T. Schwarz-Selinger, W. Jacob and S. Mändl, Nucl. Fusion **50**, 2 (2010)

[6] Sputtering by Particle Bombardment III , R. Behrisch and W. Eckstein (Edts.) Springer, Berlin (2007) in: Topics Appl. Physics, vol. **110**

Oxidation of the PdCu(100) surface

L.E. Walle[1], J. F. Aase[1], M. H. Farstad[1], I.-H. Svenum[2], T. H. Andersen[3], J. Gustafson[4], E. Lundgren[4], J. N. Andersen[4], and A. Borg[1]

1 Dept. of Physics, Norwegian University of Science and Technology (NTNU), Trondheim, Norway (Corresponding author: mari.farstad@ntnu.no)

2 Dept. of Chemical Engineering, NTNU, Trondheim, Norway

3 Sør-Trøndelag University College (HiST), Faculty of Technology, Trondheim, Norway

4 Div. of Synchrotron Radiation Research, Institute of Physics, Lund University, Lund, Sweden

Palladium has high solubility, permeability and selectivity for hydrogen, thus being a suitable membrane material for hydrogen separation. Pure Pd suffers from embrittlement when exposed to hydrogen due to formation of hydride phases [1-3]. For this reason, Pd-based alloys are often used instead, with Pd/Ag and Pd/Cu as commonly chosen alloys. Recently it has been found that Pd/Cu membranes consisting of 40wt% Cu have almost similar permeability to that of pure palladium, but with much higher resistance to hydrogen sulfide and sulfurous constituents in gas mixtures [4]. Both in the case of Pd/Ag [5] and Pd/Cu [6] membranes, heat treatment in air has been reported to enhance the hydrogen permeation, possibly due to the formation of a thin surface oxide. However, a full understanding of the thermal treatment effects is still lacking.

As a model system for surface oxidation of Pd/Cu we have investigated the clean and oxide covered surface of a $Pd_{57}Cu_{43}(100)$ alloy single crystal, applying highly surface sensitive synchrotron based photoelectron spectroscopy at beam line I311 of the MAX-lab synchrotron facility, and scanning tunneling microscopy (STM). The behavior of this surface is compared to oxide formation on $Pd_{75}Ag_{25}(100)$ and pure Pd(100).

For the clean PdCu surface the surface composition depends on the annealing temperature. As illustrated in figure 1, increased temperatures result in a less pronounced low binding energy shoulder, due to the Pd surface core level shift in the Pd $3d_{5/2}$ spectra, indicating a lower Pd contents at the surface. The surface core level shift to lower binding energy is similar to the shift observed for Pd(100), which is in strong contrast to the shift towards higher binding energy observed for PdAg.

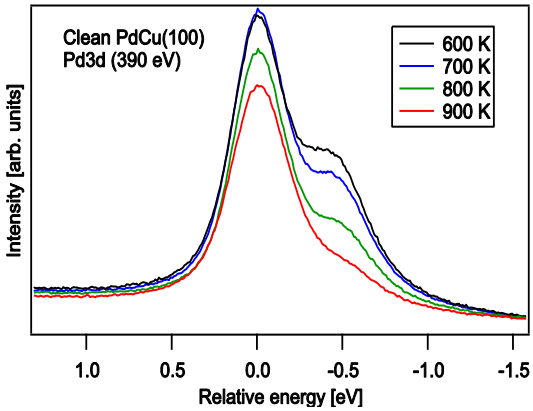

Figure 1: Pd $3d_{5/2}$ spectra of the clean PdCu surface annealed at different temperatures. The surface component of Pd clearly decreases with increasing annealing temperature, indicating a higher Cu content in the surface.

Before onset of bulk oxide formation a $(\sqrt{5}\times\sqrt{5})R27°$ surface oxide is formed on Pd(100) [7,8]. A similar oxide is observed on $Pd_{75}Ag_{25}(100)$ [9]. For $Pd_{57}Cu_{43}(100)$ the high-resolution photoemission results show that upon oxidation the surface shoulder present in the clean Pd $3d_{5/2}$ spectra disappears, leaving only the bulk Pd signal, which is in contrast to Pd(100) and $Pd_{75}Ag_{25}(100)$ where peaks at higher binding energies due to oxidized spices of Pd are formed [7,9]. Furthermore oxidized $Pd_{57}Cu_{43}(100)$ displays c(2x2) and p(2x2) low energy

electron diffraction (LEED) patterns, similar to the oxide structures on Cu(100) where a c(2x2) phase is reported [10]. The different LEED patterns and corresponding STM results indicate that the oxide structure is strongly dependent on annealing temperature and temperature during oxidation. For oxidation with 3400 L O_2 and 300°C annealing and oxidation temperature an oxide with island growth, regular step edges and boundary lines is formed as shown in figure 2. At 600°C a different type of oxide is formed for the same oxygen dose, at large scale it appears disordered, but on a smaller scale ordered patches appear, see figure 3. Both of these structures have similarities to the oxide structures reported on Cu(100) [10], supporting the conclusion that a Cu-oxide is formed on $Pd_{57}Cu_{43}$(100). In contrast to the Pd-oxides on Pd(100) and $Pd_{75}Ag_{25}$(100), this oxide shows very little reduction with CO, both for Pd and Cu enriched surfaces.

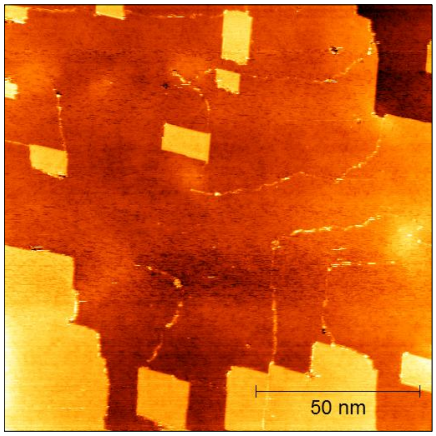

Figure 2: STM image of the oxidized PdCu surface prepared with 3400 L O_2 at 300°C. The oxide islands, step edges and boundary lines are similar to those observed on Cu(100) [10].

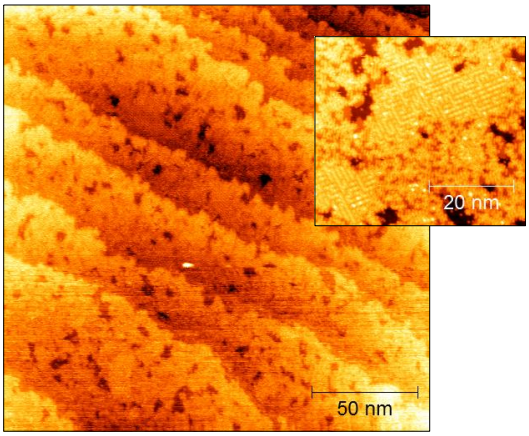

Figure 3: STM image of the oxidized PdCu surface prepared with 3400 L O_2 at 600°C. The oxide covers the surface, leaving only small openings. The inset displays a close up of the oxide surface and reveals an intricate pattern with similarities to what was found for Cu(100) [10].

[1] R. Hughes, Membr. Tech. **131**, 9 (2001).
[2] G.J. Grashoff, C.E. Pilkington and C . W. Corti, Plat. Met. Rev. **27**, 157 (1983).
[3] A. K. M. Kibria Fazle, T. Tanaka and Y. Sakamoto, Int, J. Hydrogen Energy **23**, 891 (1998).
[4] H. T. Hoang Hoang et al., Materials Letters **58**, 525 (2004).
[5] A. L. Mejdell et al., J. Membr. Sci. 307, 96 (2008).
[6] F. Roa and J. D. Way, Appl. Surf. Sci. 240, 85 (2005).
[7] M. Todorova et al., Surf. Sci. **541**, 101 (2003).
[8] P. Kostelnik et. al, Surf Sci. **601**, 1574 (2007).
[9] L. E. Walle et al., in preparation.
[10] K. Lahtonen, M. Hirsimäki, M. Lampimäki, and M. Valden, J. Chem. Phys. **129**, 124703 (2008).

Graphene Nanoribbon Heterojunctions

Stephan Blankenburg, Jinming Cai, Pascal Ruffieux, Rached Jaafar, Daniele Passerone, Xinliang Feng[1], Klaus Müllen[1], Carlo A. Pignedoli, and Roman Fasel

Empa, Swiss Federal Laboratories for Materials Science and Technology, nanotech@surfaces Laboratory, 8600 Dübendorf, Switzerland (corresponding author: R. Fasel, e-mail: roman.fasel@empa.ch)

[1] *Max Planck Institute for Polymer Research, Ackermannweg 10, 55124 Mainz, Germany*

Graphene nanoribbons (GNRs) are promising building blocks for novel graphene-based electronic devices, because variations of the geometry of a GNR allow for gap tuning through one-dimensional (1D) quantum confinement. In general, decreasing the ribbon width leads to an overall increase of the band gap, with superimposed oscillation features that are maximized for armchair GNRs (AGNRs). More complex geometries, including GNR heterojunctions, have been subject to computational investigation to explore quantum effects such as conductance oscillations, electron lensing and focusing [1].

The strong interest in heterojunctions and heterostructures derives from the fact that they are the fundamental building blocks of modern high-speed- and opto-electronics. Semiconductor heterostructures are usually manufactured by stacking crystalline materials exhibiting different electronic band gaps, which requires the use of molecular beam epitaxy or chemical vapor deposition technologies in order to precisely control the 2D interface. *Lateral* heterojunctions represent an even harder challenge. Polycrystalline graphene allows to exploit (intrinsically lateral) grain boundaries acting as 1D interfaces, and the orientation of confining domain boundaries can be related to the electronic and transport properties, both experimentally and theoretically [2]. Going from 1D interfaces to “0D” heterojunctions consisting of a finite set of atoms with controlled structure thus appears to be a highly appealing next step.

In this respect, intra-GNR heterostructures might provide a completely new concept for the realization of (opto-)electronic devices. Indeed, using GNRs as building blocks, their unique quantum properties can be fully exploited, and the interface between different GNRs can potentially be realized without defects. Band gap tuning of the heterojunction can then simply be achieved by varying the width of the components rather than their chemical composition, potentially allowing for “all-carbon” device components. Due to the inherent limitations of lithographic methods and of other known approaches to fabricate graphene nanostructures, however, the experimental realization of GNR heterojunctions with the required atomic precision has remained elusive. Bottom-up approaches based on cyclodehydrogenation reactions have recently emerged as promising routes to the synthesis of nanoribbons and

nanographenes [3]. Here we show that a recently reported bottom-up approach based on metal surface-assisted intermolecular coupling and intramolecular cyclodehydrogenation [3] not only allows for the fabrication of ultra-narrow GNRs but also gives access to GNR heterojunctions with the required atomic precision.

We report the realization of graphene nanoribbon heterojunctions with lateral dimensions below 2 nm via controllable dehydrogenation of polyanthrylene oligomers self-assembled on a Au(111) surface from molecular precursors. Atomistic simulations reveal the microscopic mechanisms responsible for intra-ribbon heterojunction formation. We further demonstrate the capability to selectively modify the heterojunctions by activating the dehydrogenation reaction on single units of the nanoribbons by electron injection from the tip of a scanning tunneling microscope, which suggests that GNR heterostructure imprinting might become feasible using electron beam "writing".

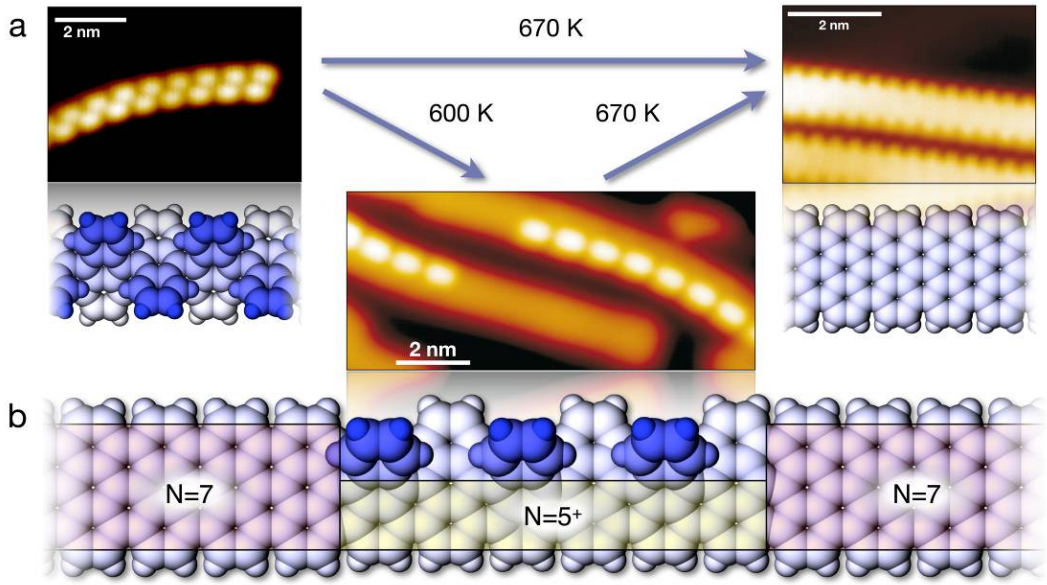

Figure 1. *Realization of GNR heterojunctions by partial cyclodehydrogenation of polyanthrylene oligomers.* ***a****, STM measurements and corresponding atomistic models demonstrating the synthesis of AGNRs starting from polyanthrylene chains assembled on a Au(111) substrat e (left) and subsequent cyclodehydrogenation upon annealing at 670 K.* ***b****, Annealing at a reduced temperature of 600 K results in partial cyclodehydrogenation and produces intra-ribbon heterojunctions between fully reacted N=7 AGNRs and partially reacted polyanthrylene segments (N=5*$^{+}$*).*

[1] (a) Kim, P.; Han, M. Y.; Young, A. F.; Meric, I.; Shepard K. L. Graphene Nanoribbon Devices and Quantum Heterojunction Devices. *IEEE* IEDM09 **2009,** 241-244; (b) Young, A. F.; Kim, P. Quantum Interference and Klein Tunneling in Graphene Heterojunctions. *Nature Phys.* **2009,** 5, 222-226.

[2] (a) Lahiri, J.; Lin, Y., Boskurt, P.; Oleynik, I. I.; Batzill, M. . An Extended Defect in Graphene as a Metallic Wire. *Nature Nanotech.* **2010,** 5, 326-329; (b) Yazyev, O.; Louie, S. Electronic Transport in Polycrystalline Graphene. *Nature Mater.* **2010,** 9, 806-809.

[3] (a) Cai, J.; Ruffieux, P.; Jaafar, R.; Bieri, M.; Barun, T.; Blankenburg, S.; Mouth, M.; Seitsonen, A. P.; Moussa, S.; Feng, X.; *et al.* Atomically Precise Bottom-Up Fabrication of Graphene Nanoribbons. *Nature* **2010,** 466, 470-473. (b) Treier, M.; Pignedoli, C. A.; Laino, T.; Rieger, R.; Müllen, K.; Passerone, D.; Fasel, R. Surface-Assisted Cyclodehydrogenation Provides a Synthetic Route Towards Easily Processable and Chemically Tailored Nanographenes. *Nature Chem.* **2011,** 3 61-67.

H-atom relay reactions in real space

T. Kumagai[1], A. Shiotari[1], H. Okuyama[1], S. Hatta[1,2], T. Aruga[1,2], I. Hamada[3], T. Frederiksen[4,5] and H. Ueba[5]

[1] *Department of Chemistry, Graduate School of Science, Kyoto University, Kyoto 606-8502, Japan*
[2] *JST CREST, Saitama 332-0012, Japan*
[3] *WPI-Advanced Institute for Materials Research, Tohoku University, Sendai 980-8577, Japan*
[4] *Donostia International Physics Center (DIPC), 20018 San Sebastián, Spain*
[5] *Division of Nano and New Functional Materials, Graduate School of Science and Engineering, University of Toyama, Toyama 930-8555, Japan*

(e-mail: thomas_frederiksen@ehu.es)

Hydrogen bonds are the path through which protons and hydrogen atoms can be transferred between molecules. The relay mechanism, in which H-atom transfer occurs in a sequential fashion along hydrogen bonds, plays an essential role in many functional compounds. The relay reaction from one molecular unit to the next is considered to involve coordinated, and often complex, rearrangements within the network, and its study dates back to the idea of 'structural diffusion' introduced by Grotthuss two centuries ago to explain the anomalously high mobility of protons in liquid water. However, microscopic characterization of relay reactions at the atomic scale is extremely challenging in complex environments.

Here we use the scanning tunnelling microscope (STM) to construct and operate a test-bed for real-space observation of H-atom relay reactions at a single-molecule level [1]. We demonstrate that the transfer of H-atoms along hydrogen-bonded chains assembled on a Cu(110) surface is controllable and reversible, and is triggered by excitation of molecular vibrations induced by inelastic tunnelling electrons. The experimental findings are rationalized by ab initio calculations for adsorption geometry, active vibrational modes and reaction pathway, to reach a detailed microscopic picture of the elementary processes.

[1] T. Kumagai, H. Okuyama, S. Hatta, T. Aruga, I. Hamada, T. Frederiksen, and H. Ueba, Nature Materials, Advance Online Publication 27 Nov. 2011 (doi:10.1038/nmat3176).

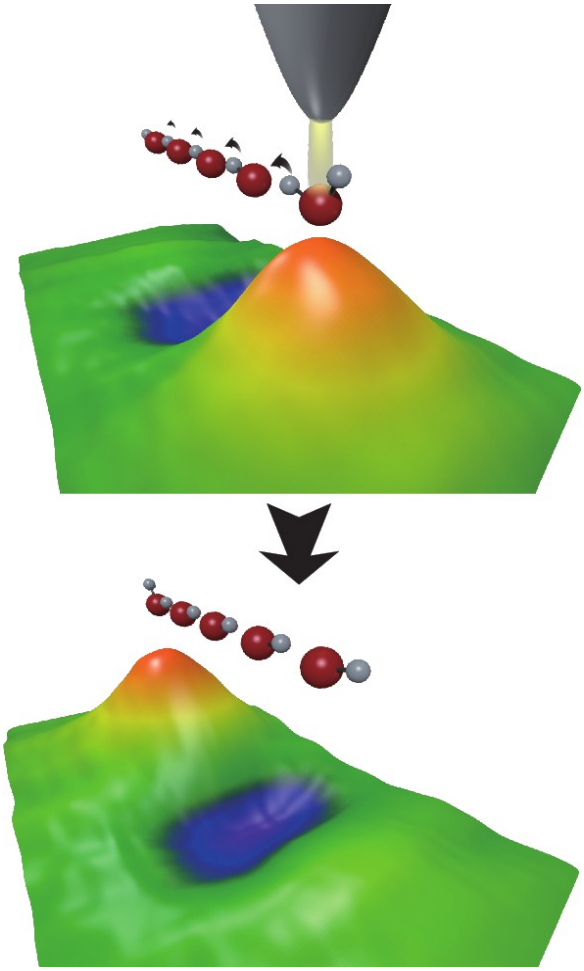

Figure 1: Illustration of the H-atom relay reaction. The tip of a scanning tunneling microscope (STM) is placed over a water molecule (H_2O) at one end of a hydrogen-bonded molecular chain (top panel). By driving an electrical current through the water molecule (yellow beam at the top) energy is delivered to the atoms and the hydrogen atoms (gray spheres) move down the chain in a concerted fashion (black arrows). The result of the collective reaction is that the initial water molecule is decomposed and a new water molecule is assembled at the other end of the chain (lower panel). The transfer process is directly visualized as a shift of the orange protrusion from one end to the other in the STM images (3D plots below the structures) [Graphics by H. Okuyama].

Tuning the growth orientation of oxide films via the interface chemistry

L. Hammer, F. Mittendorfer[1], M. Gubo, C. Ebensperger, W. Meyer, J. Redinger[1], and Klaus Heinz

Lehrstuhl f. Festkörperphysik, Universität Erlangen-Nürnberg, Staudtstr. 7, D-91058 Erlangen, Germany (corresponding author: L. Hammer, email: lutz.hammer@physik.uni-erlangen.de)
[1] Institut für Angewandte Physik and Center for Computational Materials Science, Technische Universität Wien, Gußhausstr. 25/134, A-1040 Wien, Austria

The growth of epitaxial films of transition-metal oxides on metal surfaces has been intensely investigated in the past (for a recent review see e.g. [1]). While ultrathin films when only one or at most a few layers thick often assume completely new phases, the films' structure gradually approaches the bulk structure with further increasing thickness. However, the growth direction, i.e. the crystallographic orientation of the film's surface, depends in an unforeseen way on the substrate properties. It is generally assumed that for small lattice misfit the film adopts the substrate's orientation as, initially, the film suffers only from little stress allowing for pseudomorphic growth. Film relaxation takes place gradually with increasing thickness via dislocation formation. For large misfits films are expected to be more or less close-packed terminated at the interface side in order to minimize the rumpling induced by the binding. In the whole discussion stress minimization at the interface is always regarded to dominate the film growth.

In the present study we have investigated the growth of CoO films on an unreconstructed Ir(100) substrate, whereby cobalt has been reactively deposited in an ambient oxygen atmosphere and subsequently annealed. When starting with a clean substrate this leads in the whole investigated range of Co deposition (1 - 50 ML) to the formation of CoO film oriented in [111] direction despite the square symmetry of the underlying substrate (cf. Fig. 1 a,b) [2]. The films grown in this way are thermally stable up to about 700°C, where the surface starts to facet into the non-polar [100] direction. The [111] orientation near the interface, however, remains stable until the film decomposes above 1000°C.

The situation changes completely when film growth is performed with one or several interfacial monolayers of unreacted cobalt prior to film preparation. Now the orientation of the growing CoO film is exclusively in [100] direction (Fig. 1 c,d) [3]. And again, these films are stable up to their decomposition temperature beyond 1000°C. Obviously, the strain at the interface cannot be the decisive factor in this case, since the Co layer(s) at the interface are pseudomorphic with respect to the Ir(100) substrate and so the misfit between film and the layers below is conserved. It is only the strength of the chemical binding between film and substrate which has changed (or, in order to be more precise, the corrugation of the binding potential is different).

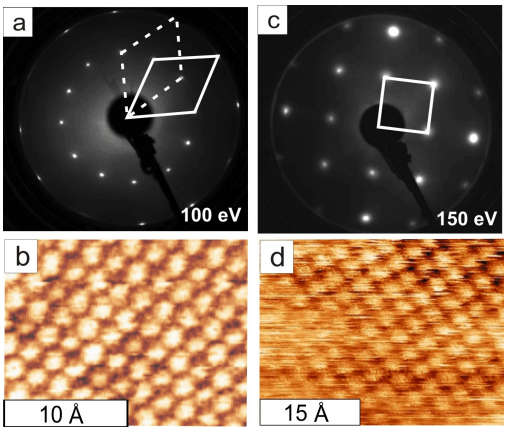

Fig. 1: LEED and STM images of CoO films grown on bare Ir(100) (a,b) and on a Co-precovered substrate (c,d)

Support for this model comes from DFT calculations. Since the further growth of the films could also be kinetically stabilized, we have concentrated on the initial film growth. On both the bare and the Co precovered Ir(100) surface precursor oxides were found comprising of one single monolayer of Co: a c(10x2) and c(8x2) phase on bare Ir(100) with CoO and CoO_2 stoichiometry, respectively [4], and a c(4x2)-Co_3O_4 phase on the Co-precovered surface [3]. All these phases exhibit the same local symmetry as the corresponding thicker films. For the c(10x2) and the c(4x2) phase the crystallographic structure was independently determined by full-dynamical LEED intensity analyses [5, 3], whereby the derived model parameters never deviated by more than 0.10 Å from those of the DFT calculations.

The relative stability of all three films on both the bare Ir(100) substrate and one precovered with 1 ML Co was calculated as a function of the chemical potential of oxygen (Fig. 2). The c(4x2) structure turns out to be never the energetically most favourite phase in case of the clean Ir(100) substrate, while it becomes the stable phase over a wide range of the chemical potential when interfaced by a single layer of cobalt. On the other side, the interface stress induced by the c(4x2) phase, is *increased* by the interfacial Co layer, i.e. *the stability switch is not driven by stress reduction* in this case. Already from a comparison of the energy axes in Fig. 2 it can be estimated that the chemical binding of the film towards the interface is strengthened by the introduction of cobalt. However, this effect is much more pronounced for the c(4x2) phase than for the other ones and so the hierarchy changes. A reason for this behaviour might be that in the c(4x2) phase the oxygen species are on top of the underlying Co atoms, so mimicking the local bond configuration of rocksalt CoO already at this stage.

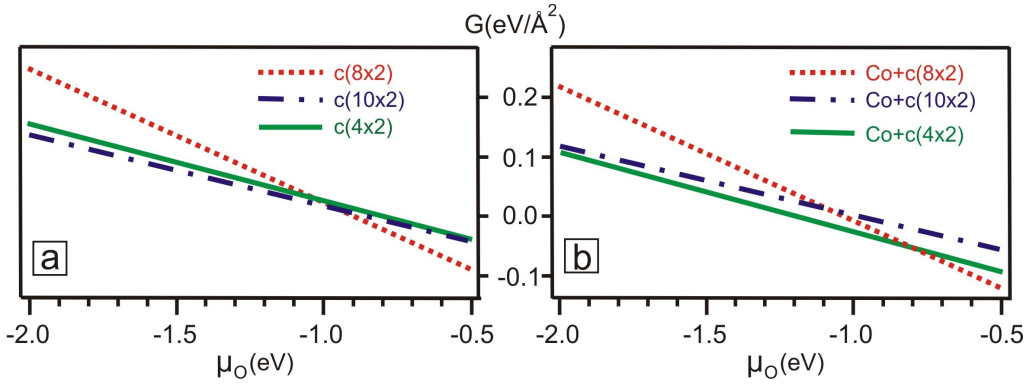

Fig. 2: Phase diagram for a single cobalt-oxide layer on (a) the bare Ir surface and (b) on 1ML Co/Ir. G is the surface free energy, $_O$ the chemical potential of oxygen.

In total we have shown that the mere introduction of a single (or several) monolayer(s) of an external material deposited on the substrate can switch the energetics of a film and its equilibrium orientation. There is no obvious reason why this effect shouldn't be more general though it was proved so far only for CoO/Ir(100).

The authors are grateful for financial support by the Deutsche Forschungsgemeinschaft and the Austrian Science Fund: F4511-N16 and for the computer support of the Vienna Scientific Cluster.

[1] F. P. Netzer, F. Allegretti, and S. Surnev, J. Vac. Sci. Technol. B 28, 1 (2010).
[2] K. Biedermann, M. Gubo, L. Hammer, and K. Heinz, J. Phys.: Cond. Matter 21 (2009) 185003.
[3] M. Gubo, C. Ebensperger, W. Meyer, L. Hammer, K. Heinz, F. Mittendorfer and J. Redinger, Phys. Rev. Letters, accepted.
[4] M. Gubo, C. Ebensperger, W. Meyer, L. Hammer, and K. Heinz, Phys. Rev. B 83 (2011) 075435.
[5] C. Ebensperger, M. Gubo, W. Meyer, L. Hammer, and K. Heinz, Phys. Rev. B 81 (2010) 235405.

Time-resolved femtosecond Se 3d core level photoemission spectroscopy at the Mott insulator $TiSe_2$

Hatem Dachraoui, Tobias Milde, Michael Porer[1], Norbert Müller, Recardo Manzke[2], Walter Pfeiffer, Rupert Huber[1] and Ulrich Heinzmann

Molecular and Surface Physics, Faculty of Physics, Bielefeld University, Germany
(corresponding author: U. Heinzmann, uheinzm@physik.uni-bielefeld.de)

[1] *Ultrafast Quantum Electronics and Photonics, Faculty of Physics, Regensburg University, Germany*

[2] *Elektronische Eigenschaften und Supraleitung, Faculty of Physics, Humboldt-University Berlin, Germany*

Strongly correlated materials exhibit interesting dynamics and phase transitions for which the underlying mechanisms are still under debate. fs-laser induced dynamics provide information about the phase transition mechanism [1]. The recent progress in the creation of femtosecond EUV pulse generation (by means of high harmonic Generation HHG [2]) offers the feasibility of time-resolved core level photoelectron spectroscopy which is capable of probing ultra-fast light driven processes at surfaces [3]. Here we use 20 fs EUV-pulses to directly study the ultrafast dynamics of the charge density wave in $TiSe_2$ after near-infrared excitation (1.5 eV). Structural transitions, evidenced by a dynamic shift of Se 3d core-levels, occurs before electrons lattice thermalization is established.

Support by the DFG SFB 613 is gratefully acknowledged.

[1] H. Dachraoui, N. Müller, G. Obermeier, C. Oberer, S. Horn and U. Heinzmann, "Interplay between Electronic Correlations and Coherent Structural Dynamics during the Monoclinic Insulator to Rutile Metal Phase Transition in VO_2", J. Phys.: Condens. Matter 23, 435402 (2011)

[2] H. Dachraoui, T. Auguste, A. Helmstedt, P. Bartz, M. Michelswirth, N. Müller, W. Pfeiffer, P. Salieres and U. Heinzmann, "Interplay between absorption, dispersion and refraction in high-order harmonic generation", J. Phys. B: Atomic, Molecular & Optical Physics 42, 175402 (2009)

[3] H. Dachraoui, M. Michelswirth, P. Siffalovic, P. Bartz, C. Schäfer, B. Schnatwinkel, J. Mattay, W. Pfeiffer, M. Drescher and U. Heinzmann, "Photoinduced reconfiguration cycle in a molecular adsorbate layer studied by femtosecond inner-shell photoelectron spectroscopy", Phys. Rev. Lett. 106, 107401 (2011)

Theoretical Description of Material Transport During Germanium Nanowire Growth

R. Kalousek[1], M. Kolíbal[1,2], and T. Šikola[1,2]

[1] *Institute of Physical Engineering, Brno University of Technology, Brno, Czech Republic*
(corresponding author: R. Kalousek, e-mail: kalousek@fme.vutbr.cz)

[2] *CEITEC BUT, Brno University of Technology, Technická 10, 61669 Brno, Czech Republic*

When dealing with nanowires their surface is a place of interest instead of a bulk and, hence, facet orientation and nanowire cross-section are essential properties to be controlled in effort to achieve optimum behavior of nanowire-based devices [1]. Nanowires grown by vapor-liquid-solid (VLS) technique with the assistance of a metal catalyst droplet possess usually a hexagonal cross-section [2].

To explain some aspects of the nanowire growth by physical vapor deposition (PVD) in more detail, we have adopted the model of Fröberg et al. [3] and modified it to account for the droplet activity. The boundary condition for adatom concentration at the nanowire sidewall $n_w = 0$ (which makes the droplet an ideal sink for all incoming adatoms) was replaced by $n_w = n_d$, which allows us to model the possible effects of actual germanium concentration in the droplet n_d on the growth rate in the PVD experiment. The resulting formula for the growth rate of a nanowire with the radius r and length L for short wires ($L \ll \lambda_s$) is

$$\frac{dL}{dt} = 2F\Omega\alpha\left[1 + (1-\Gamma)\frac{K_1(r/\lambda_s)}{K_0(r/\lambda_s)}\frac{r}{\lambda_s}\right]$$

where

$$\Gamma = \frac{2\sigma\Omega}{rk_BT\ln(p/p_{eq})}$$

Ω is the germanium atomic volume, F the deposition rate, λ_s the diffusion length of adatoms on the substrate, K_0 and K_1 are the modified Bessel function of the second kind, σ is the surface tension of the droplet, k_B is the Boltzmann constant, T is the droplet temperature, and p and p_{eq} are the actual vapor pressure during deposition and equilibrium vapor pressure of germanium, respectively. Γ is the coefficient accounting for Gibbs-Thompson effect (adopted from [3]) and $\alpha = 1 - n_d/(R\tau)$ is the coefficient reflecting the droplet activity (being 1 when the droplet acts as an ideal sink and 0 if the droplet does not collect the adatoms at all), τ being an average time for which adatom diffuses on the surface before being incorporated into the nanowire or desorbed.

The validity of the model is supported by experimental data.

This work was supported by the research programmes of the Ministry of Education of the Czech Republic (Project Nos. MSM0021630508 and LC06040), GAAV (Project No. KAN400100701), European Regional Development Fund – (CEITEC - CZ.1.05/1.1.00/02.0068).

[1] Sheenan, P. E.; Whitman, L. J. Nanoletters 5 (2005), 803.

[2] Fortuna S A, Li X, Semicond. Sci. Technol. 25 (2010) 024005.

[3] Fröberg L. E., Seifert W., Johansson J., Phys. Rev. B 76 (2007) 153401.

Carbon and Nitrogen/Carbon Modified Titania for Visible Light Photocatalysis

Horst Kisch*, Dariusz Mitoraj, and Przemek Zabek

Institute of Inorganic Chemistry, Department of Chemistry and Pharmacy, University of Erlangen-Nürnberg

Modification of *only UV active* but already commercially utilized titania photocatalysts for *visible light response* is a central topic of semiconductor photocatalysis.

In this contribution we summarize our recent findings on the chemical nature of commercially available carbon-modified titania and of an *N,C*-modified photocatalyst prepared from titania and urea (*TiO_2-N,C)* [1,2]. Surprisingly, during the preparation titania acts as thermal catalyst for the conversion of urea into organic poly(*s*-triazine) compounds, reported the first time already by J. von Liebig [3].

Wavelength dependent measurements of the quasi-Fermi potential of electrons in *TiO_2-N,C* and a nitrogen-modified material prepared by ammonia treatment suggest an only weak electronic coupling between the titania valence band and poly(*s*-triazine) or nitrogen localized surface states. It is found that the chemical structure of the photogenerated hole controls the interfacial electron transfer from formic acid. As a consequence thereof only *TiO_2-N,C* but not *TiO_2*-N photocatalyzes formic acid oxidation. This surprising difference is rationalized by assuming efficient hole stabilization through electronic delocalization within the aromatic poly(*s*-triazine) sensitizer, which is absent in *TiO_2-N*.

References

[1] P. Zą̨bek, J. Eberl, H. Kisch, Photochem. Photobiol. Sc. 8(2009)264.

[2] (a) D. Mitoraj, H. Kisch, Angew. Chem. 120(2008) 10123. (b) Chem. Eur. J.16(2010)261.

[3] J. von Liebig, Pharm. Zentralblatt 5(1834)671.

Hidden problem of atomic scale friction: Critical damping

S. Yu. Krylov [1] and J. W. M. Frenken

Kamerlingh Onnes Laboratory, Leiden University, 2300 RA Leiden, The Netherlands
(corresponding author: S.Yu. Krylov, e-mail: krylov@physics.leidenuniv.nl)

[1] *Institute of Physical Chemistry, Russian Academy of Sciences, 119991 Moscow, Russia*

With the application of atomic force microscopes to friction (friction force microscopy—FFM) atomic-scale access has been acquired to the origin of dissipative surface forces, boosting the rapidly developing field of nanotribology. There are many physical parameters which can be important for atomic scale friction, but two of them seem really crucial. One is the corrugation of the effective (mean force) contact potential: the lateral barriers faced by the slider are responsible for the appearance of stick-slip motion and sizable friction experienced. The other is the inherent dissipation rate, which describes how the energy invested into the system is losing irretrievably to the outside world. These two key parameters are never known in advance, not only because of uncontrolled contact conditions but also in view of nontrivial physics involved. This is in contrast to practically all other system parameters, which can be taken directly from experiments (like mass and flexibility of the tip and cantilever) or reasonably estimated. It looks like satire of Nature: just the most important parameters remain shrouded in mystery. In our earlier work [1] we have shown how FFM experiments can be analyzed in a consistent way in spite of the lack of initial knowledge with respect to the contact potential corrugation. In this work we concentrate on some hidden problems concerned with the dissipation rate.

In the theory related with FFM experiments, one usually follows a one-effective-spring (Prantdl-Tomlinson) model. To explicitly account for dissipation and thermal noise, one usually uses a Langevin type equation for the slider motion. Its applicability for the current problem is always postulated but never discussed critically from physical point of view. The value of damping factor in this equation (which is just the inherent dissipation rate) is always chosen *a priory*, without any physical justification. One serious problem is met on this way, but it is almost always hidden from discussion. In order to reproduce sliding dynamics similar to what is observed in typical experiments, one is forced to assume that damping is close to critical. Although nearly critical damping is suggested by experiments, it is absolutely unclear what could be physical reasons for that. Moreover, the critical damping actually looks very strange, if not to say non-physical. Indeed, it implies that the dissipation rate is mainly determined by the characteristic frequency (i.e. by the flexibility and mass of the measuring system) but it is practically independent of the contact conditions and the substrate where energy is dissipated. Certainly, one would expect just the opposite.

In principle, the problem of critical damping could be an artifact of the oversimplified one-effective-spring model. This traditional approach ignores dynamical consequences of the experimentally proven fact that the measuring system is only weakly coupled to the substrate via the tip (asperity) apex which actually is the most flexible and rapidly moving element of the system. In this work, we have analyzed friction as a function of damping factor(s) in the framework of an advanced two-mass-two-spring approach [2-4] which takes explicitly into account the flexibility and ultra-low effective mass of the tip apex. Our results show that the problem is not fixed but it is reproduced in even a more pronounced form. First, damping of the cantilever (through the tip—surface interaction) must be close to critical. If it exceeds the critical value by about one order of magnitude or more, the force-vs-position dependence loses its characteristic saw-tooth-like shape, in contrast to experiments. If it is lower than critical by more than one order of magnitude, stick-slip motion loses its regularity, again in contrast to experiments. Second, damping of the tip apex motion must be somewhat smaller than critical (to allow multiple slips which are sometimes observed in experiments) but not much smaller (otherwise the multiple slips would be typical but not occasional phenomenon). Since the characteristic frequencies of the cantilever and the tip apex differ by many (4 to 6) orders of magnitude, the problem appears to be very general. If the characteristic frequency of an object in contact with a surface is ω, damping of its motion is close to (somewhat smaller than) 2ω, regardless of its nature. We conclude that the strange nearly-critical damping is not an artifact but the fact which should have a rational physical explanation. A strongly counterintuitive character of these observations constitutes an outstanding theoretical problem.

We suggest that the key to solve the problem of critical damping is concerned with an essentially nonlocal character of dissipation and pronounced role of memory effects. The possible memory effects are ignored in the framework of the traditional Langevin approach (actually without any physical justification) and, as far as we know, this issue has never been discussed in the context of dry friction. We propose two simple, conceptually different atomistic models that lead to similar results, explain nearly critical values of the dissipation rate for both the tip and cantilever, and visualize an essentially memory character of energy dissipation in dry, atomic scale friction.

Support by the Fonds of the European Comission (Grant ERC-2010-AdG_20100224) and the Foundation for Fundamental Research on Matter (FOM, The Netherlands) is gratefully acknowledged.

[1] S.Yu. Krylov and J.W.M. Frenken, Phys. Rev. B 80, 235435 (2009)
[2] S.Yu. Krylov, J.A. Dijksman, W.A. van Loo, and J.W.M. Frenken, Phys. Rev. Lett. 97, 166103 (2006)
[3] D.G. Abel, S.Yu. Krylov, and J.W.M. Frenken, Phys. Rev. Lett. 99, 166102 (2007)
[4] S.Yu. Krylov and J.W.M. Frenken, New J. Phys. 9, 398 (2007)

Site-selective epitaxial growth of Substrate supported Metal-organic Framework by using AFM Nanografting

Tatjana Ladnorg, Christof Wöll

Karlsruhe Institute of Technology, Institute of Functional Interfaces, IFG,
(corresponding author: T .Ladnorg, e-mail: Tatjana.Ladnorg@kit.edu)

Atomic force microscopy is an invaluable tool for characterizing the surface of several organic, inorganic or biological materials at high resolution. With this technique it is possible to determine material properties like elasticity, frictional force, conductivity or simply get an image of topography. But Atomic force microscopy can not only be used for imaging the topography, friction or conductivity, it is also a versatile tool for manipulation and structuring of surfaces. The applied loading force is the main parameter to switch between imaging and manipulation [1]. During imaging, the loading forces are minimized to prevent any deformation of the biological structures under investigation. Upon increasing the load in localized predefined areas, adsorbed molecules can be removed in a straightforward fashion. In connection with self assembled monolayers (SAMs) [3] (e.g. thiols on gold) this methodology is known as nanoshaving [2].

While shaving implies only removal of molecules, nanografting [2] is performed in an organothiol containing solution, enabling the site-selective substitution of the removed SAM molecules by other molecules. Both described methods allow lateral structuring with resolutions of several nanometers.

In this work we show the application of AFM nanografting as a tool to control the site-selective growth of substrate supported metal-organic frameworks on surfaces (SURMOFs).

Metal organic frameworks (MOFs) are highly crystalline micro-porous materials consisting of metal precursor nodes which are linked with each other by organic ligands. As particulate system this class of material is already applied in the field of nanotechnology, as e.g. gas storage and gas separation, catalysis, delivery of therapeutic agents and sensor devices [4]. However, the idea of an epitaxial growth of quasi-monocrystalline substrate supported MOFs on the surface of substrates (SURMOFs) by a layer-by-layer (LBL) method is quiet new and has been developed in our group. As it is shown in [5] SURMOFs show highly selective growth on self-assembled monolayers [5], terminated by functional groups like COOH-, OH- and pyridine Here we demonstrate that nanografting with an AFM can be used to produce patterned substrates for site selective growth of a HKUST-1 SURMOF by substituting SAM molecules not specific for SURMOF growth by those which are. The proof for the site selective SURMOF growth is done by FT-IR spectroscopy with high lateral resolution.

[1] S. Xu, S. Miller, P. E. Laibinis, G. Y. Liu, *Langmuir* **1999**, *15*, 7244.
[2] M. Liu, N. A. Amro, G. Y. Liu, *Annual Review of Physical Chemistry* **2008**, *59*, 367.
[3] C. D. Bain, G. M. Whitesides, *Angewandte Chemie-International Edition in English* **1989**, *28*, 506.
[4] R. J. Kuppler, D. J. Timmons, Q.-R. Fang, J.-R. Li, T. A. Makal, M. D. Young, D. Yuan, D. Zhao, W. Zhuang, H.-C. Zhou, *Coordination Chemistry Reviews* **2009**, *253*, 3042.
[5] C. Munuera, O. Shekhah, H. Wang, C. Woll, C. Ocal, *Physical Chemistry Chemical Physics* **2008**, *10*, 7257.
[6] O. Shekhah, H. Wang, S. Kowarik, F. Schreiber, M. Paulus, M. Tolan, C. Sternemann, F. Evers, D. Zacher, R. A. Fischer, C. Wöll, *Journal of the American Chemical Society* **2007**, *129*, 15118.

Phase diagram for nanostructuring CaF_2 surfaces by slow highly charged ions

A.S. El-Said,[1,2] R. Heller,[1] R. A. Wilhelm,[1] G. Wachter,[3] R. Ritter,[4] S. Facsko,[1] C. Lemell,[3] J. Burgdörfer,[3] and F. Aumayr[4]

[1]*Institute of Ion Beam Physics and Materials Research, Helmholtz-Zentrum Dresden-Rossendorf, 01328 Dresden, Germany, EU*

[2]*Physics Department, Faculty of Science, Mansoura University, 35516 Mansoura, Egypt*

[3]*Institute for Theoretical Physics, Vienna University of Technology, 1040 Vienna, Austria, EU*

[4]*Institute of Applied Physics, Vienna University of Technology, 1040 Vienna, Austria, EU*

Impact of individual slow highly charged ions on halide surfaces creates nano-scale surface modification. For different materials and impact energies a wide variety of topographic alterations have been observed, ranging from regularly shaped pits to nano-hillocks. We present experimental evidence supported by simulations involving the initial electronic heating and subsequent molecular dynamics which allow to construct a unifying phase diagram underlying these diverse observations. By chemically etching CaF_2 samples after irradiation with slow highly charged ions both above and below the potential energy threshold for hillock formation we provide evidence for the existence of another threshold above which triangular etch pits are produced (see Fig. 1). This threshold depends on both the potential and kinetic energies of the incident ion.

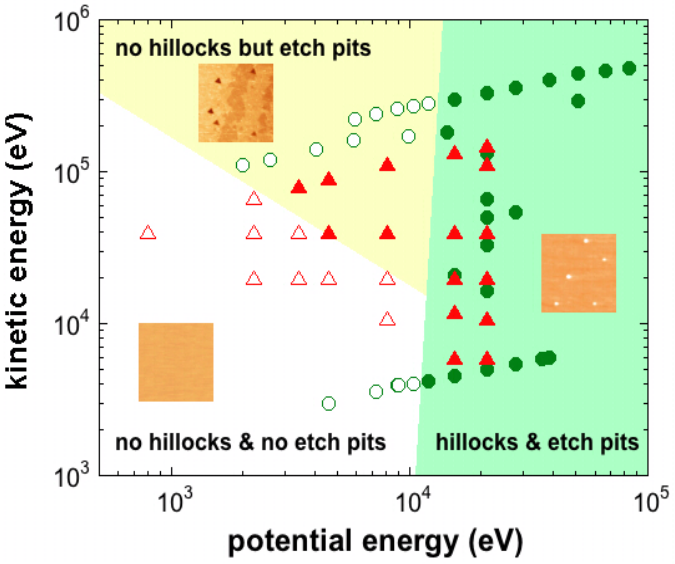

Fig. 1: Hillock and etch pit formation on CaF_2 (111) due to irradiation with highly charged Xe ions. Full (open) circles show pairs of potential and kinetic energies where hillocks are produced (absent) after irradiation, full (open) triangles indicate pairs where pits are present (missing) after etching the irradiated samples.

These experimental findings suggest the following scenario for nanostructure formation on CaF_2 qualitatively supported by simulations involving a sequence of three steps: initial heating of electrons by multiple electron transfer and Auger relaxation, hot electron transport and dissipation with accompanying lattice heating by electron-optical phonon coupling, and subsequent molecular dynamics. The following qualitative trends can be readily extracted. For HCI in "low" charge states (Fig. 2, left) only a few (i.e. low density) individual defects (point defects, single vacancies) are created at or below the surface. These defects either remain below the surface, easily anneal or are too small to be detected by means of AFM. Since the etchability of CaF_2 is strongly coupled to the creation of large defects aggregates rather than to point defects, no pits are observed after etching. Our MD simulations do not yield any significant number of lattice displacements for low q.

For larger q and, correspondingly, larger energy, the potential sputtering yield strongly increases. The density of defects (excitons, color centers) is now large enough leading to defect clusters and aggregates (Fig. 2 center column). The material in the vicinity of the impact region is not ablated but structurally weakened and forms the nucleus of an etchable defect subsequently removed by a suitable etchant. The synergistic effect contributed by the kinetic energy originates from kinetically induced defects created in the collision cascade which enhance the trapping of the color centers created by potential energy and therefore increases defect agglomeration. Consequently, the borderline between the regions A (stable) and B (etchable surface defects) has a negative slope in the phase diagram (Fig. 1).

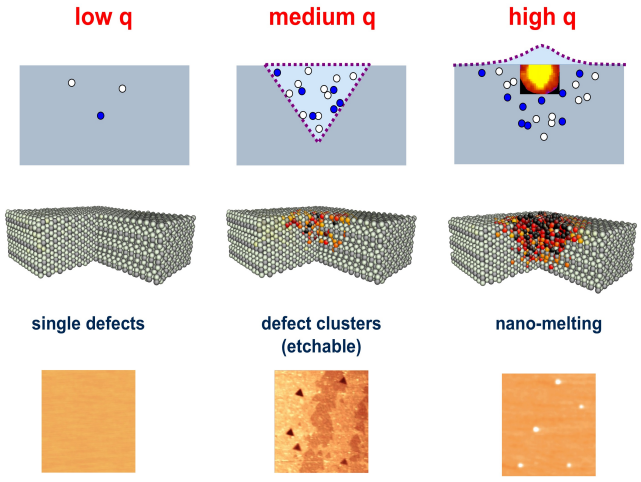

Fig. 2: Scenario for surface modification as a function of charge q of the HCI. Upper row: the charge state controls the created surface modification from non-etchable single defects (low q) to defect aggregates (medium q) and to locally molten zones (high q). Center row: typical results of MD simulations: the initial electronic excitation and energy transfer to the lattice lead to a considerable number of displacements even before melting of the surface sets in (right column). Lower row: AFM images.

R. R. is a recipient of a DOC-fellowship of the Austrian Academy of Sciences. This work has been supported by the European Community as an Integrating Activity 'Support of Public and Industrial Research Using Ion Beam Technology (SPIRIT)' under EC contract No. 227012. Support from the EU-network ITS-LEIF, the Austrian Science Foundation FWF under Proj. No. SFB-041 ViCoM, and the International Max Plank Research School on Advanced Photon Science APS (G.W.) is acknowledged.

Spin-resolved photoemission spectroscopy of $[Mn^{III}_6Cr^{III}]^{3+}$ single-molecule magnets (SMM) deposited on surfaces and of Mn compounds as reference substances, cross comparison with XMCD

Andreas Helmstedt, Aaron Gryzia, Niklas Dohmeier, Norbert Müller, Armin Brechling, Marc Sacher, Ulrich Heinzmann, Veronika Hoeke[1], Erich Krickemeyer[1], Thorsten Glaser[1], Karsten Küpper[2], Mikhail Fonin[3], Samuel Bouvron[3], Philipp Leicht[3], Thomas Tietze[4]

Molekül- und Oberflächenphysik, Fakultät für Physik, Universität Bielefeld, D-33501 Bielefeld, Germany
(corresponding author: N.Müller, e-mail: nmueller@physik.uni-bielefeld.de)

[1] *Fakultät für Chemie, Universität Bielefeld, D-33501 Bielefeld, Germany*

[2] *Abteilung Festkörperphysik, Universität Ulm, D-89069 Ulm, Germany*

[3] *Fachbereich Physik, Universität Konstanz, D-78457 Konstanz, Germany*

[4] *Max-Planck-Institut für Intelligente Systeme, D-70569 Stuttgart, Germany*

The Mn-based single-molecule magnet (SMM) $[Mn^{III}_6Cr^{III}]^{3+}$ is of special interest due to its magnetic properties: This molecule contains six Mn^{III} ions arranged in two bowl-shaped trinuclear triplesalen building blocks which are linked by a hexacyanochromate. The strong antiferromagnetic coupling of the central Cr^{III} ion with the six terminal Mn^{III} ions leads to a large spin ground state of $S_T = 21/2$. This high spin ground state in combination with a strong easy-axis magnetic anisotropy and a C_3 symmetry results in an energy barrier for spin-reversal and thus in a slow relaxation of the magnetization at low temperatures. The blocking temperature of $[Mn^{III}_6Cr^{III}]^{3+}$ SMM is about 2 K [1,2].

To study the spin state and the orbital state of the atomic constituents it is not necessary to use magnetic circular dichroism (MCD) at low temperatures in high magnetic fields, but spin-resolved photoelectron spectroscopy using circularly polarized radiation performed on paramagnetically ordered systems at room temperature can be applied as well [3]. This method is reasonable since for circularly polarized radiation, core-valence transitions are determined by the relativistic selection rules, independent from magnetic order. Therefore the resulting core hole orientation in the non-ordered system and the helicity-dependent absorption probability in the ordered system correspond to each other. The core hole orientation can be probed via the spin polarization of Auger electrons following the primary excitation. This method has been successfully proven for Gd/W(110) [4] and for Mn^{II} constituents in molecular adsorbates [3].

We have applied this method to obtain data about the spin and the orbital state of the manganese centres in $[Mn^{III}_6Cr^{III}]^{3+}$ SMM. Thereby we have measured the spin polarization of $L_{2,3}M_{2,3}V$ Auger electrons emitted from $[Mn^{III}_6Cr^{III}]^{3+}$ SMM targets after excitation with

circularly polarized synchrotron radiation in the paramagnetic phase at room temperature for selected energies in the Mn-$L_{2,3}$ excitation region. With **$[Mn^{III}_6Cr^{III}]^{3+}$** SMM as with other metal-organic compounds containing transition metal centers investigations by X-ray-based methods are complicated by the occurrence of radiation damage [5,6]. We have limited these effects by scanning the sample pointwise during data acquisition, so a total integration time exceeding the lifetime on a single sample position has been achieved. As preparation method for the required large-scale homogeneous samples we have used air brush spraying of a methanolic solution of the SMM with perchlorate counterions **$[Mn^{III}_6Cr^{III}]^{3+}$** $(ClO_4)^-_3$ onto Au coated glass plates. With all samples the Mn ionic state has been probed by XAS [7]. It turned out that **$[Mn^{III}_6Cr^{III}]^{3+}$** SMM can be deposited onto metallic or semiconducting surfaces without damage by electron transfer. However, reduction of the Mn^{III} constituents Mn^{II} can occur upon sample transfer into vacuum, if sources of free electrons and metastables, such as ionization vacuum gauges, are present during pump down [7].

The spin polarization results obtained from **$[Mn^{III}_6Cr^{III}]^{3+}$** SMM are compared with spin polarization data from Mn_2O_3 and Mn^{II}acetate references measured in zero magnetic field at room temperature as well as with corresponding XMCD asymmetries measured at low temperatures of 5-15K and high magnetic fields of 5-7T.

Special thanks are due to Helmholtz Zentrum Berlin (BESSY II), MAX-lab, Lund and Swiss Light Source (SLS), Villingen and their staff for continuous support at the beamlines. This work is supported by the Deutsche Forschungsgemeinschaft within Research Unit 945. M F acknowledges financial support by the Deutsche Forschungsgemeinschaft within Collaborative Research Center 767 and from the Baden-Württemberg Stiftung.

[1] T. Glaser, M. Heidemeier, T. Weyhermüller, R.-D. Hoffmann, H. Rupp, P. Müller, Angew. Chem. Int. Ed. 45, 6033 (2006)

[2] T. Glaser, Chemical Communications 47, 116 (2011)

[3] A. Helmstedt, N. Müller, A. Gryzia, N. Dohmeier, A. Brechling, M. D. Sacher, U. Heinzmann, M. Neumann, J. Phys.: Condens. Matter 23, 266001 (2011)

[4] N. Müller, T. Lischke, M. R. Weiss, U. Heinzmann, J. Electron. Spectrosc. Relat. Phenom.114–116**,** 777-782 (2001)

[5] J. Yano, J. Kern, K.-D. Irrgang, M. J. Latimer, U. Bergmann, P. Glatzel, Y. Pushkar, J. Biesiadka, B. Loll, K. Sauer, J. Messinger, A. Zouni, V. K. Yachandra, PNAS 102, 12047 (2005)

[6] L. Rulíšek, U. Ryde, J. Phys. Chem. B 110, 11511 (2006)

[7] A. Helmstedt, M. D. Sacher, A. Gryzia1, A. Brechling, N. Müller, U. Heinzmann, V. Hoeke, E. Krickemeyer, T. Glaser, S. Bouvron, M. Fonin, J. Electron. Spectrosc. Relat. Phenom. 184, 583 (2012)

Nature of the peak-to-peak spacing oscillations measured by RHEED during epitaxial growth

J. D. Fuhr[1] and P. Müller[2]

[1] *Centro Atómico Bariloche, CNEA, and CONICET, Av. E. Bustillo 9500, R8402AGP, Bariloche, Argentina.*
[2] *CINaM-CNRS, UPR 3118, Université d'Aix-Marseille, Campus de Luminy, Case 913, 13288 Marseille Cedex, France*

Since their first experimental evidence[1], it has been admitted that peak-to-peak oscillations observed by Reflection High Energy Electron Diffraction (RHEED) during crystal growth have an elastic origin and can be attributed to the lattice mismatch between the substrate and the deposited film. It was thus surprising to find peak-to-peak oscillations in homo-epitaxial growth with, obviously, no lattice mismatch[2,3]. Our goal is to revisit the problem of the origin of these peak-to-peak oscillations. For this purpose we perform solid-on-solid KMC simulations to describe the growth and we use kinematical approximation to simulate RHEED intensity profiles.

We write the RHEED intensity as:

$$\overline{I} \propto \int d^3k_i \, g(\vec{k}_i) \left| \sum_i \beta_i \left(\sum_{n\in i} f_n \left(\vec{k}_f - \vec{k}_i \right) \mathrm{e}^{i(\vec{k}_f - \vec{k}_i)\cdot\vec{r}_n} \right) \right|^2$$

where the incident and diffacted beams respectively have wave vectors $\vec{k}_i$ and $\vec{k}_f$. $g(\vec{k}_i)$ gives the dispersion reflecting the experimental conditions and $\beta_0 = 1$, $\beta_{i\neq 0} = 0$ for ideal RHEED calculations.

To calculate the previous integral we use Monte Carlo integration with a dispersion relation chosen as

$$g(\vec{k}_i) = A \frac{a_\parallel^2}{a_\parallel^2 + (k - \overline{k}_i)^2} \frac{a_\perp^2}{a_\perp^2 + (k_\perp)^2}$$

where $k = |\vec{k}_i|$ is the total wave vector with mean value $\overline{k}_i$, $k_\perp$ is the perpendicular component of $\vec{k}_i$ with respect to the mean incident direction given by α_i. The parameters $a_\parallel$ and $a_\perp$ represent incident energy and angular dispersions repectively, and A is a normalization factor. The parameters needed for the calculations are: the incident wave vector $k_i = |\vec{k}_i|$, the incident angle α_i, the dispersion parameters $a_\parallel$ and $a_\perp$, and the crystal structure of the surface, which defines the distance between layers and the lateral positions of the atoms in each layer.

A typical RHEED pattern calculated for a flat surface is shown in Fig. 1. The RHEED intensity profile, recorded along a straight line, is then analytically fitted to accurately determine the exact position of the maxima.

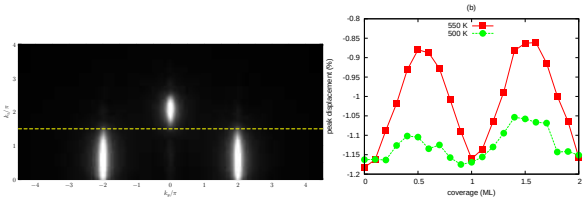

Figure 1: Typical calculated RHEED pattern for a flat surface and displacement of the maximum of the RHEED profile versus coverage during 2D crystal growth. The oscillation amplitude depends on temperature by means of the island density.

We thus simulate the 2D growth by solid-on-solid Kinetic Monte Carlo (KMC) simulations. The corresponding RHEED patterns are then calculated for increasing coverage. We find that the peak position of the RHEED streaks oscillates with coverage (Fig. 1) with a period of 1ML as reported in the experiments. We analyse the effect of the dispersion parameters $a_\parallel$ and $a_\perp$ on the oscillation amplitude and show that the oscillation essentially originates from the angular dispersion[4]. We believe that it is the fundamental reason for which in-plane lattice spacing oscillations have only be reported in RHEED experiments but not in X-ray diffraction measurements, for which energy and angular dispersions are close to zero compared to RHEED apparatus. We will thus sketch the physical origin of the oscillations on the basis of two main ingredients **(i)** the angular dispersion of the incident wave-vector and **(ii)** the size effect that enlarges the reciprocal rods of the smaller islands.

[1] J.Massies, N.Grandjean, Phys. Rev. Lett. 71 (1993) 1411.
[2] J. C. J. H. G. V. L.Carbonell, S.Tatarenko, A.Arnoult, Appl. Surf. Sci. 123/124 (1998) 283.
[3] L. P. Turban, S.Andrieu, Surf. Sci. 446 (2000) 241.
[4] J. Fuhr, P. Muller, Phys. Rev. B X (2012) X.

Hybrid materials design with DFT: Silane coupling agent on TiO_2 rutile surfaces

Wolfgang Heckel, Beatrix Elsner, and Stefan Müller

Technische Universität Hamburg-Harburg,
Institut für Keramische Hochleistungswerkstoffe,
Denickestr. 15, D-21075 Hamburg
∗ *e-mail: stefan.mueller@tuhh.de*

For a couple of years, the effort in material science to create hierarchically structured multicomponent materials has been increased continuously. For the design of such called hybrid materials with desired mechanical (e.g. hardness, stiffness, ductility) and electronic (e.g. conductivity) properties, a detailed knowledge of the structure and stability at the interface between individual types of materials plays a crucial role. Indeed, the interaction of the different composite ingredients, such as hard inorganic materials, ductile metals or soft polymers, controls the mechanical properties.

Our research focuses on the first hierarchical level. Density functional theory has been applied in order to study the crystallographic and electronic atomic structure and the energetical stability. For this, the biggest challenge is to find the ground state structure of hybrid materials in order to create a model system being still small enough to allow for its application on state-of-the-art computer systems.

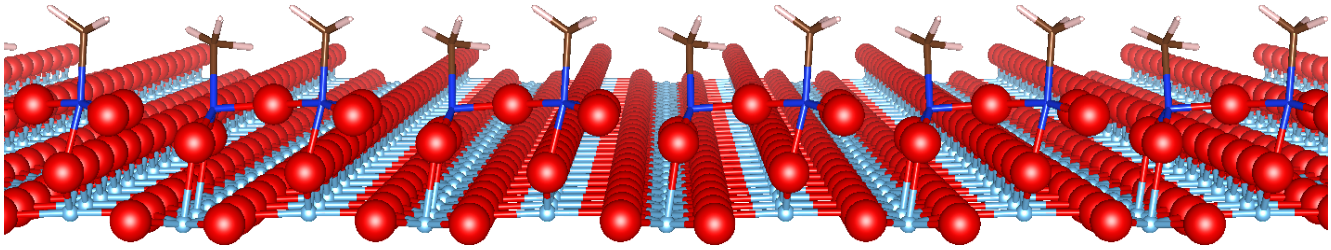

Figure 1: Energetically most favourable adsorption sites for an silane coupling agent arrangement on the TiO_2 (110) surface.

As one of the most important hybrid system we have investigated TiO_2 surfaces in the rutile structure, one of the most important hard ceramics, covered by so-called silane coupling agents (SCA) representing the contact layer to the soft part consisting of PMMA molecules (Figure 1). More precisely, we analyzed the bonding behaviour of single SCAs and SCA arrays on low-index, bulk-terminated surfaces of TiO_2 relying on ref. [1] illustrating that the energetically favoured TiO_2 (011) surface in atmosphere is – in contrast to the (2×1) reconstruction in vacuum ([2]) – the non-reconstructed one. Here, a good choice for the exchange-correlation functional plays an important role ([3]).

The resulting energetics are strongly linked to surface stability and adsorption geometry. We found that the less stable surfaces allow for higher coupling agent coverage as they contribute

more dangling bonds to the adsorbate. The release of binding energy depends heavily on the adsorption sites. Evidently, the energetically most favourable molecular arrangements show only weak bonding to the surface due to the tendency of the adsorbing molecules to form clusters before adsorption. Further the divergency from ideal silicon tetrahedral angles displays a strong influence on the binding energy, as sketched in Figure 2.

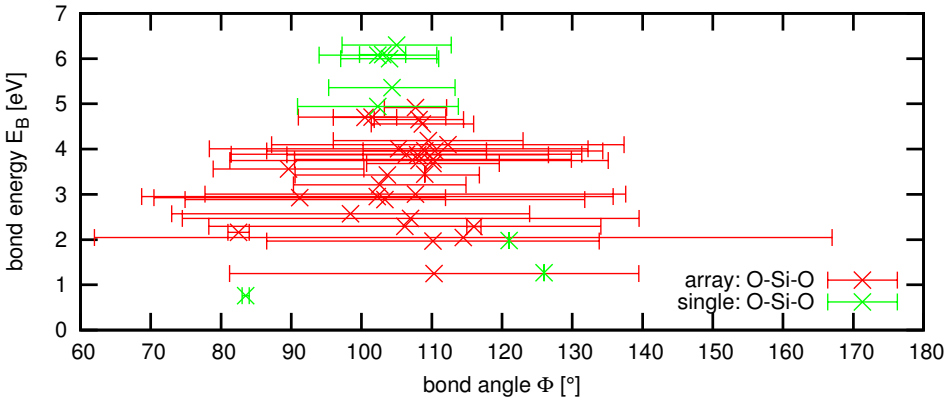

Figure 2: Total bond energy of an adsorbate as a function of the average O-Si-O angles: No matter, whether a single molecules adsorbes or a broad array, the less the O-Si-O angles deviate from the ideal silicon tetrahedral angle the higher is the probability to get a strong bonding to the surface.

References

[1] U Aschauer, and A Selloni, Phys. Rev. Lett. **106**, 166102 (2011).

[2] X Gong, N Khorshidi, A Stierle, V Vonk, C Ellinger, H Dosch, H Cheng, A Selloni, Y He, O Dulub, and U Diebold, Surf. Sci. **603**, 138 (2009).

[3] L Schimka, J Harl, and G Kresse, J. Chem. Phys. **134**, 024116 (2011).

Surface Terminations of $Fe_3O_4(001)$

Zbyněk Novotný[1], Gareth S. Parkinson[1], Thomas A. Manz[2], Zoltán Édes[1], Peter Varga[1,4], Phillip T. Sprunger[3], Richard L. Kurtz[3], Michael Schmid[1], David S. Sholl[2], and Ulrike Diebold[1]

[1] *Institut für Angewandte Physik, Technische Universität Wien, A-1040 Wien, Austria (corresponding author: U. Diebold, e-mail: diebold@iap.tuwien.ac.at)*

[2] *School of Chemical & Biomolecular Engineering, Georgia Institute of Technology, Atlanta, Georgia, USA*

[3] *Department of Physics and Astronomy, Louisiana State University, Baton Rouge, Louisiana, USA*

[4] *CEITEC - Central European Institute of Technology, Brno University of Technology*

Magnetite, Fe_3O_4, crystallizes in the inverse spinel structure with an fcc oxygen sublattice and Fe cations located in tetrahedral and octahedral interstitial sites. The energetically favourable surface termination in the (001) orientation is a distorted octahedral B layer with $(\sqrt{2}x\sqrt{2})R45°$ symmetry [1]. The lattice distortion is linked to charge order in the subsurface layers [2], leading to an inequivalence between the Fe(A) bulk continuation sites in the 'narrow' and 'wide' regions of the unit cell.

We investigated antiphase domain boundaries (APDBs) in the $(\sqrt{2}\times\sqrt{2})R45°$ reconstruction of the $Fe_3O_4(001)$ surface using scanning tunneling microscopy (STM) and density functional theory (DFT+U) calculations. APDBs occur in this system because the $(\sqrt{2}\times\sqrt{2})R45°$ reconstruction has two equivalent domains with respect to the bulk structure. During sputter/anneal cycles, small terraces form independently and grow during extended annealing, eventually merging to create large flat terraces. Where two inequivalent domains meet, an APDB is formed. The equilibrium structure of the APDBs is interpreted in terms of the distorted B-layer model for the $(\sqrt{2}\times\sqrt{2})R45°$ reconstruction, in which a lattice distortion coupled to subsurface charge order stabilize this polar surface. The APDBs are remarkably stable, withstanding prolonged annealing at 700 °C. DFT+U calculations reveal that the observed APDB structure is linked to a disruption in the subsurface charge order pattern, leading to an enrichment of Fe^{2+} cations at the APDB. Simulated STM images reproduce the appearance of the APDBs in the experimental data and reveal that they are preferential adsorption sites for hydroxyl groups.

In addition, we present a route to produce a reduced, well-ordered surface by evaporating Fe on the distorted B layer at room temperature. Using STM we show that the surface contains Fe monomers and Fe clusters. Mild annealing of the sample leads to a surface containing Fe

monomers and dimers with a coverage-dependent density: 2-fold coordinated Fe(A) monomers and 5-fold coordinated Fe dimers [3] at low and intermediate coverages, respectively. Both surfaces contain Fe adatoms located at the 'narrow' position within the unit cell, indicating a strong preference for sites located above Fe^{2+} cations in the subsurface. For higher Fe doses the surface exhibits an FeO-like structure with Fe atoms in both 'narrow' and 'wide' positions. ARXPS indicates that all Fe-rich surfaces contain mostly Fe^{2+}.

This material is based upon work supported as part of the Center for Atomic-Level Catalyst Design, an Energy Frontier Research Center funded by the U.S. Department of Energy, Office of Science, Office of Basic Energy Sciences under Award Number #DE-SC0001058.

[1] R. Pentcheva et al., Phys. Rev. Lett. 94 126101 (2005)
[2] Z. Lodziana, Phys. Rev. Lett. 99, 206402 (2007)
[3] G. S. Parkinson et al., Surf. Sci. 605, iss. 15-16, L42-L45 (2011)

The true explanation is typically rather simple

Günther Rupprechter, Karin Föttinger, Andreas Haghofer, Christian Weilach, Katrin Zorn

[a]*Institute of Materials Chemistry, Vienna University of Technology, Austria*
(corresponding author: grupp@imc.tuwien.ac.at)

We all know examples for that: people come up with models explaining surface processes and, sometimes, the model are rather fancy. When further results disagree with the originally proposed and promoted model, the model is modified to be even more complex.

However, in many cases, the original model may simply be wrong.

The current contribution discusses 4 examples of this "phenomenon",

i) the structure and selectivity of PdZn surface alloys [1,2],

ii) hydrogen adsorption on Ga_2O_3 and reactions on PdGa-Ga_2O_3 [3,4],

iii) CO dissociation on noble metals [5,6],

iv) CO oxidation on metallic vs. oxidic surfaces [7,8],

hopefully illustrating how proper experiments lead to right answers.

Do they ?

[1] Ch. Rameshan, W. Stadlmayr, Ch. Weilach, S. Penner, H. Lorenz, M. Hävecker, R. Blume, T. Rocha, D. Teschner, A. Knop-Gericke, R. Schlögl, N. Memmel, D. Zemlyanov, G. Rupprechter, B. Klötzer, Angewandte Chemie International Edition, 49 (2010) 3224.
[2] K. Föttinger, J.A. Van Bokhoven, M. Nachtegaal, G. Rupprechter, Journal of Physical Chemistry Letters, 2 (2011) 428-433.
[3] W. Jochum, S. Penner, R. Kramer, K. Föttinger, G. Rupprechter, B. Klötzer, Journal of Catalysis, 256 (2008) 278-286; 256 (2008) 268-277.
[4] A. Haghofer, K. Föttinger, F. Girgsdies, D. Teschner, A. Knop-Gericke, R. Schlögl, G. Rupprechter, Journal of Catalysis, in press. doi:10.1016/j.jcat.2011.10.007.
[5] K. Föttinger, R. Schlögl, G. Rupprechter, Chemical Communications, 2008, 320-322.
[6] Ch. Weilach; Ch. Spiel; K. Föttinger, G. Rupprechter, Surface Science, 605 (2011) 1503–1509.
[7] H. Gabasch, A. Knop-Gericke, R. Schlögl, M. Borasio, C. Weilach , G. Rupprechter, S. Penner, B. Jenewein, K. Hayek, B. Klötzer, Physical Chem. Chem. Physics, 9 (2007) 533.
[8] K. Zorn, S. Giorgio, E. Halwax, C. R. Henry, H. Grönbeck, G. Rupprechter, Journal of Physical Chemistry C, 115 (2011) 1103–1111.

Electronic and Magnetic Properties of Partially Sulphur-Terminated Graphene Nanoribbons on Au(111)

Pepa Cabrera-Sanfelix,[1] Andrés Arnau[1,2,3] and Daniel Sánchez-Portal[1,2]*

[1] *Donostia International Physics Center (DIPC), UPV/EHU, Paseo Manuel de Lardizabal 4, San Sebastián 20018, Spain*

[2] *Centro de Física de Materiales (CFM-MPC) CSIC-UPV/EHU, Paseo Manuel de Larizabal 5, San Sebastián 20018, Spain*

[3] *Departamento de Física de Materiales UPV/EHU, Facultad de Química, Apdo. 1072, San Sebastián 20080, Spain*

* *sqbsapod@ehu.es*

Using density functional theory calculations, we have analyzed the electronic and magnetic properties of ultrathin zigzag graphene nanoribbons (ZGNR) with different edge saturations. We have compared a symmetric hydrogen saturation of both edges with an asymmetric saturation in which one of the edges is saturated with sulphur atoms or thiol groups. We have also considered the vertical adsorption of such partially thiolated ZGNRs on Au(111). We find that the functionalization with sulphur atoms or thiol groups removes the corresponding edge state from the Fermi energy and kills the associated spin polarization. However, this effect is very local and the electronic and magnetic properties of the mono-hydrogenated edge (H-edge) remain unaffected. Thus, the system develops a spin moment mainly localized at the H-edge. This property remains unmodified when the partially thiolated ribbon is attached to a gold substrate, and is quite independent on the width of the ribbon. Therefore, the vertical adsorption of partially thiolated ZGNRs can be an effective way to decouple the spin-polarized channel provided by the H-edge of such ZGNRs from an underlying metallic substrate. These observations might open a novel route to build spin-filter devices using ZNGR's on gold substrates.

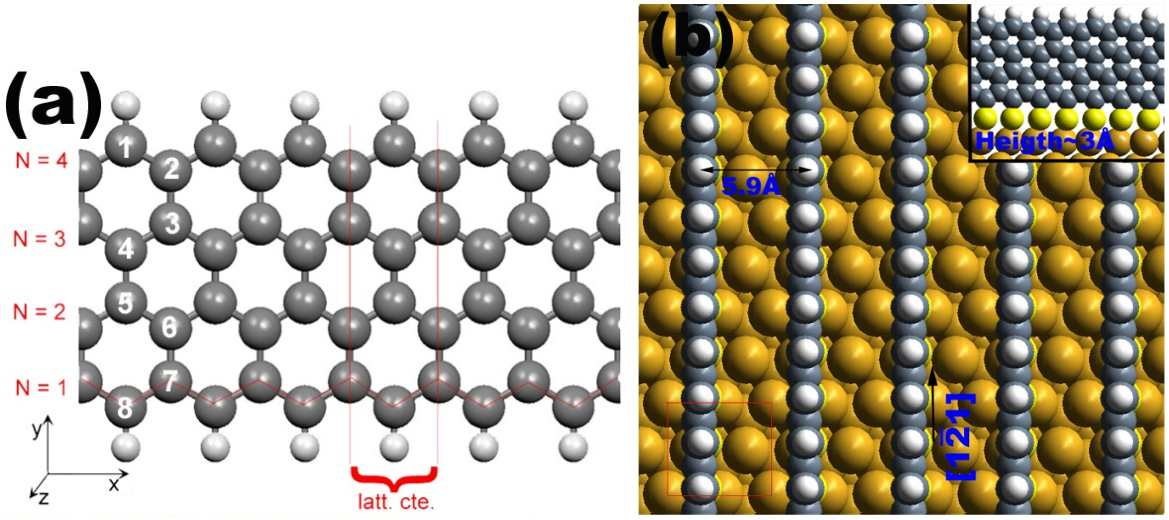

Figure. (a) Ultrathin zigzag graphene nanoribbon formed by N=4 trans-polyacetylene-chains (N=4)-ZGNR and saturated by hydrogen atoms at both edges. (b) Asymmetric S-(N=4)-ZNGR-H ribbon vertically adsorbed on the Au(111). Ribbons run along the $[1\bar{2}1]$ direction. Red thin lines delimit the rectangular 2x2 surface supercell used in the calculations.

We acknowledge support from Basque Departamento de Educación, UPV/EHU (Grant No. IT-366-07), the Spanish Ministerio de Educación y Ciencia (Grant No. FIS2010-19609-C02-00), and the ETORTEK research program funded by the Basque Departamento de Industria and the Diputación Foral de Gipuzkoa. PCS acknowledges support by the Diputación Foral de Gipuzkoa.

Dynamical Coulomb blockade observed in nano-sized electrical contacts

C. Brun[1,2], K. H. Müller[3], I.-P. Hong[1,4], F. Patthey[1], C. Flindt[3], and W.-D. Schneider[1]

[1]*Institut de Physique de la Matière Condensée, Ecole Polytechnique Fédérale de Lausanne (EPFL), CH-1015 Lausanne, Switzerland*
[2]*Institut des Nanosciences de Paris, CNRS-UMR 7588, Université Pierre et Marie Curie-Paris 6 UPMC, F-75252, Paris, France*
[3]*Département de Physique Théorique, Université de Genève, CH2111 Genève, Switzerland*
[4]*Institut für Experimentelle und Angewandte Physik, Christian-Albrechts-Universität zu Kiel, D-24098 Kiel, Germany*
(corresponding author: W.-D. Schneider, e-mail: wolf-dieter.schneider@epfl.ch)

Electrical contacts between nano-engineered systems are expected to constitute the basic building blocks of future nano-scale electronics. However, the accurate characterization and understanding of electrical contacts at the nano-scale is an experimentally challenging task. Here we employ low-temperature scanning tunneling spectroscopy to investigate the conductance of individual nano-contacts formed between flat Pb islands and their supporting substrates. We observe a suppression of the differential tunnel conductance at small bias voltages due to dynamical Coulomb blockade effects. The differential conductance spectra allow us to determine the capacitances and resistances of the electrical contacts which depend systematically on the island-substrate contact area. Calculations based on the theory of environmentally assisted tunneling agree well with the measurements [1].

As model systems for nanocontacts we have chosen to grow Pb islands of various lateral sizes and thicknesses down to a few nanometers on Si(111)-7x7, HOPG, BN/Ni(111), NaCl/Ag(111) and on Cu(111). Lead was thermally evaporated in an ultrahigh vacuum (UHV) chamber onto these different substrates. In each case the substrate temperature, the Pb flux and the Pb evaporation time were controlled and adapted to achieve favourable island growth conditions. The samples were transferred *in situ* into a custom-built STM operated in UHV at a base temperature of 4.6 K [2]. On Si(111) and on Cu(111) single crystal flat top Pb islands grow along the (111) direction on top of a one monolayer (ML) thick wetting layer (WL) [3,4]. On HOPG, BN/Ni(111), and on NaCl/Ag(111) flat top Pb islands grow on top of the substrate without the formation of a WL. The local imaging capabilities of the STM are used to precisely determine the nano-contact size and thickness on the atomic scale.

The present work facilitates quantitatively investigations of electrical nano-contacts and is important for future studies of the physical and chemical properties of supported nano-structures in relation to superconductivity, magnetism, and catalysis.

Support by the Swisss National Science Foundation is gratefully acknowledged.

[1] C. Brun, K. H. Müller, I-Po Hong, F. Patthey, C. Flindt, and W.-D. Schneider, Phys. Rev. Lett., submitted.
[2] R. Gaisch, J.K. Gimzewski, B. Reihl, R.R. Schlittler, M. Tschudy, and W.-D. Schneider, Ultramicroscopy 42-44, 1621 (1992).
[3] I.-P. Hong, C. Brun, F. Patthey, I. Yu. Sklyadneva, X. Zubizarreta, R. Heid, V. M. Silkin, P. M. Echenique, K. P. Bohnen, E. V. Chulkov, and W.-D. Schneider, Phys. Rev. B 80, 081409(R) (2009), and references therein.
[4] C. Brun, I.-P. Hong, F. Patthey, I. Yu. Sklyadneva, R. Heid, P. M. Echenique, K. P. Bohnen, E. V. Chulkov, and W.-D. Schneider, Phys. Rev. Lett. 102, 207002 (2009), and references therein.

Low-energy collective electronic excitations in thin metallic films

V. M. Silkin[1,2,3], J. P. Echeverry[1], V. Despoja[2], P. M. Echenique[1,2,4], and E. V. Chulkov[1,2,4]

[1] *Dpto. de Física de Materiales, Facultad de Ciencias Quimicas, Universidad del País Vasco, Apto. 1072, E-20080 San Sebastián/Donosita, Spain*
(corresponding author: V. M. Silkin, e-mail: waxslavas@sc.ehu.es)

[2] *Donostia International Physics Center (DIPC), P. de Manuel Lardizabal 4, E-20018 San Sebastián/Donosita, Spain*

[3] *IKERBASQUE, Basque Foundation for Science, E-48011 Bilbao, Spain*

[4] *Centro de Física de Materiales CFM/Materials Physics Center MPC, Centro Mixto CSIC-UPV/EHU, P. de Manuel Lardizabal 5, E-20018 San Sebastián/Donosita, Spain*

The physical and chemical properties of metallic objects are affected markedly by size and shape when the size shrinks down to the scale of the electron Fermi wavelength which in most metals is comparable with interatomic distances [1]. Hence when the characteristic size decreases to the atomic scale, quantum effects can become important. A remarkable example of such effects is quantization of electronic states in the case of thin semiconducting and metallic films [2]. As a result of this quantization, description of the electronic excitations in such systems may not be described properly by classical theories and a true quantum-mechanical treatment should be applied. In the case of semiconducting heterostructures the previous such studies of collective electronic excitations or plasmons have shown that the sub-band (or quantum-well states) structure in the electronic spectrum produces strong quantum effects in a low-energy excitation spectra. In particular, in addition to the conventional intra-sub-band plasmon, an analogue of a pure two-dimensional plasmon [3], the inter-sub-band transitions give origin to higher-energy inter-sub-band plasmons [4,5,6]. However, in the case of metallic films this approach based on the electronic band structure obtained with the use of a quasi free-electron-like model may be inadequate. In particular, such a model can not reproduce the surface electronic states which have a strong implication in many phenomena occurring at the metal surfaces. In the case of thin metallic films this effect can be even stronger and, in particular, can affect significantly the excitation spectra.

Here we present results of self-consistent calculations of the excitation spectra of atomically thin Ag(111) films taking into account its band structure evaluated using a model potential [7] constructed some time ago to describe in realistic manner the surface electronic

structure of variety of metals. Our study demonstrates how the quantization of electronic states in such thin metallic films is reflected in the excitation spectra in the low-energy domain, where several modes can be observed [8]. Thus, in addition to the conventional two-dimensional plasmon, we find modes related to the slab-split surface electronic states and other modes originated from the interband transitions between these surface-like states and the bulk-like quantum-well states. The influence of these modes on the IR optical properties of the metallic films is investigated as well.

[1] N. W. Ashcroft and N. D. Mermin, *Solid State Physics* (Holt, Rineheart & Winston, New York, 1976)

[2] T.-C. Chiang, Surf. Sci. Rep. 39, 181 (2000)

[3] F. Stern, Phys. Rev. Lett. 18, 546 (1967)

[4] D. A. Dahl and L. J. Sham, Phys. Rev. B 16, 651 (1977)

[5] T. Ando, A. B. Fowler, F. Stern, Rev. Mod. Phys. 54, 437 (1982)

[6] J. K. Jain and S. Das Sarma, Phys. Rev. B 36, 5949 (1987)

[7] E. V. Chulkov, V. M. Silkin, P. M. Echeniqiue, Surf. Sci. 437, 330 (1999)

[8] V. M. Silkin, T. Nagao, V. Despoja, J. P. Echeverry, S. V. Eremeev, E. V. Chulkov, P. M. Echeniqiue, Phys. Rev. B 84, 165416 (2011)

CO oxidation on individual grains of polycrystalline Pd: Laterally-resolved reaction kinetics by PEEM

D. Vogel[1,2] Ch. Spiel[1], Y Suchorski[1], R. Schlögl[2], G. Rupprechter[1]

[1]*Institute of Materials Chemistry, Vienna University of Technology, A-1210 Vienna, Austria*

[2]*Fritz-Haber-Institut der Max-Planck-Gesellschaft, D-14195 Berlin, Germany*

(corresponding author: Y. Suchorski, e-mail: yuri.suchorski@imc.tuwien.ac.at)

To describe the behavior of a heterogeneous catalyst, laterally-resolved studies of reaction kinetics are necessary. Up to date, experimental kinetic studies of heterogeneous surfaces were mainly performed by mass spectroscopy (MS) and suffer from spatial averaging over the whole catalyst.

A certain improvement can be achieved by ‘‘scanning-MS’’ using gas sampling via a capillary leak (with a lateral resolution of about 0.2 mm [1]). Nevertheless, as with every scanning procedure, a real *parallel* measurement on different grains or facets is not possible within such an approach.

We have demonstrated newly, that it is possible to obtain the local kinetic data (on a μm-scale) in CO oxidation on a polycrystalline Pt foil by analysis of the local PEEM intensities during the reaction [2]. The approach is based on the fact that the local photoemission yield during the reaction is related (via the local work function) to the CO or oxygen coverage. The mentioned coverage governs also directly the rate of the CO oxidation reaction [3]. Thus the analysis of the local photoemission yield (i.e. local PEEM intensity) might provide the local kinetic data [2, 4, 5]. Simultaneously, the global kinetics can be monitored by mass-spectrometry (MS, Fig.1).

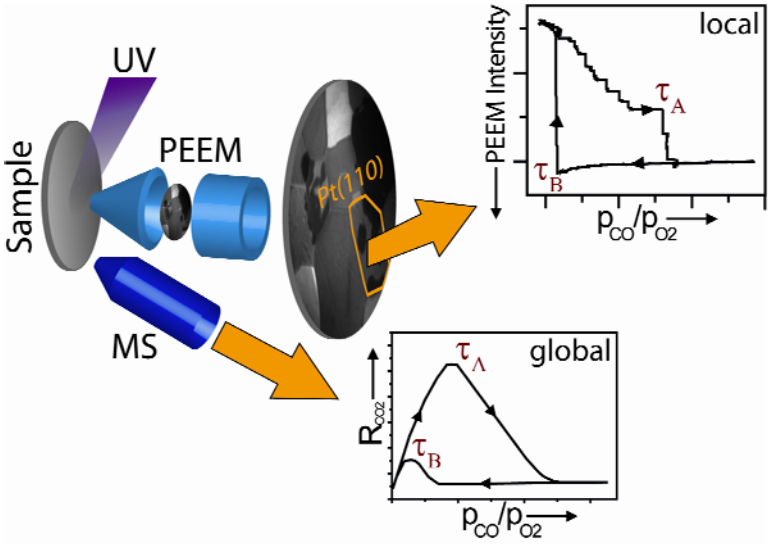

Fig.1. Scheme of the experiment: Simultaneous monitoring of the CO oxidation by PEEM and MS allows to determine the global (via MS) and local kinetic phase transitions (τ_a and τ_b) on the hetero-geneous samples.

.

In present contribution, we apply this approach to study the kinetic transitions in CO oxidation on individual crystalline grains of a polycrystalline Pd foil. The analysis of the local intensity of video-PEEM images recorded *in situ* during the catalytic CO oxidation in the 10^{-5} mbar pressure range yielded the local kinetic transitions between the high- and low-activity steady states on the individual (100), (110) and (111) orientations. From these transitions local kinetic phase diagrams were obtained for all three orientations at exactly the same experimental conditions (since in one experiment on one polycrystalline sample) and compared to the global (simultaneously measured by MS) phase diagram. As already has been observed in our earlier studies on a polycrystalline Pt foil [2, 4, 5], a quasi-independent reaction behaviour of the particular grains under the present reaction conditions could be found

To study the structure-reactivity relation, surface defects were artificially created by Ar^+-sputtering of the annealed surface. The Ar^+-sputtering lead to a shift of the (global and local) kinetic phase diagrams to higher CO pressures indicating a higher reactivity of the artificially defected surface. In addition, the independent behavior of the individual grains vanishes because of the similar sputtering-induced defect density on the differently oriented grains and of the transboundary reaction-coupling between the domains via CO diffusion.

Support by the Fonds zur Förderung der Wissenschaftlichen Forschung (SFB-F45-04 FOXSI) is gratefully acknowledged. Authors also thank Johannes Frank (IMC, TU Vienna) for his technical support.

[1] M. Johansson, J. Hoffmann Jørgensen, I. Chorkendorff, Rev. Sci. Instrum. 75, 2082 (2004)

[2] Y. Suchorski, Ch. Spiel, D. Vogel, W. Drachsel, R. Schlögl, G. Rupprechter, Chem.Phys.Chem. 11, 3231 (2010)

[3] G. Ertl, Science 254, 1750 (1991)

[4] C. Spiel, D. Vogel, Y. Suchorski, W. Drachsel, R. Schlögl, G. Rupprechter, Cat. Lett, 141, 625 (2011)

[5] D. Vogel, C. Spiel, Y. Suchorski, A. Urich, R. Schlögl, G. Rupprechter, Surf. Sci. 605, 1999 (2011)

MEMS devices as fast STM scanners: options and difficulties, an overview

F.C. Tabak[1], H. Borsboom[1], J.W.M. Frenken[1], W.M. van Spengen[2]

1. LION, Leiden Institute of Physics, Leiden University, Niels Bohrweg 2, 2333 CA Leiden, The Netherlands (corresponding author F.C. Tabak, tabak@physics.leidenuniv.nl).

2. 3mE, Faculty of Mechanical, Maritime and Materials Engineering, Delft University, Mekelweg 2, 2628 CD Delft, The Netherlands

MEMS (Micro-Electro Mechanical Systems) scanners can be designed to perform fast STM scanning motion [1]. The main advantage of these MEMS scanners is their high resonance frequency: resonance frequencies up to the MHz range can be achieved. Due to the small weight, the MEMS scanner will not excite resonances in the mechanical loop of the scanner.

We have investigated the possibilities of employing a MEMS device as STM scanner. We present various solutions to encountered difficulties, along with an overview of problems that need to be solved before MEMS scanners can be used on a regular basis.

While it is the goal to, finally, design a MEMS scanner that can perform fast scanning motion in three directions, we first design a scanner which performs fast scanning motion in the z-direction only. We incorporate this MEMS device on top of a piezo scanning element. The piezo element will perform x,y-scanning and the large-range z motion. The MEMS scanner has a range of motion of approximately 600 nm.

In implementing a MEMS scanner in an STM system, we need to solve two design problems. First, we need to deposit a tip on the MEMS scanner which has a good conductivity. Second, we need to integrate the MEMS scanner on the piezo element in a way that minimizes crosstalk and prevents crashes between the chip and the sample. These two elements will be discussed briefly.

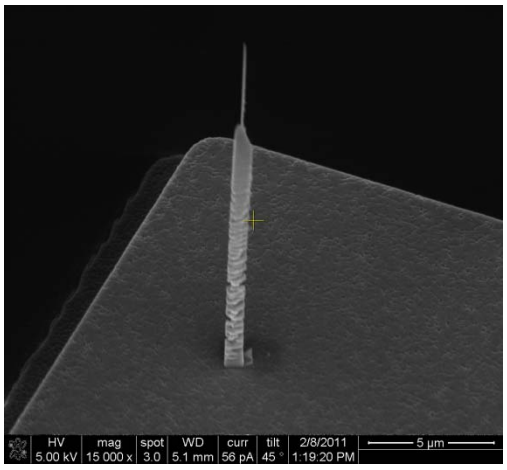

Figure 1: (Part of) MEMS scanner with platinum tip deposited by EBID.

We deposit an EBID (electron-beam-induced deposition) platinum tip on the MEMS scanner. The size ratio between the sample and scanner / tip is different than in a piezo element-based scanner: the tip is approximately 10 micrometers long and placed on the scanner which is 40 micrometers in diameter (see figure 1). The scanner is on a chip with a size of 2.5 mm. We have to be careful to not crash a side of the scanner or even the chip onto the sample during the approach.

In addition, since the MEMS scanner slightly deforms while being actuated, if the tip is not situated in the middle of the scanner, it will tilt

during z-motion and this will lead to image deformation. We have tested the deformation of the scanning membrane in a white-light interferometer and find that the membrane deformation is smaller than 20 nm. This means that in the worst-case scenario, with the tip located completely at the far edge of the scanner, the image deformation will be at most 4 nm. We have tested the electrical conductivity of the lower parts of the tips and find that the resistance is relatively high: in the MΩ range. Although this is high, it is relatively small compared to that of the tunnel gap (~1GΩ). However, we find that we are not able to obtain atomic resolution with these tips. We have tested them in a 'regular' STM by depositing an EBID tip at the end of a conventional PtIr tip and scanning on HOPG. Even in this 'simple' configuration atomic resolution could not be reached, even though SEM inspection shows that the tip apex was sufficiently sharp. We suspect that due to the nature of EBID deposition, the conductivity of the apex has been poor and non-uniformly distributed.

The second challenge is to integrate the MEMS device on the piezo element in a way that minimizes crosstalk and prevents crashes between the chip and the sample. We have minimized crosstalk by shielding the MEMS scanner with a flexible piece of copper – this is a temporary solution while a MEMS-holder is being developed that incorporates proper shielding. This can fit the MEMS device on the piezo element and make electrical contact with the contact pads on the MEMS device, making wire bonding no longer necessary. In addition, we have designed a scanner with on-chip shielding.

We have used the MEMS scanner in a first experiment, scanning on HOPG. We placed the MEMS scanner on top of a piezo scanning element, which performed the scanning motion. The MEMS scanner and tip were on top and made the tunneling contact to the sample; however, the MEMS scanner was not actuated. Although we establish a stable tunneling contact, we see that the images exhibit poor resolution, which we again attribute to the conductivity of the tip apex.

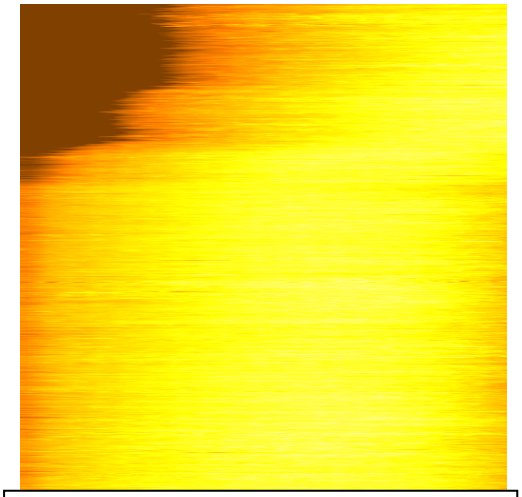

Figure 2: First MEMS STM image, taken with a MEMS scanner with a Pt EBID tip on top of a piezo scanning element. The sample is HOPG and the scan size is ~500 nm x 500 nm. The color scale spans a height range of a few nm.

In conclusion, we have found that although MEMS scanners are promising as fast STM scanners, the tip quality needs to be improved for these scanners to become useful in practical experiments. We propose the use of gold tips, which can be deposited with a high purity by EBID deposition.

1. F.C. Tabak, E.C.M. Disseldorp, G.H. Wortel, A.J. Katan, M.B.S. Hesselberth, T.H. Oosterkamp, J.W.M. Frenken and W.M. van Spengen, Ultramicroscopy 110 (2010)

Information depth of low-energy ion scattering in the reionization regime

D. Primetzhofer, M. Spitz, P. Bauer

Institut für Experimentalphysik, Johannes Kepler Universität Linz, A-4040 Linz, Austria

E. Taglauer

Max-Planck-Institut für Plasmaphysik, EURATOM Association, D-85748 Garching bei München, Germany (taglauer@ipp.mpg.de)

Probabilities for charge transfer can be determined from Time-of-Flight low-energy ion scattering experiments. In the present study He+ ions in the primary energy range from 1 to 10 keV were scattered from Cu(100) and CuAu(100) single crystal and polycrstalline Cu surfaces. From the experimental results probabilities were deduced for resonant neutralization and reionization in close collisions. The relative yields were calculated for backscattered particles that have undergone distinct charge exchange processes. Our results indicate a strong contribution to the ion yield that originates from particles reionized during a close collision in deeper layers if the experiments are performed at energies where reionization is prominent. The surface sensitivity of the ion signal at different primary energies is quantified, see e.g. Fig. 1.

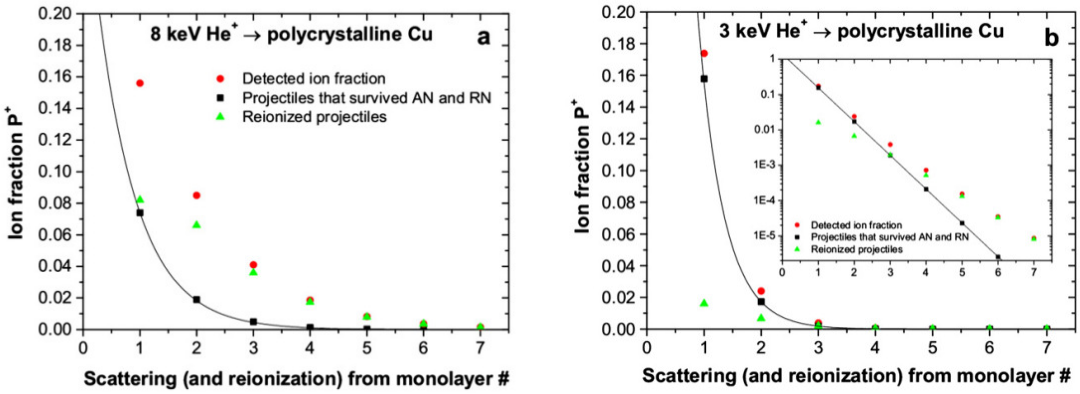

Fig. 1: Calculated ion fractions for
a) 8 keV He^+ projectiles scattered from the first seven monolayers in polycrystalline Cu,
b) 3 keV He^+ projectiles scattered from the first seven monolayers in polycrystalline Cu.

The total ion fraction (red circles), the fraction of projectiles reionized in a close collision (green triangles), and the fraction of projectiles, which survived Auger neutralization (AN) and resonance neutralization (RN) in a close collision (black squares) is shown. The inset in b) shows the same data with logarithmic ordinate.

Based on these results, the total ion spectrum was quantitatively modelled by two different but consistent approaches [1], see Fig. 2.

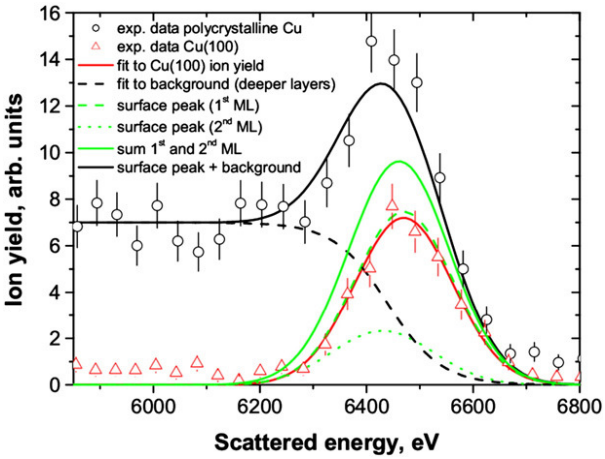

Fig. 2. Experimental ion spectra for 8 keV He+ ions scattered from polycrystalline Cu (black open circles) and a Cu(100) single crystal in double alignment geometry (red open triangles). Also shown is a fit to the low energy background for the polycrystal (dashed black line) and calculations for the expected ion yield from scattering from the first two monolayers (dashed and dotted green (grey) lines respectively) based on the single crystal data. The sum of the fitting models (black full line) shows very good agreement with the experiment.

This work was supported by the Austrian Science Fund (FWF) under Contract No. P20831.

[1] D. Primetzhofer, M. Spitz, E. Taglauer, P. Bauer, Surf. Sci.605 (2011) 1913.

Cap-shaped noble metal particles adsorbed on a solid support as a platform for surface-enhanced colorimetric, fluorescence and Raman spectroscopies

H. Takei[1], N. Bessho, T. Kawakami,
R. Shitara, and Y. Kuriyama

Department of Life Sciences, Toyo University, 1-1-1 Izumino, Itakura-machi, Gunma, 374-0193, Japan
(corresponding author: H. Takei, e-mail: h_takei@toyo.jp)

[1]Bio-Nano Electronic Research Center, Toyo University, 2100, Kujirai, Kawagoe, Saitama, 350-8585, Japan

In this work, we discuss various forms of surface-enhanced optical detection schemes based on surface-adsorbed noble metal nanoparticles. Surface-enhancement is a phenomenon based on what is called an optical "near-field" generated in the close vicinity of a noble metal nanostructure upon irradiation by an electromagnetic wave, most typically in the UV-Vis/Near IR region [1]. The near-field is characterized by an intense electromagnetic field, more than a few orders of magnitude greater in intensity than that of the incident field.

When molecules to be analyzed are brought into the optical near-field, signals can be enhanced. The scale of enhancement depends critically on the shape, size, material of nanoparticles as well as the interaction among nanoparticles [2]. We have been developing a method whereby a single layer of monodisperse SiO_2 spheres is formed on a solid support, followed by deposition of a noble metal by thermal evaporation. This leads to formation of a dense monolayer of cap-shaped noble metal particles [3]. It has much similarity with the widely-known nanosphere lithographic technique developed by Van Duyne et al. [4], but our system consists of randomly positioned nanospheres rather than a well-ordered array, which lead to unique characteristics.

To demonstrate usefulness of such particles, we have explored applications with colorimetric, fluorescence and Raman spectroscopies. Previously there has been a report that a common substrate could be useful for both surface-enhanced Raman and infrared absorption [5]. Even though various analytical techniques based on photon detection can benefit from the near-field, the substrate must be uniquely optimized for different techniques [6]. The spatial distribution of a near-field is greatly influenced not only by the shape and size of individual particles but also by inteactions among adjacent particles as well as with the underlying surface. Moreover, the positioning of the target molecule within the near-field can be of critical importance. For example, molecules need to be located in so-called „hot spot", a narrow region sandwiched by

two neighboring particles, in direct contact with the metal surface for Raman spectroscosy, but for fluorescence, there must be a separation on the order of 10 nm between the molecule and metal, in order to suppress quenching. On the other hand, for colorimetric detection, it is crucial that the particles exhibit a sharp absorption, with a narrow band width [10], because the sensing is based on shift in the absorption peak wavelength upon change in the dielectric constant of the surroundings.

For colorimetric assays, we deposited alkaline phosphatase on Au nanoparticles, 100 nm in diameter with 20 nm of Au. Addition of a substrate, NBT/BCIP, leads to formation of a non-soluble product, which can be readily detected by change in color of Au nanoparticles. The increase in the signal is estimated to be 4-fold against controls. For fluorescence and Raman, we have deposited rhodamine 6 G as a model compound on Ag nanoparticles. The enhancement factors for these detection methods are estimated to be ten-fold and more than one thousand fold respectively.

Optimization involves explorations of the nanosphere size, metal deposition thickness, metal species, nanosphere adsorption density etc. on one hand, and on the other hand, search for methods for capturing target molecules becomes a crucial issue. For immunoassays, it is clear that antibodies must be anchored to the surface, but even for other applications, it is desirable to have a surface with some affinity toward the target molecules. We will desribe various schemes for efficient capture.

In addition, we will also describe how the random arrangement of adsorbed spheres can be exploited; in recent years, it is being recognized that random systems, some with nanospheres with varying diameters, are more advantageous for surface-enhanced spectroscopies [12]. We will show that mixing nanospheres with different diameters in a random system indeed improves the enhancement ratio for Raman spectroscopy.

[1] S. Nie and S. R. Emory, *Science* 275, 1102 (1997)
[2] K. L. Wustholz, A.-I. Henry, J. M. McMahon, R. G. Freeman, N. Valley, M. E. Piotti, M. J. Natan, G. C. Schatz and R. P. Van Duyne, JACS 132, 10903 (2010)
[3] H. Takei, J. Vac. Sci. Technol. B 17, 1906 (1999)
[4] A. D. Ormonde, E. C. M. Hicks, J. Castillo and R. P. Van Duyne, Langmuir 20, 6927 (2004)
[5] F. Le, D.W. Brandl, Y. A. Urzhumov, H. Wang, J. Kundu, N. J. Halas, J. Aizpurua and P. Nordlander, ACS Nano 2, 707 (2008)
[6] S. Lai, N. K. Grady, J. Kundu, C. S. Levin, J. B. Lassiter and N. J. Halas, Chem. Soc. Rev. 37, 898 (2008)
[7] H. Wang, C. S. Levin and N. J. Halas, JACS 127, 14992 (2005)
[8] J. Zhang and J. R. Lakowicz, Optics Express 15, 2598 (2006)
[9] T. Yamaguchi, T. Kaya, M. Aoyama and H. Takei, Analyst 134, 776 (2009)
[10] M. Himmelhaus and H. Takei, Sensors and Actuators B 63, 24 (2000)
[11] H. Takei and T. Yamaguchi, Phys. Chem. Chem. Phys. 12, 4505 (2010)
[12] M. Baia, L. Baia and S. Astilean, Che Phys. Lett. 404, 3 (2005)

The relative influence of work function and stoichiometry of GaAs(001) surface on Cs - promoted oxygen adsorption

K.V. Toropetsky, H.E. Scheibler and A.S. Terekhov

Institute of Semiconductor Physics SB RAS, 630090, Novosibirsk, Russia

e-mail: terek@ngs.ru

It was found many years ago [1], that the probability of oxygen adsorption on the GaAs(110) surface is as low, as ~ 10^{-6}, but it increases up to ~ 1, if surface is covered with ~ 0.7 ML of Cs. It was observed also, that Cs-promoted O_2-adsorption is not saturated if the oxygen exposure is increased up to ~ 10^6 L and it is accompanied by the oxidation of GaAs [2]. No details of Cs-promoted O_2-adsorption and oxidation were elucidated. To understand more the "driving force" of these processes, we investigated Cs-promoted O_2-adsorption on polar GaAs (001) surface with Ga-terminated reconstruction (4x2) at low Cs-coverages ($\theta_{Cs} < 0.5$ ML) and moderate O_2-exposures ($D_{Ox} < 15$ L) [3]. XPS data show, that Cs-promoted O_2-adsorption at GaAs surface occurs, if θ_{Cs} exceeded threshold value $\theta_{Cs}^{th} \sim 0.1$ ML. The amount of the adsorbed oxygen increased with the increase of O_2-exposure up to ~ 2 L, but at $D_{Ox} > 2$ L oxygen adsorption saturated. Measurements of work function φ of GaAs(Cs, O) surface along with Cs- and O_2-adsorption revealed the following: (i) Cs-promoted O_2-adsorption "starts", when the work function of GaAs(Cs) surface is lowered by Cs-adsorption below threshold value $\varphi^{th} \sim 3.1$ eV and (ii) Cs-promoted O_2-adsorption "stops", when the work-function of GaAs(Cs, O) surface is increased by O_2-adsorption above the same $\varphi^{th} \sim 3.1$ eV. In the present work we continued to study Cs-promoted O_2-adsorption on GaAs, having in mind to answer two questions: (i) does φ_{th} depend on the stoichiometry of GaAs(001) surface? and (ii) why the Cs-promoted O_2-adsorption on GaAs(Cs) surface is not saturated, if $\theta_{Cs} \approx 0.7$ ML? To answer the first question we studied both Ga-terminated and As-terminated GaAs(001) surfaces with (4x2)- and (2x4)-reconstructions, respectively. Integral UV photoemission and photoelectron energy distribution curves (EDC) were used for the detection of adsorption of both Cs and oxygen atoms and for the measuring of the work function, respectively. The measuring procedure was as follows. Surface of p-doped GaAs was illuminated with UV-light from the deuterium lamp and the integral photoemission current $J_{ph}(t)$ was measured. Then the oxygen pressure $P_{ox}(t)$ within UHV-chamber was periodically "modulated" by the computer-controlled O_2-dispenser. The oxygen dose in every pulse was equal to 0.1 ± 0.01 L. No influence of O_2-exposers on $J_{ph}(t)$ was detected. Then the calibrated cesium dispenser was turned on and Cs-layer began to grow on the GaAs-surface at the rate 7.5×10^{-4} ML/min.

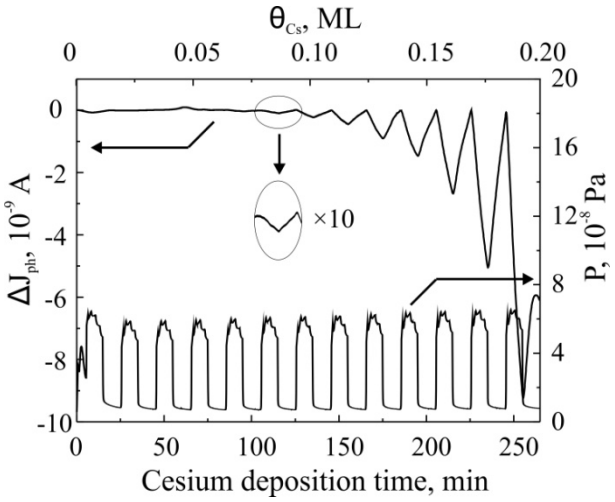

Growth of θ_{Cs} immediately manifested itself by monotonous growth of $J_{ph}(t)$, but GaAs(Cs) surface was still insensitive to the O_2-exposers up to the moment, when θ_{Cs} exceeded the θ_{Cs}^{th} Since that every O_2-exposer provoked kink on $J_{ph}(t)$. To increase the of measured data we subtracted smooth component of $J_{ph}(t)$. The resulted $\Delta J_{ph}(t)$-curve together with $P_{ox}(t)$ are shown of figure. One can see, that the falling edge of every O_2-exposer corresponds to the maximum of negative pulse of $\Delta J_{ph}(t)$. The position of first negative pulse of $\Delta J_{ph}(t)$ is marked by arrow. Value of θ_{Cs}^{th} was estimated to be 0.075 ± 0.005 ML. To determine $\varphi(t)$, energy distributions of emitted electrons were measured. The described techniques were used not only for the determination of θ_{Cs}^{th}, but for the detection of the saturation of Cs-promoted O_2-adsorption and for the study Cs-promoted oxidation of GaAs also. Results obtained led us to the following findings: (i) the existence of threshold values of θ_{Cs}^{th} and φ^{th} is confirmed by new techniques; (ii) more accurate data for threshold values of θ_{Cs}^{th} and φ^{th} were obtained; (iii) the influence of stoichiometry (reconstruction) of the GaAs(001) surface on values of θ_{Cs}^{th} and φ^{th} is not found within the experimental accuracy; (iiii) Cs-promoted oxygen adsorption on GaAs(Cs, O) surface is not saturated at $\theta_{Cs} \approx 0.7$ ML because under such conditions the work function is not increased above ~ 2.8 eV, which is lower than φ^{th}, even at very high O_2-esposures. Summarizing our experimental findings, we come to the following conclusion: Cs-promoted oxygen adsorption on GaAs(001) surface and the Cs-promoted oxidation of this surface are dominated by the surface work function and, within the experimental accuracy of our measurements, do not depend on the fine details of the atomic structure and chemical composition of initial atomically clean GaAs(001) surface. Theoretical model, which explain our findings and conclusion can be found in [4]. This work was supported by The Russian Foundation for Basic Research (grant № 12-02-00418-a).

[1] J. E. Ortega, J. Ferron, R. Miranda, C. Laubschat, M. Domke, M. Prietsch, G. Kaindl, Phys. Rev. B 39(17), 12751 (1989)

[2] W. Monch, Surf. Sci. 168, 577 (1986)

[3] K.V. Toropetsky, O.E. Tereshchenko, A.S. Terekhov, JETP Letters 88, 520 (2008)

[4] B. Hellsing, Phys. Rev. B 40, 3855 (1989)

Formation and spectroscopic analysis of conditioning films on self assembled monolayers

I.Thomé[1*], M. E. Pettitt[2], M. E. Callow[2], J.A. Callow[2], M. Grunze[1,3] and A. Rosenhahn[1,3]

[1] Institute for Functional Interfaces, IFG, Karlsruhe Institute of Technology, PO Box 3640, 76021 Karlsruhe, Germany
[2] School of Biosciences, University of Birmingham, Birmingham B15 2TT, United Kingdom
[3] Applied Physical Chemistry, Ruprecht-Karls-University Heidelberg, Im Neuenheimer Feld 253, 69120 Heidelberg, Germany

*e-mail: Isabel.Thome@kit.edu

Biofouling is a ubiquitously occurring phenomenon in intertidal zones worldwide [1]. To prevent unwanted effects caused by biofouling, suitable non-toxic coatings for these environments are required. Changing the surface chemistry and the composition of a coating changes not only its properties but most likely also affects the formation and composition of conditioning layers. In our study self-assembled monolayers (SAMs) on gold are used as highly controlled surface chemistries which allow to fine tune the physicochemical surface properties. In order to correlate colonization with surface conditioning, the surface chemistry and thus their wetting properties were varied. In agreement with previous work, chemical termination of the surface affects the settlement kinetics of spores of the macrofouler *Ulva linza* [2]. To disentangle both effects, *Ulva* settlement on the pristine surface chemistries and the successive formation of conditioning layers depending on the surface chemistry was investigated in greater detail by surface analytical techniques. Spectral ellipsometry was used to measure the increasing conditioning layer thickness over a timescale of 48 hours. Contact angle measurements revealed that formation of this protein layer changes the wettability of the surfaces and with IRRAS it was possible to show, that the surface chemistry changes the composition of the conditioning film. It also could be shown, that organism settlement is significantly changed if pristine chemistries are compared to conditioned surfaces and especially for longer biological assays conditioning needs to be taken into account.

[1] M.E. Callow, J.A. Callow, J.D. Pickett-Heaps, R. Wetherbee, “Primary Adhesion of Enteromorpha (Chlorophyta, Ulvales) Propagules: Quantitative Settlement Studies and Video Microscopy”, *J. Phycol*., **1997**, *33*, 938.

[2] M. E. Callow, J. A. Callow, L. K. Ista, S. E. Coleman, A. C. Nolasco, G. P. López, “Use of self-assembled monolayers of different wettabilities to study surface selection and primary adhesion processes of green algal (*Entero-morpha*) zoospores“, *Appl. Environ. Microbiol*., **2000**, *66*, (8), 3249-3254.

Thursday

Porphyrin nanochemistry – a 2D perspective

Johannes V. Barth
Physik Department E20, TU München, James-Franck Str., D-85748 Garching, Germany

The comprehensive characterization and engineering of low-dimensional nanostructures on surfaces is of significant current interest, both from a scientific and technological point of view. Specifically, the fabrication of molecular nano-architectures on metal surfaces, applying self-assembly protocols inspired from supramolecular chemistry, is a maturing and rapidly advancing field of research. Here we present recent insights putting particular emphasis on results elaborated with porphyrins. Given their intriguing variety of functional properties, which are exploited in both biological and artificial systems, porphyrins are ideally suited both as individual functional units and versatile building blocks in surface-confined nanosystems. Using scanning tunneling microscopy (STM) we determine the order characteristics and inspect or manipulate the interior of these molecules. High-resolution scanning tunneling spectroscopy (STS) allows to determine the pertaining electronic characteristics (frontier orbitals, energy level alignment). Supported with complementary theoretical modeling and space-averaging techniques we address key questions related to their functionality: How does the molecular conformation respond to surface anchoring and what are the consequences for the self-assembly? What determines the reactivity of adsorbed metalloporphyrins towards small gas molecules? Can we achieve and control conductance switches or molecular rotors?

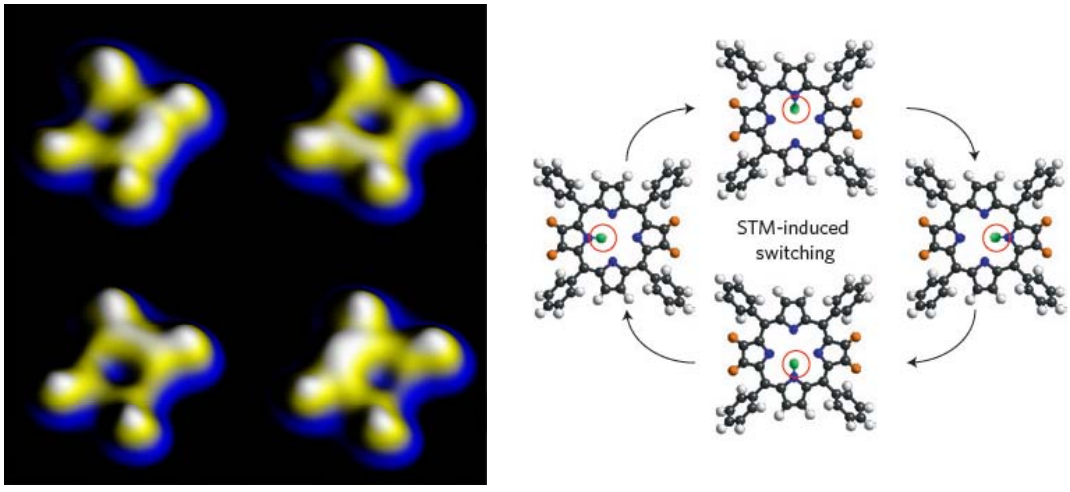

Four-level conductance switch based on single proton transfer. The atomically sharp tip of an STM is used to selectively remove one of the two hydrogen atoms from the central cavity of a free-base porphyrin molecule adsorbed on a metal surface. The position of the remaining hydrogen atom can be switched between the four different positions giving rise to four distinct electric current levels (nnano, in print).

Pore Modified Supramolecular Networks as Templates

Minna T. Räisänen[1+], Anna G. Slater[2], Neil Champness[2], Manfred Buck*

[1]*EaStCHEM School of Chemistry, University of St Andrews,*
*North Haugh, St Andrews KY16 9ST, United Kingdom, *mb45@st-and.ac.uk*
[2]*School of Chemistry, University of Nottingham,*
University Park, Nottingham, NG7 2RD, United Kingdom

Non-covalent molecular networks provide a very flexible route to atomically precise structures [1-3]. One example of a hydrogen bonded network is the system shown in Fig. 1 which consists of melamine and a derivative of perylene-3,4,9,10-tetracarboxylic di-imide (PTCDI). The triple hydrogen bond between the building blocks makes this network sufficiently robust as template for the adsorption of guest species into its pores [4,5] in a completely solvent based process.

Modification of the building blocks by introducing substituents offers additional degrees of freedom in the design of supramolecular templates besides variation in size and symmetry of the building blocks. For the PTCDI–melamine system we investigated how the introduction of adamantane moieties in the bay region of PTCDI (see Fig. 1) influences the adsorption of guest molecules namely adamantane thiol and fullerene which differ substantially in size. Compared to other substituents studied [4] adamantane represents a relatively bulky 3D structure which should have an influence different from atomic or flat lying substituents.

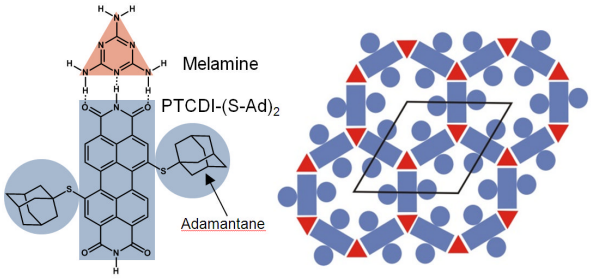

Fig. 1: Synthon (left) of a bimolecular honeycomb network (right) whose hexagonal pore is modified by adamantane moieties attached to PTCDI.

In contrast to adamantane thiol which fits seamlessly between the adamantane units and yields an arrangement identical to the empty pores [5,6], the C_{60} molecules are pronouncedly affected by the adamantane substituents. In contrast to the unsubstituted or Br-substituted PTCDI where a uniform hexagonal configuration involving 7 molecules is realised [4,7], a manifold of C_{60} arrangements is realised for the PTCDI-$(S\text{-}Ad)_2$-melamine network as evidenced by Fig. 2. Aggregates of 3-7 fullerene molecules and for a given number of molecules different geometries are discernible. The different geometries are the result of two particularities of this network. Firstly, the network consists of a mixture of PTCDI units with and without adamantane substituents. Secondly, PTCDI-$(S\text{-}Ad)_2$ is a prochiral molecule, i.e.

[+] present address: Laboratory of Inorganic Chemistry, Department of Chemistry, University of Helsinki, P.O. Box 55, 00014 University of Helsinki, Finland

on the surface two enantiomers exist. Both points give rise to different geometries of the network pore for a statistical mixture of PTCDI and enantiomers of PTCDI-$(S\text{-}Ad)_2$. For example, if a PTCDI molecule without an adamantane unit is incorporated into a network cell, two C_{60} molecules fit next to the PTCDI moiety, whereas a homochiral pore formed from 6 PTCDI-$(S\text{-}Ad)_2$ molecules (and 6 melamine molecules) leaves only space for three molecules in the centre of the pore.

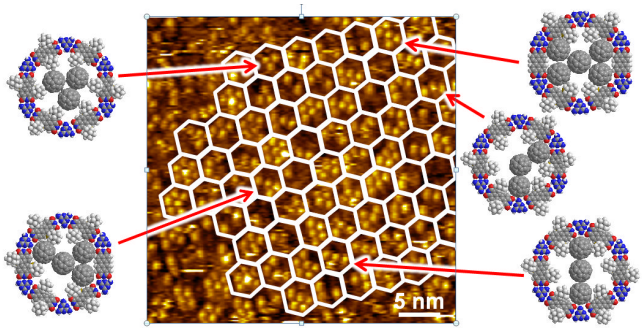

Fig. 2: STM image of C_{60} molecules adsorbed in the pores of a PTCDI-$(S\text{-}Ad)_2$–melamine network on Au(111)/mica. To guide the eye the honeycomb network is indicated by white hexagons. Protrusion represent C60 molecules, the adamantane moieties are not seen. Different configurations of C_{60} aggregates are illustrated by the models.

While the different C_{60} aggregates result from a statistical distribution of PTCDI and PTCDI-$(S\text{-}Ad)_2$ components, the example illustrates the possibilities to control the formation of aggregates of guest molecules by variation of the pore geometry through substituting moieties in the network frame.

Support by EPSRC is gratefully acknowledged.

[1] J. V. Barth, Ann. Rev. Phys. Chem. 58, 375 (2007)

[2] A. G. Slater, P. H. Beton and N. R. Champness, Chem. Sci. 2, 1440 (2011)

[3] J. Elemans, S. B. Lei and S. De Feyter, Angew. Chem-Intl Ed. 48, 7298 (2009)

[4] L. M. A. Perdigao, A. Saywell, G. N. Fontes, P. A. Staniec, G. Goretzki, A. G. Phillips, N. R. Champness and P. H. Beton, Chemistry Eur. J. 14, 7600 (2008)

[5] R. Madueno, M. T. Raisanen, C. Silien and M. Buck, Nature, 454, 618 (2008)

[6] M. T. Raisanen, A. G. Slater, N. R. Champness and M. Buck, Chem. Sci. 3, 84 (2012)

[7] J. A. Theobald, N. S. Oxtoby, M. A. Phillips, N. R. Champness and P. H. Beton, Nature, 424, 1029 (2003)

Hierarchical covalent molecular linking by sequential activation

L. Lafferentz, V. Eberhardt[1], C. Dri[2], C. Africh[2],
G. Comelli[2], F. Esch[2], S. Hecht[1], and L. Grill

Fritz-Haber-Institut, Department of Physical Chemistry, D-14195 Berlin, Germany
(corresponding author: L. Grill, e-mail: lgr@fhi-berlin.mpg.de)

[1] *Department of Chemistry, Humboldt-Universität zu Berlin, D-12489 Berlin, Germany*

[2] *Laboratorio TASC, Area Science Park, I-34149 Trieste, Italy*

A central goal of Molecular Nanotechnology is the construction of assemblies from individual functional molecules, which should be used as single-molecule "devices", and a variety of highly ordered supramolecular, i.e. non-covalent, arrangements have been reported in the last two decades [1]. However, covalent bonding, which provides high stability and the possibility of efficient charge transfer, is the desired intermolecular interaction and intense research was done in the last years to realize such structures [2]. In particular, the dehalogenation-based "on-surface-synthesis" process [3] turned out to be very successful and was used by different research groups to create a variety of well defined molecular nanostructures [4]. Its strength lies in its feasibility and the control over the final architectures, because their shape and size is directly controlled via the composition of the initial molecular building blocks, i.e. the position of the halogen substituents. However, so far only rather simple structures could be obtained, due to the limitation of one-step connection processes, but for the formation of sophisticated structures a step-by-step connection of molecules is required.

In this presentation, a novel strategy for the covalent connection of molecules in a hierarchical manner is presented [5], thereby generating species with a programmed reactivity. This is achieved by using different halogen species that exhibit different characteristic dissociation temperatures from the molecular building block. Hence, by controlling the sample temperature, the selective and sequential activation of specific sites within each individual molecule is induced. Such a hierarchical growth is demonstrated on Au(111) for homogeneous structures, obtaining one-dimensional chains after the first and two-dimensional networks after the second activation step (Fig.1), but also for heterogeneous networks, i.e. mixing different molecular species. In the latter case, high selectivity in the intermolecular linking, and thus final architecture, is achieved by the selective activation. By carefully comparing the defect density and size of the networks for non-hierarchical and hierarchical growth, an improved network quality is found for the latter one.

By using an anisotropic surface, substrate-directed growth and a preferred orientation of the molecular nanostructures are achieved [5]. In contrast to the flat Au(111) sample, a reconstructed Au(100) surface exhibits straight rows of vertically displaced atoms, which cause a preferred orientation and anisotropic diffusion of the molecules. Consequently, molecular chains and networks adsorb in a preferential orientation on the surface. This pre-arrangement in the sequential growth leads to an increased network size of the final networks. In addition to the covalent growth on metal surfaces, also the combination with inorganic crystallites will be discussed, thus creating an organic/inorganic hybrid system [6].

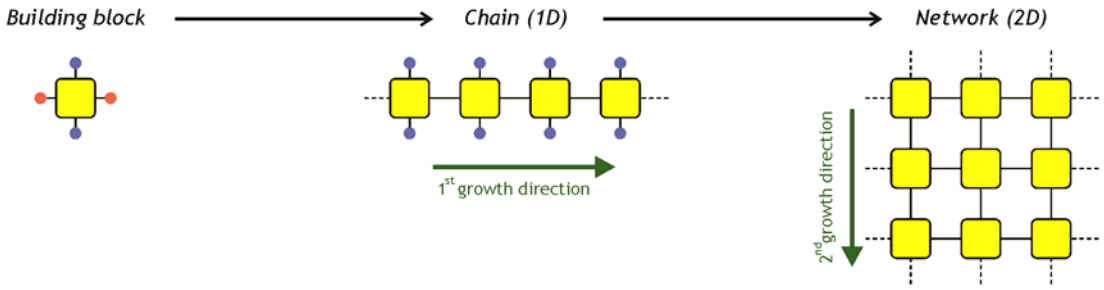

Figure 1: Concept of hierarchical covalent growth by sequential activation of different sites within each molecule (indicated in red and blue).

Finally, by pulling a polymer from a metallic surface, the conductance can be measured for a single molecular wire as a continuous function of the electrode-electrode distance [7]. Very recent results on the charge transfer through different kinds of molecular wires will be discussed. By systematically changing the bias voltage during the experiments, thus shifting the electronic levels of the electrodes with respect to the molecular orbitals, different conductance properties are measured.

Support by the Deutsche Forschungsgemeinschaft (DFG) through SFB 658 and the European Projects ARTIST and AtMol is gratefully acknowledged.

[1] L. Bartels, Nature Chem. 2, 87 (2010)
[2] D. F. Perepichka and F. Rosei, Science 323, 216 (2009)
[3] L. Grill et al., Nature Nanotech. 2 687 (2007)
[4] M. Lackinger et al., J. Phys. D : Appl. Phys. 44, 464011 (2011)
[5] L. Lafferentz et al., Nature Chem., in press
[6] C. Bombis et al., Ang. Chem. Int. Ed. 48, 9966 (2009)
[7] L. Lafferentz et al., Science 323, 1193 (2009)

Direct observation of molecular switching at and close to room temperature by STM

Stefanie Dietze, Michael Stark, Florian Buchner, Hans-Peter Steinrück
and Hubertus Marbach

Lehrstuhl für Physikalische Chemie II and Interdisciplinary Center for Molecular Materials (ICMM), Universität Erlangen-Nürnberg, Egerlandstr. 3, 91058 Erlangen, Germany, e-mail: marbach@chemie.uni-erlangen.de

An ultimate goal of nanotechnology is the usage of individual molecules as functional entities. One important example is the application of switchable molecular building blocks in information storage. In this regard the STM investigation of large organic molecules on surfaces, in particular at low temperatures (< 80 K), has become a vivid field in science with the vista to engineer functional devices. [1] The confinement on the surface in combination with molecular recognition either between absorbed molecules and/or specific substrate sites often triggers the self-assembly of long range ordered arrays. In this regard porphyrins appear to be ideal building blocks for the generation of functional molecular devices, since they combine their rigid planar framework as a structure forming element with an intrinsic functionality, mainly determined by the coordinated metal center. [2] A central aspect of our work is to gain insight into the adsorption behavior of porphyrins on different well defined metal and composite surfaces by means of scanning tunneling microscopy (STM) in ultra-high vacuum (UHV) mainly at room temperature (RT). [2-5]

Herein, we report on a metastable supramolecular ordered phase of 2H-5,10,15,20-Tetrakis-(3,5-di-tert-butyl)-phenylporphyrins (2HTTBPP) on a Cu(111) surface. The corresponding porphyrins with a metal center are well known for their conformational flexibility [2, 6] while the Cu(111) surface was recently shown to establish a strong interaction with the iminic nitrogen atoms of a related free base porphyrin. [5]. Surprisingly, 2HTTBPP molecules on Cu(111) are arranged in rows with two alternating intramolecular conformations, i.e. a concave and a convex appearance in STM (cf. Figure 1). At room temperature, frequent conformational switching of individual 2HTTBPP molecules from concave to convex and vice versa is observed (cf. Figure 2). A detailed analysis of the temperature dependence of the switching behaviour allows us to extract the activation energies and the prefactors for molecular switching in the concave and convex rows. Interestingly, at room temperature the conformational switching with the higher activation energy occurs more frequent, due to a much higher prefactor for this process. This finding was corroborated by controlled STM tip-induced switching at lower temperatures (~200 K) yielding an information storage density of $5.4\ 10^{15}$ bit/inch^2.

This work was supported by the Deutsche Forschungsgemeinschaft (DFG) through SFB 583.

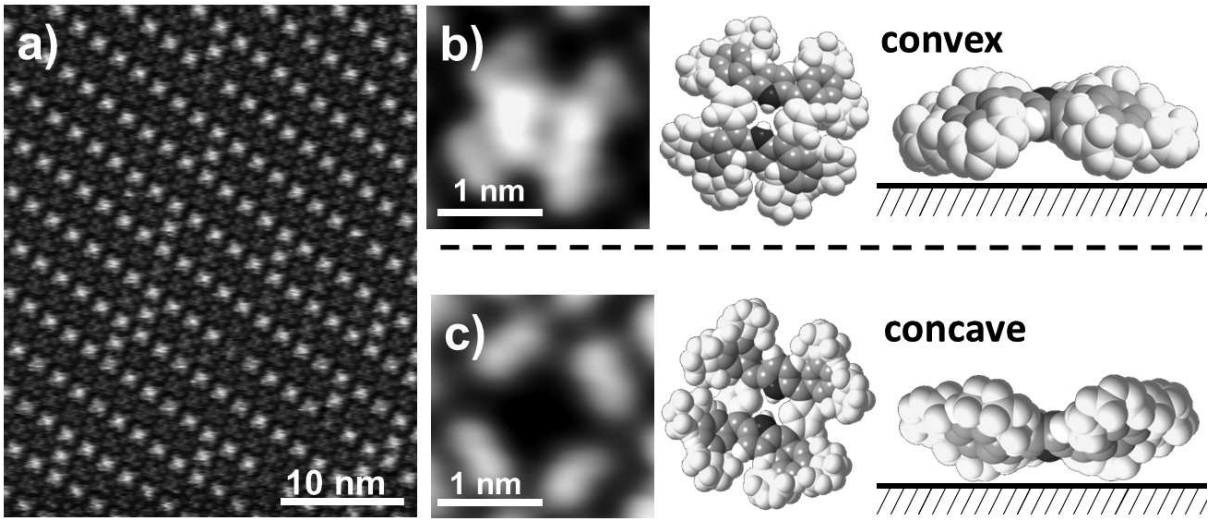

Figure 1: a) *STM image of an ordered domain of 2HTTBPP on Cu(111) acquired at room temperature (U_{Bias} = +1.81, I_{Tunnel} = 33 pA). The molecules exhibit a bimodal appearance in STM and are arranged in alternating rows.* **b), c):** *A close-up on single molecules and the corresponding models in the two intramolecular conformations, i.e. in convex and concave.*

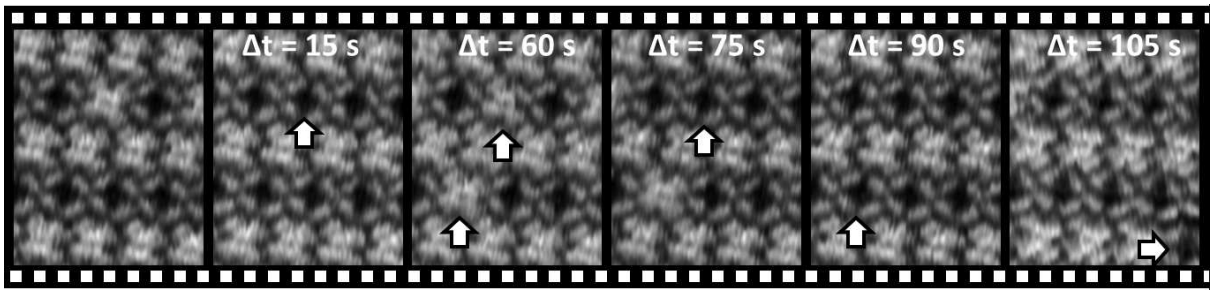

Figure 2: *Selected images from an STM movie of a 2HTTBPP domain on Cu(111) acquired at room temperature (U_{Bias} = +1.76, I_{Tunnel} = 25 pA). The arrows indicate individual molecules, which experience a spontaneous conformational switching from concave to convex or vice versa.*

[1] a) K. Morgenstern, Surf. Interface Anal., **42** (2010) 1634;
b) P. Liljeroth et al., Science, **317** (2007) 1203;
c) Y. Wang et al., JACS, **131** (2009) 3639;
d) D.M. Eigler et al., Nature, **352** (1991) 600;
d) X.H. Qiu et al., PRL, **93** (2004) 196806;
e) M. Alemani et al., JACS, **128** (2006)14446.
[2] J.M. Gottfried and H. Marbach, Z. Phys. Chem., **223** (2009) 532009.
[3] F. Buchner et al., J. Phys. Chem. C, **111** (2007) 13531.
[4] F. Buchner et al., ACS Nano, **3** (2009) 1789.
[5] F. Buchner et al., Chem. Eur. J., **17** (2011) 10226 and J. Phys. Chem. C, **115** (2011) 24172
[6] a) T.A. Jung et al.,Nature, **386** (1997) 696;
b) F. Moresco et al, PRL, **86** (2001) 672 and **87** (2001) 088302;
c) C. Loppacher et al, PRL, **90** (2003) 066107

SPM study of inorganic molecular electronics

Minko van der Maas, Janneke Dickhout, Bart Ellenbroek, Serhiy Vasnyov,
Bas Hendriksen, Sylvia Speller
Institute of Molecules and Materials, Radboud University Nijmegen

Jun Yan, De-Liang Long, Lee Cronin
Department of Chemistry, University of Glasgow

Polyoxometalates are metal-oxide nanoclusters with a cage-like structure and typically consist of VO_4 MoO_6 or WO_6 subunits. They can be considered as inorganic molecules and state-of-the–art synthetic chemistry allows high control over the synthesis and functionalization of polyoxometalates and the assembly of superamolecular structures made up of polyoxometalates. Polyoxometales form an interesting class of new nanomaterials for application in catalysis, (molecular) electronics and medicine drug delivery? They are particularly interesting because of their unique reduction-oxidation properties. Most properties have been obtained by ensemble averaging methods and the nanoscale properties of individual properties are not well known.

Although several scanning tunneling microscopy (STM) studies of polyoxometaltes have been reported in the literature our experience is that POMs are difficult to image by STM in ultrahigh vacuum, we therefore used a combination of STM and atomic force microscopy (AFM) for imaging and spectroscopy to study the nanoscale properties of $Mo_{18}O_{54}(SO_3)_2$ and $Mo_{18}O_{54}(SO_4)_2$ clusters.

The $Mo_{18}O_{54}(SO_3)_2$ cluster has been demonstrated previously to exhibit thermochromic behavior due to internal charge redistribution, whereas the $Mo_{18}O_{54}(SO_4)_2$ clusters do not show such behavior. Our scanning tunneling spectroscopy data show that there are indeed differences between the two clusters, but also that the conductance of both clusters switches between several well-defined states, where the conductance switches by an order of magnitude. Based on Kelvin probe force microscopy data we propose that the conductance switching is due to variations of the oxidation state of the clusters. The observed conductance switching may provide the basis of an inorganic molecular electronic switch.

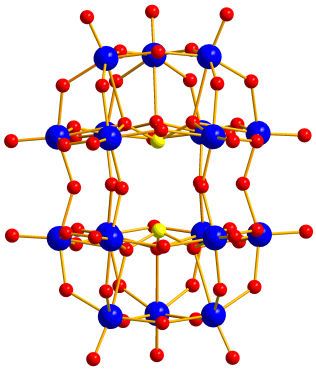

Structural model of the $Mo_{18}O_{54}(SO_3)_2$ polyoxometalate cluster

Protein interactions with the surface of gold nanoparticles: possible means of determining particle toxicity

M. E. Messing, C. R. Svensson[1], A. Schollin[2], K. Deppert, B. O. Meuller, J. Pagels[1], J. Rissler[1], M. Bohgard[1], S. Linse[2], and T. Cedervall[2]

Solid State Physics, Lund University, 221 00 Lund, Sweden
(corresponding author: M. E. Messing, e-mail: maria.messing@ftf.lth.se)

[1] *Ergonomics and Aerosol Technology, Lund University, 221 00 Lund, Sweden*

[2] *Biochemistry and Structural Biology, Lund University, 221 00 Lund, Sweden*

With the increasing amount of products and applications found in our everyday life based on nanoparticles, the concerns about possible adverse health effects of nanoparticles are being discussed intensively [1]. One of the major routes of exposure to nanoparticles is by inhalation of particles from air, leading to deposition in the respiratory tract. Many properties of nanometer-sized materials are different compared to bulk materials, and the effect of nanoparticles on biological systems is far from fully understood.

In recent years the nanoparticle interaction with biomolecules has been identified as one of the key parameters to understanding nanoparticle toxicology [2]. When biomolecules bind to the nanoparticle surface a dynamic protein/biomolecule corona is created [3]. This protein corona is dependent on the surface chemical properties, as well as the size and morphology of the particles. The protein corona is "read" by the biological system and of great relevance for the biological effects of nanoparticles.

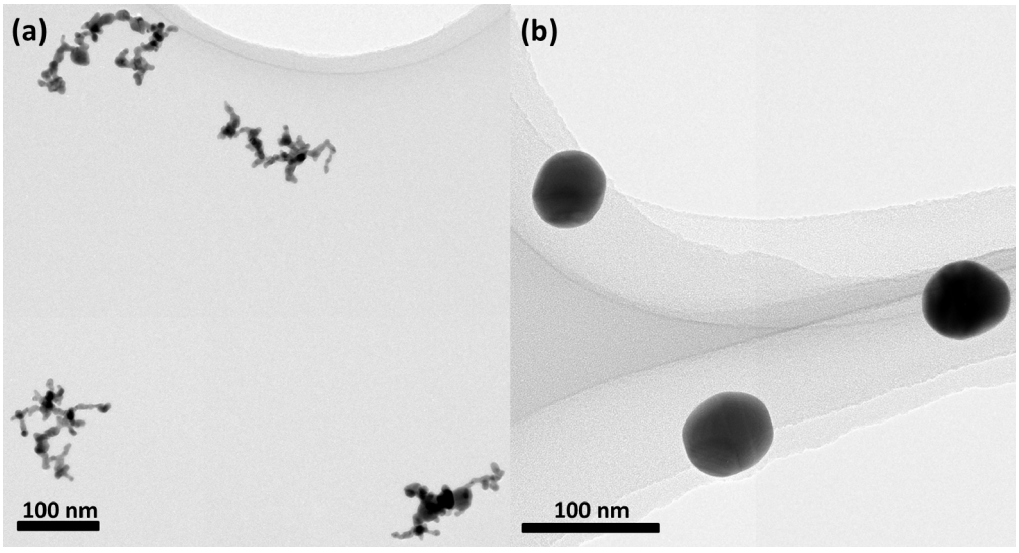

Figure 1. TEM micrographs of deposited (a) agglomerate and (b) compact gold nanoparticles.

In this work we present a method to investigate the composition of the biomolecule/protein corona formed on nanoparticles deposited into physiological fluids. Gold nanoparticles in the gas-phase were generated, and deposited, by aerosol methods [4] into bovine serum albumin (BSA), porcine serum, and porcine lung fluid. Particles with two different morphologies but the same mobility diameter, namely compact spherical particles and chainlike agglomerates (Figure 1), were generated and deposited. Before deposition the particles were thoroughly characterized on-line to determine their size, number concentration, and mass concentration [5]. Dynamic light scattering (DLS) was used to identify the particle-biomolecule complexes and the protein corona was investigated using sodium dodecyl sulfate polyacrylamide gel electrophoresis (SDS-PAGE).

DLS data indicate that nanoparticle-biomolecule complexes did indeed form for gold particles deposited into BSA and furthermore that these complexes were stable over several days. Results from SDS-PAGE strongly indicate that the protein corona is different between agglomerates and compact spherical particles deposited into porcine blood plasma (Figure 2). The result also indicates that the corona is different between particles deposited into lung fluid and blood serum. These results clearly demonstrate the usefulness of the here described deposition method for investigating the protein corona and enhancing our knowledge of nanoparticle toxicity.

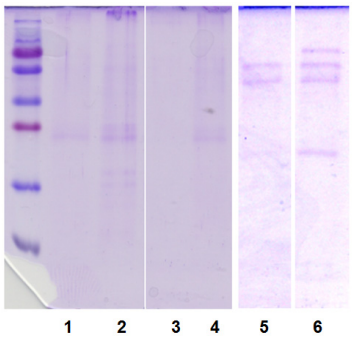

Figure 2. Results from SDS-PAGE for gold nanoparticles mixed with porcine blood. 1 and 2 show the corona signature for Au nanoparticles in full plasma and 10 times diluted, respectively. 3 and 4 show corona signature for agglomerates in full and 10 times diluted, respectively. Bands 5 and 6 show the background signature of 10 times diluted and full blood plasma.

This work was supported by the Nanometer Structure Consortium at Lund University (nmC@LU) and the Swedish research council FAS through project 2009-1291 and the FAS-centre METALUND.

[1] G. Oberdorster, E. Oberdorster and J. Oberdorster, Environ. Health Perspect. 113, 823 (2005)

[2] I. Lynch, A. Salvati and K. A. Dawson, Nat. Nanotechnol. 4, 546 (2009)

[3] T. Cedervall, I. Lynch, S. Lindman, T. Berggard, E. Thulin, H. Nilsson, K. A. Dawson and S. Linse, PNAS 104, 2050 (2007)

[4] M. E. Messing, K. A. Dick, L. R. Wallenberg and K. Deppert, Gold Bull. 42, 20 (2009)

[5] M. E. Messing, C. R. Svensson, B. O. Meuller, K. Deppert, J. Pagels and J. Rissler, submitted to Nanotoxicology (2012)

Nucleation and growth of rod-like organic molecules on inert substrates: 6P on mica

L. Tumbek and A. Winkler

Institut für Festkörperphysik, Technische Universität Graz, A-8010 Graz, Austria
(corresponding author: Adolf Winkler, a.winkler@tugraz.at)

The understanding and tailoring of organic thin film growth is a challenging issue in the context of modern organic electronics. Whereas the nucleation and growth of (metal) atoms is well understood [1], there is still lack of a comprehensive description for the nucleation and growth of larger (anisotropic) organic molecules. Although experimental evidence exists that in many cases organic film growth can be described sufficiently well with the models developed for single atom nucleation [2], there are also indications that substantial differences exist [3]. It is obvious, that the specific features of organic molecules can lead to a larger variety of growth mechanisms than for point like particles.

In this contribution we describe the nucleation and sub-monolayer formation of para-hexaphenyl (6P) on mica surfaces as a model system for the interaction of rod-like organic molecules with weakly interacting substrates. It has been shown that on freshly cleaved mica 6P forms needle like islands which are composed of flat lying molecules (Fig. 1a) [4]. However, a modification of the mica surface by argon ion sputtering changes the film formation drastically: dendritic islands form which are composed of standing molecules (Fig. 1b) [5]. From the island density as a function of the deposition rate a critical island size of 2-3 molecules was obtained, by applying the nucleation model of diffusion limited aggregation (DLA). However, the temperature dependence of the island density exhibited some unusual features and it was argued that the anisotropic diffusion probability and/or orientation dependent attachment probability of the monomers at the rim of the islands might be responsible for these features. Here we demonstrate that in addition to diffusion the attachment probability governs the nucleation and growth of 6P on mica, depending on the surface preparation by ion sputtering.

The most frequently discussed nucleation mode is the diffusion limited aggregation. According to Venables et al. [6] the island density N_x in the aggregation regime can be described as a function of the deposition rate F by a power law: $N_x \propto (F/D)^{\chi}$, where D is the surface diffusion coefficient and $\chi = i/(i+2)$, with i being the critical island size. In this case the exponent χ can only vary between 0.33 (i = 1) and 1 (for large i). This was indeed fulfilled for 6P deposited on a heavily sputtered mica surface [3]. However, it was found that the 6P island density can be strongly influenced by the sputter dose. Moreover, it was observed that on weakly sputtered mica the deposition rate dependence cannot be explained with the DLA mechanism, because the experimentally observed exponent χ was larger than 1.

Kandel [7] and more recently Venables and Brune [8] considered a scenario where the incorporation of the approaching monomers at the island edge is the limiting factor for nucleation, rather than diffusion. In this case the scaling exponent $\chi = 2i/(i+3)$. With this scenario we can well describe the experimental data and from the obtained $\chi = 1.4 \pm 0.1$ we determine a critical island size of 7 ± 2.

A second interesting feature of 6P film growth on mica is the frequently observed bimodal island size distribution, both in the case of the freshly cleaved surface (Fig.1a) as well as on the sputter modified surface (Fig. 1b). We studied this phenomenon with AFM and TDS, which allows us to identify a possible wetting layer and its influence on the film formation. In particular, we performed TDS before and after venting the vacuum chamber and re-evacuation. It turns out, that the small 6P islands (clusters) on both, the freshly cleaved and the sputter-modified mica surface, are the result of post-nucleation during the exposure of the 6P covered mica surface to air, caused by the co-adsorption of water.

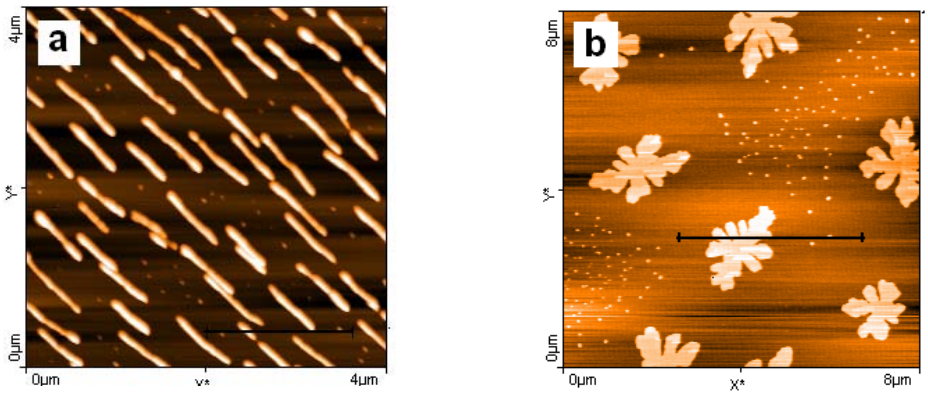

Fig.1 AFM images of 6P on freshly cleaved mica (a) and sputter modified mica (b)

Support by the Fonds zur Förderung der Wissenschaftlichen Forschung (Project P 23530)

[1] H. Brune, Surf. Sci. Rep. **31**, 121 (1998).

[2] G. Hlawacek, P. Puschnig, P. Frank, A. Winkler, C. Ambrosch-Draxl, and C. Teichert, Science **321**, 108 (2008).

[3] T. Potocar, S. Lorbek, D. Nabok, Q. Shen, L. Tumbek, G. Hlawacek, P. Puschnig, C. Ambrosch-Draxl, C. Teichert, and A. Winkler, Phys. Rev. B **83**, 075423 (2011).

[4] A. Andreev, G. Matt, C.J. Brabec, H. Sitter, D. Badt, H. Seyringer, and N.S. Sariciftci, Adv. Mater. **12**, 629 (2000).

[5] P. Frank, G. Hlawacek, O. Lengyel, A. Satka, C. Teichert, R. Resel, and A. Winkler, Surf. Sci. **601**, 2152 (2007).

[6] J.A. Venables, G.D.T. Spiller, and M. Hanbücken, Rep. Prog. Phys. **47**, 399 (1984).

[7] D. Kandel, Phys. Rev. Lett. **78**, 499 (1997).

[8] J.A. Venables and H. Brune, Phys. Rev. B **66**, 195404 (2002).

Line-on-line growth mode of HCOOH on Au (111): Energetic balance between intermolecular and adsorbate-substrate interaction

G. Pirug, C. Elsässer, M. Kazempoor, M. Müller, and C. Wagner

Peter Grünberg Institut (PGI) and JARA-FIT,
Forschungszentrum Jülich GmbH, D 52425 Jülich, Germany
(corresponding author: G. Pirug, e-mail: g.pirug@fz-juelich.de)

The adsorption of formic acid (HCOOH) on a Au(111) surface has already been characterized by vibrational spectroscopy and electron diffraction using high resolution electron energy loss spectroscopy (HREELS) and low energy electron diffraction (LEED), respectively.[1] The vibrational signature indicates weak chemical substrate interaction of flat lying chains of H-bonded HCOOH molecules [2]. The corresponding LEED pattern indicates that the reconstruction of the Au(111) surface is not lifted upon adsorption. However, the intermolecular interaction results in a well ordered $\begin{pmatrix} 1.89 & -.31 \\ 1.66 & 2.70 \end{pmatrix}$ surface structure with a rectangular 6.0 x 6.8 $Å^2$ unit cell, azimuthally rotated by 8.3° with respect to the [01] substrate surface direction. Furthermore missing spots in the LEED pattern could be explained by the existence of a pg glide mirror plane symmetry, consistent with the formation of ß-chains, only slightly elongated with respect to those identified in crystalline formic acid.[3, 4] These ß-chains adsorbed on Au(111) surfaces with link lengths of 6.8 Å and separated by ~ 6 Å could be visualized by topographical STM images.

The well-defined azimuthal orientation of the HCOOH overlayer indicates an epitaxial growth. However, neither a commensurate nor a point-on-line structure [5] is feasible within the error bars of the LEED measurement. Fig. 1 shows the reciprocal adsorbate lattice for the $\begin{pmatrix} 1.89 & -.31 \\ 1.66 & 2.70 \end{pmatrix}$ structure superimposed on the reciprocal lattices of two rotational domains of the reconstructed Au(111) surface. These domains originate from two possible compression directions of the terminal Au layer rotated by 120° against each other, forming the $(22 \times \sqrt{3})$ surface reconstruction.[6] From the coincidence of higher order overlayer reciprocal lattice points with the [3,-2] and [0,3] points of the reciprocal substrate lattice it can be concluded that the HCOOH molecules grow in a line-on-line fashion on either of the two rotational domains of the reconstructed Au(111) substrate.[7, 8] This unexpected growth mode serves two purposes. Firstly, it leaves the rather rigid adsorbate unit cell only weakly perturbed, and secondly, it allows an uniform growth of a single HCOOH domain over the stripe-like rotational domains of the reconstructed Au(111) surface. Therefore, growth on [3,-2] and [0,3] lattice lines alternates on the alternating Au(111) domains.

These findings nicely illustrate the delicate energetic balance of the molecule-molecule and molecule-substrate interaction that is typical for the layer growth of chemically interacting molecules on rather inert surfaces like Au(111). While the intermolecular interaction due to H-bonding within the adsorbed layer results in a bulk-like periodic surface structure, the comparably weak adsorbate substrate interaction leads to its azimuthal alignment. Although the energetic gain from the line-on-line epitaxial growth is expected to be small, compared to commensurate or point-on-line epitaxy [5, 7], the observed growth mode seems to be the most favorable one with respect to the total potential energy of the adsorbate layer, i.e., the sum of intermolecular and molecule-substrate interactions.

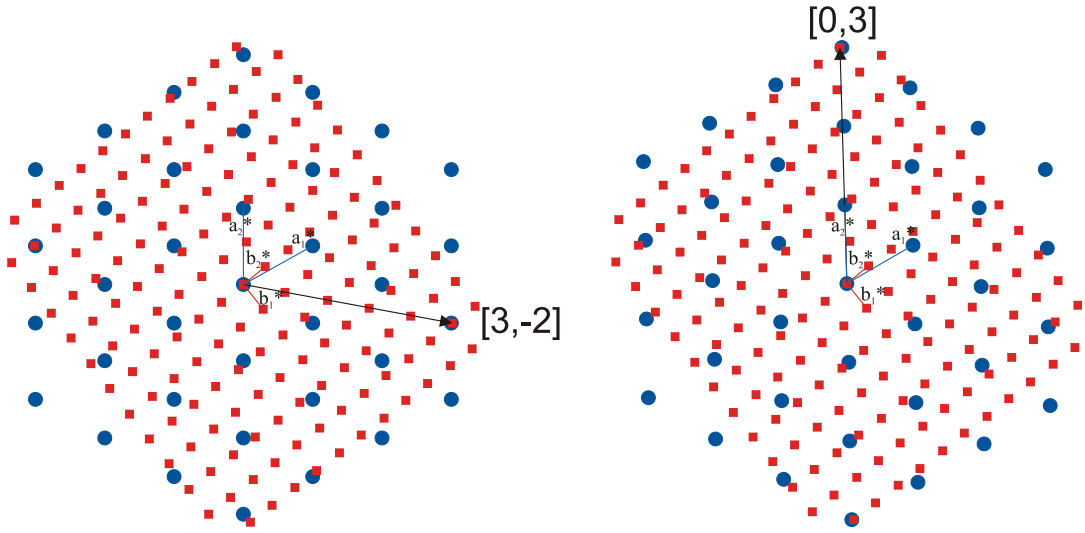

Fig 1: Reciprocal lattice of a $\begin{pmatrix} 1.89 & -.31 \\ 1.66 & 2.70 \end{pmatrix}$ HCOOH surface structure (■) on two rotational domains of the reconstructed Au(111) surface (●) with a) [3,-2] and b) [0,3] line-on-line coincidence.

[1] G. Pirug, M. Müller, and M. Kazempoor, in: F. Aumayr, C. Lemell and P. Varga (Eds.), Symposium on Surface Science, 2010, 37
[2] M. Kazempoor, and G. Pirug, Appl. Phys. A87, 435 (2007)
[3] F. Holtzberg, B. Post, and I. Fankuchen, Acta Cryst. 6, 127 (1953)
[4] I. Nahringbauer, Acta Cryst. B34, 315 (1978)
[5] D. E. Hooks, T. Fritz, and M. D. Ward, Advanced Materials 13, 227 (2001)
[6] J. V. Barth, H. Brune, G. Ertl, and R. J. Behm, Physical Review B 42, 9307 (1990)
[7] S. C. B. Mannsfeld, K. Leo, and T. Fritz, Physical Review Letters 94, 056104/1 (2005)
[8] D. Kasemann, C. Wagner, R. Forker, T. Dienel, K. Müllen, and T. Fritz, Langmuir 25, 12569 (2009)

Evidence of a strong hybridization between surface states and 1-D quasimolecular states of a Cu-O chain in the reconstructed O(2x1)/Cu(110) surface

Pepa Cabrera-Sanfelix,[1] Daniel Sánchez-Portal[1,2] and Andrés Arnau[1,2,3]

[1] *Donostia International Physics Center (DIPC), UPV/EHU, San Sebastián 20018, Spain*

[2] *Centro de Física de Materiales (CFM-MPC) CSIC-UPV/EHU, San Sebastián 20018, Spain*

[3] *Departamento de Física de Materiales UPV/EHU, Facultad de Química, Apdo. 1072, San Sebastián 20080, Spain*

(corresponding author: Andrés Arnau, e-mail: andres.arnau@ehu.es)

It is well known that a reconstruction of the Cu(110) surface occurs upon oxygen adsorption. Some experimental techniques such as low energy electron diffraction (LEED [1] and scanning tunneling microscopy (STM) [2], together with ab-initio calculations [3,4] established unambiguously that the adsorption of ½ monolayer of oxygen on Cu(110) induces reconstruction of the surface according to the added-row geometry, where every second [001] row of Cu atoms in the topmost layer is missing, and the Cu – O – Cu chains along the (001) direction keep their oxygen atoms located in the long bridge sites. However, contrary to what one would expect, the electronic structure of this surface reconstruction has not been characterized accurately enough neither by different experimental techniques nor by first-principles calculations, so that a complete consensus about both of them does not exist presently in the literature. In particular, there is a controversy about the occupancy, character, dispersion (and even the existence) of an antibonding band of the Cu-O chain that is precisely the main motivation of this work.

The electronic structure of the Cu(110)-p(2x1)O surface has been investigated experimentally by photoemission [5] and by inverse photoemission experiments[6]. Also, DFT [3,7,8] and tight-binding calculations [9] were performed to compare with the experimental data. Three occupied bonding bands were clearly identified, appearing below the *d* bands of the Cu(110) substrate between -8 and ~-5.5 eV along the ΓY direction, with O p_x, p_y and p_z character. There is a reasonable agreement between theoretical results and experimental data with respect to the bonding bands dispersion. There is, however, some controversy concerning the three corresponding antibonding bands and their occupancy, as only two of them with O($2p_x$)

and O($2p_z$) character have been clearly identified [5]. Previous calculations based on the linear combination of atomic orbitals (LCAO) method and self-consistent slab calculations reveal a third antibonding band with p_y symmetry but its energy location at the Y point of the surface Brillouin zone and its dispersion are a controversial matter. Using angle resolved photoemission, Courths et al [5] showed that the occupied surface state of the pristine Cu(110) surface at the high symmetry point Y shifts upwards in energy as the surface is exposed to oxygen already at low O coverages, although it was not possible to follow the evolution of the corresponding spectral feature for high enough O coverages. However, an earlier inverse photoemission study of the O(2x1)/Cu(110) surface by Jacob et al. [6] clearly showed an unoccupied surface state at the Y-point located about 0.5 eV above the Fermi level. More recently, this surface state has been clearly identified in scanning tunneling spectroscopy and density functional theory calculations [10], in which a large enough number of Cu layers are used to represent the Cu(110) surface. As the occupied Cu(110) surface sate band has p_y symmetry and crosses the Fermi level, it is a good candidate to hybridize with the Cu-O "missing" antibonding band with O($2p_y$) character. The question is how to characterize the hybridization of these bands.

Here, we proof that, due to the interaction with the Cu(110) surface, this band splits into two components: one mixes with the pristine Cu(110) partially occupied surface state that becomes unoccupied, while the other strongly hybridizes with bulk Cu sp- and d-bands. Our strategy to reach these findings is based on a systematic study of the electronic structure in which the distance between the added row Cu-O chain and the Cu(110) surface is artificially varied. Our basic findings are: (i) there is a significant degree of ionicity in the Cu-O bonds, i.e., charge transfer from the Cu to the O atoms, of the Cu-O chain, which has partially filled bands, (ii) the Cu(110) surface transfers charge to the Cu-O chain (about 0.5 electrons per Cu-O unit), (iii) due to the interaction between the Cu-O chain and the Cu(110) surface the three bonding bands with O(2p) character are shifted down in energy below the Cu d-bands without suffering a strong mixing, being the one with O($2p_z$) character the one that hybridizes more, while the antibonding bands suffer a much stronger mixing and splitting with components that even change its dispersion.

We acknowledge support from Basque Departamento de Educación, UPV/EHU (Grant No. IT-366-07), the Spanish Ministerio de Educación y Ciencia (Grant No. FIS2010-19609-C02-00), and the ETORTEK research program funded by the Basque Departamento de Industria and the Diputación Foral de Gipuzkoa. PCS acknowledges support by the Diputación Foral de Gipuzkoa.

[1] S. R. Parkin, H. C. Zeng, M. Y. Zhou, et al., Physical Review B **41**, 5432 (1990).
[2] D. J. Coulman, J. Wintterlin, R. J. Behm, et al., Physical Review Letters **64**, 1761 (1990).
[3] S. Y. Liem, G. Kresse, and J. H. R. Clarke, Surface Science **415**, 194 (1998).
[4] J. Harl and G. Kresse, Surface Science **600**, 4633 (2006).
[5] R. Courths, S. Hufner, P. Kemkes, et al., Surface Science **376**, 43 (1997).
[6] W. Jacob, V. Dose, and A. Goldmann, Appl. Phys. A **41**, 145-150 (1986).
[7] J. Harl, G. Kresse, L. D. Sun, et al., Physical Review B **76** (2007).
[8] F. Pforte, A. Gerlach, A. Goldmann, et al., Physical Review B **63** (2001).
[9] P. Cortona and C. Sapet, Surface Science **585**, 155 (2005).
[10] C. Corriol, J. Hager, R. Matzdorf, and A. Arnau, Surf. Sci. **600**, 4310 (2006).

Theoretical investigation of intermolecular hydrogen-bond mediated core level shifts

A. Garcia-Lekue, S. Garcia-Gil[1], P. Ordejón[2], A. Arnau[3,4]

Donostia International Physics Center (DIPC), Donostia, Spain
(corresponding author: A. Garcia-Lekue, e-mail: wmbgalea@lg.ehu.es)

[1]*Centre d'Elaboration de Matériaux et d'Etudes Structurales (CEMES), Toulouse, France*
[2] *Centre de Investigació en Nanociència i Nanotecnologia, CIN2 (CSIC-ICN), Barcelona, Spain*
[3]*Centro de Física de Materiales (CSIC-UPV/EHU), Materials Physics Center MPC, Donostia, Spain*
[4] *Departamento de Física de Materiales, UPV/EHU, Donostia, Spain*

Hydrogen bonding (H-bond) is a type of noncovalent interaction incredibly common in nature. Examples of H-bond formation can be found in many fields such as material science, biochemistry, organic chemistry or supramolecular chemistry. Many important structural functions in biology and chemistry are carried out by H bonds, including stabilization of protein folding, organization of DNA and organization of water and carbohydrates. Hydrogen bonding combines directionality and strength, due to which it has been intensively exploited in the fabrication of self-assembled nanostructures. Experimentally, hydrogen-bonds can be investigated by means of X-ray Photoemission Spectroscopy (XPS), a powerful technique to track the changes in the chemical environment of an atom through its core-level shifts (CLS). Previous studies have shown that H-bonds can induce very large CLS [1], and the influence of the distance between the constituents of the H-bond on the CLS has been examined [2]. However, an extensive investigation of the effect of hydrogen-bonding on the core-level shifts has not yet been accomplished.

For this reason, in this work we have thoroughly investigated the core-level shifts induced by the formation of H-bonds. As mentioned above, the high directionality of hydrogen bonding enables the formation of highly oriented structures from units capable of forming head-to-tail interactions. For a selected set of such units, we have performed a systematic study of the effect of distance and angle on the H-bond mediated CLS. In particular, we have considered isonicotinic acid as a model system for the study of the N1s core-state, oxalic acid for the O1s core-state and the adenine-thymine base pair for the study of both N1s and O1s core-states.

For the calculations of the core-level shifts we have employed the initial and final state approximations as implemented within the SIESTA framework [3]. In the initial state approximation, only the state of the system before the photoionization process is considered,

i.e. no relaxation effects are included [4]. The final state approximation instead, includes the effects due to the rearrangement of the charge originated by the ionization of the core [5]. Hence, it reflects the variations in the screening of the core hole created in the photoemission process.

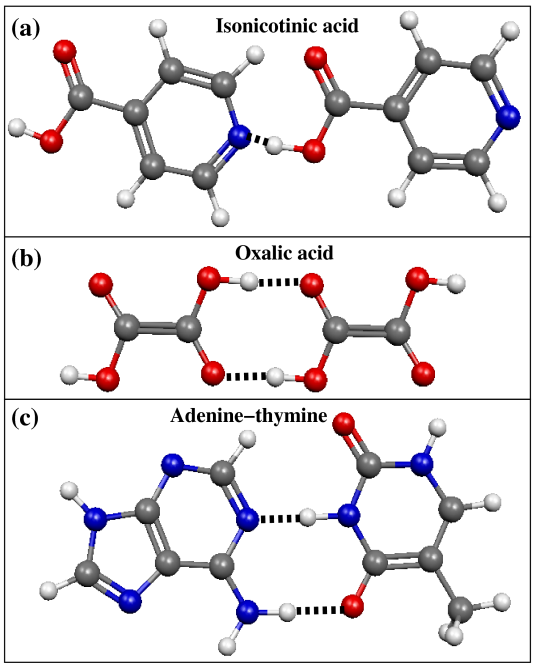

Figure 1: Systems used in the investigation of H-bond induced CLS. (a) isonicotinic acid dimer, (b) oxalic acid dimer and (c) adenine-thymine base pair.

From our results, we conclude that the strength of the CLS strongly depends on the angle and distance between the atoms involved in the H-bond, and that shifts of more than 1eV might be induced. Besides, comparing the calculations performed within the initial and final approximations, we are able to extract information about the screening of the core hole left behind by the photoemission process.

Support from the Spanish Ministerio de Ciencia e Innovación (Grant No. FIS2010-19609-C02-00), the ETORTEK program funded by the Basque Departamento de Industria and the Diputación Foral de Guipuzcoa are gratefully acknowledged.

[1] J. N. O'Shea, J. Schnadt, P.A. Brühwiler, H. Hillesheimer and N.Mårtenson, J. Phys. Chem. B 105, 1917 (2001)

[2] G. Tu, Y. Tu, O. Vahtras and H. Ågren, Chem. Phys. Lett. 468, 294 (2009)

[3] S. Garcia-Gil, PhD Thesis, Universitat Autònoma de Barcelona, 2011

[4] X. Blase, A.J.R. da Silva, X. Zhu and S.G. Louie, Phys. Rev. B 50, 8102 (1994)

[5] E. Pehlke and M. Scheffler, Phys. Rev. Lett. 71, 2338(1993)

One Dimensional Structures at Low Water Coverage on Cu(110)

P. Cabrera-Sanfelix,[1] Y. Shi,[2,3] B-Y. Choi,[2] A. Arnau,[1,4] M. Salmeron[2,3] and D. Sánchez-Portal.[1,4]

[1]*Donostia Int. Phys. Center, P. Manuel de Lardizabal 4, San Sebastian 20018, Spain*
[2]*Materials Sci. Division, Lawrence Berkeley National Lab., Berkeley, CA 94720, USA*
[3]*Dep. of Materials Sci. and Engineering, Univ. of California Berkeley, CA 94720, USA*
[4]*Centro de Física de Materiales CSIC-UPV/EHU, Materials Physics Center MPC, P. Manuel de Lardizabal 5, San Sebastian 20018, Spain*

Water growth on metal surfaces has been a topic of debate during many years. The self-organization of water in metallic surfaces is determined by the competition between inter-molecular and metal-substrate interactions. So, the molecules (i) cluster in a 3D-phase, (ii) wet the surface following a well-ordered 2D-adlayer or even, in a more complicated scenario, (iii) a significant fraction of water molecules undergo partial dissociation.[1, 2]

The wetting of Cu(110) has been recently reported. Thus, at low temperature and coverage water forms one dimensional arrays of side-sharing pentagons on Cu(110).[3] We present in here that the pentagon row structure can evolve to hexagon row structure as the coverage of water increases beyond 0.2 layers, according to the experimental evidence. We show that this transformation is mediated by the formation of lobe structure (LS) clusters made of n pentagons connected to a central hexagonal ring (n-LS). The most frequent configuration, the 4-LS, is believed to act as a catalyst for the propagation of H-bond re-orientation along the chain of pentagons and thus, they could be considered the precursors of the transformation to the hexagonal row structure. DFT calculations compare the structures and energetics of pentagon and hexagon infinite row structures and explore the possible structures for the isolated 4-LS, depending merely on the molecules orientation. Finally, we present the several 4-LS "defects" into the pentagon row structure.[4]

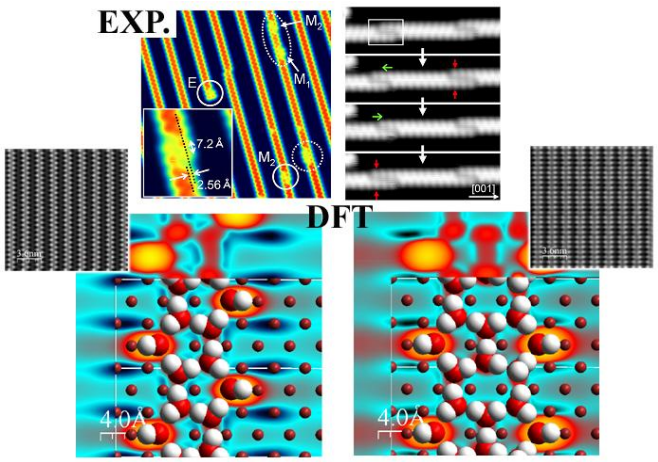

Figure 1. Upper panels: exp. STM images (30nm × 30nm) of the Cu(110) surface covered by 0.2 ML water after annealing to 120 K. Downward panels: DFT images for pentagonal row structure and the proposed hexagonal row structure based on the propagation of 4-LS clusters.

[1] P. Cabrera-Sanfelix, A. Arnau, et al., *Physical Review B* **2008**, *78*.
[2] A. Michaelides, A. Alavi, et al., *Phys. Rev. B* **2004**, *69*, 113404.
[3] J. Carrasco, A. Michaelides, et al., *Nature Materials* **2009**, *8*, 427.
[4] Cabrera-Sanfelix P et al., *In preparation*.

Abstract 3S-12: Symposium on Surface Science 2012, St. Christoph am Arlberg, Austria, March 11-17, 2012

The self-assembly of $(WO_3)_3$ clusters on Cu(110) surfaces

M. Denk[1], D. Kuhness[1], M. Wagner[1], S. Surnev[1], F.R. Negreiros[2], L. Sementa[2], G. Barcaro[2], A. Fortunelli[2], F.P. Netzer[1]

falko.netzer@uni-graz.at

[1] *Surface and Interface Physics, Institute of Physics, Karl-Franzens Universität Graz, A-8010 Graz, Austria*

[2] *CNR-IPCF, Istituto per i Processi Chimico-Fisici, I-56124 Pisa, Italy*

W oxides have interesting applications in the fields of catalysis, gas sensors or electrochromic devices, which are all related to their tendency towards nonstoichiometry and the easy formation of oxygen vacancies. Most applications involve fundamental surface processes, which need to be characterized at the atomic scale for high-level use in nanoscopic device technology. Moreover, it is a challenging scientific question, how structure concepts of defects in W oxide bulk samples, e.g. the so-called crystallographic shear planes, transfer into low-dimensional nanostructures or 2-D W oxide nanolayers. The preparation of high quality epitaxial oxide films, prerequisite for the elucidation of fundamental surface properties, by the preferred physical vapour deposition method, i.e. the reactive evaporation of the metal in oxygen atmosphere, is hampered in the case of W oxide by the difficulty of evaporating W in UHV. An alternative approach is to use self-assembly concepts and to build up thin layers from molecular-type building blocks of W-O clusters on a suitable substrate surface. Here we explore the feasibility to fabricate W-oxide nanostructures (nanolayers) on metals via self-assembly of $(WO_3)_3$ clusters, deposited directly from the gas phase on two surfaces with different chemical reactivities, namely on a Cu(110) surface and on an oxygen-covered Cu(110)2x1 surface reconstruction.

It has been shown recently that $(WO_3)_3$ cluster molecules, formed by vacuum sublimation of WO_3 powder at ~900-1000°C, can be deposited as monodispersive clusters on solid surfaces [1,2]. STM imaging shows that the clusters adsorb as intact units on the bare Cu(110) and the oxygen-reconstructed Cu(110)2x1-O surfaces at low temperature (<15K), but that the adsorption geometries and the cluster surface interactions are significantly different on the two substrate surfaces (see Fig. 1). As detailed by DFT calculations, on clean Cu(110) the overall cluster distortion is minor, whereas on the Cu-O surface the clusters and also the substrate are significantly distorted due to the strong oxygen affinity of the W atoms. On both surfaces, cluster and Cu electronic states are appreciably mixed, and electron charge is donated by the surface to the cluster, with stronger charge transfer from Cu-O. The different surface interactions of the $(WO_3)_3$ clusters on bare Cu and Cu-O are directly

reflected in their W 4f XPS core level signatures, which show a shift to lower binding energy on both the bare Cu and the Cu-O substrate, as illustrated in Fig. 2. On warming to room temperature and above, the $(WO_3)_3$ clusters react with the Cu substrate surfaces and between themselves and condense into 2-D layers. Fig. 3 shows an STM image and a LEED pattern of an extended 2-D WO_x monolayer, which corresponds to an incommensurate stripe phase formed on Cu(110)2x1-O. The structure is row-matched in the [001] direction of the substrate, suggesting a templating effect of the Cu-O surface. The W atoms have been partly reduced from the 6+ state in the clusters to 5+ and possibly 4+ in the 2-D layer as a result of the condensation reaction, as investigated by XPS. Several ordered surface structures are also observed in second and subsequent oxide layers, where the $(WO_3)_3$ units retain most of their cluster ring structure.

Work supported by the ERC Advanced Grant SEPON.

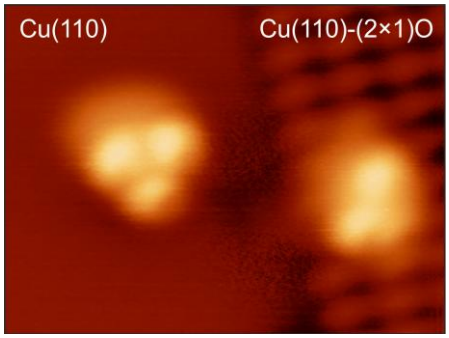

Fig.1: STM images of $(WO_3)_3$ clusters on Cu(110) (left) and Cu(110)2x1-O (right), recorded at 5K.

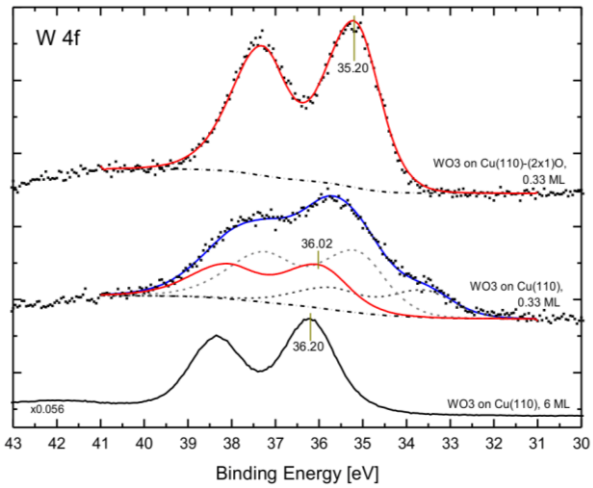

Fig.2: W 4f XPS core level spectra of $(WO_3)_3$ clusters at 80K. A spectrum of 6ML of $(WO_3)_3$ is shown for comparison (bottom)

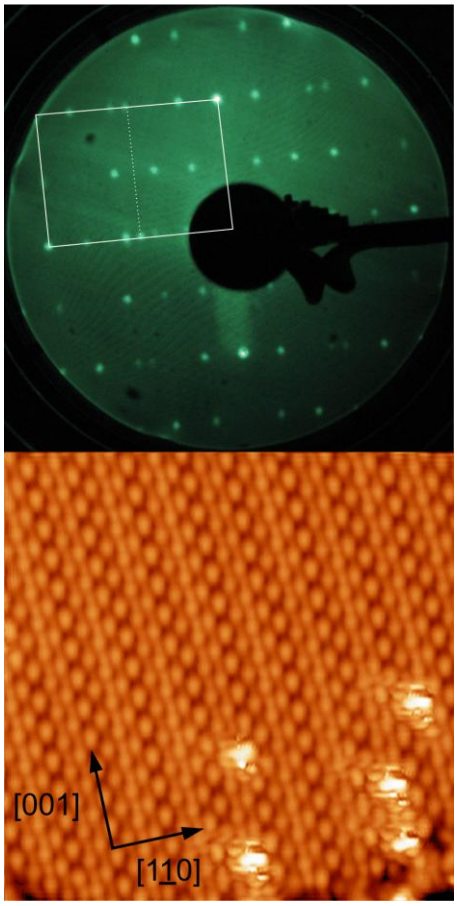

Fig.3: STM and LEED of a 2-D WO_x monolayer on Cu-O

[1] O. Bondarchuk, X. Huang, J. Kim, B.D. Kay, L.-S. Wang, J. M. White, Z. Dohnalek, Angew. Chem. Int. Ed. 45(2006)4786

[2] M. Wagner, S. Surnev, M.G. Ramsey, G. Barcaro, L. Sementa, F.R. Negreiros, A. Fortunelli, Z. Dohnalek, F.P. Netzer, J. Phys. Chem. C115(2011)23480

Friday

Field states and their lifetime on nano

Ch. Zaum, K.Morgenstern

Institute für Festkörperphysik, Abteilung für Atomare und Molekulare Strukturen (STMOS), Leibniz Universität Hannover, Appelstr. 2, D-30167 Hannover, Germany
(corresponding author: K. Morgenstern, e-mail: morgenstern@fkp.uni-hannover.de)

The electrostatic potential of a surface has important consequences for e.g. the reactivity of surfaces. A sensitive method to determine the electrostatic potential of a surface is the measurement of image potential states.

Image potential states are a Rydberg-like series of unoccupied states in the front of a metallic surface that are stabelized by the interaction of an electron with its image charge in the metal. The energetic position of these states is closely related to the vacuum level of the metal. Thus they are sensitive measures for changes in work function, which in turn contains information about the electrostatic potential.

The image potential stateswere intensely probed in photo emsision experiments [1] and theory [2] for a long time. The states can also be probed by scanning tunneling microscopy (STM) [3], though the strong electric field leads to a Stark shift [4], such that the states are shifted beyond the vacuum energy and are consequently probed in the field emission range. These shifted states are conventionally named field states [5]

The lifetime of electrons within the image state depends on its energetic position with respect to the projected band gap and increases with quantum number. It has been investigated by time-resolved two-photon photemission spectroscopy [6]. Also this lifetime is affected by the Stark shift [7].

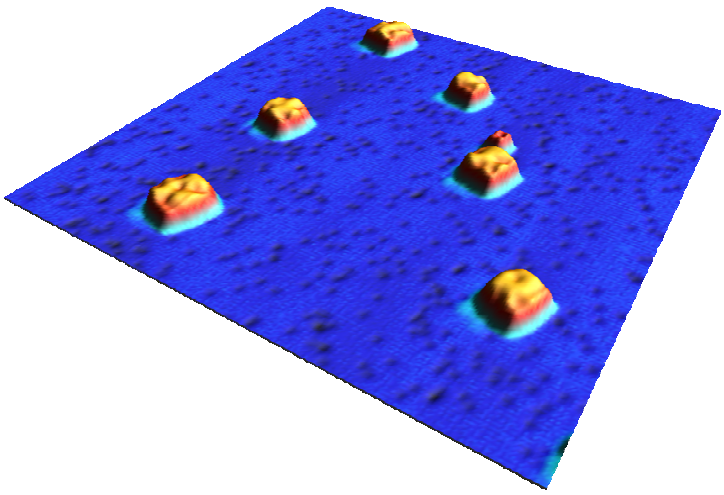

Figure1: STM image of Cu and Cu/Ag islands on alloyed Ag(100).

We investigated the field states by low-temperature (5K) scanning tunneling microscopy for an alloyed system formed by the deposition of Cu on Ag(100) at room temperature. At this temperature, a surface alloy forms through exchange diffusion [8] (see Fig. 1). Furthermore, either incommensurate pure copper islands or commensurate Ag/Cu alloy islands form in dependence of their size with a transition between 4 nm^2 and 7 nm^2 [8].

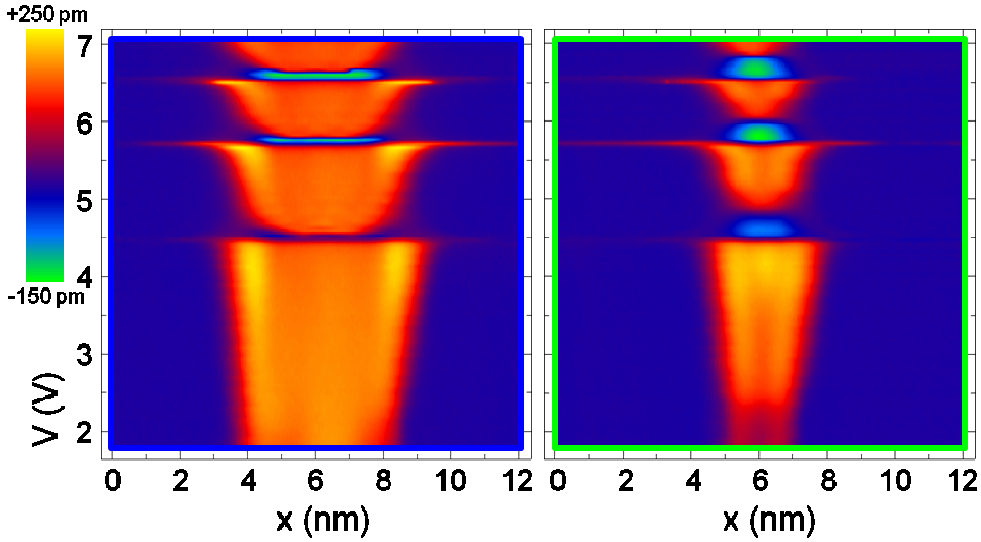

Fig. 2: Spatially dependent dI/dV spectra for Cu/Ag alloy island (left) and Cu island (right).

We measure and map the position and the width of field states on the two types of islands (see Fig. 2) and compare those to the values on the alloyed terrace. Remarkable changes in the position and width of the field states give spatially resolved information about the local variation in electrostatic potential. In particular the energetic shift of the first two image potential states differ for the two types of islands not only quantitatively, but also qualitatively. Furthermore, the lifetime is considerably enhanced on the pure copper islands despite its much smaller size.

The obtained values are compared to the field states measured on terraces and close to step edges on pure Ag(100) and Cu(111). Through this comparison we are able to differentiate between field effects, nano-size effects and chemical shifts of the field states.

[1] V. Dose, W. Altmann, A. Goldmann, U. Kolac, J. Rogozik, Phys. Rev. Lett. 52 (1984) 1919

[2] E.V. Chulkov, V.M. Silkin, P.M. Echenique, Surf. Sci. 437 (1999) 330.

[3] P. Wahl, M.A. Schneider, L. Diekhöner, R. Vogelsang, K. Kern, Phys. Rev. Lett. 91 (2003) 107402

[4] L. Limot, T. Maroutian, P. Johanson, R. Berndt, Phys. Rev. Lett. 91 (2003) 196801

[5] G. Binnig, K.H. Frank, H. Fuchs, N. Garcia, B. Reihl, H. Rohrer, F. Salvan, A.R. Williams, Phys. Rev. Lett. 55 (1985) 991.

[6] U. Höfer, I.L. Shumay, Ch. Reuß, U. Thomann, W. Wallauer, Th. Fauser, Science 277 (1997) 1480; P.M. Echenique, R. Berndt, E.V. Chulkov, Th. Fauster, A. Goldmann, U. Höfer, Surf. Sci. Rep. 52 (2004) 219.

[7] S. Crampin, Phys. Rev. Lett. 95 (2005) 046801; J.I. Pascual, C. Corriol, G. Ceballos, I. Aldazabal, H.-P. Rust, K. Horn, J.M. Pitarke, P.M. Echenique, A. Arnau, Phys. Rev. B 75 (2007) 165326.

[8] Ch. Zaum, M. Rieger, K. Reuter, K. Morgenstern, Phys. Rev. Lett. 107 (2011) 046101

Dynamics of truly monodisperse clusters under the STM

M. König, Y. Fukamori, B. Wang, F. Esch, and U. Heiz

Technische Universität München, Catalysis Research Center,
Chair of Physical Chemistry, Lichtenbergstr. 4, 85748 Garching, Germany
(corresponding author: F. Esch, e-mail: friedrich.esch@tum.de)

The use of clusters promises to revolutionize our ability to design and control the selectivity and efficiency of catalytic processes owing to the unique chemical and physical properties of these structures [1]. Nanostructures and molecular clusters behave quite differently than bulk materials due to quantum size effects that become dominant upon reducing the dimensionality of the material grains. "Every atom counts" – and thus size becomes a third dimension to the periodic table. A deeper understanding of the interplay between morphology and electronic structure as function of the cluster size will guide the development of a new generation of atomically designed nanostructures for catalysis.

In order to access the ultimate fundaments of the non-scalable size regime of supported cluster chemistry, we developped the preparation of truly monodisperse cluster-assembled materials, i.e. with every cluster of same size and adsorption site and thus chemical environment. To this purpose, we deposited size-selected, soft-landed Pd_N clusters ($7 \leq N \leq 31$) on epitaxial graphene and boron nitride films (see Fig. 1). Moiré moieties formed on graphene films have been shown to be good candidates for the stabilization of clusters [2]. Such well defined samples allow for the first time to fully complement these local with integrating measurements on cluster reactivity and electronic structure and to study isomer effects at the atomic scale.

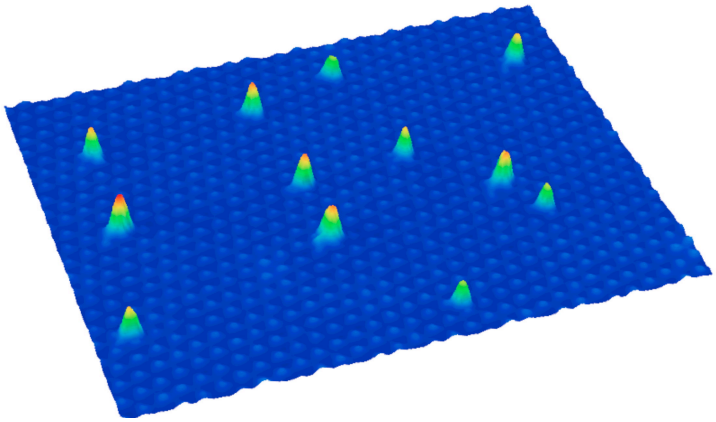

Fig. 1: STM image of Pd_{20} clusters soft-landed on a graphene layer on Ru(0001) at room temperature. All clusters are adsorbed on a single type of Moiré moiety.

Our STM measurements show that the Pd clusters are well-dispersed on the graphene surface at room temperature, without any preferential aggregation at the step edges, contrary to what occurs upon physical vapour deposition [3]. Pd_{20} clusters show a 2-3 monolayer high atomic structure, comparable to that of free-standing clusters in the gas phase. Neither cluster fragments nor surface damage is observed, confirming a well-controlled soft-landing on the graphene surface.

On graphene, the clusters are exclusively adsorbed on one of the two ring hollow registries of the superstructure, indicating a strong carbon-metal interaction and a softening of the carbon-carbon bonding at this local registry. Different isomers of Pd_{20} are observed, and isomerization processes can occur during continuous STM scanning. Clusters can be manipulated by the Push mode or can be removed in a controlled way, leaving behind the pristine surface. Astonishingly, the electronic structure of different clusters with same topographic appearance in the STM image reveals huge differences, as manifested in the conductance maps.

The STM study reveals that the cluster mobility/stability depends not only on the cluster size, but also on the footprint specific to isomers of different height. An investigation on the thermal stability of larger, Pd_{20} clusters by annealing clearly indicates different mechanisms in the sintering process: cluster diffusion dominates at temperatures below 500 K, Ostwald ripening at temperatures above 500 K. Two approaches are currently implemented in order to increase the STM time resolution for the study of these cluster-assembled materials under reactive gas environments [4].

Support by the EUROCORES FANAS project NOMCIS, by the Luxemburg National Research Found (Y.F.) and the Friedrich Ebert-Stiftung (M.K.) is gratefully acknowledged.

[1] U. Heiz and U. Landman, editors, *Nanocatalysis (NanoScience and Technology)* (Springer, 2006), p. 519

[2] A. T. N'Diaye, S. Bleikamp, and P. J. Feibelman, Physical Review Letters **97**, 215501 (2006)

[3] Z. Zhou, F. Gao, and D. W. Goodman, Surface Science **604**, L31-L38 (2010)

[4] F. Esch, C. Dri, A. Spessot, C. Africh, G. Cautero, D. Giuressi, R. Sergo, R. Tommasini, and G. Comelli, The Review of Scientific Instruments **82**, 053702 (2011)

CO oxidation over Pt group metals studied by *in situ* high pressure XPS

J. Gustafson, S. Blomberg, N. M. Martin, V. Fernandes[1], A. Borg[1], R. Chang[2], Z. Liu[2] and E. Lundgren

Division of Synchrotron Radiation Research, Lund University, Sweden

(corresponding author: J. Gustafson, e-mail: johan.gustafson@sljus.lu.se

[1] *Norwegian University of Science and Technology, Trondheim, Norway*

[2] *Advanced Light Source (ALS), LBNL, Berkeley, USA*

The catalytic CO oxidation reaction over Pd, Pt and Rh single crystals and nanoparticles has been studied for decades. Although most surface science studies have been performed at conditions close to UHV, some notable exceptions exist, in which infrared (IR) spectroscopy, Surface X-Ray Diffraction (SXRD) and Scanning tunnelling microscopy (STM) have been used at pressures relevant for industrial catalysis. Among these, the SXRD and STM studies find that the catalytic surface oxidizes when the activity gets high [1-9], while the IR spectroscopy generally agrees with the previously general belief, that the catalytically active phase is metallic [10-12]. Consequently, there has been a strong debate concerning the active phase of these catalysts during CO oxidation.

While IR spectroscopy probes the properties of the adsorbate (CO), SXRD is sensitive to the surface structure of the substrate. In contrast, X-ray Photoelectron Spectroscopy (XPS) probes both the adsorbate and the substrate, and in the case of High Pressure (HP-) XPS, also the gas phase. Hence, the chemical properties of the surface, the adsorbate as well as the composition of the gas phase can be studied simultaneously. In this contribution we show *in situ* HP-XPS results of CO oxidation over Pd(100) and Rh(100) obtained at beamline 9.3.2 at the Advanced Light Source in Berkeley.

Fig. 1 shows continuous O 1s scans following the CO oxidation over Pd(100) and Rh(100) respectively. In these experiments, the chamber was filled with 0.33 mbar CO and 0.33 mbar O_2 and the temperature ramped up and down in order to reveal the ignition and extinction of the catalytic reaction. The behaviour of both samples is similar and a wealth of information is obtained at once. At low temperatures, the main features are the peaks corresponding to adsorbed CO (which for Pd overlaps with the Pd 3p peak) and CO + O_2 in gas phase. As the reaction ignites, all signs of CO have disappeared from the spectra, and instead we detect O on the surface and CO_2 in the gas phase.

These results agree well with previous reports, saying that adsorbed CO efficiently poisons the CO oxidation reaction, while the oxygen covered surface is catalytically active. In the active state, the residence time of the CO on the surface is so short that it cannot be detected by XPS, which explains why no CO can be observed in IR spectroscopy. The fact

that CO is not seen in the gas phase over the active surface, shows that the catalyst is mass transfer limited. From Fig. 1, it is difficult to judge the exact nature of the surface oxygen, but in contrast to recent SXRD reports, more detailed measurements show that the Rh surface is metallic in the active state, while the Pd surface oxidizes in high enough pressures and temperatures. We will discuss the consequences of these results.

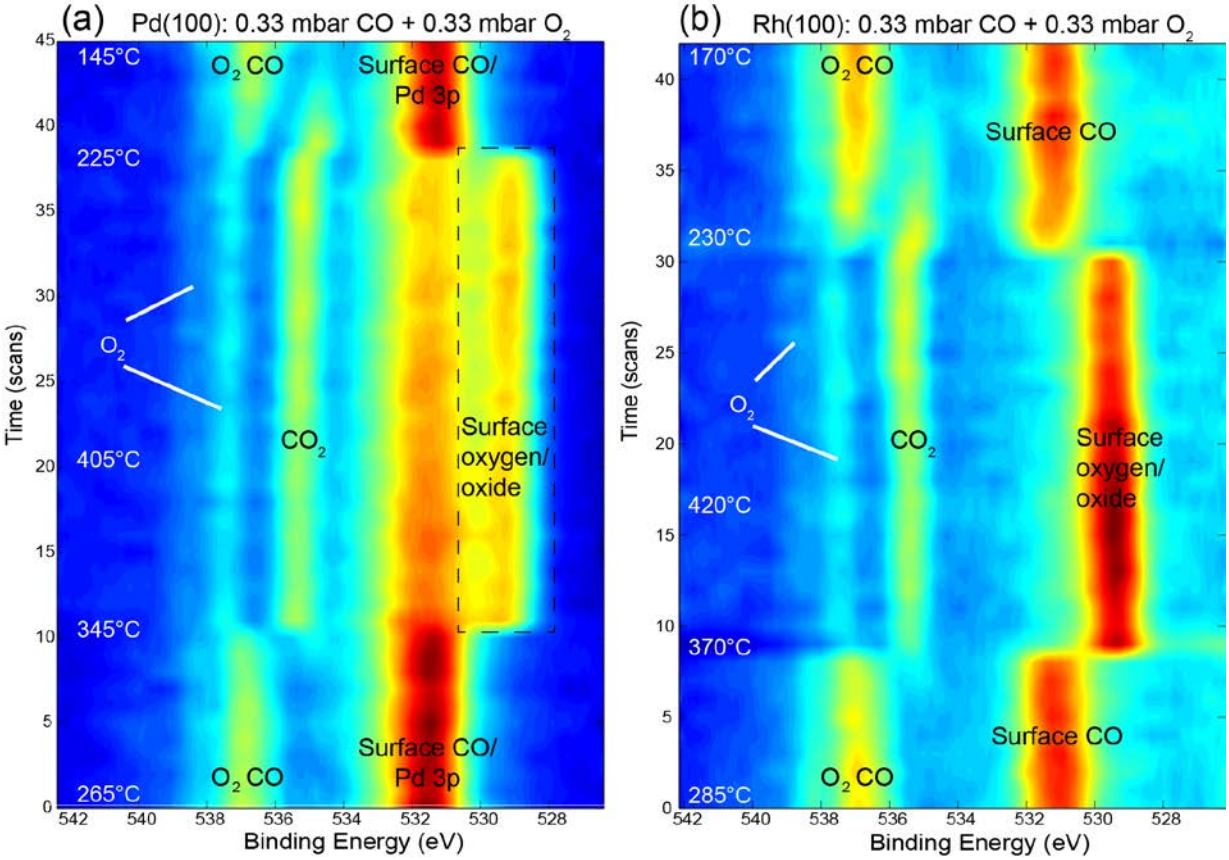

Figure 1 CO oxidation in a gas mixture of 0.33 mbar CO and 0.33 mbar O_2 over (a) Pd(100) and (b) Rh(100).

[1] H. Over, *et al.*, Science **287** (2000) 1474.

[2] H. Over, and M. Mühler, Prog. Surf. Sci. **72** (2003) 3.

[3] H. Over, O. Balmes, and E. Lundgren, Catalysis Today **145 (**2009) 236.

[4] B. L. M.Hendriksen, and J. W. M. Frenken, Phys. Rev. Lett. **89** (2002) 046101.

[5] B. L. M. Hendriksen, S. C. Bobaru, and J. W. M. Frenken, Surf. Sci. **552** (2004) 229.

[6] M. D. Ackermann, *et al.*, Phys. Rev. Lett. **95** (2005) 255505.

[7] R. Westerström, *et al.*, Phys.: Condens. Matter **20** (2008) 184019.

[8] J. Gustafson, *et al.*, J . Phys. Rev. B **78** (2008) 045423, Catalysis Today **145** (2009) 227, J. Phys. Chem. C. **114** (2010) 4580, J. Phys. Chem. C **114** (2010) 22372.

[9] R. van Rijn, *et al*., J. Phys. Chem. C. **114** (2010) 6875, Phys. Chem. Chem. Phys., **13** (2011) 13167.

[10] M. S. Chen, *et al.*, Surf. Sci. **601** (2007) 5326.

[11] F. Gao, *et al.*, Surf. Sci. **603** (2009) 65, J. Phys. Chem. C **113** (2009) 174, J. Phys. Chem. C **113** (2009) 182. J. Phys. Chem C **114** (2010) 6874.

[12] S. M. McClure, and D. W. Goodman, Chem. Phys. Lett. **469**, (2009) 1.

Liquid Organic Hydrogen Carriers: Surface Science and Model Catalytic Studies

M. Sobota, S. Schernich, M. Amende, I. Nikiforidis[1], B. Sanmartín Zanón, T. Staudt, O. Höfert, Y. Lykhach, C. Papp, W. Hieringer[1], M. Laurin, D. Assenbaum[2], P. Wasserscheid[2], H.-P. Steinrück[1], A. Görling[1], J. Libuda

Lehrstuhl für Physikalische Chemie II and Erlangen Catalysis Resource Center, Friedrich-Alexander-Universität Erlangen-Nürnberg, D-91058 Erlangen, Germany
(corresponding author: J. Libuda, e-mail: libuda@chemie.uni-erlangen.de)
[1]Lehrstuhl für Theoretische Chemie, Universität Erlangen-Nürnberg, D-91058 Erlangen, Germany
[2] Lehrstuhl für Chemische Reaktionstechnik, Universität Erlangen-Nürnberg, D-91058 Erlangen, Germany

Hydrogen has attracted considerable attention as an energy carrier, e.g. as an alternative fuel for CO_2-free vehicle propulsion. The most serious challenge of hydrogen technology is related to storage, with existing technologies requiring either high pressures or cryogenic temperatures.[1] Chemical hydrogen storage represents an interesting alternative, with so-called Liquid Organic Hydrogen Carriers (LOHCs) providing particularly promising properties. N-ethylcarbazole (NEC) has been identified as an attractive candidate which is reversibly hydrogenated to dodecahydro-N-ethylcarbazole (H_{12}-NEC), taking up 5.8 wt% of hydrogen. As H_{12}-NEC has many physico-chemical similarities to Diesel, LOHC systems based on NEC/ H_{12}-NEC could make use of the existing energy infrastructure and, therefore, enable step-wise replacement of the existing hydrocarbon fuels.[2] Besides, LOHC technology provides a very attractive new way to store temporary energy over-production from renewable sources, even at longer timescales. The current challenge for implementation of LOHCs in mobile applications is related to the noble-metal demand of conventional dehydrogenation catalysts. Sufficiently fast and dynamic dehydrogenation requires catalysts containing large amounts of supported Pt or Pd. Careful design of dehydrogenation catalysts that combine highest activity, selectivity, and stability with low noble metal content could pave the way for LOHCs in future energy technology.

Despite the great technical potential of the concept, very little is known on the underlying reaction mechanisms at the microscopic scale. Therefore, we have started to investigate the catalytic reaction mechanisms and associated microkinetics using a surface science and model catalysis approach.[3] Here, we present selected results from model studies addressing the interaction of H_{12}-NEC with single crystal surfaces, Pd(111) and Pt(111), and single-crystal-based model catalysts, $Pd/Al_2O_3/NiAl(110)$ and $Pt/Al_2O_3/NiAl(110)$, under ultrahigh-vacuum (UHV) conditions. Adsorption, dehydrogenation, and decomposition of H_{12}-NEC is investigated using time-resolved infrared reflection absorption spectroscopy (TR-IRAS), high-resolution photoelectron spectroscopy (HR-PES) with synchrotron radiation (BESSY

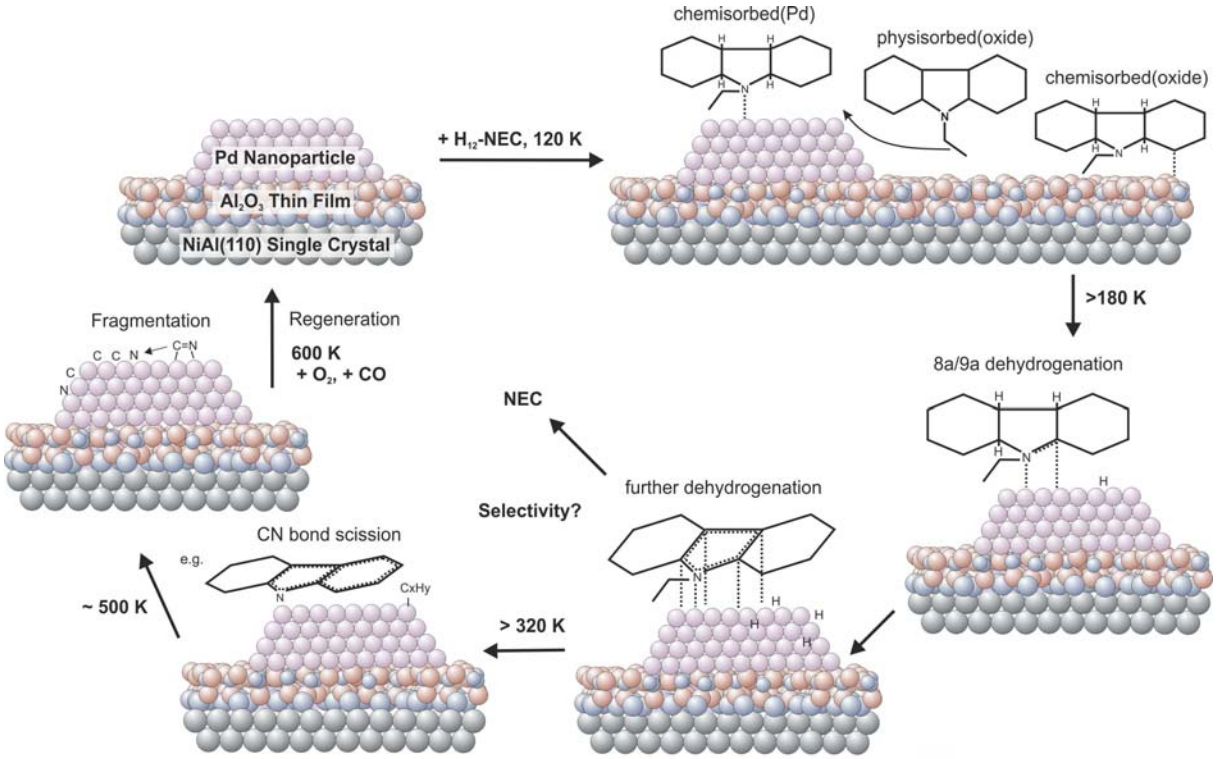

II), and molecular beam (MB) techniques, complemented by density functional theory (DFT) calculations.

H_{12}-NEC is found to adsorb molecularly on all surfaces at low temperature (120 K). On Pd surfaces initial activation of the molecule occurs via C-H bond scission at specific position (8a, 9a) of the carbazole skeleton at temperatures above 170 K (see Figure). Interestingly, differences in activation barriers can be identified comparing Pd(111) and Pd nanoparticles. Dehydrogenation successively proceeds with increasing temperature, before breakage of one C-N bond occurs at temperatures around 350 K. The decomposition intermediates reside on the surface up to 500 K and, finally, decay to small fragments and atomic species. These species block part of the reactive sites, but can be oxidatively removed by heating in oxygen to 600 K. Characteristic differences are identified concerning deactivation on Pd and Pt nanoparticles, with substantially higher temperatures required on Pt to activate C-N bond breakage. These findings could explain the different stability of technical dehydrogenation catalysts and may provide rational strategies towards the development of more stable and metal-efficient catalytic materials.

Financial support by the Deutsche Forschungsgemeinschaft (DFG) within the Excellence Cluster “Engineering of Advanced Materials” and the BMW Group, Research and Technology, is acknowledged. Additional support was provided by the Fonds der Chemischen Industrie and the DAAD. M.S. gratefully acknowledges support by the Fonds der Chemischen Industrie via a Kekule Grant. The authors thank the BESSY staff for support and the Helmholtzzentrum for travel support.

[1] U. Eberle, M. Felderhoff, F. Schüth, *Angew. Chem. Int. Ed.* 48, 6608 (2009)
[2] D. Teichmann, W. Arlt, P. Wasserscheid, R. Freymann, Energy Environ. Sci. 4, 2767 (2011)
[3] M. Sobota, I. Nikiforidis., M. Amende, B. Sanmartín Zanón, T. Staudt, O Höfert, Y. Lykhach, C. Papp, W. Hieringer, M. Laurin, D. Assenbaum, P Wasserscheid, H.-P. Steinrück, A. Görling, J. Libuda, Chem. Eur. J. 17, 11542 (2011)

Fischer-Tropsch synthesis followed at high pressures with STM and SXRD

V. Navarro, S.B. Roobol, R. van Rijn, O. Balmes, D. Wermeille, A. Resta, R. Felici, A.P. van Bavel and J.W.M. Frenken

Fischer-Tropsch synthesis (FTS) is a catalytic reaction that leads to the production of hydrocarbons from a mixture of H_2 and CO under high-temperature and high-pressure conditions. In spite of its enormous industrial and economic importance and in spite of the impressively large number of scientific studies on this reaction, many fundamental aspects of FTS are still far from being understood completely, i.e. on the atomic and molecular scale [1].

Traditional surface science techniques, with which catalyst surfaces can be investigated down to the atomic level, can usually be applied only under (high) vacuum conditions, many orders of magnitude below the pressures of industrial FTS. This extreme 'pressure gap' can easily lead to dramatic differences between laboratory and practice in terms of the catalyst structures, the reaction mechanisms and the reaction efficiencies and selectivities.

We have performed studies on the FTS with two innovative experimental techniques that approach the conditions at which the reaction takes place in industry. Scanning tunneling microscopy (STM) [2] and surface X-ray diffraction (SXRD) [3] have been used *in situ* to follow catalytic surfaces at high pressures and elevated temperatures. The two techniques are complementary, i.e. real space versus reciprocal space, and emphasis on local structures versus emphasis on periodic structures. In both cases we have configured the instruments in the form of small flow reactors, embedded inside a UHV chamber in which traditional surface science techniques are used to prepare and characterize the samples. These techniques have allowed us to study the structural changes on the surface of the catalyst while the reaction takes place.

In our studies, we have used a Co(0001) single crystal surface as a model catalyst. Much to our surprise, we find with both techniques that during the reaction, at atmospheric pressures and elevated temperatures, a polycrystalline cobalt phase, i.e. an overlayer of cobalt nanoparticles, rapidly develops on the surface of the single crystal. We attribute this 'powdering' to the formation of a highly defective layer of graphene during the reaction, through which cobalt atoms segregate and coalesce to form particles on top. This scenario has severe consequences for the FTS reaction and for our view on the structure and working mechanisms of this catalyst and also for the potential role of structural promoters.

References:

1- J. Wilson *et al*., *J. Phys. Chem*. **99**, 7860-7866 (1995).
2- C.T. Herbschleb *et al*., to be published. B.L.M. Hendriksen, *et al*., *Topics in Catalysis*, **36**, 1–4 (2005).
3- R. van Rijn *et al*., *Rev. Sci. Instrum*. **81**, 014101 (2010).

Laser Induced Fluorescence applied to catalysis

S. Blomberg[1], J. Zetterberg[2], J. Gustafson[1], PA. Carlsson[3], E. Lundgren[1]

(corresponding author: S. Blomberg e-mail: sara.blomberg@sljus.lu.se)

1. Division of Synchrotron Radiation Research, Lund University, Lund, Sweden.

2. Division of Combustion Physics, Lund University, Lund, Sweden

3. Competence Centre for Catalysis, Chalmers University of Technology, Gothenburg, Sweden

The catalytic activity of the Pt-group metals has been studied for many years. Most studies have been performed in Ultra High Vacuum (UHV) [1], hence the surface-gasphase interaction at atmospheric conditions is not as well known. During the last decade, new techniques have been developed to measure at more realistic conditions, enabling a more complete understanding of complex catalytic processes [2-4]. In order to improve and understand the catalytic process, the gas phase may also play an important role. In reactivity measurements, the gas phase is almost exclusively detected through mass spectrometry (MS), which does not contain any spatial information of the gas distribution that could provide additional information about the reactions and the catalytic activity. We have therefore combined MS with planar laser-induced fluorescence (PLIF), commonly used in many other applications e.g. combustion physics [5-7]. The technique complements the mass spectrometer with a 2D image of the probed gas and by using a laser, non-intrusive *in situ* measurements can be performed.

We report the first experiments carried out on a new *in situ* setup, which allows for detection of CO_2 close to a catalyst under realistic reaction conditions by the means of PLIF in the mid-infrared spectral range. An IR laser sheet is used to probe a ro-vibrational transition in the CO_2 gas molecule at ~2.7 μm. The fluorescence light at 4.3 μm from the de-excited molecule is then detected by an IR camera that provides 2D images of the CO_2 concentration in the reactor cell.

Due to the spatial information provided by the PLIF signal, at least two samples in the reactor cell can be studied simultaneously. By analyzing the PLIF signal we show that it is possible to distinguish which sample is actually generating the CO_2 signal. In figure 1 the CO oxidation over a 2%Pd/CeO_2 and a 2%Pt1%Pd/CeO_2 powder catalysts placed next to each other in the reactor cell is shown. The study is performed at a partial pressure of 25 mbar O_2, 25 mbar CO and 50 mbar Ar. The temperature is ramped and reaches 200°C as a maximum. The 2D PLIF images in figure 1 a) are an average of 10 snapshots (each 15 μs) and each image covers a total time 1s. The 2D images contain information of the CO_2 distribution in the cell and point measurements of the CO_2 concentration over each catalyst is easy to extract. The observed CO_2 signal by PLIF is in good agreement with an increase of the CO_2 MS signal. The PLIF snapshots together with the point measurements clearly shows that the catalytic ignition occur

at different temperatures for the two samples. The sample containing Pt is active for a much shorter temperature range compared to the pure Pd catalyst.

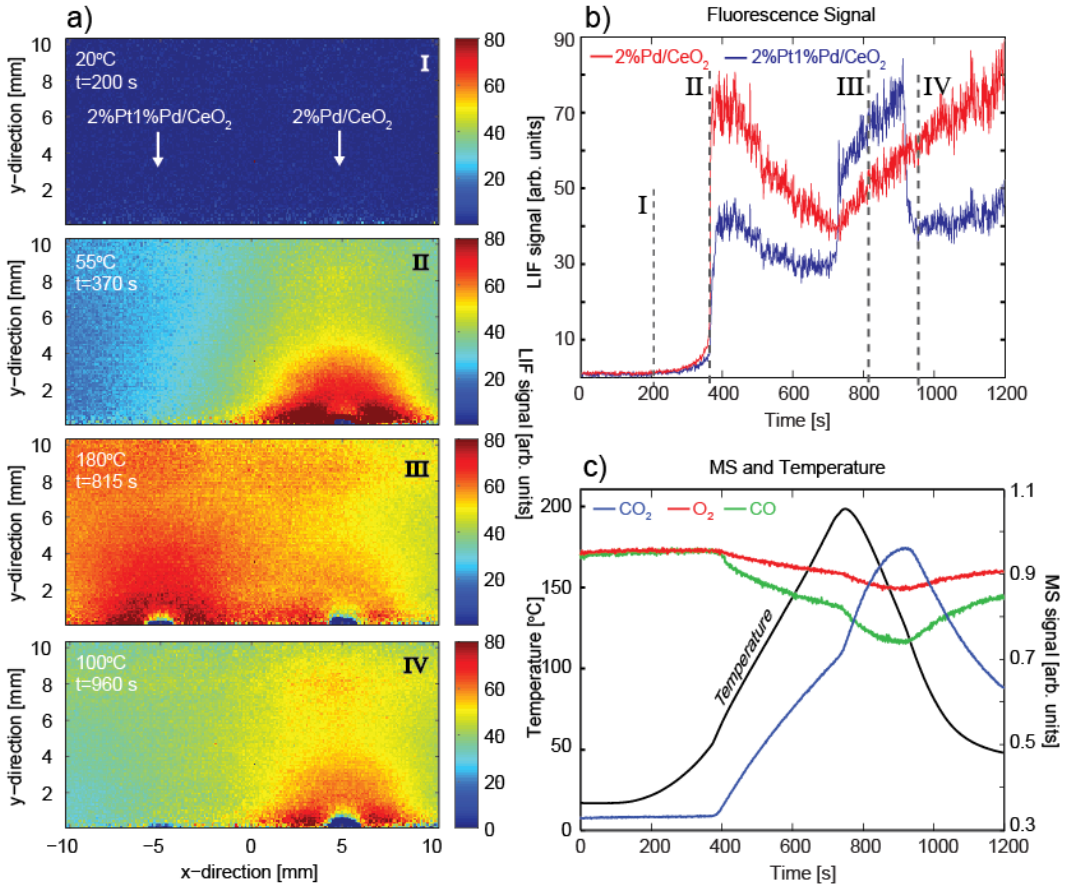

Figure 1a). 2-dimensional PLIF snapshot images during the reaction showing the CO_2 concentration over a 2%Pd/CeO_2 and a 2%Pt1%Pd/CeO_2 powder catalyst surfaces at different times and temperatures. b) The fluorescence signal over each sample (red and blue) c) The temperature of the samples together with a normalized MS signal of the CO, O_2 and CO_2.

The presented PLIF data together with other techniques allow for a more complete picture of the catalytic process, and in particular on the almost unknown gas distribution within the reactor cell. Furthermore, the combination of spatial and temporal resolution of the gas phase opens up for studies of short lived radicals and intermediate species in the gas phase close to the surface that may affect catalytic reactions and the surface active surface structure.

[1] G. Ertl, H. Knözinger, and J. Weitkamp, *Handbook of Heterogeneous Catalysis.* Wiley, New York, 1997.
[2] A. Stierle and A. Moelenbroek, MRS Bull. **32**, 1000 (2007).
[3] E. Lundgren and H. Over, J. Phys. Condens. Matter **20**, 180302 (2008).
[4] Freund, Surf. Sci. **601**, 1438 (2007).
[5] A. C. Eckbreth, *Laser diagnostics for combustion temperature and species*. (Abacus Press, Tunbridge Wells, Kent ; Cambridge, Mass., 1988).
[6] K. Kohse-Höinghaus and J. B. Jeffries, *Applied combustion diagnostics*. (Taylor & Francis, New York, 2002).
[7] J. Wolfrum, Symposium (International) on Combustion **27** (1), 1-41 (1998).

Photochemistry on nanoparticles. An overview of a typical system

D. Menzel, K. Watanabe, K. H. Kim, D. Mulugeta, and H.-J. Freund

Fritz-Haber-Institut der Max-Planck-Gesellschaft, Dept. CP, Faradyweg 4-6, 14195 Berlin, Germany
(corresponding author: D. Menzel, e-mail: dietrich.menzel@ph.tum.de)

This report intends to give an overview over the specific effects which occur in the photochemical activity on surfaces of nanoparticles (NPs), in comparison to the surfaces of bulk crystals [1]. It is based on the results of a project that has been completed after running for 7 years with the intent to get a qualitative and quantitative understanding of these specific effects using a particular adsorbate system. We believe that our results have bearing for many if not most molecular adsorbates on metallic nanoparticles. Some of the results have been described before at 3S conferences [2], and most have been or are being published (see [3-7]).

Our test system was NO dimers adsorbed on Ag NPs supported on thin alumina films on NiAl single crystals. In situ comparison with Ag(111) has always been done which has been well studied before [8,9]. The strongest channel, on which we concentrate here, is photodesorption of NO. Conversion to N_2O + O and to NO 'monomers' on the surface and photodesorption of N_2 [4,7]) also occur. Photodesorption cross sections (PCS) were obtained from signal decay under irradiation [3,5-7]. Conclusions about the mechanism were obtained from final state energies of the desorbing NO (translational energies from time-of-flight [3,7] and delays in REMPI [5]; rotational and vibrational distributions from REMPI [5]). A strong focus of the studies lay on the influence of particle size [3,5]. Clearly different behavior was observed for nanosecond [3,5,7] and for femtosecond [6] laser pulses. Some details:

Linear range (nanosecond laser pulses) [3,5,7]: Strictly linear yield vs. fluence behavior was observed here (~ 5 ns, up to several mJ/pulse). Strong PCS variations were found for particles vs. the compact surface, and with changing mean particle sizes [3,5]. These were biggest for Mie plasmon excitation and for NP size around 5 nm. Off the plasmon resonance smaller enhancement was found, compatible with ~ 1/*R* (*R*: particle radius) and explained by excitation confinement. On the other hand, the found constancy of all final state energies over most of the investigated range of photon energy and polarization, as well as of particle size, indicate that the dynamics of desorption are unchanged which, in agreement with former work on Ag(111) [9] we identify as the well-known TNI (transient negative ion) mechanism [10]. Only at photon energies high enough to excite electrons from the Ag *d*-band or the adsorbate HOMO (reached with 4.7 eV photons) to the Ag s-band, a second channel can become observable which appears to go via a transient positive ion (TPI) [3,5].

Nonlinear range (femtosecond laser pulses) [6]: For pulses of ~100 fs strong nonlinear enhancement of the photodesorption yields and enhancements of the PCS were observed on

Ag NPs even for smaller fluences, indicating strong nonlinearity of the NO desorption yield, particularly for plasmon excitation. On Ag(111) no effect was seen even at 20-fold fluences. However, NO final state energy distributions were again unchanged suggesting unchanged dynamics. Two-pulse correlation experiments indicated that the memory for excitations is very short (at most corresponding to the pulse length). We therefore exclude the established nonlinear mechanisms, "DIMET" [11], and the friction mechanism [12]. We have suggested a re-excitation mechanism of hot electrons within the NPs which can increase the yield without changing the dynamics, and which can operate only in NP systems.

In summary, we find that yield and PCS enhancement of photochemical processes at metallic NPs are induced by plasmon excitation, and - more weakly - by confinement of hot electrons. For fs pulses re-excitation of confined hot electrons can lead to strong nonlinear enhancement. However, in (almost) all cases the individual dynamics, as indicated by the final state energies, stay constant and are compatible with a TNI mechanism.

We thank Walter Wachsmann for very able technical assistance.
Support by the Deutsche Forschungsgemeinschaft within priority program SPP1093 (Dynamik von Elektronentransferprozessen an Grenzflächen), the German-Israeli Foundation (Dynamics of Electronic Processes in a Confined Environment), the Fonds der Chemischen Industrie, and the NEDO International Joint Research Grant on Photon and Electron Controlled Surface Processes is gratefully acknowledged.

[1] V. P. Zhdanov and B. Kasemo, J. Phys.: Condens. Matter 16, 7131 (2004); K. Watanabe, D. Menzel, N. Nilius, and H.-J. Freund, *Chem. Rev.* 106, 4301 (2006)

[2] See abstracts K. Watanabe et al., 3S'08, p. 57; and D. Mulugeta et al., 3S`10,

[3] D. Mulugeta, K. H. Kim, K. Watanabe, D. Menzel, and H.-J. Freund, Phys. Rev. Lett. 101, 146103 (2008)

[4] K. H. Kim, K. Watanabe, D. Menzel, and H.-J. Freund, J. Am. Chem. Soc. 131, 1660 (2009)

[5] D. Mulugeta, K. Watanabe, D. Menzel, and H.-J. Freund, J. Chem. Phys. 134, 164702 (2011)

[6] K. H. Kim, K. Watanabe, D. Mulugeta, H.-J. Freund, and D. Menzel, Phys. Rev. Lett. 107, 047401 (2011)

[7] K. H. Kim, K. Watanabe, D. Menzel, and H.-J. Freund, submitted to Surf. Sci. (Aug.2011)

[8] C. I. Carlisle and D.A. King, J. Phys. Chem. B 105**,** 3886 (2001), and references therein

[9] S. K. So, R. Franchy, and W. Ho, J. Chem. Phys. 95, 1385 (1991); T. Vondrak, D. J. Burke, and S. R. Meech, Chem. Phys. Lett. 327, 137 (2000)

[10] F. M. Zimmermann and W. Ho, Surf. Sci. Rep. 22, 127 (1995)

[11] J.A. Misevich, T.F. Heinz, and D.M. Newns, Phys. Rev. Lett. 68, 3737 (1992)

[12] P. Avouris and B.N.J. Persson, J. Phys. Chem. 88, 837 (1984)

DM is also at Physik-Department E20, Technische Universität München, 85748 Garching
Present addresses of
KW: Dept. of Chemistry, Tokyo University of Science, Shinjuku-ku, Tokyo 162-8601, Japan
KHK: Dept. Physics and Astronomy, Michigan State University, East Lansing, MI 48824-2320, USA
DMul: Dept. of Physics and Astronomy, University of Tennessee, Knoxville, TN 37996, USA

Development of novel high brightness and high spin-polarized SPLEEM and application to spintronics

T.Koshikawa, M.Suzuki, T.Yasue, E.Bauer [(1)],

Y.Takeda [(2)] and T.Nakanishi [(2)]

Osaka Electro-Communication Univ., Neyagawa, Osaka, Japan.

(1) Arizona State Univ.Tempe, Arizona, USA.

(2) Nagoya Univ.Chigusa, Nagoya, Japan

Memory size has been tremendously enlarged after the development of GMR. Recently new concept MRAM (magnetic random access memory) has been proposed, in which the magnetic domain wall can be driven with current (current-induced domain wall motion: CWM) using perpendicular magnetic anisotropy [1]. $[Co/Nix]_y$ multi-layer nano-wires might be an important candidate, which has strong perpendicular magnetic anisotropy [2]. In order to clarify the detailed magnetic thin film formation and their property, we need more sophisticated magnetic microscopy instrument which gives us high spatial resolution, dynamic observation and so on. Here we will present the results of development of a novel high spin-polarization and high brightness low energy electron microscope (SPLEEM) with new idea; strained super lattice cathodes for high spin-polarization (90%), the back side illumination of laser beam to the cathode for very high brightness ($1.3x10^7$ A/cm^2 sr) and XHV (extreme high vacuum) at the electron source chamber for long life time (over 2 months) shown in Fig. 1. We have investigated the detailed magnetization process of those multi-layer with newly developed SPLEEM [3-6]. The magnetic images of $Co/Ni_2/W(110)$ and 1 ML Au on $Co/Ni_2/W(110)$ show that Au ultra thin film conducts to the strong perpendicular magnetic anisotropy shown in Fig. 2. W(110) substrate

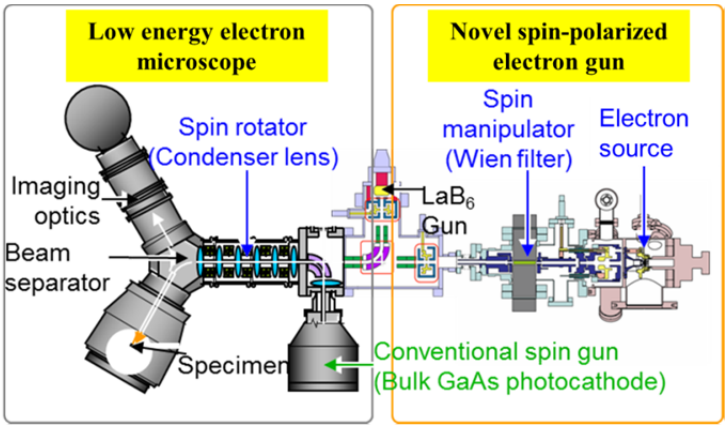

Fig. 1. High brightness and highly spin-polarized SPLEEM

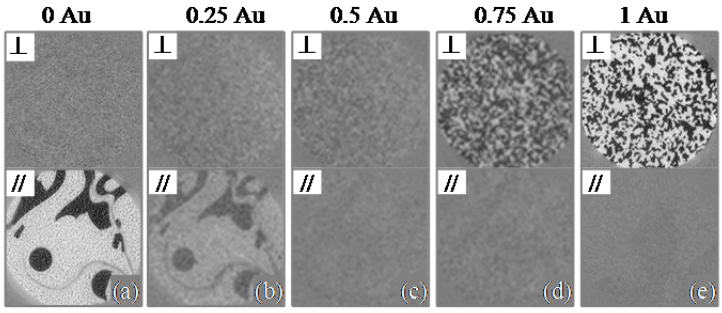

Fig. 2. Magnetic domain contrast of Au/1Co/2Ni/W (110)

gives also big effect on the perpendicular magnetization of CoNi2 thin film. This means that combination of ultra thin Au film and W substrate could be used as the cap materials.

Additional development are carried out in order to improve the high quantum efficiency of the photo-cathode with reducing the absorption of the laser light at the GaAs inter-layer and the reflection of the laser beam at the back-side surface, which makes us now improving the factor four. We are also making a compact spin gun with new idea in which we can reduce the devices for spin manipulation and rotation from two to one. This novel device can operate the spin direction in 3 dimensional ways.

[1] M.Yamaguchi et al., Phys. Rev. Lett. ,92, 077205 (2004).
[2] H.Tanigawa et al., Appl. Phys. Express, 2, 053002 (2009).
[3] N.Yamamoto et al., J.Appl.Phys., 103, 064905 (200).
[4] X.G.Jin et al., Appl.Phys. Express, 1, 045002 (2008).
[5] X.G.Jin et al., J.Cryst. Growth, 310, 5039 (2008).
[6] M.Suzuki et al., Appl.Phys.Express. 3, 026601 (2010).

*E-mail address: kosikawa@isc.osakac.ac.jp

Kinetic transitions and light-off in catalytic CO oxidation on Pt: from mesoscopic to nanoscale

Y. Suchorski[1], Ch.Spiel[1], D.Vogel[1,2], R. Schlögl[2], G.Rupprechter[2]

[1]*Institute of Materials Chemistry, Vienna University of Technology, A-1210 Vienna, Austria*

[2]*Fritz-Haber-Institut der Max-Planck-Gesellschaft, D-14195 Berlin, Germany*

(corresponding author: Y. Suchorski, e-mail: yuri.suchorski@imc.tuwien.ac.at)

The light-off in exothermic catalytic reactions such as CO oxidation in an exhaust converter is a self-accelerating step, where the reaction being governed solely by the reaction kinetics, becomes, at critical temperature, determined by mass transport due to the shifted balance between the reaction heat generation and the energy dissipation in the system [1]. Such a step is closely related to the kinetic phase transition from the catalytically inactive to active steady state. Although in contrast to the catalytic light-off where the heat and mass transport play an important role [2], kinetic phase transitions are purely kinetic phenomenon [3], the common feature is that the behaviour of a catalytic system changes qualitatively when a control parameter exceeds certain value. Unfortunately, to our knowledge, there are not so much studies where the isobar kinetic transitions for differently oriented surfaces are investigated, the early studies of Rinnemo et. al. [2] and by Garske and Harold [4] on a Pt wire are rather exceptions.

In present contribution, we apply the photoemission electron microscopy (PEEM) and field ion microscopy (FIM) to study *in situ* the light-off in CO oxidation on a polycrystalline Pt foil and on an apex of a Pt nanotip, correspondingly. We have shown recently, that it is possible to monitor the isothermal kinetic phase transitions in CO oxidation on individual grains of a polycrystalline Pt foil analysing the local PEEM intensities during the reaction [5]. The idea of the approach is based on the obstacle that the local PEEM intensity (i.e. the local photoemission yield) of the CO or oxygen covered Pt surface is directly related, via the local work function, to the CO or oxygen coverage. In turn, the rate of the CO oxidation reaction, as was shown in the pioneering work of Ertl [6], depends on the CO or oxygen coverage. From these two findings the dependence of the local PEEM image intensity on the local reaction rate may be concluded, which allows the spatially-resolved monitoring of the local kinetic phase transitions on a heterogeneous surface [5, 7, 8].

In present work we use this approach to determine the *isobar* kinetic transition at light-off in CO oxidation in the 10^{-5} mbar pressure range on individual μm-sized grains of a polycrystalline Pt foil. Similar approach is used to determine the kinetic transition on individual facets of a nm-sized Pt tip used as a model of a single catalytic particle. In the case of the Pt-tip we use the proper orthogonal decomposition (POD), also known as Karhunen–Loeve (KL) decomposition for the image analysis. On catalytic surfaces POD has been applied by us already earlier for the analysis of the reaction-induced fluctuation using field electron microscopy (FEM) as the imaging method [9]. In present contribution, we use the

POD for the first time to analyse the FIM video-frames in order to distil coherent spatiotemporal modes.

The experiments have detected a quasi-independent light-off behaviour of the individual grains (50-100 μm size) of a polycrystalline Pt-foil, thus the obtained results may be generally valid for the corresponding single crystal orientations. Similarly, as in the case of the *isothermal* kinetic transitions at similar conditions on the same sample [5, 7, 8], neither diffusion coupling nor gas phase coupling nor heat transfer processes are able to synchronize the light-off on different domains. In turn, the light-off on a Pt-tip at similar pressure and temperature range occurs well synchronized for different surface orientations, as follows from the POD-analysis of corresponding FIM video-sequences.

Since the gas phase coupling and heat transfer were similar in both, “foil” and “tip” cases, the observed striking differences in the light-off behaviour can be caused solely by the differences in the diffusion processes. Indeed, the individual domains on the foil are confined rather by μm-deep “clefts”, whereas the facets on the apex of the tip are confined by atomic steps solely. It is clear that the surface diffusion of CO might overcome the microscopic defects such as atomic steps but hardly the mesoscopic barriers between crystalline grains.

From the isobar kinetic transition points obtained at increasing and decreasing temperature, local kinetic phase diagrams for individual Pt(100), Pt(110), and Pt(111) domains were constructed which are in a quantitative agreement with corresponding isothermal diagrams obtained earlier via cyclic variation of the CO pressure [5].

Support by the Fonds zur Förderung der Wissenschaftlichen Forschung (SFB-F45-04 FOXSI) is gratefully acknowledged. Authors also thank Johannes Frank (IMC, TU Vienna) for his technical support.

[1] D.A. Frank-Kamenetskii, Diffusion and Heat Transfer in Chemical Kinetics, 2nd ed. (Plenum, New York, 1969).

[2] M. Rinnemo, D. Kulginov, S. Johansson, K.L. Wong, V.P. Zhdanov, B. Kasemo, Surf. Sci. 376, 297 (1997)

[3] V.P. Zhdanov, B. Kasemo, Surf. Sci. Rep. 20, 111 (1994)

[4] M.E. Garske and M.P. Harold, Chem. Eng. Sci. 47, 623 (1992)

[5] Y. Suchorski, Ch. Spiel, D. Vogel, W. Drachsel, R. Schlögl, G. Rupprechter, Chem.Phys.Chem. 11, 3231 (2010)

[6]G. Ertl, Science 254, 1750 (1991)

[7] C. Spiel, D. Vogel, Y. Suchorski, W. Drachsel, R. Schlögl, G. Rupprechter, Cat. Lett, 141, 625 (2011)

[8] D. Vogel, C. Spiel, Y. Suchorski, A. Urich, R. Schlögl, G. Rupprechter, Surf. Sci. 605, 1999 (2011)

[9] Y. Suchorski, J. Beben, R. Imbihl, Surf. Sci. 454-456, 331 (2000)

Author Index

SPECS Systems

SPECTROSCOPY AND MICROSCOPY UNDER
NEAR AMBIENT CONDITIONS

NAP-XPS & NAP-SPM

„In order to understand real world chemical processes, we need to analyze them as they occur in the real world.“

Miquel Salmeron, Berkeley Lab

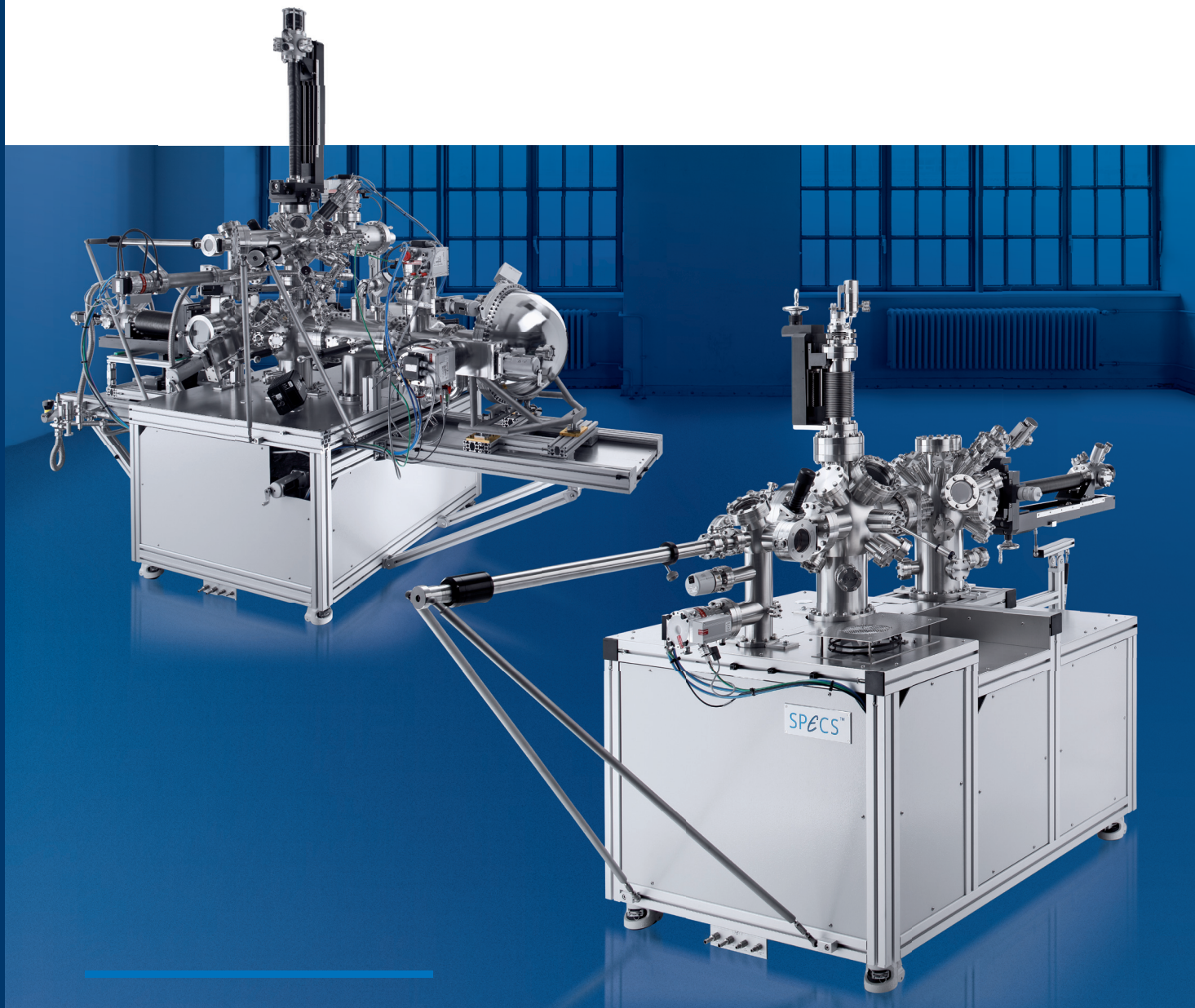

SPECS Surface Nano Analysis GmbH

T +49 (0)30 46 78 24-0
E support@specs.com
H www.specs.com

SPECS™

SYMPOSIUM ON SURFACE SCIENCE 2012
St. Christoph am Arlberg, Austria
March 11 - March 17, 2012

Friedrich Aumayr, Ulrike Diebold and Peter Varga, organizers
Institute of Applied Physics, Vienna University of Technology (TU Wien)

Sunday, 11 March 2012	Monday, 12 March 2012	Tuesday, 13 March 2012	Wednesday, 14 March 2012	Thursday, 15 March 2012	Friday, 16 March 2012
	07:15 - 08:00 BREAKFAST	07:15 - 08:00 BREAKFAST	07:15 - 08:00 BREAKFAST	07:15 - 08:00 BREAKFAST	07:15 - 08:00 BREAKFAST
	chair: ***ECHENIQUE***	*chair:* ***HEINZMANN***	*chair:* ***KISCH***	*chair:* ***BOVENSIEPEN***	*chair:* ***AUMAYR***
	08:00 - 08:20 GIESSIBL	08:00 - 08:20 GREBER	08:00 - 08:20 LUNDGREN	08:00 - 08:20 BARTH	08:00 - 08:20 MORGENSTERN
	08:20 - 08:40 GÖLZHÄUSER	08:20 - 08:40 MITTENDORFER	08:20 - 08:40 STIERLE	08:20 - 08:40 BUCK	08:20 - 08:40 ESCH
	09:15 - 12:00 SKIING INSTRUCTIONS	09:15 - 12:00 SKIING INSTRUCTIONS	09:15 - 12:00 SKIING INSTRUCTIONS	09:15 - 12:00 SKIING INSTRUCTIONS	09:15 - 12:00 GIANT SLALOM RACE
	12:00 - 13:00 LUNCH	12:00 - 13:00 LUNCH	12:00 - 13:00 LUNCH	12:00 - 13:00 LUNCH	12:00 - 13:00 LUNCH
	13:30 - 15:30 SKIING INSTRUCTIONS	13:30 - 15:30 SKIING INSTRUCTIONS	13:30 - 15:30 SKIING INSTRUCTIONS	13:30 - 15:30 SKIING INSTRUCTIONS	13:30 - 15:30 SKIING INSTRUCTIONS
	chair: ***SÁNCHEZ-PORTAL***	*chair:* ***TAGLAUER***	*chair:* ***HAMMER***	*chair:* ***SCHNEIDER W D***	*chair:* ***DIEBOLD***
16:00 - 18:30 REGISTRATION	16:30 - 16:50 BRUNE	16:30 - 16:50 DIL	16:30 - 16:50 KAMPEN	16:30 - 16:50 GRILL	16:30 - 16:50 GUSTAFSON
	16:50 - 17:10 WEINELT	16:50 - 17:10 OKUDA	16:50 - 17:10 MAIER	16:50 - 17:10 MARBACH	16:50 - 17:10 LIBUDA
	17:10 - 17:30 EBERHARDT	17:10 - 17:30 IBACH	*chair:* ***RUPPRECHTER***	17:10 - 17:30 HENDRIKSEN	17:10 - 17:30 NAVARRO
	17:30 - 17:50 JOHANSSON	17:30 - 17:50 LINSMEIER	17:10 - 18:30 POSTER INTRODUCTION	17:30 - 17:50 MESSING	17:30 - 17:50 BLOMBERG
	17:50 - 18:10 STARKE	17:50 - 18:10 STEURER		17:50 - 18:10 WINKLER	17:50 - 18:10 MENZEL
	18:10 - 18:30 KNUDSEN	18:10 - 18:30 KLIMOV		18:10 - 18:30 PIRUG	*chair:* ***FASEL***
					18:30 - 18:50 KOSHIKAWA
18:30 - 19:30 DINNER	18:30 - 19:30 DINNER	18:30 - 19:30 DINNER	18:30 - 19:30 DINNER	18:30 - 19:30 DINNER	18:50 - 19:10 SUCHORSKI
					19:10 - 19:35 GIANT SLALOM RACE AWARD CEREMONY
20:00 - 20:20 OPENING	*chair:* ***ALTMANN***	*chair:* ***MÜLLER P***	19:30 - 21:30 POSTERSESSION	*chair:* ***BAUER***	
chair: ***VARGA***	19:30 - 19:50 REUTER	19:30 - 19:50 RENAUD		19:30 - 19:50 ARNAU	20:00 CONFERENCE DINNER
20:25 - 20:45 SCHEFFLER	19:50 - 20:10 HELLMAN	19:50 - 20:10 LEROY		19:50 - 20:10 GARCIA-LEKUE	
20:45 - 21:05 WÖLL	20:10 - 20:30 BORG	20:10 - 20:30 ORTEGA		20:10 - 20:30 CABRERA-SANFELIX	
21:05 - 21:25 DRAXL	20:30 - 20:50 SCHNEIDER M A	20:30 - 20:50 CHULKOV		20:30 - 20:50 NETZER	